Biogenic volatile organic compound emissions from bioenergy plants and potential impacts on air chemistry

Felix Havermann

München 2019

Biogenic volatile organic compound emissions from bioenergy plants and potential impacts on air chemistry

Felix Havermann

Dissertation
an der Fakultät für Physik
der Ludwig-Maximilians-Universität
München

vorgelegt von
Felix Havermann
aus München

München, den 1. Oktober 2019

Erstgutachter: Prof. Dr. Mark Wenig
Zweitgutachter: Prof. Dr. Hans Peter Schmid
Tag der mündlichen Prüfung: 15. November 2019

Zusammenfassung

Es wird erwartet, dass der Anbau von Bioenergiepflanzen in Europa in naher Zukunft stark zunehmen wird. Dies hat nicht nur Einfluss auf die Ressourcenversorgung, sondern auch auf die Umwelt. Da viele Energiepflanzen andere Emissionsmengen und Gruppierungen von hochreaktiven biogenen flüchtigen organischen Verbindungen (BVOCs) aufweisen als die meisten sonstigen Agrarpflanzen, könnte die chemische Zusammensetzung der Atmosphäre beeinflusst werden. BVOCs in der Atmosphäre können zu einer Zunahme der Konzentrationen von Ozon und sekundären organischen Aerosolen (SOA) führen, sowie die Lebensdauer des klimaschädlichen Gases Methan (CH_4) durch Reaktionen mit dem Hydroxyl-Radikal (OH) verlängern. Diese negativen Einflüsse durch den vermehrten Anbau von Bioenergiepflanzen auf die Luftqualität und das regionale Klima sind jedoch schwer zu quantifizieren, da ausreichende Feldmessungen an diesen Pflanzen fehlen. Deshalb habe ich biogenic volatile organic compound (BVOC)-Flüsse aus den in Deutschland meistgenutzten Bioenergiepflanzen Mais, Weidelgras und Raps mittels Feldmessungen und biogeochemischer Modellierung genauer untersucht. Die Pflanzen wurden in Dedelow, Brandenburg, Deutschland angebaut und während der gesamten vegetativen und reproduktiven Entwicklungsstadien untersucht. Mit einer Kombination aus sich automatisch öffnenden und schließenden Großkammern und einem Protonentransferreaktionsmassenspektrometer (PTR-MS) konnte ich hohe Emissionsanteile von hochgradig reaktiven Terpenoiden sowie anderen BVOCs, darunter Alkohole, Aldehyde, Ketone, Benzonoide und Fettsäurederivate quantifizieren. Die Saisona-lität der BVOC-Flüsse konnte in charakteristische Gruppen eingeteilt und den verschiedenen Entwicklungsstadien der Pflanze zugeordnet werden. Die Beobachtungen aus den Feldmessungen wurden unter anderem dafür verwendet, ein physiolo-gisch-orientiertes BVOC Modell, das an ein biogeochemisches Ökosystem gekoppelt wurde, weiter zu entwickeln und zu parametrisieren. Die Parameter wurden für jeden einzelnen Stoff angepasst und beinhalten den Standardemissionsfaktor, den Krümmungskoeffizienten der Emissionsfunktion und den Anteil der lichtabhängigen und lichtunabhängigen Emissionsfunktion. Dazu wurde in dieser Arbeit ein Modell zusammengeführt, welches Emissionen von neu gebildeten Stoffen (lichtabhängige) und Emissionen aus dem Stoffspeicher (lichtunabhängig) simulieren kann. Das Mo-dell wurde anschließend dazu verwendet, Jahresbilanzen der Emissionen zu erstellen, die nicht nur von der direkten meteo-

rologischen Situation angetrieben werden, sondern auch vom Pflanzenwachstum und der Photosynthese abhängen. Simulierte jährliche BVOC-Gesamtemissionen weichen zwischen den Bioenergiepflanzen um den Faktor 37 zwischen der Art mit den niedrigsten und der mit den höchsten Emissionen ab (2.5 $\pm$ 0.1, 15.7 $\pm$ 0.6, and 91.3 $\pm$ 8.0 mmol m^{-2} a^{-1} aus Mais, Weidelgras und Raps). Aufgrund des hohen Anteils von hochreaktiven Terpenoiden an den emittierten BVOCs aus Mais, sind die Unterschiede von möglichen Auswirkungen auf die Luftchemie zwischen den Pflanzen weniger stark ausgeprägt. Bei Berücksichtigung der potentiellen OH-Reaktivität (ein Maß, dass den Einfluss auf O_3 und SOA Bildung, sowie den indirekten Klimaeinfluss wiedergibt) verringert sich dadurch der Unterschied zwischen den Arten in Bezug auf die Luftchemie auf den Faktor 6. Wenn zusätzlich auf die theoretische produzierbare Menge Strom skaliert wird, ergibt sich sogar nur ein Unterschied von dem Faktor 4.5. Die Ergebnisse zeigen, dass BVOC-Flüsse aus großflächigem Bioenergieanbau in Zukunft besser differenziert werden sollten. Dazu müssen eine Vielzahl unterschiedlicher Stoffe berücksichtigt werden. Da für den Einfluss auf die Luftchemie häufig eine zeitlich hoch aufgelöste Einschätzung der BVOC-Emission notwendig ist, muss zudem berücksichtigt werden, dass sich die Emissionsfaktoren mit dem Entwicklungsstadium ändern. Daher sollten auch Messungen verstärkt über längere Messzeiträume durchgeführt werden, die über mehrere Entwicklungsstufen hinweg gehen.

Abstract

Bioenergy plant production is expected to rapidly expand in Europe in the near future. This might not only affect resource availability but will also influence the environment. Since many bioenergy plants do emit different amounts and different compositions of biogenic volatile organic compounds (BVOCs) compared to conventional agricultural crops, the new blend of highly reactive compounds might change the chemical composition of the atmosphere. BVOCs have a strong potential to enhance the photochemical O_3 production, increase the formation of secondary organic aerosols (SOA), and prolong CH_4 lifetime due to fast reactions with OH. These environmental impacts of bioenergy plants on air quality and the regional climate, however, are difficult to evaluate since accurate field observations of relevant crops are not available. Therefore, I studied a large range of BVOC fluxes from the most prominent bioenergy plants in Germany, which are maize, ryegrass, and oilseed rape, by applying field measurements and biogeochemical modeling. The plants were cultivated in Dedelow, Brandenburg, Germany and observed throughout the vegetative and reproductive development stages. Combining automatically moving large chambers and a proton transfer reaction–mass spectrometer (PTR-MS), I quantified the emission of numerous highly reactive terpenoids, together with several other BVOCs, including alcohols, aldehydes, ketones, benzenoids, and fatty acid derivatives. The characteristic seasonal BVOC flux pattern of each species, could be divided into groups and was associated to the different plant growth stages. The observations from the field campaigns were used to parameterize a biogeochemical ecosystem model coupled to a process-based BVOC emission model. The parameters for the BVOC model were fitted for each compound individually and comprise the standardized emission factor, an emission function curvature coefficient, and the fractionation into a light dependent (*de novo* emission) and light independent (pool emission) function. Therefore, I merged a mechanistic process-based *de novo* model with a pool emission approach into a joint BVOC emission model which was embedded in the biogeochemical framework LandscapeDNDC. Finally, total annual emissions were calculated in dependence on simulated plant growth and photosynthesis. Simulated BVOC emissions show that considerable differences between the investigated bioenergy plants exist with oilseed rape having 37-fold higher total annual emissions than maize (oilseed rape: 91.3 $\pm$ 8.0 mmol m^{-2} a^{-1}; maize: 2.5 $\pm$ 0.1; and ryegrass: 15.7 $\pm$ 0.6). The differences in

potential annual impacts on air chemistry are less pronounced between the plants, due to the large fraction of highly reactive terpenoids in the maize BVOC emissions. In particular, the difference is reduced to the 6-fold when the potential impact on OH-reactivity (a measure for O_3 and SOA forming potential as well as indirect radiative forcing) is considered and to the 4.5-fold when the theoretically produced electricity yield is additionally taken as a reference. Thus, the results indicate that BVOC fluxes from large-scale bioenergy fields should be better differentiated, especially with regard to BVOC composition and reactivity. Additionally, the large impact of plant phenology on emission factors demands for elaborated models that should be based on measurements that cover the whole plant growth period.

Contents

Acronyms

AVOC	anthropogenic volatile organic compound
BVOC	biogenic volatile organic compound
GC-MS	gas chromatography–mass spectrometry
GHG	greenhouse gas
GLV	green leaf volatile
GPP	gross primary production
`JJv`	BVOC emission model based on electron transport J and J_v
LDF	light dependent fraction
`LandscapeDNDC`	landscape denitrification and decomposition
LOX	lipoxygenases
`MEGAN`	model of emissions of gases and aerosols from nature
MEP	methyl erythritol 4-phosphate
MVA	mevalonic acid
m/z	mass to charge ratio
NEE	net ecosystem CO_2 exchange
NSE	Nash-Sutcliffe modeling efficiency
OVOC	oxygenated volatile organic compound
PAR	photosynthetically active radiation
PPFD	photosynthetic photon flux density
PTR-MS	proton transfer reaction–mass spectrometer
$\mathbf{R_{eco}}$	ecosystem respiration
ROS	reactive oxygen species
SEF	standardized emission factor
SIV	stress-induced volatiles
SOA	secondary organic aerosols
VOC	volatile organic compound

1. Introduction into BVOCs and bioenergy plants

Vegetation plays a pivotal role in the exchange of trace gases between land surface and atmosphere. For example, on the short term, plants assimilate more carbon dioxide (CO_2) by photosynthesis than they release by respiration, and more oxygen (O_2) is emitted than taken up. However, on the longer term, the carbon and oxygen cycles are balanced for most natural ecosystems. In addition, plants exchange a very large group of biogenic volatile organic compounds (BVOCs) (Guenther et al., 2012; Peñuelas and Staudt, 2010; Arneth et al., 2010b,a; Steinbrecher et al., 2009). Due to their high chemical reactivity with other atmospheric gases, BVOC emissions have a strong impact on the atmospheric composition. Climate and land use determine the natural emission regime of BVOCs and thus, the feedback to air quality and climate warming (Harper and Unger, 2018; Szogs et al., 2017; Rosenkranz et al., 2015; Ashworth et al., 2013). An already ongoing European Union (EU) climate change mitigation strategy within the energy sector, is substituting fossil energy sources by renewable energies especially from biomass (EEA, 2013; European Commission, 2014). That is, an increased land use and land cover change to the cultivation of bioenergy crops will lead to a change in the BVOC emission regime.

1.1. BVOCs within the land–atmosphere interface

Generally, BVOCs are highly reactive molecules with a high vapor pressure which are emitted from every living organism such as animals, microorganisms, fungi, and vegetation with the largest fraction (Kesselmeier and Staudt, 1999; Williams et al., 2016). With a global mean of 760 Tg C per year (1980–2010), total BVOC emissions from vegetation, exceed those from anthropogenic sources (anthropogenic volatile organic

compound (AVOC), such as transport, solvent use, production and storage processes, and combustion processes) by far with around 110 Tg C (Sindelarova et al., 2014; Calfapietra et al., 2013a; Piccot et al., 1992). Though, AVOC emissions can be more relevant than BVOC emissions on the local scale, especially in urban areas (Ghirardo et al., 2016; Calfapietra et al., 2013a). Simulations estimate the composition of global mean BVOC emissions by 70 % of isoprene, 11 % monoterpenes, 6 % methanol, 3 % acetone, and 2.5 % sesquiterpenes (Sindelarova et al., 2014). However, there are around 35,000 different volatile organic compounds (VOCs) currently known, which differ in synthesis and emission characteristics, and vary by their respective reactivity within the atmosphere as well (Wink, 2003). The composition and magnitude of emitted compounds is generally determined by the plant species (Kesselmeier and Staudt, 1999). Additionally, emissions of those compounds which are released from specific plant storage structures mainly depend on diffusion and evaporation and are thus exponentially dependent on the temperature. The fluxes of compounds which are emitted directly after their synthesis are controlled by both, temperature and photosynthetically active radiation (PAR) as well (Niinemets et al., 2004). Though, BVOC emissions also depend on the phenological growth stage of the plants and can be additionally induced by biotic and abiotic stressors, such as herbivores and heat (Yeoman and Yeoman, 1996). Generally, the emissions of BVOCs from plants facilitate their reproduction, defense, plant to plant interaction, and protection against stress (Peñuelas and Staudt, 2010; Pichersky and Gershenzon, 2002). Once emitted to the atmosphere, BVOCs immediately start to oxidize with the hydroxyl radical (OH), ozone (O_3), nitrate radical (NO_3), and in coastal areas with chlorine (Cl) atoms, leading to first generation BVOC products (Peñuelas and Staudt, 2010). The consumption of OH radicals by the formation of first generation products prolongs CH_4 lifetime and thus indirectly enhances radiative forcing (Kaplan et al., 2006). Intermediate products and subsequent later generation products lead to the formation of O_3 (photochemically under high NO mixing ratios) and secondary organic aerosols (SOA) (Atkinson, 2000). SOA perturb the radiative transfer and support the growth of particles by acting as cloud condensation nuclei (CNN) (Carslaw et al., 2010). Thus, BVOCs are affecting air quality and the regional climate.

1.2. Bioenergy plants now and in future

To combat climate change and meeting future goals of reducing the emissions of greenhouse gas (GHG), fossil energy sources must be substituted by renewable energy sources. That is, there is a continuous global need in increasing the energy supply from wind, sun, oceanic and geothermic energies, hydro power, and biomass. In countries which are part of the Organisation for Economic Co-operation and Development (OECD), between 1990 and 2014, total primary energy supply (= total primary energy production + energy imports − energy exports − international bunkers ± storage changes) from renewable sources increased about 2.5 % each year, whereas the energy supply for conventional energy only increased about 0.5 %. Currently, biomass is the main contributor to total primary renewable energy supply (International Energy Agency, 2015; OECD, 2013). The estimates are: Germany 57 % in 2015, Europe 62 % in 2012, OECD countries 52 % in 2014, globally 72 % in 2013 (FNR, 2018b; European Commission, 2014b; International Energy Agency, 2015). Biomass sources can be divided into the three sectors of forests, bioenergy crops, and agricultural residues. Solid biomass from forests and agricultural residues can be used for heating and electricity production by combustion. Biomass from bioenergy crops and residues can be converted into liquids (biodiesel, bioethanol) and used as biofuels e.g. for transport, and into gas (biogas mixture of methane (CH_4) and CO_2) which is used used for heat and electricity production (Bentsen and Felby, 2012; REN21, 2015; International Energy Agency, 2017). In Germany, 13 % (2.3 Mha) of the total agricultural area (17.7 Mha) is currently used for bioenergy plants (FNR, 2018b). For the future, Germany has set goals to increase the fraction of renewable energy sources within total primary energy supply from currently 13 % to 18 % until 2020, and further up to 50 % until 2050 with 26 % coming from biomass (Arbeitsgemeinschaft Energiebilanzen, 2015; Erneuerbare-Energien-Gesetz, 2014). For the EU, in 2008 7.8 Mha were used to produce biomass for bioenergy (EEA, 2011). The European forested area and the usage of resources from forestry for bioenergy production have increased during the last 20 years. However, its bioenergy potential will not significantly grow with estimates ranging from 0.8 to 6.0 EJ a^{-1} in 2010 to 0.8 to 10 EJ a^{-1} until 2050. The energy potential for residues from agricultural production will similarly not change significantly with estimates from currently 0.8 to 3.9 EJ a^{-1} to 0.6 to 5.0 EJ a^{-1} in future. In contrast, bioenergy crops have considerable potential for increases and

thus are supposed to fulfill the major part of future demand for biomass as an energy source in the EU. Estimates to supply energy thus are ranging from present 0.8 to 2.0 EJ a^{-1} to 3.0 to 56 EJ a^{-1} in 2050, with grass from arable land being the most important (Bentsen and Felby, 2012). Also recent projections of the 2013 EU reference scenario show a total increase of biomass and waste for primary energy production from around 136 Mt of oil equivalent in 2015 to 164 Mt in the year 2050 in Europe (European Commission, 2014).

1.3. Motivation and scientific objectives

Changing land use from natural ecosystems (e.g. forests, wetlands) and agricultural areas for food production towards the cultivation of bioenergy plants raises ethical as well as environmental concerns (McCalmont et al., 2015). Environmental considerations include groundwater pollution by leaching of nitrate (Nikièma et al., 2012), a potential decline in biodiversity (Immerzeel et al., 2014), or the release of additional GHG, especially CO_2, CH_4, and N_2O (Crutzen et al., 2008; Nikièma et al., 2012). Thus, these environmental costs can potentially outweigh the benefits of a non-fossil energy source. BVOC emissions might put an additional burden by changing the atmospheric chemistry and potentially increasing the formation of O_3 and SOA. Since evidence exists that at least some bioenergy crops have considerably different emission patterns than most conventional crops, this effect cannot be neglected. It should therefore be carefully considered which kind of bioenergy plants are planted in which locations (rural vs. near urban areas) and which impacts on air quality and local climate can be expected (Rosenkranz et al., 2015; Porter et al., 2015; Szogs et al., 2017).

Emissions of BVOCs from different bioenergy plants have been studied before. However, these measurements have been conducted over short periods only (hours to few days) or concentrate on only few compounds (König et al., 1995; Das et al., 2003; Veromann et al., 2013; Morrison et al., 2016). Mostly, also potential changes of emission patterns with season are neglected or oversimplified. These patterns are often the result of a changing emission sensitivity to temperature and radiation which depends on previous meteorological conditions but might also depend in the plants phenological stage. Overall, there is a lack of accurate information about the emission

regime from bioenergy plants. Nevertheless, a number of modeling studies on the impact of BVOC emissions on air quality has been carried out, especially regarding the influence on ground ozone concentrations, e.g. from poplar plantation as source of biomass (Beltman et al., 2013; Ashworth et al., 2015; Zenone et al., 2016). Since poplars are large isoprene emitter, these efforts have neglected the huge variability of different BVOCs from various other bioenergy plants (Porter et al., 2012; Beltman et al., 2013). In some studies, also the large variation in measured emission potentials and the resulting uncertainty for modeling has been addressed (Münzenberg-St.Denis and Renner, 1999; Renner and Münzenberg, 2003). Thus, it can be concluded that intensive measurement campaigns on BVOC emissions of relevant bioenergy plants are urgently needed.

Therefore, this study aims to derive various important BVOC emission parameters from field campaigns conducted at a high temporal resolution continuously throughout several weeks. The long term observations will also enable to investigate the dependencies of these parameters on environmental and phenological drivers of BVOC fluxes. By improving the parameterization of a process-based physiologically BVOC emission model which was coupled to an ecosystem model within the scope of this study, total annual fluxes could be estimated to characterize the potential impact on atmospheric chemistry for the considered bioenergy plants. These were maize, oilseed rape, and ryegrass, which are either already widely planted or are supposed to play an important role for renewable energy production in the future (Bentsen and Felby, 2012; FNR, 2018b). Thus, the major scientific objectives of this work are:

1. **to determine the composition and amount of seasonal changing BVOC emission fluxes from the most important bioenergy plants in Germany throughout their major growth periods under field conditions;**
2. **to evaluate the impact of meteorological factors (in particular temperature and radiation), as well as phenological stages on the source strength of BVOC emissions;**
3. **to upscale observed BVOC fluxes of the different bioenergy plants to the annual scale and evaluate their potential impact on air chemistry (especially reactions with OH).**

These objectives are examined by carrying out field campaigns and measuring BVOC

fluxes from maize, oilseed rape, and ryegrass with a high temporal resolution throughout different plant growth stages. The results from these measurements are used to improve the parameterization of a BVOC emission model, which will be coupled to a biogeochemical modeling framework in order to estimate total BVOC fluxes for the whole growing season. Thus, additional methodological aims of the thesis include:

- **to test the applicability of large automatic chambers for detecting BVOC emissions from bioenergy plant canopies**
- **to develop and evaluate an BVOC model that considers *de novo* as well as pool emissions and can be applied to investigate trace gas exchanges from bioenergy plants.**

2. Theory and background of BVOC research

As an introduction into the research field of biogenic volatile organic compounds (BVOCs), or shorter just plant volatiles (BVOC emissions from animals and humans are several orders of magnitude lower (Dicke and Loreto, 2010; Williams et al., 2016)), this chapter aims to answer the questions: What are plant volatiles and why do plants emit them? Why, as a meteorologist, should one investigate plants and BVOCs? How can one observe and model BVOCs emitted from plants? And finally, what has already been done in conducting research on maize, oilseed rape, and ryegrass in relation to plant volatiles?

All findings and results which are explained and briefly described in the following, originate from studies that are conducted mostly with only a single or few plant species. Although one can hardly transfer species specific findings to vegetation in general, the information about the exact species from the cited experiments will not be provided in the following. Also, as findings about a specific plant species can strongly vary between different studies as well. For this reason, the investigated plant species are only reported if essential.

2.1. BVOC emissions from plants

Globally, terrestrial ecosystems play a major role regarding energy, water, momentum and trace gas exchanges between the land surface and the atmosphere (Heimann and Reichstein, 2008). Energy and water fluxes, within the hydrological cycle, are mainly controlled by plant transpiration via the stomatal aperture of the plant's leaves leading to a partitioning of the incoming energy flux into latent and sensible

heat fluxes. Via stomatal conductance, the plant's transpiration is directly linked to trace gas exchanges, especially of carbon dioxide (CO_2), which enters the leaves via the stomata and is transformed together with water (H_2O) under exposure of light into glucose ($C_6H_{12}O_6$) and oxygen (O_2). A process of carbon assimilation that is called photosynthesis. Plants use glucose to gain energy by consuming oxygen and emitting CO_2 back to the atmosphere—the respiration, which is the opposite reaction of that for photosynthesis and also named carbon dissimilation. The energy from respiration is mainly used for building up stable plant structures (e.g., roots, stem, branches, leaves) and the maintenance of these structures (Whiting et al., 2014). A minor part of assimilated carbon is converted to compounds that are released again by root exudation or trace gas emissions, such as biogenic volatile organic compounds (BVOCs)

BVOCs can be briefly described as lipophilic liquids which have a low molecular mass and high vapor pressure at ambient temperatures (Dudareva et al., 2013). These organic trace gases other than CO_2, carbon monoxide (CO), and CH_4 are sometimes also termed nonmethane VOCs (NMVOCs). According to their chemical structure (Kesselmeier and Staudt, 1999; IUPAC, 1997), these highly reactive gaseous compounds (chemical lifetimes of few minutes to few days) can be divided into the folowing major groups:

- terpenes: compounds with $C_{5n}H_{8n}$ skeletons with $n \in \mathbb{Z}$ like hemiterpenes (C_5H_8) monoterpenes ($C_{10}H_{16}$), sesquiterpenes ($C_{15}H_{24}$), diterpenes ($C_{20}H_{32}$), etc.
- alkanes: only single bonds between carbon and hydrogen atoms C_nH_{2n+2}
- alkenes: two carbon atoms double bonded, C=C (C_nH_{2n+2})
- carbonyls: carbon atom double bonded to an oxygen atom, C=O
- alcohols: hydroxyl bound to a carbon, e.g. ethanol with C_2H_5OH
- organic esters: derived from a carboxylic acid and an alcohol, thus having C=O, e.g. methyl salicylate
- ethers: an oxygen atom bonded to any two carbon hydrogen molecules, e.g. dimethyl ether $CH_3{-}O{-}CH_3$
- and organic acids, especially carboxylic acids: organic compounds containing a

carboxyl group (C(=O)OH), e.g. acetic acid.

The group of carbonyls, alcohols, and acids is typically summarized as oxygenated volatile organic compounds (OVOCs). All groups have a large variety of species which all differ in their structure or elemental composition and thus in their physiochemical and atmospheric properties (Kesselmeier and Staudt, 1999). For example, within the group of monoterpenes ($C_{10}H_{16}$) (see Fig. 2.1.1) several compounds exist that all have the same elemental composition and the same molecular mass but a different structure. These are called isomers. Due to the difference in their structure, isomers have

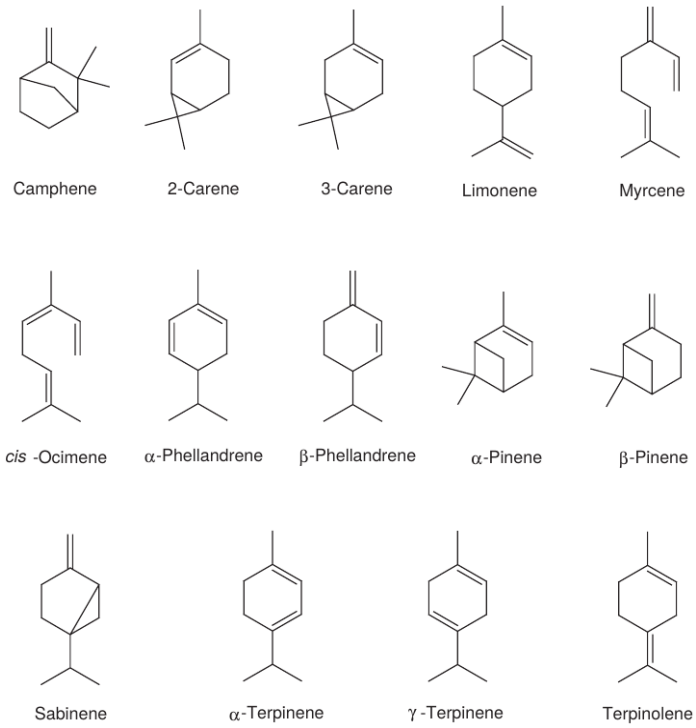

Figure 2.1.1.: Structural formulas of selected monoterpenes ($C_{10}H_{16}$) as an example of isomer diversity (from Atkinson and Arey, 2003).

different chemical reaction lifetimes within the atmosphere. Hence, they consequently have a different impact on atmospheric chemistry. For example, α-pinene (globally estimated as the third highest BVOC emitted after isoprene and methanol (Guenther et al., 2012)) has a lifetime of 2.6 hours with the hydroxyl radical (OH), 4.6 hours with ozone (O_3), and 11 minutes with the nitrate radical (NO_3). Whereas, under the same atmospheric trace gas concentrations, α-terpinene has shorter lifetimes of 47 minutes with OH, 2.8 hours with O_3, and 2 minutes with NO_3 (Atkinson and Arey, 2003).

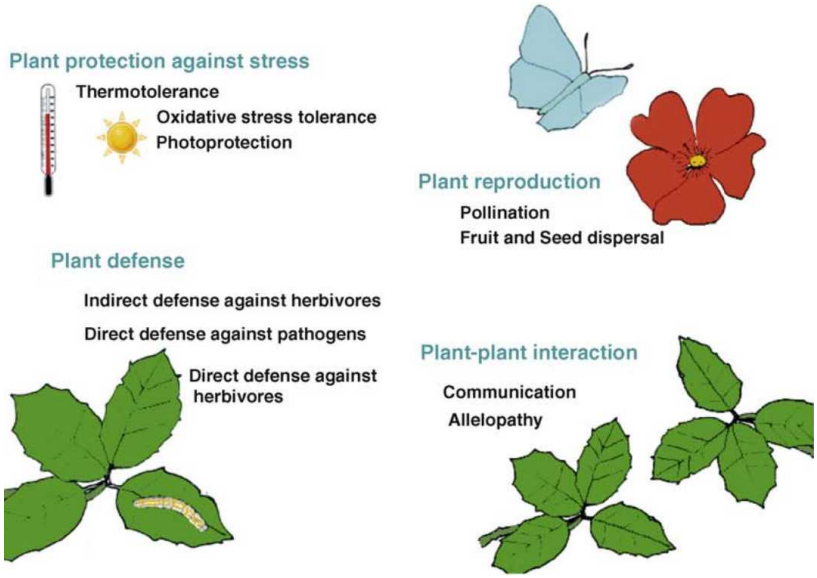

Figure 2.1.2.: Main benefits from BVOCs emitted by plants. VOCs as a medium for communication is described by the plant defense, plant reproduction and plant-plant interaction. VOCs as a response to plant stress is described by plant protection against stress (adapted from Peñuelas and Staudt, 2010).

Plants emit BVOCs in very different compositions and in very different intensities, so that the compound composition of emitter plants varies strongly. Why is this the case? BVOC production comes with a cost because the required carbon cannot be used for other purposes (such as growth or maintenance) and also because the energy requirements for formation of most BVOC are relatively high. Plants are thus likely to have benefits from these investments.

2.1.1. Communication and protection

Emissions of BVOCs have various plant biological and ecological functions (Niinemets, 2018). It is apparent that the particular BVOC blend from a specific plant under certain environmental conditions is a medium for communication (Baldwin et al., 2006; Kreuzwieser et al., 2014). This communication happens among plants of the same or different species as well as between plants and animals, especially insects (see Fig.2.1.2). Possible paths of plant-animal communication are depicted in Fig. 2.1.3. The interaction among plants-insects and plant-animals for the purpose of plant reproduction is triggered by fragrant flowers or fruit flavor attracting a recipient.

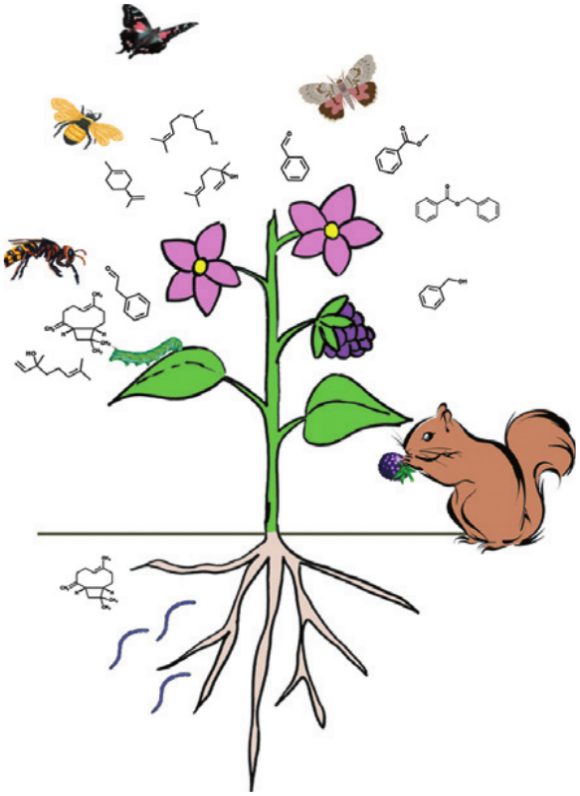

Figure 2.1.3.: Illustration of plant-animal communication by BVOCs above and below ground for pollination, seed dispersal, and defense against herbivores (from Dudareva et al., 2013).

Thereby insects as well as animals detect emitted compounds by their olfactory system and serve the plant as pollinators (plant-pollinator interaction) and seed dispersers (plant-frugivore interaction) when interacting with the plants during their foraging (Peñuelas and Staudt, 2010; Dudareva et al., 2013; Rosenkranz and Schnitzler, 2016; Xu and Turlings, 2018). A species specific floral BVOC profile can also act as a reproductive isolation when closely related plant species lacking a mechanism which prevents mutual pollination (Dudareva et al., 2013). Besides reproduction, plant-insect interaction by volatiles also serves as a direct or indirect defense, especially against herbivore attacks or microbial pathogen infestation above and below ground. After being attacked, induced BVOCs (see Sect. 2.1.2 for more information on stress-induced volatiles (SIV) and herbivore-induced volatiles) ones emitted, can directly repel the attacker by affecting its behavior or physiology. An indirect plant defense mechanism is to attract the natural enemies of the attacker, either by the compounds emitted from the flower or fruit as an alternative food source, or by signaling the

natural enemy of a specific herbivore its presence (Pierik et al., 2014; Xu and Turlings, 2018).

The neighboring plants of SIV emitting plants can receive this signal and may begin to emit SIVs without being exposed to the stress themselves, or increase the emission of SIV without a stronger exposure to the stress, or be better prepared to start emitting SIVs (primed) in case of stress exposure. These plant-plant communication mechanisms of inducing or priming BVOC emissions, enhances the stress resistance of a whole plant community (Baldwin et al., 2006; Kegge and Pierik, 2010). Other than communication, BVOCs can also serve allelopathy. For example, root emitted monoterpen can inhibit seed germination of competitor plant species (Kegge and Pierik, 2010). Plant-plant competition for light, nutrients (especially nitrogen and phosphorus), and water is a common stressor in high density stands as e.g., in monocultures of intensive industrial farming. In some plants, there is a change in magnitude and blend of BVOCs between nutrient rich and nutrient poor (deficiency) soils. For example in Mediterranean species, monoterpene or sesquiterpene emissions increase during intraspecific competition (Kegge and Pierik, 2010; Pierik et al., 2014).

In addition to the protection and defense from biotic stress such as herbivores, pathogens, and plant competitors, BVOCs can also protect their emitters from abiotic stress, i.e., intense radiation, high temperatures, or the oxidative impact of air pollutants (Dudareva et al., 2013; Peñuelas and Staudt, 2010). Radiation, heat and strongly oxidative agents such as ozone can damage plant tissues and proteins and thus impair the plant metabolism, i.e. inhibit photosynthesis (primary metabolism). On the longer term, it can also reduce volatile emissions (secondary metabolism, see Sect. 2.1.2 for more details), especially isoprene, but in the short-term, emissions tend to be increased. It could be shown that photosynthesis of isoprene and monoterpene emitting plants is getting less damaged from heat stress and recovers faster, thus endures a higher thermotolerance, of emitting compared to non-emitting plants (Vickers et al., 2009; Sharkey et al., 2008). For example, it was observed that the photosynthesis damage of non-emitting leaves at 35 ℃ was the same than that of leaves which were exposed to isoprene at 45 ℃ (Sharkey and Yeh, 2001; Peñuelas et al., 2005). The hypothesis behind the thermotolerance effect is that the thylakoid membrane (see Fig.2.1.4 for an illustration) which surrounds the site inside a chloroplast where the light dependent reactions of photosynthesis take place, become permeable during heat stress. Isoprene can enter the leaky thylakoids (isoprene is synthesized inside the

chloroplast, cf. Sect.2.1.2) and stabilizing the membrane by enhancing the hydrophobic interactions due to its lipophilic property. (Sharkey and Yeh, 2001; Vickers et al., 2009).

Another protecting effect of BVOCs is that it acts as an anti-oxidant against reactive oxygen species (ROS) such as superoxide anion (O_2^-), the hydroperoxyl radical (HO_2), hydrogen peroxide (H_2O_2), and OH. ROS appear in response to the impact of oxidative compounds such as ozone (O_3). O_3 is a toxic gas, thus, periods of higher tropospheric O_3 concentrations are a serious threat to animals (including humans) and plants, especially to their productivity. Oxidation damage by O_3 within plants can lead to leaf injuries and a reduction in biomass growth and yield. The damage depends on the amount of molecules that enter the plants via stomata, the plant's defense system, and the sensitivity of tissue to oxidative stress (Tiwari et al., 2016). After O_3 enters the plant, it reacts with liquid phase compounds of the apoplast leading to the formation of ROS and thus enhancing the level of oxidative compounds within the plant. ROS are extremely reactive species that damage lipids, pigments, and proteins, amongst others. However, O_3 also triggers the production of compounds that detoxify ROS. A potential part of this defense system is an increased emission rate of various BVOCs with high reaction rates. Thus, BVOCs, especially isoprene, may also prevent plant damage from high O_3 concentration exposure due to their anti-oxidative properties (Sharkey et al., 2008; Tiwari et al., 2016).

Altogether, there are strong evidences in literature that emissions of BVOCs improve plant protection and reproduction. It should also be noted, that BVOCs supply us with aroma compounds for perfumes, flavour constituents, food preservatives, chemotherapeutics, and anaesthetics (Rosenkranz and Schnitzler, 2016).

2.1.2. Biosynthesis and driving forces of constitutive and induced emissions

This section summarizes how plant volatiles are synthesized and what mainly drives constitutive and induced emissions.

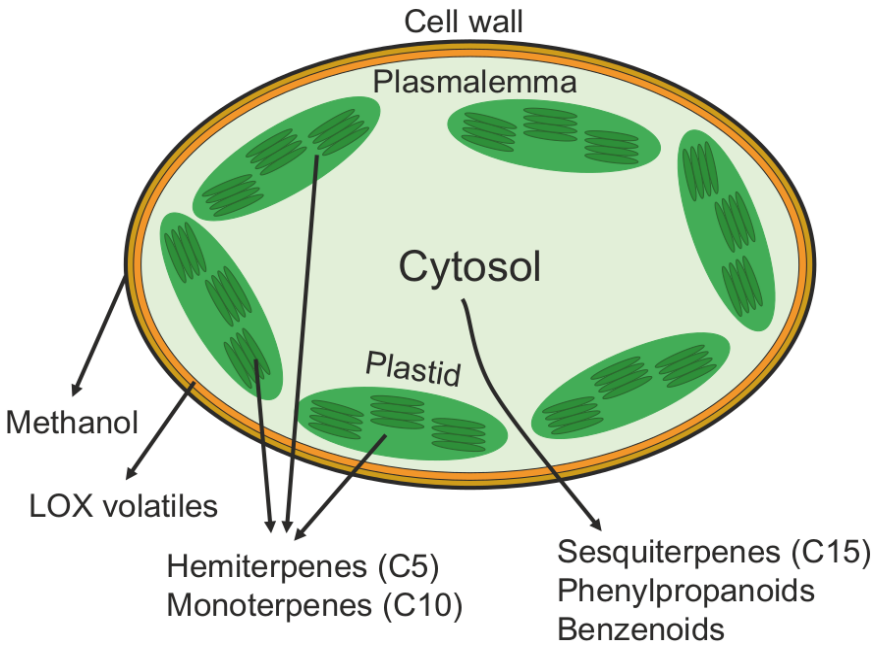

Figure 2.1.4.: Illustration of a plant cell with examples where the groups of terpenoids (hemiterpenes, monoterpenes, and sesquiterpenes), phenylpropanoids and benzenoids, LOX volatiles (fatty acid derivatives), and methanol are being synthesized. Additional note: the dark green discs inside the plastids (e.g., chloroplasts) are called thylakoids (from Niinemets, 2018).

Metabolic pathways and biosynthesis

Synthesis of BVOCs depends on availability of C, nitrogen (N), and sulfur (S), as well as energy from the primary metabolism (Dudareva et al., 2013). Plant metabolism—the chemical reactions within a living plant which are controlled by enzymes—can be divided into primary and secondary metabolism. Metabolic pathways within the primary metabolism synthesize and utilize primary metabolites which are a variety of sugars, amino acids, fatty acids, nucleotides and their polymers. Generally, primary metabolites are essential for the plant's survival, whereas secondary metabolites aid in functions such as protection, competition, and species interactions. Secondary metabolic pathways can be restricted to specific plant species or genus and might be only active during particular plant growth stages or during stress events (Yeoman and Yeoman, 1996). This is why around 35,000 different secondary metabolites are currently known, with more than 20,000 representatives from the group of terpenes (Köllner et al., 2004a; Wink, 2003) which make up a large part of BVOCs. An alternative to grouping BVOCs by chemical structure, which was introduced at the

beginning of Sect. 2.1, they can be also divided by their synthetic origin into terpenes, phenylpropanoids/benzenoids, and fatty acid derivatives (see Fig. 2.1.4) (Dudareva et al., 2013; Rosenkranz and Schnitzler, 2016) although a few plant species-/plant genus specific compounds are not covered by these classes (Dudareva et al., 2013). In the following, the main pathways and some of their metabolites will be briefly described, by having the focus on these compounds which were detected during the field experiments conducted for this thesis.

The basic skeleton for all terpenes ($C_{5n}H_{8n}$) is formed by terpene enzymes or terpene synthases (TPS) from the precursors isopentenyl diphosphate (IDP; or alternatively isopentenyl pyrophosphate (IPP)) and dimethylallyl diphosphate (DMADP; or alternatively dimethylallyl pyrophosphate (DMAPP)). From both, IDP and DMADP, isoprene can already be formed. Monoterpenes are formed by the addition of geranyl diphosphate (GDP), sesquiterpenes are formed by the addition of farnesyl diphosphate (FDP), and diterpenes by geranyl geranyl diphosphate (GGDP) (see Fig. 2.1.5 for a detailed schematic) (Degenhardt et al., 2009; Loreto and Schnitzler, 2010; Li and Sharkey, 2013; Richter et al., 2016). So, different TPS are responsible for the formation of different terpenes. Since isoprene is the largest fraction of terpenes being emitted, isoprene synthases (ISPS) became one of the most studied TPS compared to mono-TPS and others. Both isoprenoid precursors are formed via two pathways which are spatially separated from each other: the methyl erythritol 4-phosphate (MEP) pathway which is located in the plastids involving seven enzymatic steps, and the mevalonic acid (MVA) pathway in the cytosol with six enzymatic reactions. The MVA pathway synthesizes sesquiterpenes as well as precursors of oxidative degradation for irregular terpenes (e.g. the irregular acyclic homoterpene (*E*)-4,8-dimethyl-1,3,7-nonatriene (DMNT)) (Dudareva et al., 2006). Within the MEP pathway, IDP and DMADP for isoprene and monoterpenes are synthesized as well as carotenoid derivatives with carbon skeletons ranging from C_8 to C_{18} (Dudareva et al., 2013; Loreto and Schnitzler, 2010; Richter et al., 2016).

Phenylpropanoid and benzenoid compounds originate from phenylalanine (Phe), an aromatic amino acid that is synthesized via seven enzymatic reactions of the shikimate pathway and additionally three of the arogenate pathway. The biosynthesis of Phe takes place in plastids whereas phenylpropanoids and benzenoid volatiles are converted afterwards in the cytosol (Dudareva et al., 2013). Benzenoids and their derivatives from the shkikmate pathway are e.g. benzyl acetate, indole, and methyl

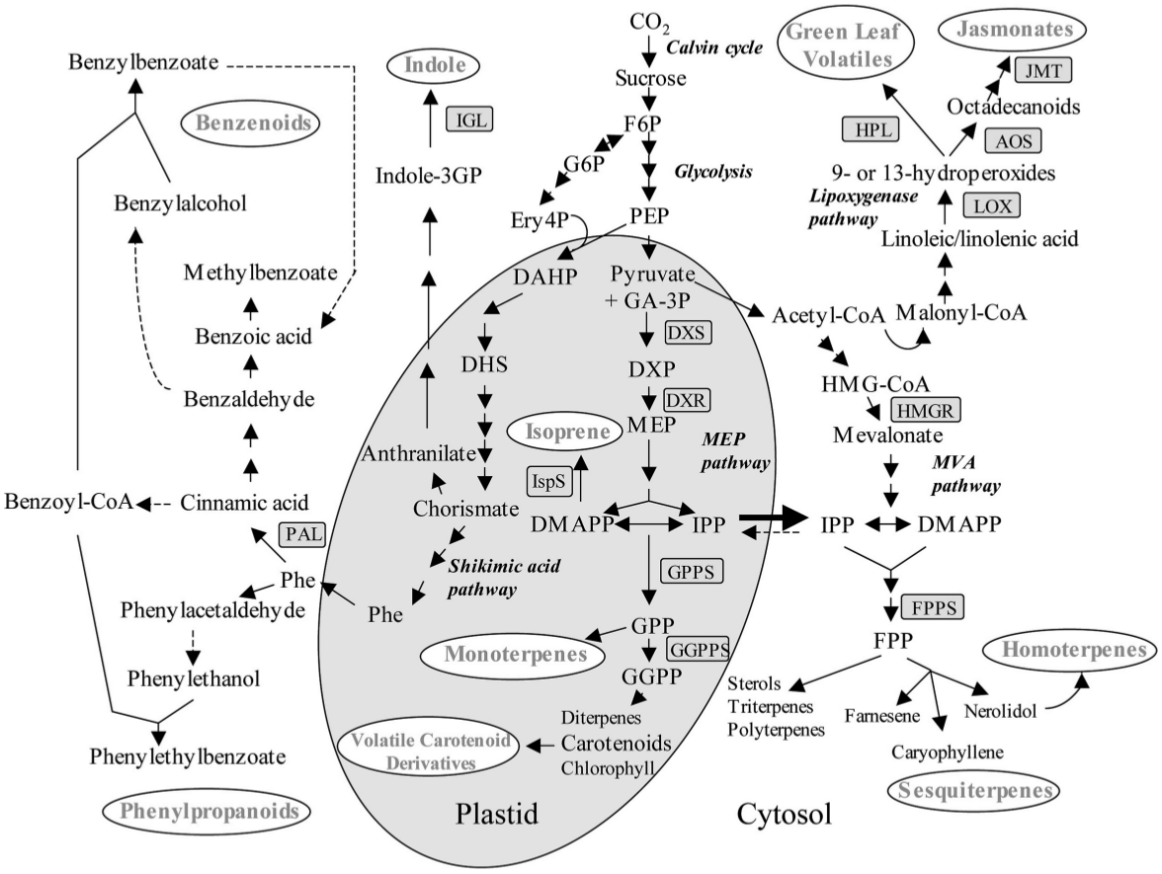

Figure 2.1.5.: Detailed schematic of different pathways for the biosynthesis of various BVOCs. The illustration shows metabolic pathways italicized, BVOCs in bold and enzymes are boxed. (Explanations of all abbreviations can be found in the caption of original illustration from Dudareva et al., 2006).

salicylate (Pańka et al., 2013; Ghirardo et al., 2016).

Fatty acid derivatives are formed by the lipoxygenases (LOX), which initiate the octadecanoid pathway from linolenic or linoleic acid—unsaturated fatty acids—as the substrate. Two specific ways of oxygenation from the unsaturated fatty acids form several intermediate products involving a multitude of enzymatic reactions to be finally converted to C_6 (13-hydroperoxy intermediates) and C_9 (9-hydroperoxy intermediates) volatiles such as n-hexanal, (Z)-3-hexenal, n-nonanal, (Z)-3-nonenal, and mehtyl jasmonate (C_{13}). Due to the formation by LOX, the C_6 and C_9 aldehydes and alcohols are commonly referred to as LOX products, or also green leaf volatiles (GLVs) due to their induced synthesis in the green plant organs after wounding which has a characteristic fresh hay (Loreto and Schnitzler, 2010; Dudareva et al., 2013).

Another group of plant volatiles are short-chained oxygenated compounds such as methanol, acetaldehyde, and ethanol. Methanol is synthesized by degradation and formation of cell wall pectins. Thus, in periods of relaxation and rigidification of cell walls, e.g. during the leaf growth, methanol emissions are enhanced. Similarly, ethanol emissions can be enhanced during periods of flooded root zone. Thereby, ethanol is formed in the roots, transported to the leaves, and can be further enzymatically oxidized to acetic acid and acetaldehyde (Niinemets, 2018).

Still, there are volatiles emitted whose metabolic origin is in debate (Loreto and Schnitzler, 2010). It should be also noted that some volatiles can be just intermediates of the described pathways above and that these BVOCs may be released from certain plant tissues because the chemical or mechanical resistances are reduced e.g. during specific growth stages of the plant growth (cf. methanol).

Driving forces of leaf *de novo* and pool emissions

Constitutive emission rates of BVOCs are generally determined by their synthesis rates, diffusivity, volatility, and solubility, that is, by internal as well as external factors (Peñuelas and Staudt, 2010). After being synthesized, it is assumed that there are two different ways of emission: Either they are released from leaves directly after biosynthesis, known as *de novo* emission, for example via the leaf stomata. Hence, the emission rate correlates with the biosynthetical production rate. Or as emissions from specific plant storage structures, known as pool emission, for example from resin ducts, glands, or trichomes. In this case the emission rate depends mainly on diffusion and evaporation (Niinemets et al., 2014). Generally, independent from the source of emission (pool or *de novo* emission, vegetative or reproductive plant tissue), a linear increase in temperature always leads to an exponential increase in a variety of terpenoids for many kind of woody and herbaceous species and in angiosperms as well as gymnosperms (Holopainen and Gershenzon, 2010). Thus, temperature is the most important driver for BVOC emissions.

If a plant species lacks specialized storage structures, BVOC release mainly depends on its *de novo* synthesis. However, it could be shown that many plant species have the ability to store small amounts of BVOC, particular those that are water soluble, even without the existence of specialized storage structures (Niinemets et al., 2004).

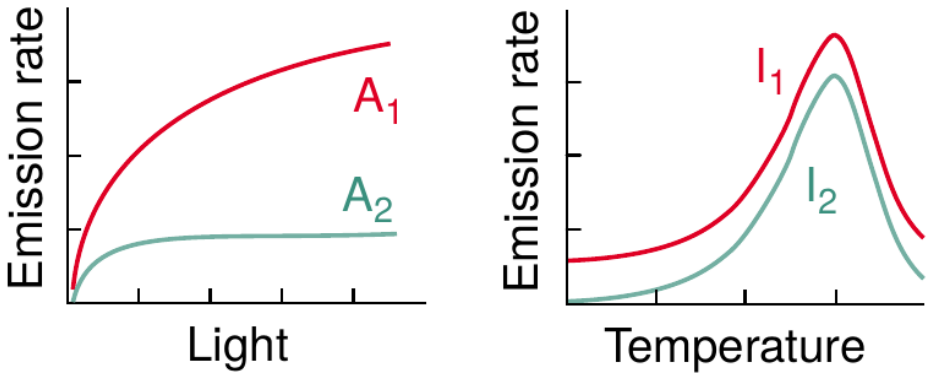

Figure 2.1.6.: Generalized dependence of plant volatile *de novo* emissions on photosynthetically active radiation (light) and temperature. The availability of substrate from photosynthesis for different secondary metabolic pathways for biosynthesis is mainly controlled by light with a higher substrate generation for A_1 than for A_2. The activity of synthases within the pathways are mainly controlled by temperature with a specific temperature optimum and higher synthase activity for I_1 than for I_2 (from Niinemets et al., 2004).

Generally, directly released BVOCs mainly depend on temperature and the absorbed spectrum of radiation (photosynthetically active radiation (PAR) or photosynthetic photon flux density (PPFD)) (see Fig. 2.1.6), similarly to photosynthesis, especially the Calvin cycle (Sharkey and Yeh, 2001). Emissions exponentially increase with increasing temperatures until an optimum temperature and then subsequently decrease. Leaf temperature optima, or actually the temperature optima of the biosynthesis apparatus, is higher than that of photosynthesis (25–30 °C for C_3 plants) with maximum emission rates from *de novo* emissions at temperatures of up to 40–45 °C on the short term, depending on the plant species. Increasing the light intensity leads to an asymptotically increase of the emission rates. It could be shown, that absorbed PAR controls the amount of available substrate (Niinemets, 2018; Li and Sharkey, 2013; Sharkey and Yeh, 2001; Dudareva et al., 2013).

As ambient CO_2 concentration affects photosynthesis, also the *de novo* emission is affected. It could be observed, that volatile emissions increase from CO_2 free air until the CO_2 compensation point of photosynthesis (carbon assimilation equals respiration) at around 50 ppm CO_2. A further increase in ambient CO_2 concentration leads to decreasing emissions, known as CO_2 inhibition. Though, CO_2 inhibition itself is temperature dependent with less inhibition at higher temperatures. Together with the aforementioned exponential emission increase with increasing temperature, BVOC emissions may still rise in a warmer climate despite the CO_2 suppression effect. The

interaction between temperature and ambient CO_2 concentration is a crucial aspect for simulating future BVOC emissions. Thus, it is also concerned in most model algorithms (Li and Sharkey, 2013; Guenther et al., 2012; Grote et al., 2014).

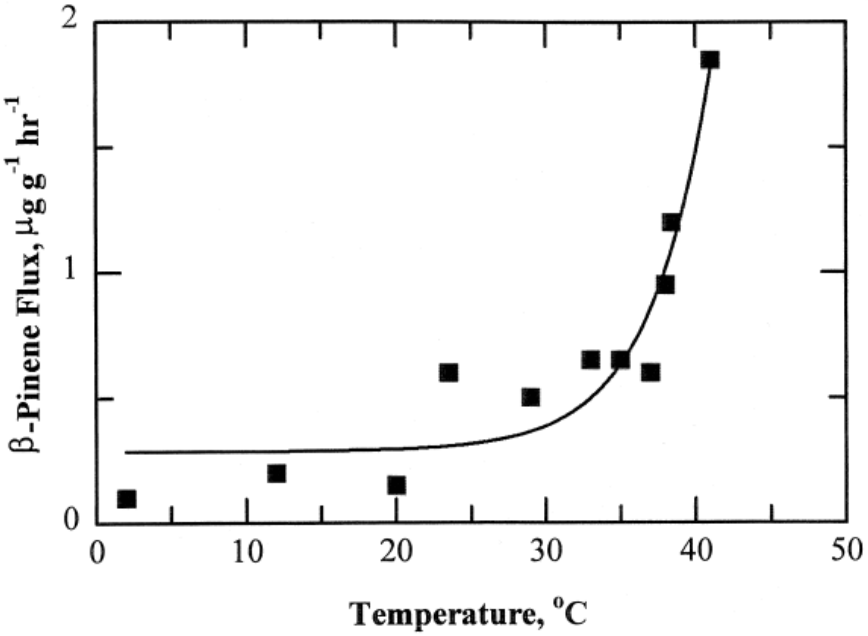

Figure 2.1.7.: An example of measured monoterpene emissions (β-pinene) together with a fitted exponential curve as a function of temperature illustrating the general temperature dependence of plant volatile pool emissions showing no temperature optimum (from Fuentes et al., 2000).

Whereas *de novo* emissions are controlled by plant physiology (synthase availability and activity limiting biosynthesis), pool emissions are only controlled physiochemically by volatility and diffusion. Additional partitioning of BVOCs between gas and liquid phase inside the plants follows the Henry's law constant (e.g. for isoprene $H = 7780$ Pa m^3 mol^{-1} and methanol $H = 0.46$ Pa m^3 mol^{-1} at 25 ℃), thus emissions very much depend on temperature. In addition, mechanical and chemical resistances between the source of emission inside the plants (e.g. resin ducts of conifers or glandular cells of broadleaved trees) and the atmosphere may change, e.g. due to damaging by herbivores, wind, precipitation or fire. The BVOC pools are filled over time periods of days to months and are therefore mostly uncoupled from BVOC biosynthesis. Some BVOCs can also be stored in the leaf mesophyll and thus depend on stomatal conductance as a major resistance term to diffusion. As shown in Fig. 2.1.7, in contrast to *de novo* emission, there is no temperature optimum for pool emissions (Niinemets

et al., 2004; Loreto and Schnitzler, 2010; Niinemets, 2018).

Ecosystem emissions other than from leaves

Besides plant volatile emissions from leaves, BVOCs can be also emitted from other plant tissues and the soil as well. Especially the reproductive plant tissues, i.e. flowers, can largely contribute to the plant's total terpenoid emissions (Köllner et al., 2004a; Wiß et al., 2017). Up to date 1,700 different floral volatiles have been detected that are synthesized via MEP, MVA, shikimate, and LOX pathways—similar to those of leaf volatiles as described before. Floral terpenoids consist mainly of monoterpenes ($\sim$ 53 %), sesquiterpenes ($\sim$ 28 %), and diterpenes ($\sim$ 1 %). The BVOC bouquet from flowers serves to attract of pollinators (mainly by benzenoids) and to defend against pathogens and florivores (again terpenoids and benzenoids all with molecular masses less than 300 g mol^{-1}) (Muhlemann et al., 2014; Knudsen et al., 2006). Thus, floral volatiles ensure the reproduction and evolutionary success of plants.

Additionally, the soil ecosystem with its multi trophic interaction can act as both, a BVOC source as well as a sink. Soil microbial decomposition provides the largest contribution to soil BVOC emissions. Thereby, dead plant organic matter serves as substrates for the microbial degradation. Resulting BVOCs typically are intermediates or final products synthesized in metabolic pathways of fermentation and respiration (aerobic and anaerobic). The activity and thus BVOC emission from microbes can rise during rain events when the microbial activity increases. Also plant roots (fine roots and total roots) can directly release BVOCs as intermediates or final products of their secondary metabolism. BVOC emissions from the soil can also origin from storages within the litter or from solutions in the soil. After rain events, VOCs dissolved in the water from soil pores can evaporate from these solutions, leading to typical emission bursts. However, soil ecosystems can also act as a sink mainly due to the consumption of BVOCs by microbes as a carbon source but also by adsorption of volatiles to surfaces of mineral soil particles (Peñuelas et al., 2014).

It should be noted that magnitude and composition of emissions from tissues other than leaves show a distinct seasonality which is related to the phenology of the plant as well as the availability of litter on the ground.

Induced biotic and abiotic emissions

It is already mentioned in Sect. 2.1.1 that BVOC emissions can be induced, in particular by stress. stress-induced volatiles (SIV) and more specifically herbivore-induced volatiles serve as a medium for plant-plant and plant-insect communication as well as to protect plants against oxidative stress. A demonstrative way of inducing emissions is to rub a leaf (especially from all kind of cuisine condiments) or a small flower between fingers. Thereby, the pools from ducts or glands are disrupted and, although the human olfactory system is extremely selective, BVOC bouquets from many plants can be experienced. As depicted in Fig. 2.1.8, induced emissions can be driven by biotic (pathogens, parasitic plants and herbivores) and abiotic stress factors (high temperatures, mechanical wounding, air pollution and oxidative stress) (Niinemets, 2010; Peñuelas and Staudt, 2010; Loreto and Schnitzler, 2010; Dicke and Loreto, 2010). Plants can be exposed to a variety of stress factors although studies about the impact of multiple stresses on plant volatiles are rare, but it is known that a multitude of stresses can have additive as well as counteractive effects on BVOC emissions (Holopainen and Gershenzon, 2010).

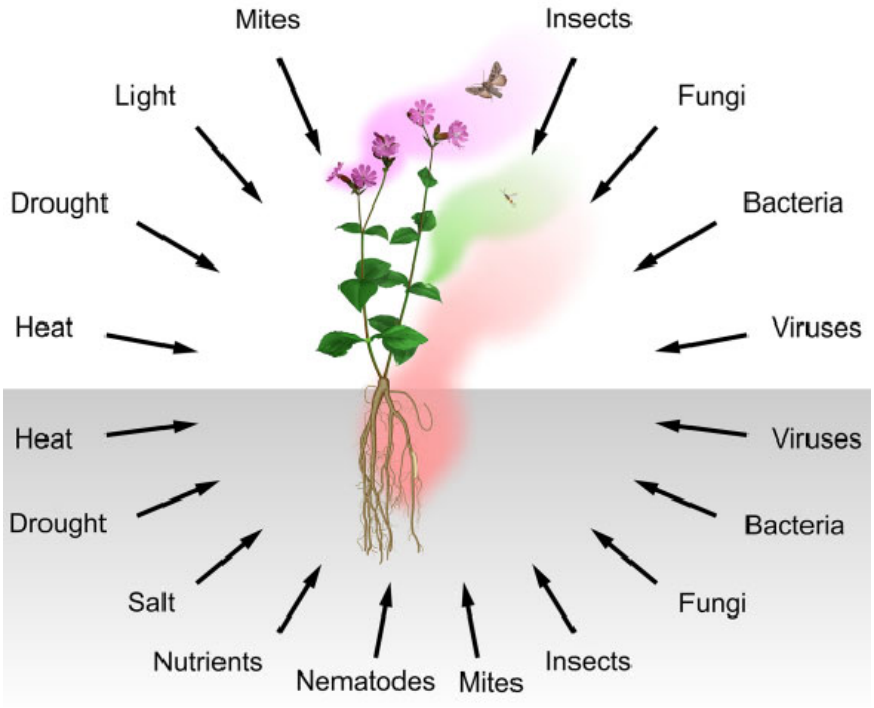

Figure 2.1.8.: Potential biotic and abiotic stressors leading to BVOC emissions from different plant tissues above and below ground (from Loreto et al., 2014).

Induced plant volatiles can be emitted from all plant species in contrast to constitutively emitted volatiles which are only synthesized by specific species. In case plants emit both kinds of BVOCs, the composition of induced emissions is typically different from constitutive ones. Additionally, different stressors can also induce different BVOC compositions. Current findings about induced emission diversity is still very limited (Niinemets, 2018). However, as an introduction into the topic, some examples about stress induced compounds are given in the following. At the occurrence of one or more stresses, induced BVOC emissions will immediately rise until a maximum is reached. When the stress magnitude decreases, also the induced emissions will gradually decrease until a constitutively level is reached.

In many cases, the first rapid increase of stress induced BVOCs is from short-chained alcohols and aldehydes such as GLVs and methanol. Emissions either increase when internal or external secretory pool structures are ruptured or, when synthesis is triggered, typically when membranes are damaged (e.g. by herbivore attacks and exposure to severe heat, frost, and oxidative stress). For GLVs, the most important production pathway is the LOX pathway which are formed from membrane lipids within seconds (Pichersky and Gershenzon, 2002; Niinemets, 2010, 2018). These compounds have antibiotic properties, which is why induced emissions can combat the invasion of damaged plant tissues. They are also typical compounds for plant-plant communication especially for inducing or priming emissions of unaffected plants (Loreto and Schnitzler, 2010). Increased methanol emissions can be also induced due to increased pectin methylesterases which catalyzes methanol formation (Loreto and Schnitzler, 2010; Kegge and Pierik, 2010; Niinemets, 2018).

Furthermore terpenoids (esp. isoprene, monoterpenes, and sesquiterpenes) as well as benzenoids can also be stress induced (Niinemets, 2010). The synthesis and emissions of these compounds are starting or increasing few moments after stress occurrence. This time lag of emission increase can be explained by the time consuming gene expression and protein synthesis to activate terpene synthases (Pichersky and Gershenzon, 2002; Niinemets, 2018). Typical herbivory induced terpenoids are monoterpenes (e.g., β-phellandrene, α-pinene, p-cymene, (+)-2-carene), sesquiterpenes (e.g., β-caryophyllene) and benzenoids (e.g., methyl salicylate), which have defense and toxic properties (Dudareva et al., 2013; Misztal et al., 2015). Increased emissions, e.g. of benzenoids, are induced by the activiation of secondary metabolic routes leading to enhanced concentrations of chorismate and isochorismate which are final products

of the shikimate pathway (Misztal et al., 2015).

Moderate drought stress induces terpenoid emissions, especially isoprene, despite the fact that photosynthesis and stomatal conductance is reduced directly which decrease carbon supply to the MEP pathway. Thus, alternative carbon sources such as those from respiration or starch breakdown can be used to induce high emissions (Loreto and Schnitzler, 2010). Reduced stomatal opening does not affect the diffusion rates of terpenoids due to their high Henry's law constant. Additionally, rewatering of heat stressed plants can result in emission bursts due to the recovery of the carbon source from photosynthesis (Loreto and Schnitzler, 2010). However, it has been observed that heavy drought stress results in decreasing terpenoid emissions due to the altered carbon supply. In the case that the drought stress level damages membranes and cell walls, strong emission bursts of GLVs were observed after the damage occurred (Loreto and Schnitzler, 2010). Under non-stressed conditions, the carbon loss from plants due to constitutive BVOC emissions is relatively small (around 1 % relative to net ecosystem CO_2 exchange (NEE) e.g. in poplar trees (Portillo-Estrada et al., 2015) or below 1 % in crops e.g. maize (Wiß et al., 2017)). However, during stress periods with reduced photosynthesis activity (especially abiotic stresses), the carbon investment in BVOC bursts can lead to a substantial carbon loss especially in relation to gross primary productivity (Loreto et al., 2014; Dicke and Loreto, 2010).

As already mentioned in Sect. 2.1.1, high reaction rates of O_3 and ROS with terpenoids serve as a protection against oxidative stress. It has been found that high O_3 concetrations, hence strong oxidative stress, induce isoprene and monoterpene emissions whereas moderate oxidative stress tend to decrease emissions (Loreto and Schnitzler, 2010). Strong oxidative stress leads to a higher expression of isoprene synthase gene mRNA with a probable increased activity of the enzyme and the protein level, whereas moderate stress levels may act vice versa. Oxidative stress can be usually recognized first by the denaturation of lipids in the cell membrane. Thus, similar to drought stress, emission bursts of GLVs as well as increases of methanol can occur (Loreto and Schnitzler, 2010).

Generally, most BVOCs, regardless if emitted constitutively or as induced emissions, fulfill specific functions for their emitter plants. An example is the sesquiterpene β-caryophyllene. It can serve as an antimicrobial agent, reducing bacterial growth when emitted from the flowers or act as an indirect below ground defense by attract-

ing root pest killing parasitic wasps and entomopathogenic nematodes, when emitted from the roots (Dudareva et al., 2013). However, emitted BVOCs do not only have positive effects for their emitting plants, but they can also affect the air chemistry.

2.2. BVOCs in the troposphere

After an introduction into the benefits for plants to emit BVOCs, this section introduces the major atmospheric impacts caused by these compounds. Generally, emissions of BVOCs, are a direct input of highly reactive compounds into the planetary boundary layer and subsequently into the whole troposphere. They potentially alter ambient air oxidative status, atmospheric particle condensation, and cloud cover (Niinemets, 2018). After being emitted, molecules react with other atmospheric trace gases, start to fragment, condensate and deposit on particles and surfaces, and split until being finally oxidized to CO_2 (Peñuelas and Staudt, 2010). In the end, all potential mechanisms lead to impacts on air quality and climate.

There are two important chemical steps: first, the primary reactions (loss processes or degradation of BVOCs) especially with OH, O_3, NO_3, and Cl atoms (but mainly in marine and coastal areas, which is why Cl reactions will be neglected in the following); and secondly, subsequent reaction steps, their products, and intermediate products which potentially lead to the formation of SOA and O_3 (Atkinson, 2000; Heald et al., 2008; Hallquist et al., 2009; Ziemann and Atkinson, 2012). The physical loss processes of dry and wet deposition play a minor role (Fuentes et al., 2000). But before looking deeper into air chemistry reaction processes, the presence of O_3, OH, and NO_3 should be briefly explained.

2.2.1. The role of ozone, hydroxyl radical, and nitrate radical

Ozone (O_3)

Two processes lead to the presence of the toxic GHG O_3 in the troposphere: Firstly, it is formed by ultraviolet (UV) radiation and O_2 as a substrate in the stratosphere, where it is known as the ozone layer protecting life on earth from highly energetic UV radiation by absorption. The turbulent process of eddy diffusion transports O_3

from the stratosphere into the troposphere (Atkinson and Arey, 2003). Secondly, it is formed photochemically by the interaction of nitric oxides (NO_x; the sum of NO and NO_2) and VOCs which will be further explained below. Both tropospheric source processes are balanced by in situ photolysis, dry deposition on various surface types, and reactions with BVOCs leading to ambient concentrations of 10–40 ppb at remote sites (Fuentes et al., 2000; Atkinson and Arey, 2003).

Hydroxyl radical (OH)

The hydroxyl radical (OH) is the most important oxidant of the troposphere, i.e. it reduces the level of oxidative compounds in the atmosphere. It is formed by the photolysis ($+h\nu$) of tropospheric O_3 and the subsequent reaction of the O atom (more precisely the singlet oxygen atom which is the first excited state of the oxygen atom, $O(^1D)$) with water vapor, which can be described in a simplified form as:

$$O_3 + h\nu \longrightarrow O_2 + O(^1D) \tag{2.1a}$$

$$O(^1D) + H_2O \longrightarrow 2\,OH \tag{2.1b}$$

Due to its strong dependence on radiation ($h\nu$), OH concentrations vary during the diurnal cycle with peak ambient concentrations during periods of highest radiation. Another significant source of OH can be the reaction of O_3 and BVOCs, especially alkenes (e.g., isoprene and monoterpenes). Minor formation of OH can also occur from the photolysis of nitrous acid (HNO_2). An annual global mean of 24 hour averaged OH concentrations is estimated as 1.0×10^6 molecule cm^{-3} (Atkinson and Arey, 2003; Fuentes et al., 2000).

Nitrate radical (NO_3)

The formation of NO_3 in the troposphere depends on the presence of NO_x. NO is emitted to a large part from fossil fuel combustion processes, but also from agricultural as well as natural soils and natural fires. Additionally, it can be formed in-situ by lightnings (Ciais et al., 2013). Following the reactions 2.2, NO is subsequently oxidized

with O_3 to NO_2, which can be further oxidized to NO_3.

$$NO + O_3 \longrightarrow NO_2 + O_2 \tag{2.2a}$$

$$NO_2 + O_3 \longrightarrow NO_3 + O_2 \tag{2.2b}$$

Generally, fast photolysis rates of NO_3 lead to short lifetimes of ~ 5 s during noon, which can be chemically described by

$$NO_3 + h\nu \longrightarrow NO + O_2 \tag{2.3a}$$

$$NO_3 + h\nu \longrightarrow NO_2 + O(^3P) \tag{2.3b}$$

where $O(^3P)$ is the ground-state of oxygen atom. In the nighttime NO_3 concentrations can range up to 1×10^{10} molecule cm^{-3} with a 12-hour nighttime average concentration of 5×10^8 molecule cm^{-3} (Atkinson, 2000; Atkinson and Arey, 2003; Fuentes et al., 2000).

2.2.2. Implications on air quality

Degradation of BVOCs by O_3, OH, and NO_3

The reactions of different BVOCs with O_3, OH (mainly daytime), and NO_3 (mainly during evening and nighttime) (Peeters et al., 2007; Ziemann and Atkinson, 2012) show a large variability, due to the compound specific chemical and structural properties (see Tab. 2.1) (Fuentes et al., 2000; Atkinson and Arey, 2003). For this reason, also the impact on atmospheric chemistry varies for all BVOCs. The degradation is most often measured and expressed as reaction rates or rate constants (k-rates) in units of cm^3 molecule^{-1} s^{-1}. These k-rates can be used to calculate tropospheric lifetimes (time for decay of the specific compound to $1/e$ of its initial concentration) under specific temperature and assumed constant concentrations of the reaction gases. Thus, as concentrations can vary strongly and those of OH and NO_3 exhibit strong diurnal cycles, the lifetimes in table 2.1 serve as an estimate under very specific atmospheric conditions (Fuentes et al., 2000; Atkinson and Arey, 2003). However, it illustrates the large lifetime differences between the compounds very well. Generally, terpenes have shorter atmospheric lifetimes (minutes to hours) and thus, have a stronger impact on atmospheric chemistry than most of the OVOCs (lifetimes of hours

Table 2.1.: Exemplary atmospheric lifetimes of selected BVOCs depending on reactions with OH, O_3, and NO_3. Assumptions for the lifetime calculations are ambient concentrations of 2.0×10^6 molecules cm^{-3} of OH for 12-h daytime average, 7×10^{11} molecules cm^{-3} of O_3 for 24-h average, and 2.5×10^8 molecules cm^{-3} of NO_3 for 12-h nighttime average. All values taken from Atkinson and Arey (2003).

Biogenic volatile organic compound	Lifetime for reactions with OH	O_3	NO_3
Isoprene	1.4 h	1.3 day	1.6 h
(oxygenated) Monoterpenes			
Camphene	2.6 h	18 day	1.7 h
Limonene	49 min	2.0 h	5 min
Myrcene	39 min	50 min	6 min
cis-/trans-Ocimene	33 min	44 min	3 min
α-Pinene	2.6 h	4.6 h	11 min
β-Pinene	1.8 h	1.1 day	27 min
α-Terpinene	23 min	1 min	0.5 min
1,8-Cineole	1.0 day	> 110 day	1.5 year
Linalool	52 min	55 min	6 min
Camphor	2.5 day	> 235 day	> 300 day
Sesquiterpenes			
β-Caryophyllene	42 min	2 min	3 min
α-Humulene	28 min	2 min	2 min
Longifolene	2.9 h	> 33 day	1.6 h
other VOCs			
Acetone	61 day	> 4.5 year	> 8 year
cis-3-Hexen-1-ol	1.3 h	6.2 h	4.1 h
cis-3-Hexenyl acetate	1.8 h	7.3 h	4.5 h
Methanol	12 day	> 4.5 year	2.0 year

to days). For the primary reactions of BVOCs there are generally two mechanisms:

1. the addition to C=C bonds by all three gases which is the dominant mechanism, and
2. the H-atom abstraction from C−H bonds by OH and NO_3 radicals.

There are a multitude of products which are formed from these reactions, which is why these products are also called first generation BVOC products. Similar important are intermediate products of these primary reactions, such as hydroperoxyl radical HO_2,

alkyl radicals (R), alkoxy radicals (RO), and alkyl peroxy radicals (RO_2) (Atkinson, 2000; Atkinson and Arey, 2003; Fuentes et al., 2000; Ziemann and Atkinson, 2012; Calfapietra et al., 2013a). As these intermediate products are formed also from AVOCs, especially in urban areas, this group will not be excluded in the following paragraph, which is why the abbreviation VOC is used.

Formation of O_3 from VOCs

Besides the turbulent transport of toxic O_3 from the stratosphere into the troposphere, O_3 is also formed directly in the troposphere by two mechanisms involving VOC–NO_x–O_3–HO_x reactions First, under conditions of low VOC concentration O_3 production is dominated by the photolysis of NO_2 via:

$$NO_2 + h\nu \longrightarrow NO + O(^3P) \tag{2.4a}$$

$$O(^3P) + O_2 + \text{air} \longrightarrow O_3 + \text{air} \tag{2.4b}$$

However, as O_3 again reacts rapidly with NO (see reaction 2.2), these reactions neither lead to a formation nor loss of O_3, rather to a specific photoequilibrium between NO, NO_2 and O_3 (Atkinson, 2000). Secondly, under higher VOC concentration conditions, the intermediate products from VOC degradation processes, especially the hydroperoxyl (HO_2) and RO_2 radicals lead to a net formation of NO_2, following:

$$HO_2 + NO \longrightarrow OH + NO_2 \tag{2.5a}$$

$$RO_2 + NO \longrightarrow RO + NO_2 \tag{2.5b}$$

The additionally formed NO_2 in turn photolyzes to subsequently form O_3 (see reaction 2.4) resulting in a net formation of O_3. Generally, the most significant tropospheric O_3 production is the photolysis of NO_2 (Atkinson, 2000; Atkinson and Arey, 2003). Both processes, the photoequilibrium between NO, NO_2, and O_3, and the net O_3 formation are illustrated in Fig. 2.2.1. Under low NO concentration conditions, reactions of O_3 with OH and HO_2 are predominant, leading to a net loss of O_3 by production of O_2

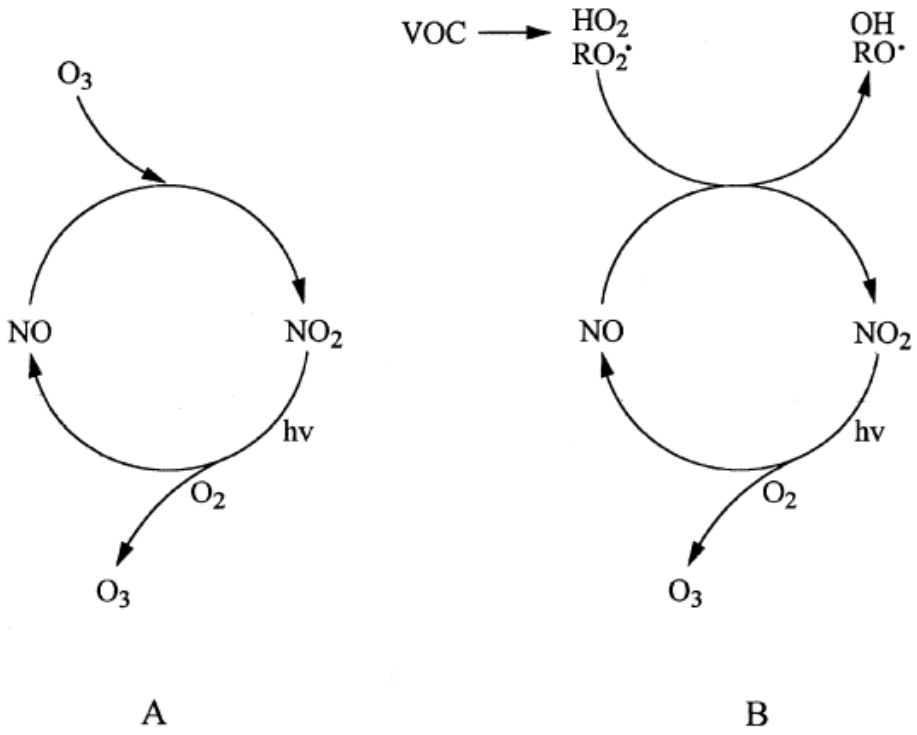

Figure 2.2.1.: Schematics of tropospheric O_3 formation. A: Photoequilibrium between NO, NO_2, and O_3 in the absence of VOCs. B: Net O_3 formation due to VOCs and subsequently formed intermediate products that additionally produce NO_2 from NO (from Atkinson, 2000).

(see reaction 2.6).

$$HO_2 + O_3 \longrightarrow OH + 2\,O_2 \tag{2.6a}$$

$$OH + O_3 \longrightarrow HO_2 + O_2 \tag{2.6b}$$

Thus, the net O_3 concentration increase or decrease under constant sunlight conditions depends on the availability of NO and is determined by the reaction rates of NO_2 production (HO_2 and NO, RO_2 and NO) versus the reaction rates of O_3 depletion (e.g., HO_2 and O_3) (Atkinson, 2000). Based on the reaction rate constants and typical radical concentrations, net photochemical O_3 formation is favored at NO mixing ratios larger than around 20^{-12}, whereas net photochemical O_3 loss is favored below that value (Atkinson, 2000). As concentrations of the most important radicals depend on VOCs and their degradation processes, the amount of O_3 concentration increase also depends on the VOC–NO_x ratio. Additionally, this ratio is determined by each

specific VOC due to different reaction rates as shown above. Nevertheless, three different mixing conditions for O_3 formation ratios can be distinguished (Calfapietra et al., 2013a):

1. a VOC limited ratio of VOC:NO_x < 4;
2. an optimum O_3 production ratio of VOC:NO_x between 4 to 15; and
3. a NO_x limited ratio of VOC:NO_x > 15.

Formation of SOA from BVOCs

BVOCs play an important role in the formation of SOA (Bonn and Moortgat, 2003; Heald et al., 2008; Hallquist et al., 2009; Li et al., 2011; Makkonen et al., 2012; Mentel et al., 2013). SOA are liquid or solid particles suspended in the air which perturb the radiative transfer by absorbing and scattering solar as well as terrestrial radiation. Additionally, SOA facilitates the growth of particles, thus acting as cloud condensation nuclei, and participate in heterogeneous atmospheric chemical reactions (Carslaw et al., 2010). They also cause negative impacts on human health by leading to all-cause, lung cancer, and cardiopulmonary mortality (Pope III et al., 2002).

Generally, SOA are formed by oxidation from gaseous precursors after being released or emitted from any kind of anthropogenic or natural source. In contrast, primary organic aerosols, also called primary biological aerosol particles, are emitted directly. Sources from terrestrial ecosystems are e.g. biomass burning, volcanic eruptions and wind-driven suspension of soil, mineral dust, sea salt and biological materials like viruses, bacteria, fungal spores, pollen, plant debris and algae. Like SOA, primary biological aerosol particles can also act as cloud condensation nuclei and ice nuclei, thus altering cloud properties and regional precipitation pattern and intensities (Hallquist et al., 2009; Carslaw et al., 2010). Especially BVOCs and AVOCs contribute to the formation of SOA. While first generation products (from reactions with O_3, OH, and NO_3) are still volatile, it is the second or later generation products with lower vapor pressures and higher water solubility that convert more easily into the particle phase. Thereby processes such as nucleation, condensation of vapors and heterogeneous and multiphase chemical reactions are the main drivers for changes in particle numbers and particle mass (Atkinson and Arey, 2003; Hallquist et al., 2009). Figure 2.2.2 illustrates an example of SOA formation from isoprene oxidation

pathways. The presented mechanism is highly simplified and focuses on OH initiated oxidation of isoprene, thereby neglecting a large amount of other BVOCs as well as other reaction pathways initiated by O_3, NO_3, and Cl.

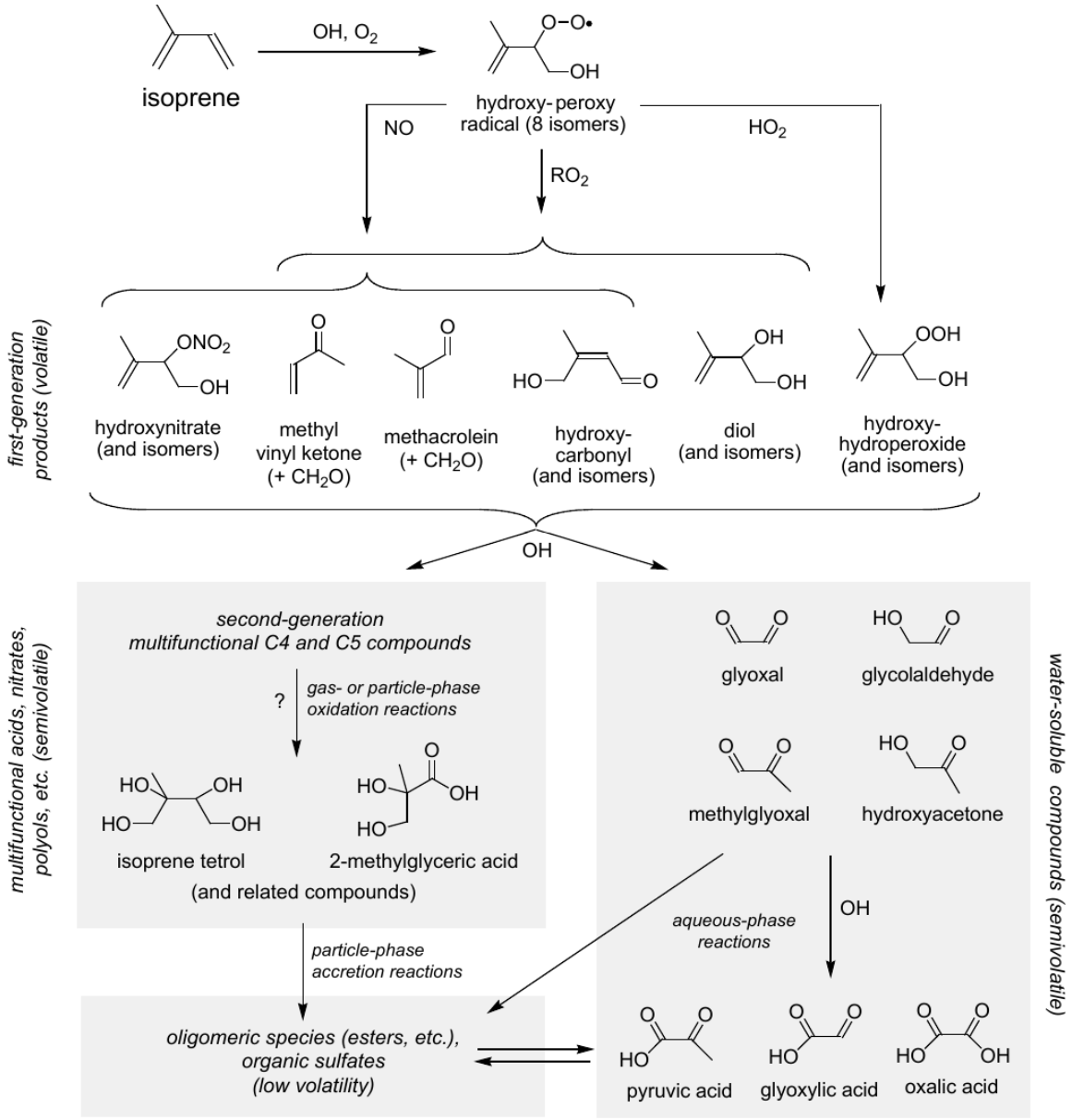

Figure 2.2.2.: Schematic of potential oxidation pathways of isoprene with OH leading to the formation of SOA (from Carlton et al., 2009).

12 to 50 % of SOA mass and 50 % of cloud condensation nuclei might origin from forest sources (Carslaw et al., 2010). Furthermore it as been estimated that even up to 90 % of the total SOA concentration in many continental European regions during

the summer months originate from organic sources (Hallquist et al., 2009).

2.2.3. Implications on climate

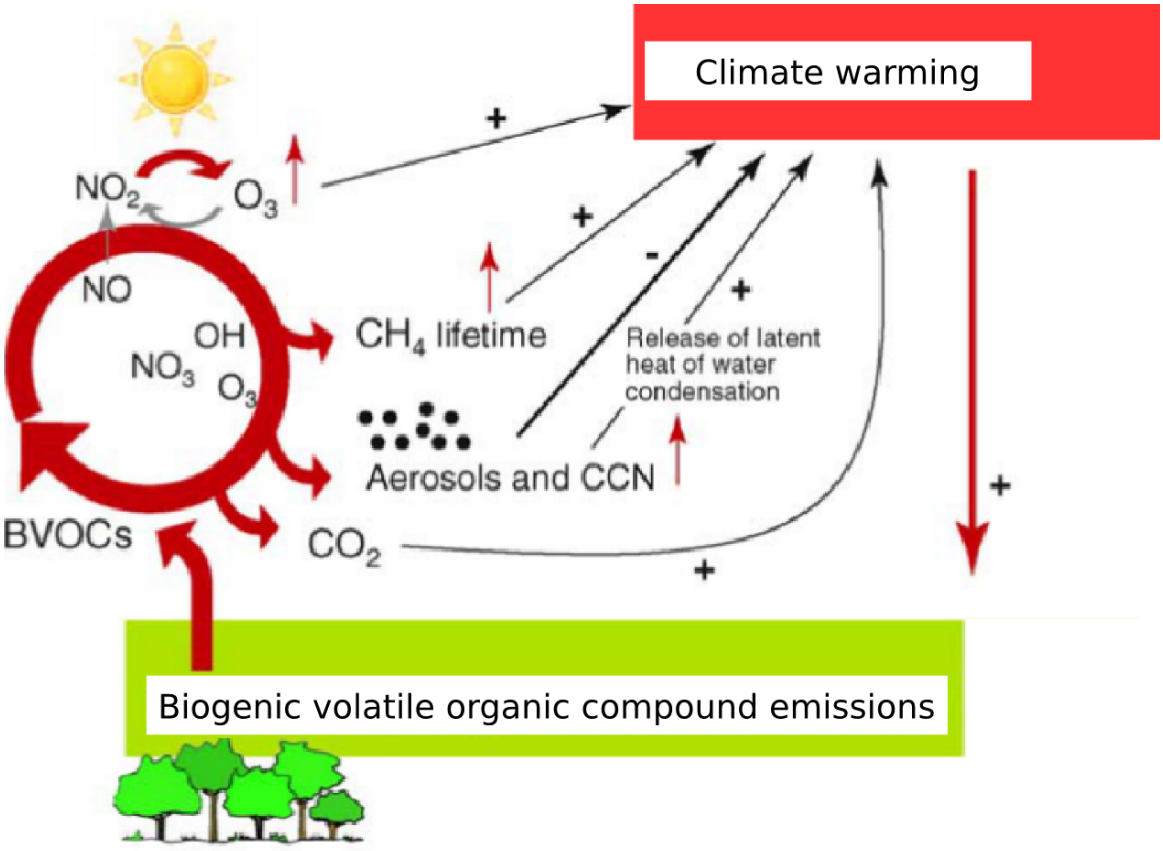

Figure 2.2.3.: Impact of BVOC emissions on atmospheric chemistry and climate by formation of O_3, prolonging CH_4 lifetime, formation of aerosols and cloud condensation nuclei (CCN), and CO_2 production (adapted from Peñuelas and Staudt, 2010).

Emitted BVOCs undergo various reactions thereby also affecting local to global climate by altering the radiative transfer (see Fig. 2.2.3). This can either have a net warming or cooling effect. A net warming results from direct and indirect impacts on GHGs via the aforementioned formation of the GHG O_3, the decrease of OH concentration and thereby increasing CH_4 lifetime (20-year global warming potential of 84), and the final oxidation of all VOCs to CO_2 (Atkinson and Arey, 2003). Thus, these direct and indirect impacts lead to a global radiative forcing of 0.10 ± 0.04 W m^{-2} (Myhre et al., 2013). Net cooling results from the aforementioned formation

of SOA and its effect on radiation absorption and scattering by the aerosol itself (aerosol–radiation interaction) as well as potential cloud formation (aerosol–cloud interaction). These SOA interactions are estimated to have a global radiative forcing of −0.03 (−0.27 to +0.20) W m^{-2} compared to pre-industrial times (Myhre et al., 2013). Until 2100, the global aerosol burden might increase by 25 to 150 % which would cause an impact of −0.04 to −0.24 W m^{-2} compared to current conditions. On the local scale, recent radiative perturbation can rise up to −14 W m^{-2}, with future values in the range of several W m^{-2} due to very strong local aerosol sources such as forests (Carslaw et al., 2010).

2.3. BVOC measurements

To assess the impact on air quality and climate, observations are required to quantify BVOC emission rates from natural vegetation, which is the first major part of this thesis. Similar to other atmospheric trace gas measurements, there are several different measurement techniques, especially the setup and the instrumentation, which are briefly summarized in the following. It should be noted that not the flux directly but only the molar mixing ratio of trace gases can be measured. Based on the temporal development of concentrations, however, the flux can be derived.

2.3.1. Chamber and micrometeorological measurement system

First, concerning the setup, one has to differentiate between a chamber or enclosed approach and a micrometeorological approach.

Chamber system

Chamber measurements can enclose small volumes as e.g. individual foliage elements with controlled environmental conditions (cf. Graus et al., 2013) medium volumes that cover branches or tree seedlings (cf. Müller et al., 2002; Mozaffar et al., 2017), as well as to larger volumes enclosing whole plants (cf. Wiß et al., 2017; Fuentes et al., 2000). This approach can be used under field as well as laboratory conditions. The enclosing covers can be bags, cuvettes, or chambers which should consist of impermeable and

inert material with a very low friction coefficient and specific absorbent and adsorbent characteristics (e.g. polytetrafluoroethylene (PTFE or Teflon), perfluoroalkoxy Teflon (PFA), polyether ether ketone (PEEK) (cf. Pagonis et al., 2017; Deming et al., 2019)), to prevent BVOC reactions or deposition at the chamber's surface.

Generally, chamber measurement techniques can be divided into flow-through (also called dynamic or open) and non-flow-through (also called static or closed) systems. In a flow-through system, gas is continuously flowing in and out of the chamber system, whereas in a non-flow-through system gas is only transported out of the system. While the flow-through system can be additionally divided into a steady state as well as non-steady state chamber condition, the non-flow-through system can only be used under non-steady state conditions (Livingston and Hutchinson, 1995).

Steady state systems are characterized by target trace gas mixing ratios which need to be constantly at equilibrium. Ideally, the characteristics of the entering carrier gas are chosen in a way that the enclosed sample air is marginally perturbed and the molecular diffusion of trace gases between the sample and air the chamber gas matrix is similar to ambient conditions. Emission rates (positive gas flux) are calculated by measuring trace gas mixing ratios of the constantly inflowing and outflowing gas, exactly knowing flow rate, enclosure volume, and size if the emitting sample the emission rate should be scaled to, e.g. the leaf area index or biomass in the case of vegetation (Livingston and Hutchinson, 1995; Fuentes et al., 2000; Peñuelas et al., 2014). In contrast, trace gas concentrations of the gas matrix in non-steady state systems are continually changing in accordance to the sample emission rate which affects the diffusion rate. Therefore, the chamber volume, the closing period as well as the ratio of outgoing flux and chamber volume should be carefully chosen (e.g., high volume to flux ratio) to minimize these potential negative feedbacks. However, when diffusion rate impacts become negligible and concentration changes remain constant, the measurement effort (concentration of the outflowing gas) for non-steady state systems is relatively low compared to steady state systems where the flow rate and the concentration of the ingoing and outgoing gas matrix need to be measured continuously (Livingston and Hutchinson, 1995; Hoffmann et al., 2015; Peñuelas et al., 2014).

Micrometeorological system

When measuring trace gas fluxes from larger spatial scales, such as field to canopy scale, micrometeorological systems can be applied. Examples are the gradient diffusion approach, the modified Bowen ratio method, the relaxed eddy accumulation technique, and the eddy covariance approach. For simplicity, only the two most important techniques, gradient diffusion and eddy covariance (Peñuelas et al., 2014), are briefly described herein. The gradient diffusion approach is based on two concentration measurements at different vertical levels above an emitter source. The gradient between both measurement is multiplied by the atmospheric eddy diffusivity of each specific BVOC which is obtained by additional measurements (especially the momentum flux) and applying Monin Obukhov similarity theory (MOST) (Fuentes et al., 2000). Another technique, the eddy covariance (EC) approach, assumes that a substantial part of the trace gas flux is carried by small eddies. To be able to detect these fluxes, the vertical wind velocity and the trace gas concentrations need to be measured at high frequencies ($\sim$ 10 Hz) at the same time (Karl et al., 2002). Therefor, the turbulent flux terms are calculated by Reynolds decomposition and averaging of the Navier Stokes equations which are used in a second step to calculate the trace gas flux based on the covariance between fluctuations of the vertical wind velocity and the trace gas concentration (Fuentes et al., 2000; Karl et al., 2002). However, the concentration measurements need to be in the same time interval which is currently not feasible with state-of-the art BVOC instruments. Thus, most studies make use of the virtual disjunct eddy covariance (vDEC) method (cf. Bachy et al., 2016; Brilli et al., 2012; Copeland et al., 2012; Hörtnagl et al., 2014; Seco et al., 2015) which is based on the EC method but without the need of exactly the same time series of the covariant elements. While vertical wind is still measured at 10 Hz, it is possible to operate a BVOC sensor at only 1 Hz storing a disjunct time series. The coinciding measurements are found by temporally shifting and synchronizing both time series performing a correlation analysis (Karl et al., 2002). However, still, foot print analyses of the emission source as well as extensive statistical post processing compared to any kind of chamber system needs to be performed and integration times of the BVOC sensor are still short which decreases the instrument's precision.

Apart from the described in-situ measuring approaches, also remote sensing approaches from the ground or with air- and space-borne sensors are used to detect

BVOC which are used particularly at large spatial scales (regional to global). For example, columns of formaldehyde can be detected (e.g. measurements by the satellite based Ozone Monitoring Instrument (OMI) or by Differential Optical Absorption Spectrometry (DOAS) from ground) and used to retrieve isoprene concentrations by inverse analysis (Schultz et al., 2015; Kaiser et al., 2018). Also, isoprene emissions can be retrieved from photochemical reflectance index from Moderate Resolution Imaging Spectroradiometer (MODIS) sensor (Filella et al., 2018; Peñuelas et al., 2013).

2.3.2. Online and offline data sampling

When using chamber or micrometeorological measurement systems it can be distinguished between online and offline data sampling methods. Online data sampling describes fast on-site analysis of a gas matrix directly after drawing the gas sample. Thereby, the analysis instrument needs to be directly connected to the measurement system, which can be cumbersome especially for remote field studies as most of the sample analyzers are fragile and heavy and thus difficult to transport. Examples of online gas sample analyzers are a PTR-MS and online gas chromatography–mass spectrometry (GC-MS) instruments (Peñuelas et al., 2014; Hakola et al., 2017). In contrast, offline data sampling means that a gas matrix sample is pumped through an adsorbent material and stored in inert cartridges (e.g. glass tubes). The gas sample can then be preserved in an cooled environment for a longer time (days to months). The solid adsorbent material can consist of poly(2, 6-diphenylphenylene oxide) known as TENAX-TA, polydimethylsiloxane (PDMS) foam, or graphitized carbon black (GCB) material (e.g. Carbopack-B/X) (Ghirardo et al., 2016; Hakola et al., 2017). The material prevents further chemical degradation or reactions during the time of storage. Analysis is usually performed by GC-MS or gas chromatography–flame ionization detection (GC-FID) after being thermally (at high temperatures) or chemically (e.g. using disulphide–methanol) desorbed (Fuentes et al., 2000; Peñuelas et al., 2014; Schultz et al., 2015). The main advantage of offline data sampling is that no gas analyzer needs to be transported to the sample site, which enables e.g. sampling with unmanned aerial vehicles (UAV) (cf. McKinney et al., 2019). The main disadvantage is the low sampling frequency as the adsorbent material is normally flushed for several minutes up to few hours which only provides one data point.

2.3.3. Proton transfer reaction–mass spectrometry (PTR-MS)

As already mentioned above, PTR-MS and GC-MS are the most widely used analysis instruments to detect BVOC concentrations. Especially the PTR-MS has been proven as a valuable tool in numerous atmospheric measurement campaigns within all different kind of setups and environments including aircraft-, ship- and vehicle-based experiments (see Yuan et al. (2017a) for a comprehensive review and list of literature). Also in this study a PTR-MS is used during the field experiments which is why a short introduction into the instrument is given in the following.

A PTR-MS is used for online real-time detection of VOCs with relatively high sensitivity and low detection limits (Lindinger et al., 1998; Hansel et al., 1999). This soft chemical ionization technique, which is characterized by low fragmentation rates, uses a reagent ion, e.g. hydronium (H_3O^+), to interact with a BVOC molecule. Alternatively, NO^+ and ${O_2}^+$ or Kr^+ and Xe^+ can be used (IONICON, 2013). Figure 2.3.1 shows the schematic of a PTR-MS built by Ionicon Analytik, Innsbruck, Austria. The reagent ion H_3O^+, which is produced by protonation of water vapor, is generated in the ion source. The ion source is followed by the drift tube or reaction chamber with a very low pressure ($\sim$ 2–4 mbar) where VOC molecules within the gas sample get chemically ionized by proton transfer following the simplified reaction

$$H_3O^+ + R \longrightarrow RH^+ + H_2O \tag{2.7}$$

Only those trace gas molecules (R) with a higher proton affinity than water (691 kJ mol^{-1}) will get protonated (RH^+), thus most common fractions of ambient air (N_2, O_2, Ar, CO_2) remain unchanged (IONICON, 2013, 2011; Yuan et al., 2017a). Most VOCs have a higher proton affinity than water except for formaldehyde whose proton affinity (713 kJ mol^{-1}) is similar to that of water. This is the reason why PTR-MS detection sensitivity of formaldehyde is relatively low and strongly depends on air humidity because it affects the protonation equilibrium between HCHO and H_2O (Inomata et al., 2008; Vlasenko et al., 2010; Yuan et al., 2017a).

$$H_3O^+ + HCHO \rightleftarrows HCHO \cdot H^+ + H_2O \tag{2.8}$$

The quadrupole mass spectrometer (QMS) separates the gas sample according to a predefined mass to charge ratio (m/z). As the charge number with PTR-MS mea-

surements is 1 when using H_3O^+ as the reagent ion, the m/z value equals the molar mass of the target ion plus 1 from the added proton. For example, isoprene (C_5H_8) has a molar mass of around 68 g mol^{-1}, thus its m/z= 69. The secondary electron multiplier (SEM), which follows the QMS, detects the mass as count rates, which can then be converted to VOC mixing ratios using the specific parameters of the reaction chamber such as voltage, temperature, pressure, and length (IONICON, 2016, 2013).

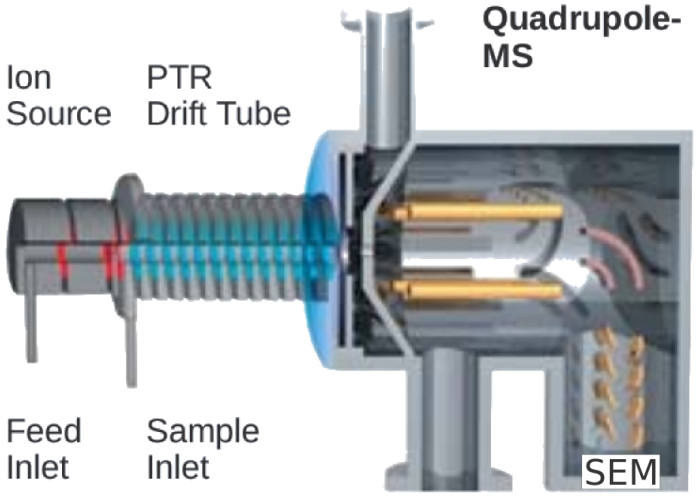

Figure 2.3.1.: A schematic of the core functionality of a proton transfer reaction–quadrupole mass spectrometer (PTR-QMS) illustrating the three major parts of ionization region with an inlet for the reagent ion, the drift tube or reaction chamber with an inlet for the gas sample upstram, the quadrupole mass spectrometer for separating the protonated chemical species, and the secondary electron multiplier (SEM) for detecting the count rates (adapted from IONICON, 2013).

In the late 2000s, the PTR-MS technology was further developed from the robust PTR-QMS to a more fragile and cost intensive PTR-TOF-MS which measures the time of flight (TOF) of each mass instead of detecting the counting rates (Yuan et al., 2017a). Thereby, improving the transmission of protonated molecules from the reaction chamber to the time of flight region, the resolution of detectable masses could be significantly enhanced (Jordan et al., 2009; Yuan et al., 2017a). In order to separate specific compounds with the same nominal mass e.g. between isomers of monoterpenes or isoprene and fragments of 2-methyl-3-buten-2-ol, sampling with a PTR-QMS should be accompanied with any kind of GC-MS instrument (online or offline) (Ghirardo et al., 2010).

2.4. BVOC modeling

To study the impact of BVOCs on air quality and climate on a broader spatial scale (regional and global level) and to analyze potential future emission changes due to climate or land use and land cover change, models of BVOC emissions need to be applied (Arneth et al., 2010a). Different approaches have been applied that yielded estimates with a large variability in particularly for global monoterpene fluxes (30 to 128 Tg C a^{-1}) while the range of simulated isoprene emission was fairly narrow (412 to 601 Tg C a^{-1}) (Carslaw et al., 2010). Besides different BVOC model approaches, these ranges are the result of changed vegetation distribution, climatologies, and spatial and temporal resolutions using a set of global model frameworks. Large uncertainties still exist regarding seasonal variation and emission of coumpounds other than isoprene that can only be mitigated with model improvements. The second major part of this thesis is thus the modeling BVOC emissions using field measurements as evaluation. Therefore, different common modeling approaches are described in the following.

2.4.1. Different modeling approaches

Current BVOC emission models can be divided into two main approaches: (1) empirical models from a leaf-level process perspective and (2) process-based models which are established from a plant physiological perspective reflecting biosynthesis pathways (Grote and Niinemets, 2008; Monson et al., 2012; Grote et al., 2013). Both approaches are briefly summarized below. The BVOC model which is used in this thesis will be explained in section 2.4.2 in more detail.

Empirical models

The first mathematical formulation of an isoprene emission model to describe its temperature and radiation dependency of *de novo* emissions was formulated by Tingey et al. (1979) (Grote et al., 2013), using the following general logistic function

$$\log(E_{\text{iso}}) = \frac{a}{1 + \exp\{-b(x - c)\}} + d \tag{2.9}$$

with E_{iso} as isoprene emission depending on empirical parameters a, b, c, and d, as well as x, which is a substitute for either radiation as PPFD or leaf temperature. The empirical parameters are determined by fitting Eq. 2.9 to measured isoprene emissions from live oak via non-linear least-squares (Monson et al., 2012). The approach was modified to describe monoterpene emissions with a temperature dependence only (Tingey et al., 1980), thus assuming a strict emission from storage pools and an an infinite source which is only constrained by volatility and diffusive resistances (Grote et al., 2013). Further model development during the 1980s lead to differentiated non-linear emission response shapes for the main controlling environmental factors (leaf) temperature and PPFD. Also, emission is now calculated in one equation, combining both drivers (Monson et al., 2012). Additionally, it was detected that a distinct relationship exists between isoprene biosynthesis and plant CO_2 assimilation (Niinemets et al., 1999; Sharkey and Yeh, 2001). This lead to a revised formulation of emissions by Guenther et al. (1991, 1993) which is based on radiation and temperature dependencies similar to those used by photosynthesis models (Grote et al., 2013). For isoprene, Guenther et al. (1993) estimated emissions via

$$E_{\text{iso}} = \text{SEF}_{\text{iso}} * C_L * C_T \tag{2.10}$$

with SEF_{iso} as the standard emission factor of isoprene, which defines plant species specific basal emissions in units of μg g^{-1}DW h^{-1} at the standardized environmental conditions of PPFD = 1000 μmol m^{-2} s^{-1} and T_S = 303.15 K.

The light dependent factor C_L is defined as

$$C_L = \frac{\alpha c_{L1} \text{PPFD}}{\sqrt{1 + \alpha^2 \text{PPFD}^2}} \tag{2.11}$$

with the coefficients $\alpha\,(= 0.0027)$ and $c_{L1}\,(= 1.066)$. The values of these coefficients were derived empirically by non-linear best fit procedures applied to isoprene emission observations from eucalyptus, sweet gum, aspen, and velvet bean. Thereby, α is the initial slope of the graph, relating PPFD to isoprene emission. It can be interpreted as the light quantum use efficiency. The coefficient c_{L1} is chosen to set the whole function C_L to 1 under environmental standard conditions. The hyperbolic shape of C_L (see Fig. 2.4.1) in response to light is similar to the light dependency of photosynthesis (Guenther et al., 1993).

The temperature response of enzymatic activity, factor C_T, is defined as

$$C_T = \frac{\exp\left\{\frac{c_{T1}(T - T_S)}{R_G T T_S}\right\}}{1 + \exp\left\{\frac{c_{T2}(T - T_M)}{R_G T T_S}\right\}} \tag{2.12}$$

with R_G (= 8.314 J K^{-1} mol^{-1}) as the ideal gas constant, and c_{T1} (= 95,000 J mol^{-1}), c_{T2} (= 230,000 J mol^{-1}), and T_M (= 314 K) as empirical coefficients which were estimated again by non-linear best fit procedures to observed emission rates (Guenther et al., 1993).

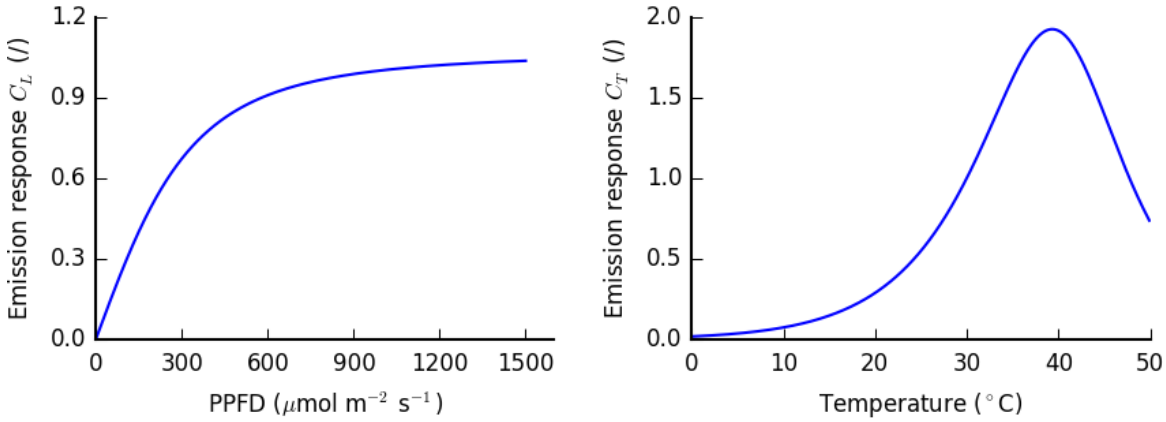

Figure 2.4.1.: Normalized *de novo* BVOC emission rates depending on temperature and PPFD based on Eq. 2.10 from Guenther et al. (1993). Left: emission response of factor C_L following Eq. 2.11 depending only on PPFD; Right: emission response of factor C_T following Eq. 2.12 depending only on temperature.

The emission responses shown in Fig. 2.4.1 agree well with general understanding of leaf *de novo* emissions (see Sect. 2.1.2 and Fig. 2.1.6). On the one hand, emissions increase almost linearly with increasing PPFD until a certain light level is reached and light response increases asymptotically due to light saturation. On the other hand, emissions increase exponentially with increasing temperature followed by a subsequent decreasing after an optimum temperature is reached due to enzyme denaturation or substrate limitations (Guenther et al., 1993). This light and temperature dependencies are comparable to that of photosynthesis, but with a higher optimum temperature than that of photosynthesis (Niinemets et al., 1999; Grote et al., 2013).

The simulation of short-term emission changes of BVOCs from specific storages, mainly monoterpenes, has been related to changes in leaf temperature, relative hu-

midity, and PPFD. However, except for temperature, at least their short-term influences were found either non-significant or negligible (Tingey et al., 1980; Guenther et al., 1993). Thus only temperature dependence has been formally described for the use with models via

$$E_{\text{mono}} = \text{SEF}_{\text{mono}} * \exp\{\beta(T - T_S)\} \tag{2.13}$$

with SEF_{mono} as the standard emission factor of monoterpenes and β being an empirical coefficient determining the gradient change of exponential growth (K^{-1}). Similar to the SEF, the value of β is highly dependent on the species and varies according to Guenther et al. (1993) between 0.057 and 0.144 K^{-1} with more than 50 % of the considered 28 studies being in the range of 0.09 ± 0.015 K^{-1}.

The aforementioned approaches for modeling *de novo* and pool emissions do not account for seasonal changes and external environmental control mechanisms other than light and temperature. Also, it is apparent that emissions of monoterpenes and many other BVOCs cannot be explained solely by a pool emission approach. Thus, empirical leaf scale models were further developed (cf. Niinemets et al., 2010; Grote et al., 2013) leading to the most widely used approach of model of emissions of gases and aerosols from nature (`MEGAN`) currently in version 2.1 (Guenther et al., 2006, 2012).

The latter model, still applies a plant- and BVOC specific standardized emission factor (SEF) (other nomenclatures are (standard) emission potential, emission factor) similar to Eqs. 2.10 and 2.13. However further influences are introduced that describe the emission responses to environmental and phenological conditions which are now explicitly related to the canopy scale. The recent empirical emission model by Guenther et al. (2012) is defined as

$$E_{\text{BVOC}} = \text{SEF}_{\text{BVOC}} \times \text{C}_{\text{CE}} \times \text{LAI} \times \gamma_{\text{P, BVOC}} \times \gamma_{\text{T, BVOC}} \times \gamma_{\text{A, BVOC}} \times \gamma_{\text{SM, BVOC}} \times \gamma_{\text{C, BVOC}} \tag{2.14}$$

with BVOC dependent activity factors (γ) for PPFD (γ_{P}), temperature (γ_{T}), leaf age (γ_{A}), soil moisture (γ_{SM}), and CO_2 inhibition (γ_{C}). The emissions are further scaled by a canopy environment model dependent parameter (C_{CE}) and the leaf area index (LAI) to yield a flux in units of μg m^{-2} ground area h^{-1}.

Another major improvement in `MEGAN` is the consideration of seasonality. Therefore, the activity factors for PPFD and temperature in Eqs. 2.10 and 2.13 are set in relation

to temperature and light conditions of the last ten days. Finally, *de novo* and pool emissions are separately calculated for each BVOC. The idea of such a two-component approached evolved from the fact, that the same biogenic component can be emitted from storages and from *de novo* biosynthesis at the same time, as it could be shown for monoterpenes by stable isotope $^{13}CO_2$ labeling by Ghirardo et al. (2010). Ghirardo et al. (2010) further developed a hybrid model using equations from the approach in Guenther (1997) by fractioning between *de novo* (58 %) and pool (42 %) emissions which significantly improved simulation results. Stavrakou et al. (2011) used a similar modeling approach on the global scale with `MEGAN` for methanol by designating 80 % to the *de novo* emissions. Thus, Guenther et al. (2012) assume that all BVOCs can be emitted by separately considering emissions from light dependent (LDF) and light independent (LIF) sources. Thereby, BVOC specific activity factors γ_{P} and γ_{T} from the formerly equations for isoprene (see Eq. 2.10) and monoterpenes (see Eq. 2.13) are rearranged to

$$\gamma_{\mathrm{P,\,BVOC}} = 1 - \mathrm{LDF_{BVOC}} + \mathrm{LDF_{BVOC}}\gamma_{\mathrm{P\_LDF}} \tag{2.15a}$$

$$\gamma_{\mathrm{P\_LDF}} = C_P \left(\frac{\alpha \mathrm{PPFD}}{\sqrt{1 + \alpha^2 \mathrm{PPFD}^2}} \right) \tag{2.15b}$$

which is similar to Eq. 2.11 but parameters α and C_P are estimated from past PPFD conditions by

$$\alpha = 0.004 - 0.0005 \ln(P_{240}) \tag{2.16a}$$

$$C_P = 0.0468 \exp\{0.0005(P_{24} - P_{\mathrm{past}})\}(P_{240})^{0.6} \tag{2.16b}$$

with P_{24} and P_{240} as the average PPFD over the last 24 and 240 hours, respectively, and P_{past} as the standard PPFD conditions over the past 24 hours with 200 and 50 μmol m^{-2} s^{-1} for sunlit and shade leaves, respectively. The activity factor for temperature dependent emissions γ_{T} is calculated as follows

$$\gamma_{\mathrm{T,\,BVOC}} = 1 - \mathrm{LDF_{BVOC}}\gamma_{\mathrm{T\_LIF,\,BVOC}} + \mathrm{LDF_{BVOC}}\gamma_{\mathrm{T\_LDF,\,BVOC}} \tag{2.17}$$

with $\gamma_{\mathrm{T\_LIF,\,BVOC}}$ similar to Eq. 2.13 but BVOC specific applicable to all light independent emissions. Factor $\gamma_{\mathrm{T\_LDF,\,BVOC}}$ is similar to Eq. 2.12 but with coefficients

that reflect temperature conditions over the past ten days, following

$$\gamma_{\text{T\_LDF, BVOC}} = E_{\text{opt}} \frac{c_{T2} \exp\left\{c_{T1,\text{ BVOC}} * \dfrac{1/T_{\text{opt}} - 1/T}{R_G}\right\}}{c_{T2} - c_{T1,\text{ BVOC}}\left(1 - \exp\left\{c_{T2} * \dfrac{1/T_{\text{opt}} - 1/T}{R_G}\right\}\right)} \tag{2.18}$$

with $c_{T1,\text{ BVOC}}$ as an empirical BVOC specific parameter and coefficients E_{opt} and T_{opt} defined as

$$T_{\text{opt}} = 313 + (0.6(T_{240} - T_{\text{past}})) \tag{2.19a}$$

$$E_{\text{opt}} = C_{\text{eo, BVOC}} \exp\{0.05(T_{24} - T_{\text{past}})\} \exp\{0.05(T_{240} - T_{\text{past}})\} \tag{2.19b}$$

with $T_{\text{past}}\,(= 293K)$ as the plant physiological past standard temperature for leaves, T_{24} and T_{240} as the leaf temperature averaged over the last 24 and 240 hours, respectively, and $C_{\text{eo, BVOC}}$ as an BVOC specific empirical coefficient.

Generally, the modeling framework `MEGAN` was developed to be applied as a standalone version on the local/ecosystem scale, coupled to atmospheric chemistry models (e.g. the Weather Research and Forecasting model coupled with chemistry (`WRF-chem`) version 3.4.1 (Knote et al., 2014)) or linked to a land surface model (e.g. within the Community Land Model (`CLM`) version 5 (Lawrence et al., 2018)). Thus, the model can be used to estimate BVOC fluxes and analyze impacts of climate- and land use change scenarios (Guenther et al., 2012). In order to be applicable with global scale models parameters and SEF values had to be defined for plant functional types (PFTs) instead of the specific plant species, which is further discussed in Niinemets et al. (2010). It should be noted that the approach can be only used to simulate constitutive emissions, whereas those from induction (biotic/abiotic, stress, priming) as described in Sect. 2.1.1 are not considered. Additionally, the environmental drivers affect the emission in an additive way assuming that they are independent from each other. However, indications exist that this might not always be the case (Niinemets et al., 2010; Grote et al., 2013).

During the late 1990's main pathways of BVOC biosynthesis were discovered (see Sect. 2.1.2), which lead to more mechanistically based models which describing linkages to photosynthesis and controls over the chemical kinetics more explicitly (Grote et al., 2013).

Process-based models

Apart from empirical models BVOC emissions can be simulated with semi-mechanistic and mechanistic models which focus on the link to photosynthesis, eventually considering biochemical processes of BVOC biosynthesis (Niinemets et al., 1999; Grote et al., 2006; Monson et al., 2012; Grote et al., 2013). This development was mainly driven by the discovery of the MEP pathway, which uses primary metabolites as substrates and chemical energy (from adenosine triphosphate, ATP) as well as reducing power (from nicotinamide adenine dinucleotide phosphate, NADPH) from primary metabolism, to synthesize isoprenoids (see Sect. 2.1.2) (Niinemets et al., 1999; Grote and Niinemets, 2008). Thus, the additionally observed high correlations between isoprenoid emissions and CO_2 assimilation lead to process-based isoprenoid models which are associated to and rely on process-based photosynthesis models (e.g., Farquhar et al. (1980); Farquhar and Sharkey (1982)) (Grote and Niinemets, 2008). Niinemets et al. (1999) found that leaf photosynthetic electron transport is related to leaf isoprene synthesis and thus emissions. The relation between net CO_2 assimiliation rate (A, in units of μmol m^{-2} leaf area s^{-1}) and photosynthetic electron transport rate (J, also in units of μmol m^{-2} leaf area s^{-1}) can be described as

$$A = J\frac{C_{ic} - \Gamma^*}{4C_{ic} + 8\Gamma^*} - R_d \tag{2.20}$$

with C_{ic} as the leaf intercellular CO_2 mole fraction, Γ^* as the photosynthetic CO_2 compensation point (where gross CO_2 assimilation equals photorespiration in units of μmol mol^{-1}), and R_d as the mitochondrial or dark respiration rate in units of μmol m^{-2} leaf area s^{-1} (Niinemets et al., 1999; Monson et al., 2012). Generally, J supplies the required ATP and NADPH for isoprene synthesis (Sharkey and Yeh, 2001; Arneth et al., 2007). The Eq. 2.20 can be transformed to relate isoprene emission to J:

$$E_{\text{iso}} = \varepsilon \times J \times \alpha \tag{2.21}$$

with J as the photosynthetic electron transport rate in units of μmol m^{-2} leaf area s^{-1}, ε as the fraction of J used for isoprene synthase, and α as a scaling factor converting electrons and isoprene synthase masses to isoprene molecules per leaf dry mass (Niinemets et al., 1999; Grote and Niinemets, 2008; Monson et al., 2012). Factor ε can be described as the ratio of isoprene synthase activity and the rate of total pho-

tosynthetic electron transport, both in dependence on an enzyme catalyzed reaction depending on temperature:

$$k = \frac{\exp\left\{c - \frac{\Delta H_a}{R_G T}\right\}}{1 + \exp\left\{\frac{\Delta S}{R_G} - \frac{\Delta H_d}{R_G T}\right\}} \tag{2.22}$$

with ΔH_a and ΔH_d as an activation and deactivation energy, respectively, in units of J mol^{-1}, S as an entropy term in units of J mol^{-1} K^{-1}, and c as a scaling constant (Niinemets et al., 1999; Monson et al., 2012). Factor α can be written as

$$\alpha = \frac{C_{ic} - \Gamma^*}{6(4.67C_{ic} + 9.33\Gamma^*)} \tag{2.23}$$

with the numbers in the denominator reflecting 6 moles of carbon necessary as substrate for isoprene in the MEP pathway as well as stoichiometric relations of electron transport for isoprene synthesis at the excess of CO_2 assimilation dependent on intercellular CO_2 mol fraction (C_{ic}) and CO_2 compensation point (Γ^*) (Niinemets et al., 1999; Monson et al., 2012). The calculation of E_{iso} could then be related to PPFD from photosynthesis models (cf. Monson et al., 2012) by

$$J = \frac{\alpha \text{PPFD}}{\sqrt{\left(1 + \frac{\alpha^2 \text{PPFD}^2}{J_{\text{max}}^2}\right)}} \tag{2.24}$$

with J_{max}^2 as the maximum photosynthetic electron transport rate describing the upper limit of $J = J_{\text{max}}$ at saturating PPFD (Monson et al., 2012). The Eq. 2.24 corresponds pretty much to Eq. 2.15 because it relates emission to a photosynthesis product that itself depends on PPFD. The difference is that other influences on photosynthesis will also affect isoprene emission without the need of an explicit introduction of the emission equation (Monson et al., 2012). In contrast to the numerous ecosystem/biochemical simulation frameworks that use `MEGAN`, only few land use models have implemented an adapted version of the approach of Niinemets et al. (1999, 2002) to simulate BVOC emissions. Examples are the dynamic global vegetation model Lund Potsdam Jena general ecosystem simulator (`LPJ-GUESS`) (Arneth et al., 2007; Schurgers et al., 2009; Hantson et al., 2017)) and the model `E2-YIB` (Zheng

et al., 2015; Harper and Unger, 2018).

Models were further developed as it became more and more evident that other compounds than isoprene are also emitted from light dependent *de novo* production and not (solely) from specific storage structures (Niinemets et al., 2002; Grote et al., 2006). Martin et al. (2000) developed a model following a concept, where isoprene production is simulated as the minimum of the three potentially limiting processes: (1) rate supply of carbon as a substrate from photosynthesis and photorespiration, (2) rate supply of ATP to produce IDP and DMADP as universal terpene precursors, (3) and the maximum temperature dependent isoprene synthase activity (Martin et al., 2000; Arneth et al., 2007; Grote et al., 2013). Another follow-up development of the Niinemets et al. (1999, 2002) model is the `JJv` model, which will be described in more detail in Sect. 2.4.2.

Zimmer et al. (2000), Lehning et al. (2001), and Grote et al. (2006) established and further developed a detailed biochemical isoprenoid biosynthesis model that was combined with a seasonal isoprene synthase model to account for long-term variations (`SIM-BIM`) and the follow-up for non-stored monoterpene emissions (`SIM-BIM2`). Thereby, the synthase activity (or biosynthesis capacity) dynamically develops on a daily basis in dependence on temperature, PPFD, and the phenological state of the leaves. In a second step, each of the 8 enzymatic conversion steps to calculate isoprenoid precursors to form isoprene and monoterpenes are explicitly calculated. These calculations are based on different kinetic parameters (esp. enzyme activities, and Michaelis-Menten constants) to represent first-order Michaelis-Menten equations and the temperature dependences of the biochemical reactions (which base on Eq. 2.22) for all intermediate enzyme synthases within the MEP pathway. Finally, the production of isoprene and monoterpenes is set equal to their emission (Grote et al., 2006, 2010). The process of simulating all synthesis steps however demands various parameters that are at least partly species-specific and are difficult to measure. If they could not be provided by literature, they were mainly derived through inverse modeling and parameter fitting to observed temperature dependencies (which are mostly determined from crude leaf extracts) (Grote et al., 2013). The detailed functions and equations describing the specific steps within SIM-BIM2 are not presented here, since they are not relevant for this study. Nevertheless, it can be concluded that all described process-based models describe the light dependency by coupling emission calculations to a photosynthesis model which supplies energy and substrates, and

thereby could potentially consider further environmental influences on constitutive emissions (Grote and Niinemets, 2008; Grote et al., 2013). For example, the mechanism could be used to explain limiting effects of drought and CO_2 concentration on some of the photosynthetic metabolites and thus BVOC precursors (Grote et al., 2010). However, the incorporation of induced (especially biotic) or primed emissions is still missing in current models.

2.4.2. The BVOC emission model JJv

The BVOC emission model based on electron transport J and J_v (`JJv`) is a follow-up from the model proposed by Niinemets et al. (1999, 2002) and developed mainly by Harrison et al. (2013), Morfopoulos et al. (2013, 2014), and Grote et al. (2014) in order to be applicable in combination with earth system models. As this model will be used within this study to simulate light dependent BVOC emissions from bioenergy crops, it is described here in more detail.

The general idea is, that NADPH is limiting synthesis of the MEP pathway and is itself provided by the total electron transport (J_{tot}) from photosynthesis. The reducing power of NADPH is also required for carbon assimilation and photorespiration (photosystem II). It is assumed that the energy used for this part is described as the electron flux $J_{\mathrm{CO2+O2}}$ which consumes most of J_{tot} and only little is left for additional redox reactions in the leaf such as isopreneoid biosyntheis (J_{bvoc}) and others (J_{other}); thus: $J_{\mathrm{tot}} = J_{\mathrm{CO2+O2}} + J_{\mathrm{bvoc}} + J_{\mathrm{other}}$ (see Fig. 2.4.2) (Morfopoulos et al., 2014). Due to the different orders of magnitude of nmol for J_{bvoc} and J_{other}, and μmol for J_{tot}, a partitioning within the nmol scale remains enigmatic which is why a full mass balance seems unrealistic and thus J_{other} can be neglected in this approach (Morfopoulos et al., 2014). The supply of J_{tot} is light limited and the consumption for carbon assimilation and respiration ($J_{\mathrm{CO2+O2}}$) is limited by the capacity of ribulose-1,5-bisphosphate carboxylase/oxygenase (Rubisco), the enzyme for carbon fixation within the Calvin cycle (Harrison et al., 2013; Morfopoulos et al., 2013). Thus, using the notation of the `JJv` model, the excess energy from electron supply (J) subtracted by the electron consumption (J_v) should be related to isoprenoid biosynthesis. This interplay of electron transport rates is described by

$$\gamma_{\mathrm{ph}} = (c_1 + c_2 * max(-\Delta J_{\mathrm{sat}}, J - J_v)) * J * min(1, C_{ic}/\Gamma^*) \qquad (2.25)$$

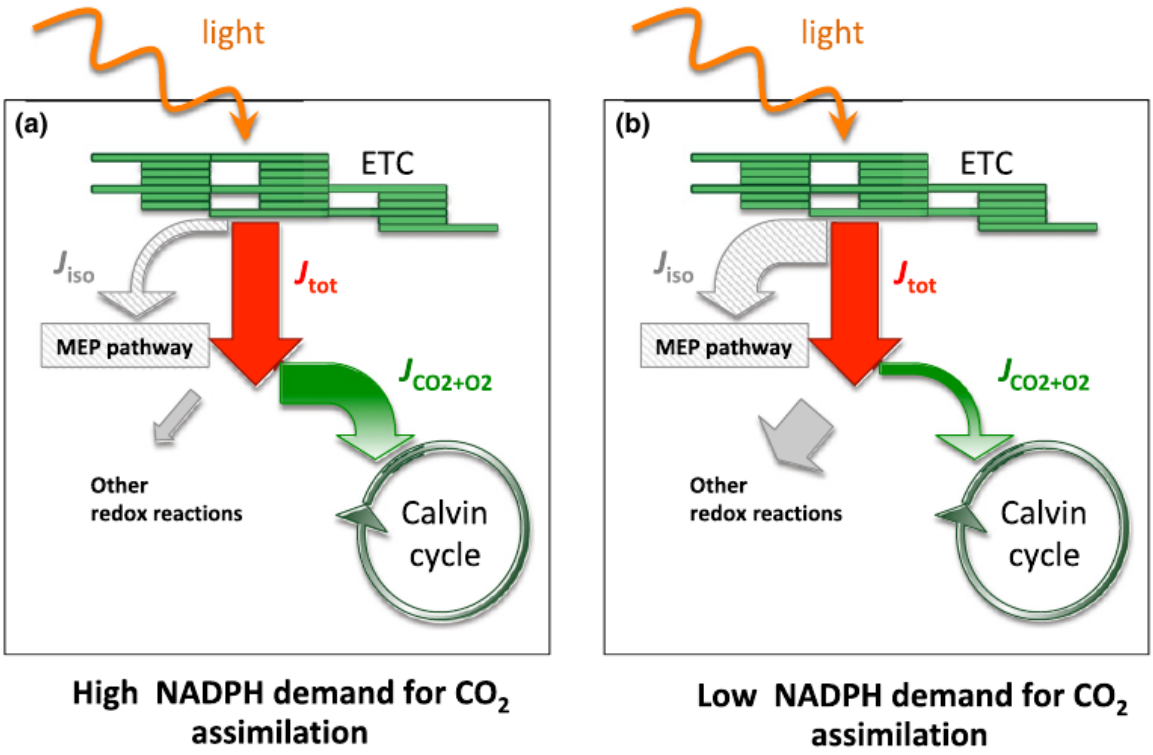

Figure 2.4.2.: Schematic of proposed hypothesis of interdependence between photosynthesis and isoprene biosynthesis underlying the `JJv` model. J_{tot} generated from light dependent reactions of photosynthesis (ETC: electron transport chain), supplies electron flux ($J_{\text{CO2 + O2}}$) and reducing power (NADPH) to Rubisco within the Calvin cycle, and to a much smaller part also to MEP pathway (J_{iso}) and other redox reactions. Under constant J_{tot}, an increased demand in NADPH (Fig. (a)) for Rubisco leads, to an increased $J_{\text{CO2 + O2}}$, and thus less J_{iso} for MEP pathway and other redox reactions and vice versa (Fig. (b)) (from Morfopoulos et al., 2014).

with c_1 ($= 0.1765e - 3$) and c_2 ($= 0.0028e - 3$) (dimensionless) as parameters for the fraction of electrons used from excess transport rate and photosynthetic transport rate, respectively, ΔJ_{sat} ($= 34$) as the saturating amount of electrons that can be supplied from other sources (in units of μmol m^{-2} s^{-1}). The parameter c_1 and c_2 were determined from hybrid aspen observations of isoprene emissions and photosynthesis and a subsequent fitting of the photosynthesis model to observations. The values of J, J_v, C_{ic}, and Γ^* need to be provided from the photosynthesis model, e.g. by Farquhar et al. (1980).

The BVOC synthase activity is calculated as a temperature dependent term, similar

to Eq. 2.22 by

$$\gamma_{\text{en}} = \frac{\exp\left\{c_0 - \dfrac{\Delta H_{a\_\text{en}}}{R_G T}\right\}}{1.0 + \exp\left\{\dfrac{\Delta S_{\text{en}}}{R_G} - \dfrac{\Delta H_{d\_\text{en}}}{R_G T}\right\}} \tag{2.26}$$

with c_0 (= 32.86 J mol^{-1}) as a scaling constant, ΔH_{a_en} (= 83129 J mol^{-1}) as the enzymatic activation energy, ΔH_{d_en} (= 284600 J mol^{-1}) as the enzymatic deactivation energy, and ΔS_{en} (= 887.5 J mol^{-1} K^{-1}) as the enzyme entropy term.

Finally, both emission functions, the photosynthetic (γ_{ph}) as well as the enzymatic (γ_{en}) emission potential, are used in the standardized form by normalizing with environmental standard conditions. `JJv` can be parameterized to plant or PFT level and BVOC specific SEF from literature or own measurements can be used according to:

$$E_{\text{bvoc}} = \text{SEF}_{\text{bvoc}} * \gamma_{\text{ph\_rel}} * \gamma_{\text{en\_rel}} \tag{2.27a}$$

$$\gamma_{\text{ph\_rel}} = \gamma_{\text{ph}} / \gamma_{\text{ph\_norm}} \tag{2.27b}$$

$$\gamma_{\text{en\_rel}} = \gamma_{\text{en}} / \gamma_{\text{en\_norm}} \tag{2.27c}$$

with $\gamma_{\text{ph\_norm}}$ and $\gamma_{\text{en\_norm}}$ as the photosynthetic and enzymatic emission potentials under environmental standard conditions, respectively.

Various modeling studies were carried out to evaluate `JJv` and to investigate its uncertainty (Harrison et al., 2013; Morfopoulos et al., 2013, 2014; Grote et al., 2014) and the model has demonstrated its capability to reproduce isoprene emission responses to changing temperature, PPFD, and CO_2 concentrations. In particularly, it could represent (1) an emission decrease with increasing ambient CO_2 concentrations ($\rightarrow$ increasing C_{ic}) due to increased NADPH demand for CO_2 assimilation; (2) an emission increase with increasing PPFD due to an increased supply of total electron transport (J_{tot}); (3) the interdependence of an higher temperature optimum for isoprene synthase and lower temperature optimum for J_{tot} leading to an intermediate temperature optimum for isoprene emissions; and (4) an emission decrease with increasing light use efficiency.

2.4.3. LandscapeDNDC framework

This thesis aims to simulate a realistic full seasonal cycle of BVOC emissions for different bioenergy crops. Therefore, it is crucial to correctly reproduce phenological (leaf biomass) development, micrometeorology, and management impacts. Concerning photosynthesis, a Farquhar-type (Farquhar et al., 1980; Farquhar and Sharkey, 1982) model is needed for the linkage with a process-based BVOC emission model such as `JJv` (Grote et al., 2014) because the input of J, J_v, C_{ic}, Γ^* is required for BVOC synthesis calculation. Here, I decided for the modeling framework landscape denitrification and decomposition (`LandscapeDNDC`) (Haas et al., 2013) which is a modular process-oriented terrestrial ecosystem model, originally based on the 1-D biogeochemical model `DNDC` (Li et al., 2000). `LandscapeDNDC` has proven its capability to simulate biosphere-atmosphere-hydrosphere exchange processes (carbon, nitrogen, and water) at site and regional scale for forest, agricultural, and grassland ecosystems (Grote et al., 2009, 2011; Haas et al., 2013; Kraus et al., 2015, 2016; Molina-Herrera et al., 2016, 2017; Klatt et al., 2017; Houska et al., 2017). Its modular design allows to select different process descriptions for for canopy microclimate, water balance, soil carbon and nitrogen processes, physiological and stand structural development which can be applied to various different ecosystems (Butterbach-Bahl et al., 2019; Grote et al., 2011; Kraus et al., 2015). For example Molina-Herrera et al. (2016) applied `LandscapeDNDC` for modeling N_2O emissions and the leakage of NO_3 into ground water for different forest and agricultural sites (maize, oilseed rape, and grassland) in Europe. BVOC emissions had been simulated for holm oak forests with the predecessor model MoBiLE using the Guenther et al. (1993), Niinemets et al. (2002), and `SIM-BIM2` models (Grote et al., 2009, 2010). However, there are no `LandscapeDNDC` studies for agricultural sites or for BVOCs other than monoterpenes.

Concerning carbon assimilation, `LandscapeDNDC` uses the stomatal conductance model from Ball et al. (1987) and the Farquhuar photosynthesis model (Farquhar et al., 1980) which are both coupled by an approach from Collatz et al. (1992) ensuring that several important input variables for the `JJv` can be provided.

The model simulates all of these variables for a dynamically plant size adjusted number of canopy layers separately, in dependence on micrometeorology (i.e. radiation separately for sunlit and shaded leaf fractions, temperature) which are calculated from measured field meteorology.

3. Bioenergy plants used in this study and their emission characteristics

In contrast to several well investigated tree species where many measurements of species specific SEF are available, large uncertainties exist about BVOC emission characteristics from crops and in particular bioenergy crops (Steinbrecher et al., 2009; Karl et al., 2009). Especially information about SEF is scarce which lead to very crude default settings of of SEF for isoprene of different crop species (either 0.0 or 0.5 μg g^{-1}DW h^{-1}) and default SEF of 0.5, 2.0, and 0.1 μg g^{-1}DW h^{-1} for monoterpenes, OVOCs, and sesquiterpenes, respectively (Karl et al., 2009). More recently, several measurements were published with focus on bioenergy plants from short rotation coppices (especially poplar) and to some part also from crops (Portillo-Estrada et al., 2018; Hu et al., 2018; Mozaffar et al., 2018, 2017; Yuan et al., 2017b; Vanzo et al., 2016, 2015; Zenone et al., 2016; Brilli et al., 2016; Bachy et al., 2016; Morrison et al., 2016). In addition modeling studies on air quality impacts of BVOCs from bioenergy crops were carried out based on these data (Hu et al., 2018; Porter et al., 2015; Ashworth et al., 2015, 2013; Beltman et al., 2013). Nevertheless, all studies report large uncertainties related to the composition of BVOCs, the dependence on phenological stages, and the emissions in response to environmental conditions others than radiation and temperature, which are mainly caused by short observation periods and methodologies that are not able to detect the full range of emission compounds and environmental conditions.

3.1. Maize (*Zea mays* L.)

With currently 197 mio ha, maize is globally one of the most important crops and the cultivated area is still increasing (FAO, 2019). In Germany, 16.7 mio ha land are used

for agriculture, with maize cultivated on 2.5 mio ha (data from 2016). From these, 0.9 mio ha (36 %) are used to produce silage maize for biogas (FNR, 2018c). Maize, has a high energy yield which is why its biomass is used as the preferred substrate for the fermentation into biogas (69 %). Its average CH_4 yield per hectare land has a theoretical potential to produce electricity of 18,731 kWh in a combined heat and power plant (FNR, 2018b,c).

To the author's knowledge, there are few studies about field BVOC fluxes from maize which are all briefly summarized below. Das et al. (2003) observed midday fluxes from maize plants by offline GC-MS and GC-FID at an early growth stage (0.5 m plant height) via concentration gradient measurements in North Carolina, USA, for 5 days in May 1995. The most abundant compounds were methanol with 75% of total mass emission flux, followed by monoterpenes, and acetone with estimated SEF of 34.5, 6.61, and 4.25 μg g^{-1}DW h^{-1}, respectively. The study also found that total BVOC emissions have a large diurnal and daily variability.

The study of Graus et al. (2013) measured BVOC fluxes from enclosed maize leaves by PTR-MS in Colorado, USA, for 2 days in September 2010. With SEF of 3.74 (60 % of total fluxes), 0.57, and 0.39 μg g^{-1}DW h^{-1} for methanol, acetone, and monoterpenes, respectively, the overall emission rate was one order of magnitude lower than what has been observed by Das et al. (2003). Besides, emissions of GLVs, toluene, benzene, as well as various others were detected. The study also revealed a clear bidirectional flux pattern of acetaldehyde.

Leppik et al. (2014) observed the diurnal variability of relative BVOC fluxes from enclosed maize leaves and from a maize ecosystem by offline GC-MS in Grignon, France, for altogether 9 days in June 2010. The study found strong diurnal cycles with different temporal emission maxima for monotpernes, sesquiterpenes, and methly salicylate.

The longest observation period is available from Bachy et al. (2016), who investigated emissions from a maize ecosystem by means of the eddy covariance method coupled to a PTR-MS for a whole growing season in Belgium. Again, methanol with a SEF of 1.64 μg g^{-1}DW h^{-1} (66 % of absolute mean fluxes) showed highest emissions, followed by 0.32, 0.06, and 0.06 μg g^{-1}DW h^{-1} of acetone, acetic acid, and isoprene. These values are one order of magnitude lower than those from Graus et al. (2013) and two orders of magnitude lower than estimated by Das et al. (2003). Additionally,

many of the detected compounds showed deposition and emission in similar magnitude. This study also indicates the soil as a potential source and sink for some of the detected BVOCs.

Finally, Mozaffar et al. (2017, 2018) detected significant emission changes of maize leaf BVOC emissions at different leaf developmental stages while measuring emissions for several days at each stage with PTR-MS and GC-MS. Generally, all detected BVOC emissions were higher for younger than for senescent leaves with the largest fraction being methanol, followed by acetaldehyde, acetic acid, and hexenals. Mozaffar et al. (2017) also highlight the dependence of methanol emissions on both, temperature and PPFD, which could also be well reproduced by a model that simulated BVOC emissions as a composite of light dependent (0.9) and light independent (0.1) terms.

3.2. Oilseed rape (*Brassica napus* L.)

Globally, around 35 mio ha are cultivated with oilseed rape each year since 2013 (FAO, 2019). In Germany, the cultivated area of around 1.3 mio ha also remains constant since the beginning of the 2000's (FAO, 2019). Oilseed rape is mainly cultivated as winter rapeseed by seeding in autumn and harvesting around July/August in the subsequent year (FNR, 2018b). Harvests from 0.71 mio ha (in the year 2017) were used to produce bioenergy from oil of the seeds which can be further processed into biodiesel (FNR, 2018b). Biodiesel is mixed with diesel fuel to run combustion engines in the transportation sector or directly to produce energy in combined heat and power plants (FNR, 2018d). Based on the assumption of 416 kg rapeseed oil t^{-1} seeds which corresponds to around 1450 l rapeseed oil ha^{-1}, oilseed rape crops can potentially yield 1392 l rapeseed oil ha^{-1} land as biodiesel for the transportation sector (based on 0.96 l motor fuel equivalent) or generate 13900 kWh ha^{-1} electricity (FNR, 2018d,b).

The study of Jakobsen et al. (1994) describes emitted BVOCs from flowers of oilseed rape plants grown under laboratory conditions. They enclosed flowers (all leaves were removed the previous day) into a 5 dm^3 glass vessel and detected major emissions of monoterpenes and to some part also sesquiterpenes using a GC-MS.

In König et al. (1995), dynamic PTFE branch enclosure (15 dm^3) measurements were used for field observations of BVOCs with offline GC-MS and GC-FID at Essling,

Austria. During the late flowering period, two days in May 1993 were observed and detected emission rates of monoterpenes (74.6–108.7 ng g^{-1}DW h^{-1}), oxygenated monoterpenes (1.0–8.9 ng g^{-1}DW h^{-1}), GLVs (30.5–47.2 ng g^{-1}DW h^{-1}) and other OVOCs (51.0–142.8 ng g^{-1}DW h^{-1}).

McEwan and Smith (1998) carried out measurements in the field throughout few days during flowering period by partially enclosing oilseed rape plants with a nylon bag using a dynamic approach and sampling BVOCs using offline GC-MS. The results of the study were quantified in relative amounts only, with monoterpenes being dominant (60–90 %). Furthermore, GLVs (max. 25 %), oxygenated monoterpenes, as well as low emissions of sesquiterpenes, acetaldehyde and acetone were detected.

Müller et al. (2002) conducted a field observation throughout 2 days during the flowering period in May 1998 by enclosing plants ($V = 82$ dm^3) and measuring with offline GC-MS in Saxony, Germany. Due to the focus of the study, only monoterpenes were detected with emission rates of 30–60 ng g^{-1}DW h^{-1}.

Himanen et al. (2009) conducted plant treatments with CO_2 and O_3 fumigation in a laboratory and observed emissions as well as additional tritrophic interactions (herbivore-induced volatiles signaling a natural enemy the presence of an herbivore) during the vegetative plant growth (no flowers or buds emerged). GC-MS measurements revealed mainly terpenoid emissions (monoterpenes, oxygenated monoterpenes, sesquiterpenes) which summed up to 78.5–163.5 ng g^{-1}DW shoot h^{-1} and very low emissions of GLVs.

Veromann et al. (2013) did laboratory experiments at PPFD 300 μmol m^{-2} s^{-1} and 24 ℃ with field grown oilseed rape plants in Jõgeva, Estonia, for two days in May 2010. One set of plants were in the bud stage and another in the flowering stage. The top of the plants was enclosed and measurements were conducted using a dynamic approach involving offline GC-MS. Major emissions of acetic acid, monoterpenes, benzaldehyde, and GLVs were detected.

Morrison et al. (2016) used dynamic vegetation enclosures for monthly average measurements via GC-MS at fields in Lincolnshire, England. By exclusively observing isoprene and monoterpenes, only little amounts of isoprene (temporally max. of 350 ng g^{-1} DW h^{-1}) were detectable while monoterpene emissions were below the limit of detection.

Renner and Münzenberg (2003) used some of the described emission estimates from oilseed rape plants (Jakobsen et al. (1994); König et al. (1995); Müller et al. (2002)) and did a chemical transport modeling study concluding that BVOC emissions may have a moderate impact on ozone formation. However, the model results suffer on the large variability of input information clearly stating that parameterization from measurements needs to be improved.

Concerning biodiesel from oilseed rape plants, it might be worth mentioning that during the last years, strong competition for rapeseed oil developed due to increasing and cheap palm oil and soy bean oil imports (BHKW Infozentrum GbR, 2018). Both, palm oil and soy bean oil originate from tropical regions often from tropical forest clearcuts, as e.g. for palm oil in Indonesia. This development is already accused to have strong negative impacts on water and heat fluxes (cf. Manoli et al. (2018); June et al. (2018)), carbon sequestration and biodiversity (cf. Dislich et al. (2017)) besides the irreversible destruction of these unique and pristine ecosystems (cf. `www.regenwald.org/themen/palmoel`).

3.3. Ryegrass (*Lolium multiflorum* L.)

Globally around, 1.8 billion ha is covered by grassland (FAO, 2019). In Germany, around 6.5 mio ha are covered with grassland (FAO, 2019) from which 5.3 mio ha are agriculturally cultivated but only grass from less than 0.25 mio ha is used for biogas production (FNR, 2018b,a). The term grassland includes many different grassy species with perennial ryegrass, timothy grass, meadow fescue, common meadow-grass, meadow foxtail, orchard grass, white clover, and red clover being the most important in Germany (FNR, 2018b,a). In contrast to the annual crops maize and oilseed, grassland is cultivated as a perennial crop with normally 3–6 cutting events each year depending on the intensity of cultivation (extensive vs. intensive). In this thesis, I studied a mixture of the two cultivars italian ryegrass (*Lolium multiflorum*, 85 %) and a hybrid ryegrass (*Lolium x hybridum*), 15 %). Regarding its importance for biogas production, grassland in Germany represents the second largest (14 %) fraction after maize and yields on average 9,549 kWh ha^{-1} electricity (FNR, 2018b).

A number of relatively new studies can be found on grassland BVOC emissions. The study of Davison et al. (2008) observed cut-induced emissions from a mixed

agricultural grassland covering 12 different grass species with *Lolium perenne* as one of it using the eddy covariance approach and applying PTR-MS together with offline GC-MS measurements throughout 4 days in June 2005 at Oensingen, Switzerland. The emission rates of the major compounds were determined as average daytime fluxes and were differentiated into the time before and after cutting. These were methanol (8.7–38 nmol m^{-2} s^{-1}), acetaldehyde (0.6–8.4 nmol m^{-2} s^{-1}), acetone (0.3–5.1 nmol m^{-2} s^{-1}), 2-butanone (methyl ethyl ketone, MEK) (0.3–2.2 nmol m^{-2} s^{-1}), and significant fluxes of GLVs. Just before cutting at the first day of measurements the LAI was 5.2 m^2 m^{-2} and the cut biomass was 510 gDW m^{-2}. The results indicate that an emission burst of all observed compounds occurred directly after cutting which quickly diminished after few hours.

The studies of Bamberger et al. (2010, 2011), Ruuskanen et al. (2011), Brilli et al. (2012), and Hörtnagl et al. (2014) measured BVOC exchanges by disjunct eddy covariance coupled to PTR-MS and PTR-TOF-MS over mountainous grassland (minimum of 4 different graminoid species and 5 forb species) in Austria. Measurements were carried out throughout the years 2008–2012. Although no ryegrass species are grown at the experimental site, it is worth mentioning that major deposition fluxes of many different compounds (monoterpenes, oxygenated monoterpenes, acetic acid, and sesquiterpenes) could be detected besides significant emissions of methanol. Up to 2 days after grass cutting, high emission bursts of methanol, GLVs, acetaldehyde, acetone, and isoprene were observed. Based on additional laboratory experiments, Brilli et al. (2012) highlight that the different grass species significantly differ in their composition of emitted BVOCs. Hörtnagl et al. (2014) focused on acetaldehyde exchange and detected major emission as well as depostion rates. The occurrence of fluxes in both directions had been explained by the specific acetaldehyde compensation point, soil temperature, and soil water content while air temperature and PPFD seemed to play minor roles. Spielmann et al. (2017) observed also isoprene and monoterpenes exchanges based on enclosure studies with the same grassland species under laboratory conditions using a PTR-TOF-MS. They conclude that especially soils are a major sink for terpenoids, although the presence of aboveground biomass could significantly decrease deposition rates.

Pańka et al. (2013) studied ryegrass in symbiotic associations with an endophytic fungi which were infected by the pathogen *Fusarium poae*. Under laboratory conditions and by using small bags which enclosed some grass plants, BVOCs were

measured with offline GC-MS. They detected significant amounts of emitted GLVs, monoterpenes, oxygenated monoterpenes, sesquiterpenes, benzyl acetate, indole and methyl salicylate.

Additionally, it should be mentioned that the fraction of harvested plant biomass that is used as bioenergy source is very small (globally 8 % in 2017/2018, Germany 14 % in 2016) compared to, e.g., forage for animals which has the highest fraction (globally 43 %, Germany even 60 %). The fraction of harvested crops which is directly used for food is globally 32 % but in Germany it is only 22 % (FNR, 2018b).

4. Conducted observations and simulations in this study

This chapter is a methodological description about my work during the three field campaigns and the subsequent modeling study.

4.1. Field study site and bioenergy crop experiments

Table 4.1.: Characterization of the three field experiments conducted at an experimental site near Dedelow, Brandenburg, Germany.

Plant species (cultivar) Binomial name	BVOC measurement period (CO_2 measurement period)	# data values daily/hourly	# chambers
Maize (Zoey) *Zea mays* L.	24 July 2015 – 16 September 2015 (April 2015 – September 2015)	48/1153	2
Oilseed rape (Pr44d06) *Brassica napus* L.	9 April 2016 – 20 May 2016 (August 2015 – July 2016)	29/801	4
Ryegrass (Country 2051) *Lolium multiflorum* L.	9 June 2017 – 29 June 2017 (August 2016 – September 2017)	16/396	4

Atlogether, I conducted three intensive field experiments on two field sites during the years 2015 to 2017 (see Tab. 4.1 and Fig. 4.1.1). The site is at an experimental field station close to the research station Dedelow which is located in northeastern Germany, in the region of the Uckermark, Brandenburg (exactly at N 53.3793 and E 13.7856). The site is embedded into the CarboZALF project (Sommer et al., 2016) which provides the necessary infrastructure for measuring trace gas exchanges in the field from different crop species with an automatic closed-chamber approach, also measuring relevant meteorological variables. The maize and ryegrass experiment in

2015 and 2017 were conducted at a site called D15, whereas the oilseed rape experiment in 2016 took place at D14 due to the overlap with the preceding maize experiment. Therefore, also the automatic measurement chambers and the measurement hut needed to be moved in between each campaign.

A Maize 11 August 2015

B Ryegrass 6 June 2017

C Oilseed rape 18 May 2016

Figure 4.1.1.: Bioenergy plants, automatic chambers, and measurement hut of the three field campaigns conducted at Dedelow, Germany during 2015 and 2017.

Within the scope of the project Volatile Organic Compound Emissions (VOCE), in which this thesis is embedded, the general idea was to measure BVOC emissions from bioenergy crops during different environmental conditions and different plant development stages. In this setup, neither the number of different plant species, nor the particular species exactly, nor the period during which each field campaign

was conducted was defined. Thus, all project partners had to decide together about the specifics of the experimental setups, including the species to grow. This resulted in the decision to cultivate maize during 2015, oilseed rape during 2016, and ryegrass during 2017. The basis for this decision was:

- Importance: Which are the most important plants for the production of renewable energy in Germany today and which might have a larger potential in the future (for both, transportation and energy sector)?
- Knowledge gaps: For which crops is crucial information about BVOC emissions still missing? In particular regarding field performance during different growth stages. In this respect, it is a benefit to investigate species that belong to different types regarding the source of their energy supply (i.e. oil, starch or fiber).
- Facilitation: Only crops can be selected that have a chance for sufficient growth and development at the investigation site. It is regarded a benefit if local farmers and technicians of the CarboZALF project are experienced in the required management techniques (seeding, fertilizing, harvesting etc.) and further analyses (determination of the growth stages, measuring the biomass, etc.).

Details about the importance and the available information for the selected crop species can be found in Chapt. 3.

4.1.1. Field management of the cultivated crops

In the following, a brief description is given about field management and plant development, which was conducted and observed by the technical staff at ZALF. More detailed can be found in the appendix chapter C.

Field management of maize

At the end of April 2015, 11 maize grains per m^2 were seeded (an energy and food cultivar Zoey from Advanta Seeds DMCC) within the 690 m^2 agricultural parcel called CarboZALF D15. The maize was harvested within the chambers at 14 September 2015 while the rest of the field remained until late September. The respective cultivar

is relatively small (maximum height around 2 m) which makes it convenient to be used within automatic chambers. To ensure sufficient plant nutrients and following conventional farming procedures, the field was fertilized around the seeding days with potassium, phosphor, and 160 kg N ha^{-1} as urea. Information about nitrogen fertilizer is later on considered for modeling of the plant growth because the selected soil model provides a full carbon and nitrogen balance in dependence on nutrient inputs (see Sect. 4.4.1). Additionally, herbicides, fungicides, and insecticides were applied in April, May, and beginning of July 2015. Since BVOC measurements did not start before the end of July, the application of fertilizers and plant protecting agents that might potentially induce volatilizations, could not have any direct impacts. Maize growth started slowly as the spring period was relatively cool and dry than on average. The summer, however, was very warm with only few rain events. Thus, the maize development was quite good, although the plants grew somewhat shorter than expected.

Field management of oilseed rape

In late August 2015, 50 grains of oilseed rape per m^2 were seeded (the semi-dwarf hybrid cultivar PR44D06 from Pioneer MAXIMUS®) on the parcel CarboZALF D14. The plants within the chambers were harvested at 19 May 2016 and the rest of the field was removed end of July. Herbicides and insecticides were applied in September, October 2015, and at 5 April 2016 (4 days before starting of the field campaign). The last applied compounds were the insecticides *Karate* and *Plenum* containing lambda-cyhalothrin $C_{23}H_{19}ClF_3NO_3$ and pymetrozin $C_{10}H_{11}N_5O$ which are solid under normal environmental conditions and seen as non-volatile. Besides phosphor and potassium, the field was fertilized with 30 kg N ha^{-1} as calcium ammonium nitrate (CAN) in September 2015, 80 kg N ha^{-1} as urea in March 2016, and 60 kg N ha^{-1} as CAN at 6 April 2016 (3 days before the field campaign). I expect no impact on BVOC measurements from this last application, since the fertilizer (a mixture of calcium ammonium nitrate) contains no hydrocarbon compounds and it was additionally applied by hand, not by combustion machines potentially emitting AVOCs.

In September 2015, the oilseed rape started to grow and developed normally until the end of the vegetation period (2 January 2016). Due to the cold winter and spring with only short warm periods, the plants developed slowly until beginning of May

2016 when temperatures increased. Due to the warmer conditions and some rain, plants grew fast and reached the flowering stage.

Field management of ryegrass

In late August 2016, 40 kg ha^{-1} of ryegrass seeds were planted on the parcel CarboZALF D15 (the cultivar mixture COUNTRY 2051 applicable as fodder and as a substrate for biogas plants, which consists of 85 % italian ryegrass (*Lolium multiflorum*) and 15 % hybrid ryegrass (*Lolium x hybridum*)). Generally, grassland is cultivated as a perennial crop and can be cut 3–6 times a year. In the current field campaign the ryegrass was cut at 17 May 2017, 26 June 2017, and 4 August 2017. After the third cut the campaign was completed and no more cuts were necessary. BVOC measurements started shortly after the first cut and lasted until a few days after the second cut. The ryegrass was fertilized in March, May, and July 2017 with 80, 50, and 30 kg N ha^{-1} as CAN, respectively. No plant protecting agents were applied. Consequently, no direct impacts on the BVOC measurements from any fertilizers or plant protecting agents are expected.

Due to a drought period that lasted until early September 2016, the grass had to be sown two times but emerged successfully after rain events in September and developed further until the end of the year. The winter was cold with snow until February 2017, but after mild temperatures end of February the grass started growing again. During the whole growing season, the weather was unsettled with alternate warm and cold as well as dry and moist periods. Nevertheless, the grassland developed normally and cutting was done as usually after reaching a specific developmental stage.

4.1.2. Main characteristics of the field experiments

Based on previous investigations, I expect only very low emissions during very early growth stages with a low plant biomass (see the review in Ch. 3). Thus, measurement periods where selected so that plants were at least in a late vegetative, early reproductive growth period. This is also recommended in order to include the flowering and fruit development, which is known to provide a sometimes unnoticed and a more elaborated BVOC bouquet than previous periods. Following Meier (2001), vegetative

plant growth of agricultural crops can be divided into the principal plant development stages germination, leaf development, formation of side shoots, stem elongation and shoot development, and development of vegetatively propagated organs. The reproductive growth can be divided into inflorescence emergence, flowering, development of fruit, and ripening or maturity of fruit and seed. The last principal growth stage is defined as senescence which does not belong to the reproductive development. The agricultural practice of cutting grassland for straw as a source for fodder or as a substrate for biogas plants usually occurs during the beginning of the flowering period (the first stage of reproductive growth) (Verch, G. (head of the research station), 2017; personal communication).

The maize, oilseed rape, and ryegrass BVOC experiments ran for 55 days, 42 days, and 21 days, respectively. Due to maintenance periods and technical problems during field experiments (see Sect. 4.1.3) the actual period of the BVOC fluxes were 48 days (1153 hours), 29 days (801 hours), and 16 days (396 hours) for maize, oilseed rape and ryegrass field studies. I defined the threshold to calculate a daily flux when at least 75 % of the day is covered by observed fluxes. It should be noted that only two automatic chambers could be used for the maize campaign, which were closed once within one hour, resulting in 36 flux observations per day ($24 \times 2 \times 0.75$). During the oilseed rape and ryegrass experiment, I could use four automatic chambers which were closed once within one hour, resulting in a minimum of 72 flux observations per day ($24 \times 4 \times 0.75$). I defined an hourly flux when a minimum of 50 % of chamber measurements is available (1 flux observation for maize, and 2 for oilseed rape and ryegrass). Additionally, periods for the campaigns were restricted by the availability of the PTR-MS instrument which was provided by the project partners from Helmholtz Zentrum München.

4.1.3. Difficulties during the field experiments

In this section, general and experiment specific problems are listed which occurred during the measurement periods. This includes difficulties related to data acquisition apart from the BVOC field experiments, especially meteorological measurements, which are necessary as input data for the modeling study.

General difficulties for the whole three years of data acquisition

- **Time:** The absolute time of the different measurement systems could not be synchronized automatically (e.g., by using a software tool like Tardis 2000), thus I converted all recorded measurements to local standard time (LST) which was the Central European Summer Time (CEST; UTC+2) during the BVOC experiments.
- **Status:** The status of the valves and the chambers was often not appropriately saved within the PTR-MS data set, and needed intensive post processing after the experiments.
- **Radiation:** I detected a relatively large bias of 15–20 % between a PAR sensor next to the chambers and a PAR sensor from a neighbored field (ca. 30–50 m). Since the remote sensor was closer in line with radiation data from a DWD weather station nearby, it was agreed with the responsible person at ZALF (Mathias Hoffman) to disregard the PAR data from the chamber.
- **Precipitation:** Unfortunately, ZALF could only provide subdaily precipitation data for 2015, daily sums for 2016, but no data for 2017 for our site. Thus, for 2017, I could use daily sums of precipitation data from a station around 2 km away.
- **Outage:** During the period of August 2016 until November 2016 which was outside any BVOC measurement campaign all devices related to the chambers were off. However, the gap could be fully substituted by meteorological measurements from a neighbored site.

Field experiment specific difficulties

- **Maize 2015:** During the explicitly hot summer, the measuring hut heated up leading to occasional shut-downs of the temperature sensitive PTR-MS with occasional shut downs. We decided to drill holes into the hut and install a ventilator exchanging the hot air from inside with warm air from outside which somewhat relaxed the situation.
- **Oilseed rape 2016:** An important gas tube lost its connection leading to

measurements from inside the measurement hut instead from the automatic chambers. The problem was detected after three days and immediately fixed.

- **Ryegrass 2017:** During the first half of the BVOC experiment, the automatic chambers were closed for only 5 minutes instead the regular 12 minutes, reducing the number of data points for the calculation of one flux to 3–4 instead of the usual 8–11. This problem lasted over two weeks because the recalibration of the chamber required the presence of a specific but unavailable technician. During the last two measurement days, chamber 3 did not close appropriately so that I could not use these data for further analyses.

4.2. Observations in the field

Part of the applied methods during the field experiments was already briefly explained in my publication Wiß et al. (2017) which is dedicated to observations on maize in 2015. Nevertheless, I describe the conducted methods in more detail in the following sections and will add important methodological modifications regarding the experiments on oilseed rape and ryegrass. An illustration of the measurement setup is shown in Fig. 4.2.1.

4.2.1. Automatic chambers and measurement setup

All trace gas concentration measurements which were used to obtain net trace gas fluxes from the observed species were conducted with large polycarbonate automatic chambers (wall thickness 2 mm) (see Fig. 4.1.1) of 1.5 m × 1.5 m × 2.5 m size each. The chambers are mounted onto a steel frame and are moved by an electronically controlled cable winch upwards and downwards. A similar setup was used for GHG experiments within other projects of CarboZALF (cf. Sommer et al., 2016; Hoffmann et al., 2017). By using these large chambers, all plant-atmosphere interactions including the BVOC exchanges could be observed at the whole ecosystem level. This includes trace gas exchange from the soil, where interactions of the plant species specific rhizosphere microbiome are involved. Thus the whole ecosystem emission pattern can be measured under natural field conditions, with all kind of interactions as e.g. induced emissions (see Sect. 2.1.1 for more details on induced emissions).

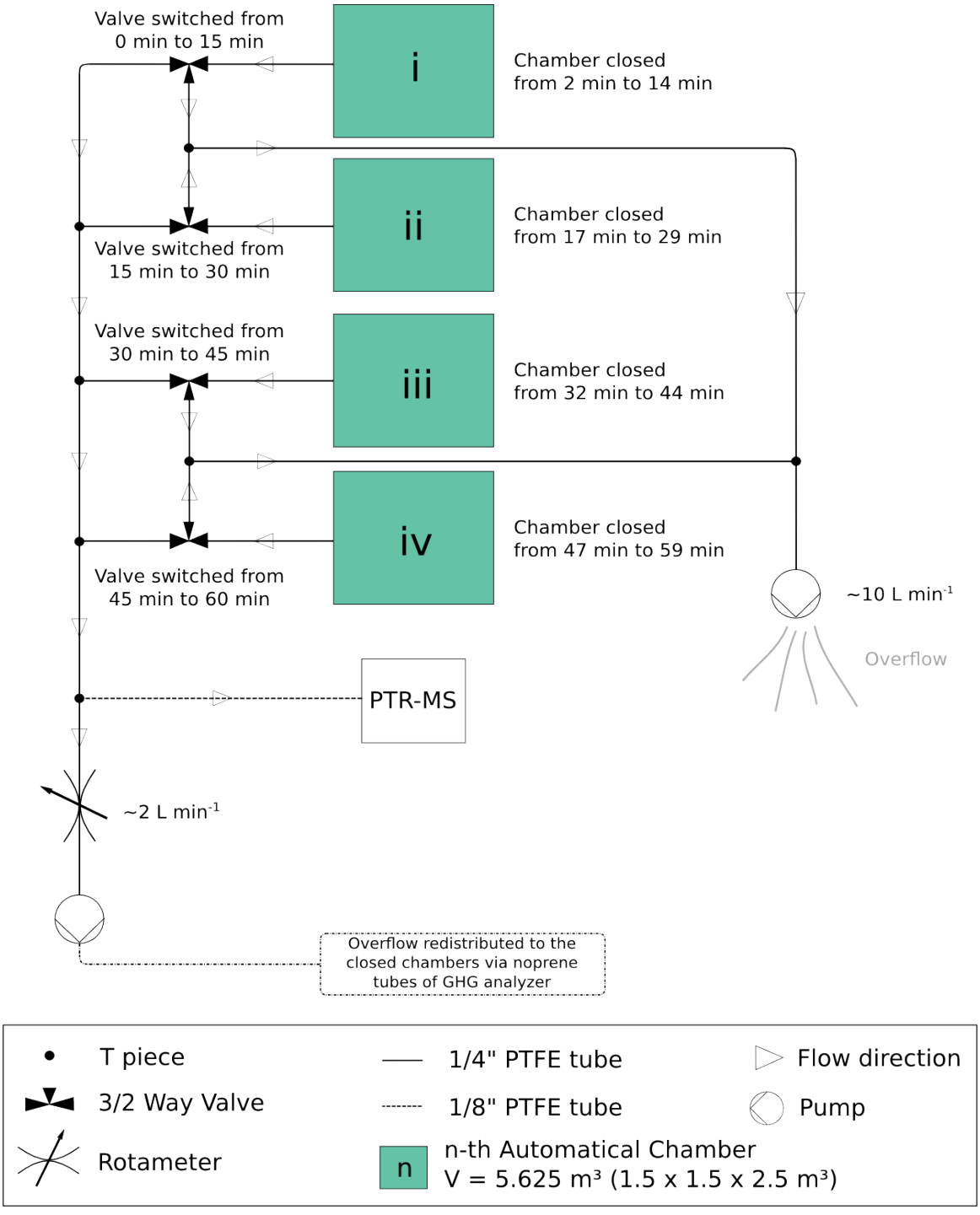

Figure 4.2.1.: Scheme of field experiment setup using four chambers (oilseed rape and ryegrass). For the maize experiment, the chambers iii and iv were not available but the chambers i and ii and their respective valves were operated the same way. The tube distances are not scaled correctly, as the tube length from the chamber to its 3/2 valve was around 95 % of the total tube length to the PTR-MS. Thus, continuously flushing of the tubes (with the second pump) during the periods while chambers were open (always three chambers at the same time) did significantly improve the measurement results.

To my knowledge, this is the first time that large automatic closed chambers under non-steady state conditions are used to study BVOC exchange rates.

The general measuring approach (see Fig. 4.2.1 for the setup) consists of a chamber system, where all of the drawn air (∼10 dm^3 min^{-1} from the BVOC and the GHG system) is redirected back into the chamber headspace, except for the 70 cm^3 min^{-1} which are used for the PTR-MS. As the gas mass losses due to PTR-MS measurements are below 1 %, the system can be defined as a flow-through non-steady-state approach, where trace gas concentrations within the headspace of the chambers can be directly linked to net ecosystem fluxes. The gas matrix is sampled from the chambers when they are closed during a period of 12 minutes, so that concentration changes from four chambers (two during the maize experiment) per hour can be measured. To minimize the impact of the chambers on the plant development and to ensure near-ambient environmental conditions, the chambers were kept open for 80 % of the time (i.e. 48 min h^{-1}). A 3/2 way polytetraflouretylen (PTFE) valve switches between drawing air from the closed chamber to the PTR-MS and drawing air from the open chamber for flushing the tubes. Preliminary tests during the setup showed that flushing of tubes significantly improves the measurement results as gas concentration memory effects within the 20 m 1/4″ PTFE tubes were minimized. In addition to valves and tubes, also the T-pieces and fittings were all made of PTFE which is resistant to the measured compounds and prevents those from being adsorbed at the surface. To avoid condensations and keep the vapor pressure high, all tubes are thermally isolated and heated to a temperature at least 6 K above ambient conditions (up to a maximum temperature of 40 ℃). Also, the chambers were built more than six months prior to the measurements to minimize potential sources of chemical noise possibly originating from the polycarbonate chamber material. In each chamber, two fans ensure homogeneous air mixing of the headspace.

4.2.2. BVOC measurements by PTR-MS

All temporally resolved BVOC measurements were quantified using a PTR-QMS 500 instrument from Ionicon Analytik (Innsbruck, Austria) (see the instrument in Fig. 4.2.2). A description of the instrument can be found in Sect. 2.3.3. This section describes how the PTR-MS was operated and calibrated during the field experiments.

Figure 4.2.2.: The PTR-QMS 500 on its way to the measurement hut.

Settings of the PTR-MS

A number of settings have to be defined for the operation of the instrument, especially regarding the drift tube, which is the chamber where the proton transfer reactions take place. I will briefly indicate the most important settings (see Tab. 4.2), which were chosen in close collaboration with Andrea Ghirardo from the Helmholtz Zentrum München.

Table 4.2.: Settings of the PTR-MS drift tube during the three field experiments. The resulting ratio of the electric field strength and the gas number density (E/N) is given in units of 1 Td which is equivalent to 10^{-17} V cm^{-2} in SI derived units.

Crop species	Pressure [mbar]	Voltage [V]	Temperature [°C]	E/N [Td]
Maize	2.2	599.4	60.0	133.9
Oilseed rape	2.2	600.5	60.0	134.2
Ryegrass	2.2	589.1	60.0	131.6

The main settings for the PTR-MS drift tube were the same for all three campaigns: a pressure of 2.2 mbar, a voltage of around 600 V, and a temperature of 60 °C, which is well within the recommendation of the manufacturer and was also used in studies before (IONICON, 2016; Yuan et al., 2017a). These settings together with constant values of the instrument's components (e.g., length of reaction drift tube) resulted in an E/N of 133 Td (E = the electric field strength, N = the gas number density; 1 Td = 10^{-17} V cm^{-2}). It is generally considered to be favorable for sensitivity keeping the level of the hydronium water clusters ($H_3O^+(H_2O)$) as reagent ions low so that pure hydronium (H_3O^+) dominate (at E/N> 100 Td). I used an E/N at around 133 Td, also to inhibit the effect of monoterpenes fragmentation due to changing relative humidity within the chamber (Tani et al., 2004).

BVOC compound selection was first directed by literature survey and was extended based on experiences made during first test measurements in the field. Finally, 18 compounds for maize, 25 for oilseed rape, and 32 for ryegrass were measured. The m/z values of the selected BVOCs ranged from 21 (H_3O^+) to 225 (potentially $C_{17}H_{20}$ or $C_{13}H_{20}O_3$) (see Tabs. 4.3, 4.4, and 4.5 in the following paragraph for more details on that), which is as far as I am aware, the largest range of molar masses investigated under field conditions. Generally, a molar mass close to 300 g mol^{-1}, is seen as an upper limit of BVOC emissions from plants, especially from the flowers (Knudsen et al., 2006).

All detected compounds with significant emissions

The Tables 4.3, 4.4, and 4.5 show all compounds differentiated by crop which are analyzed in this thesis, including the m/z values, their respective compound names, the molecular formula, and the duration each compound was measured by the PTR-MS. From all compounds measured, those with very small flux rates (maximum hourly mean fluxes < 0.01 nmol m^{-2} s^{-1}) or a negligible amount of significant fluxes (fraction of significant fluxes during measurement period below 10%) were disregarded from further analyses. These are m/z 135, 151, 153, 155, 195, 219, 223, and 225 for the oilseed rape experiment, and m/z 79, 93, 103, 107, 111, 113, 115, 118, 124, 135, 139, 143, 151, 153, 155, 165, 195, 219, 223, and 225, for the ryegrass experiment. The flux calculation from concentration measurements is described in Sect. 4.2.4.

Table 4.3.: Compounds with significant BVOC fluxes from the maize ecosystem measured during Dedelow field experiment 2015, their respective mass to charge ratio (m/z), the molecular formulas, and the dwell time for measuring each compound's concentrations in seconds.

m/z	Measured compound	Abbreviation	Formula	Dwell time
21	Hydronium ions	-	$H_3{}^{18}O^+$	0.2 s
33	Methanol	-	CH_5O^+	2 s
39	Water cluster	-	$H_3O(H_2{}^{18}O)^+$	1 s
45	Acetaldehyde	-	$C_2H_5O^+$	5 s
47	Ethanol	-	$C_2H_7O^+$	1 s
59	Acetone	-	$C_3H_7O^+$	1 s
69	Fragments of pentanal; octanal; nonanal; decanal	m/z 69	-	5 s
71	Unspecified mass feature	m/z 71	-	1 s
99	Hexenal	GLV	$C_6H_{11}O^+$	2 s
101	Hexanal	GLV	$C_6H_{13}O^+$	2 s
107	Xylenes; 1,2,3-trimethyl (fragment)	Xylenes	$C_8H_{11}{}^+$	1 s
137	Monoterpenes (mainly limonene)	MTs	$C_{10}H_{17}{}^+$	5 s
151	(*E*)-4,8-dimethyl-1,3,7-nonatriene	DMNT	$C_{11}H_{19}{}^+$	1 s
153	Camphor; (*E*)-2-caren-4-ol; Methyl salicylate; 4-ethylguaiacol	m/z 153	$C_{10}H_{17}O^+$ $C_8H_9O_3{}^+$ $C_9H_{13}O_2{}^+$	5 s
155	Oxygenated monoterpenes (mainly 1,8-Cineole)	oMTs	$C_{10}H_{19}O^+$	1 s
205	Sesquiterpenes (α-Humulene)	SQTs	$C_{15}H_{25}{}^+$	10 s
225	Unspecified mass feature	m/z 225		1 s

As already described in Sect. 2.3.3, when using the PTR-MS which measures nominal masses, the specific BVOC species can only be identified with certainty by additionally analyzing gas samples via GC-MS. Therefore, I collected altogether 8.4 dm^3 of gas samples when the chambers were closed at a flow rate of 150 cm^3 min^{-1} for 56 minutes (7 times the last 8 minutes of a closed chamber period during daylight at different growth stages). The samples were stored in glass tubes containing TENAX-TA, polydimethylsiloxane (PDMS) foam (Gerstel, Mülheim an der Ruhr, Germany), and graphitized carbon black (GCB) adsorbent material (Carbopack X).

Table 4.4.: Compounds with significant BVOC fluxes from the oilseed rape ecosystem experiment 2016 (see Tab. 4.3 for a detailed caption).

m/z	Measured compound	Abbreviation	Formula	Dwell time
21	Hydronium ions	-	$H_3{}^{18}O^+$	0.2 s
33	Methanol	-	CH_5O^+	1 s
39	Water cluster	-	$H_3O(H_2{}^{18}O)^+$	1 s
45	Acetaldehyde	-	$C_2H_5O^+$	1 s
47	Ethanol	-	$C_2H_7O^+$	1 s
59	Acetone	-	$C_3H_7O^+$	1 s
61	Acetic acid	-	$C_2H_5O_2{}^+$	1 s
69	Isoprene		$C_5H_9{}^+$	5 s
71	Methacrolein, Methyl vinyl ketone	MACR+MVK	$C_4H_7O^+$	2 s
73	Unspecified mass feature	*m/z* 73		1 s
79	Unspecified mass feature	*m/z* 79		1 s
93	Toluene			1 s
99	Hexenal	GLV	$C_6H_{11}O^+$	2 s
101	Hexanal	GLV	$C_6H_{13}O^+$	2 s
107	Xylenes	-	$C_8H_{11}{}^+$	2 s
118	Unspecified mass feature	*m/z* 118	-	2 s
137	Monoterpenes (mainly Thujene, Myrcene, Trans-β-Ocimene)	MTs	$C_{10}H_{17}{}^+$	5 s
205	Sesquiterpenes (Junipene)	SQTs	$C_{15}H_{25}{}^+$	10 s

In addition, gas samples were directly collected from the leaves of each crop species with a portable gas exchange fluorescence system (GFS-3000, Heinz Walz GmbH, Effeltrich, Germany) at 1000 μmol m^{-2} s^{-1} PPFD and 30 ℃. Furthermore, control measurements were taken when chambers were open. The sample tubes were transported to the laboratory at Helmholtz Zentrum München, stored for few days at 4 ℃, and analyzed with GC-MS by Dr. Andrea Ghirardo. A brief description of the method can be found in Sect. 4.3.

Altogether, I was measuring at relatively long dwell times (1–10 s) compared to many studies that measure 0.2–1 s per compound (Bachy et al., 2016; Yuan et al., 2017a). Increasing the dwell times leads to higher accuracies of the measurements but with less data points within 12 minutes per chamber closure, the flux calculation becomes less robust. Thus, choosing a full measuring-cycle duration of about 1 minute

Table 4.5.: Compounds with significant BVOC fluxes from the ryegrass ecosystem experiment 2017 (see Tab. 4.3 for a detailed caption).

m/z	Measured compound	Abbreviation	Formula	Dwell time
21	Hydronium ions	-	$H_3{}^{18}O^+$	0.2 s
33	Methanol	-	CH_5O^+	1 s
39	Water cluster	-	$H_3O(H_2{}^{18}O)^+$	1 s
45	Acetaldehyde	-	$C_2H_5O^+$	1 s
47	Ethanol	-	$C_2H_7O^+$	1 s
59	Acetone	-	$C_3H_7O^+$	1 s
61	Acetic acid	-	$C_2H_5O_2{}^+$	1 s
69	Isoprene		$C_5H_9{}^+$	5 s
71	Methacrolein, Methyl vinyl ketone	MACR+MVK	$C_4H_7O^+$	2 s
73	Methyl ethyl ketone	MEK	$C_4H_9O^+$	1 s
99	Hexenal	-	$C_6H_{11}O^+$	2 s
101	Hexanal	-	$C_6H_{13}O^+$	2 s
137	Monoterpenes (mainly Myrcene)	MTs	$C_{10}H_{17}{}^+$	5 s
205	Sesquiterpenes (Isolongifolene)	SQTs	$C_{15}H_{25}{}^+$	10 s

for the PTR-MS is a compromise between accuracy and number of data points.

Generally, monoterpene concentrations can be measured at *m/z* 137 (the parental ion for $C_{10}H_{16}$) and their fragmentations at *m/z* 81 (Maleknia et al., 2007; Bamberger et al., 2010; Laffineur et al., 2011; Emmerson et al., 2017; Yuan et al., 2017a). I only considered monoterpenes at the parental ion *m/z* 137 because concentrations of *m/z* 81 can also origin from fragmentated hexenal (Tani et al., 2004) which was also significantly emitted during our field experiments. In this thesis, *hexenal* is used as a synonym for all $C_6H_{10}O$ isomers, and *hexanal* for all $C_6H_{12}O$ isomers. Both groups are products from the LOX pathway and contribute to the group of GLVs (see Sect. 2.1.2).

During the maize experiment, I could not clearly identify the compounds measured at *m/z* 69, 71, 153, and 225. The *m/z* 69 is often referred to isoprene in environmental studies (Yuan et al., 2017a). However, similarly to Bachy et al. (2016), I could not detect isoprene by GC-MS analysis, but fragments of the fatty aldehydes pentanal, octanal, nonanal, and decanal instead. Also *m/z* 71, which is commonly attributed to

the sum of the isoprene oxidation products methacrolein (MACR) and methyl vinyl ketone (MVK) (Brilli et al., 2012; Yuan et al., 2017a), remained as an unspecified mass feature. The signal at *m/z* 153 reflected methyl salicylate, camphor, (E)-2-caren-4-ol, and 4-ethylguaiacol. Possible molecular formulas at signal at *m/z* 225 can be $C_{17}H_{20}$ and $C_{13}H_{20}O_3$ (possibly methyl jasmonate). As the proportion of compounds recorded at the same *m/z* could not be determined with certainty by GC-MS, the respective compounds are presented referring to the *m/z* values only.

Compared to the maize experiment, methanol and acetaldehyde were measured with shorter dwell times during the oilseed rape and ryegrass campaign. The results from the maize experiment indicated already highly accurate concentration measurements for these compounds which could therefore be measured in shorter dwell times, gaining some extra time to measure additional masses at *m/z* 61, *m/z* 73, *m/z* 79, *m/z* 93, and *m/z* 118 while keeping the overall measuring cycle at around 1 minute. In 2016, the *m/z* 69 could be clearly related to isoprene as GC-MS analyses suggest. Thus, also *m/z* 71 was likely to origin from isoprene oxidation representing the products methacrolein (MACR) and methyl vinyl ketone (MVK). The components at *m/z* 73, 79, and 118 could not be identified with certainty by GC-MS. Possible candidates for *m/z* 73 are 2-butanone (methyl ethyl ketone, MEK) (Davison et al., 2008) or methyl glyoxal and benzene for *m/z* 79. Generally, the possible compound benzene and the detected compound toluene are often associated to AVOCs. However, it was also shown that these compounds can have biogenic sources (Misztal et al., 2015; Maleknia et al., 2007; Jordan et al., 2009; Baltensperger et al., 2005). The study of Veromann et al. (2013) identified *m/z* 118 as indole.

The dwell times for the ryegrass experiment equal those from the oilseed rape experiment. All compounds measured at specific *m/z* values by PTR-MS could be clearly identified by GC-MS analyses.

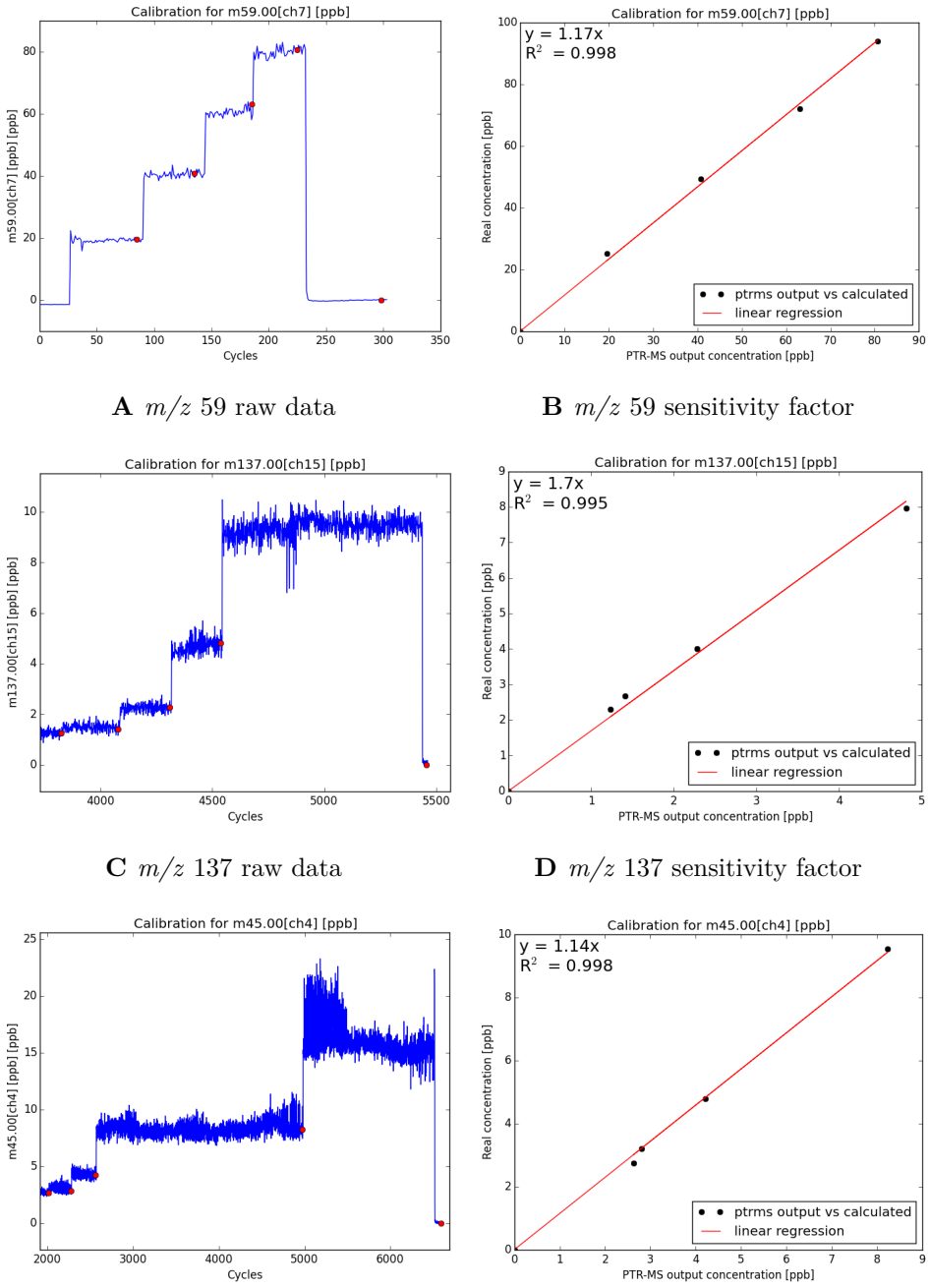

A m/z 59 raw data

B m/z 59 sensitivity factor

C m/z 137 raw data

D m/z 137 sensitivity factor

E m/z 45 raw data

F m/z 45 sensitivity factor

Figure 4.2.3.: Examples of the calibration steps. Left: Raw measured data showing stepwise increase of BVOC concentrations from changing the dilution of BVOC calibration gas with N_2 mass flows. The dots represent mean values which are used for the calibration procedure. Right: Linear regression line of observed (x-axis) and calculated concentrations from a calibration gas cylinder (y-axis) forced through the origin to yield the slope representing the sensitivity factor. **A** and **B** example m/z of maize experiment, **C** and **D** example m/z of oilseed rape experiment, **E** and **F** example m/z of ryegrass experiment.

The calibration procedure

The PTR-MS was calibrated before each field campaign by calculating sensitivity factors for all compounds within a calibration gas cylinder. This sensitivity accounts for the fragmentation within the drift tube of the PTR-MS and for the natural isotopic abundance of each specific compound. As proposed by the manufacturer (IONICON, 2016), the calibration gas was dynamically diluted with N_2 when PTR-MS was already running in operational mode as described before (see Fig. 4.2.3). After several measuring cycles (minimum around 50) with constant flow (controlled by mass flow controllers) and constant BVOC concentrations I either adjusted the mass flow of the calibration gas cylinder or the flow from the N_2 cylinder, in order to reach a BVOC concentration that is twice the expected concentration in the headspace of the chambers. The actual BVOC concentrations could then be calculated from the measured BVOC concentrations, their known uncertainties within the calibration gas cylinder, the N_2 flux and the flux of the calibration gas. For the compounds which were measured during the field experiments but were not present in the calibration gas cylinder, a custom-made setup is used which vaporized liquid VOC standards which is a procedure common at Helmholtz Zentrum München, to detect the fragmentation pattern of the compounds in the drift tube of the PTR-MS.

4.2.3. Observing meteorology, GHG exchanges, and plant physiology

Measurements of meteorological variables, GHG concentrations, and observations of plant physiological and developmental stages were all done by the project partner from ZALF. Different meteorological sensors recorded temperature (field and chamber temperatures), radiation as PPFD (1 W m^{-2} global radiation $\approx 1/(0.45 * 4.57)$ μmol m^{-2} s^{-1} PPFD), precipitation, wind speed, relative humidity, and the atmospheric pressure from July 2015 until the end of 2017. Additionally, the field site is equipped with a fast greenhouse gas analyzer (Los Gatos, San Jose, USA) to detect concentrations of CO_2, CH_4, and H_2O. The main purpose was to determine CO_2 fluxes to get information about net ecosystem CO_2 exchange (NEE), ecosystem respiration (R_{eco}), and gross primary production (GPP). The calculation of these exchange rates are all done by the project partner (Mathias Hoffmann from ZALF).

The methodology is described in detail in Hoffmann et al. (2015, 2018) but will be also briefly explained here. From CO_2 concentration changes during daylight, NEE and R_{eco} (as the sum of autotrophic and heterotrophic respiration) can be calculated similarly to the BVOC flux calculation described in Sect. 4.2.4, by using transparent and opaque chambers. Using calculated R_{eco} from earlier field experiments, a temperature dependent Arrhenius-type R_{eco} model based on Lloyd and Taylor (1994) has been derived, to simulate R_{eco} for the whole experiment, as transparent chamber data were only available during the BVOC flux experiments. Thus, R_{eco} was modeled and GPP could be calculated subtracting R_{eco} from NEE (Hoffmann et al., 2015, 2018).

The aboveground biomass from the three species was determined 3–4 times per growing period from a representative area outside the measurement chambers. After taking the samples from the field, they were weighed, subsequently dried at 105 ℃ for 72 hours in a dry oven and weighed again to detect the specific fresh and dry weight in units of dt ha^{-1} equivalent to 10 g m^{-2}.

Phenological development and growth stages were recorded each week and reported according to the Biologische Bundesanstalt, Bundessortenamt and Chemical industry (BBCH) identification keys for the annual crops maize and oilseed rape from Meier (2001) and for ryegrass according to Gustavsson (2011).

4.2.4. Flux calculation and data analyses

According to the non-steady-state approach, the exchange rate of trace gases is derived as the slope of a linear regression fitted by ordinary least squares to the concentration changes in the headspace during periods of closed chambers. If the slope of a linear regression is not significantly different from zero (H0: the slope of the regression line is zero at $P > 0.05$, two-tailed t distribution test) the ecosystem flux is set to zero. Examples from fitting the different crops are shown in Figs. 4.2.4, 4.2.5, and 4.2.6, respectively. Each time when a chamber closed, I could detect significant concentration changes during daylight hours which were represented well by the slope of linear regressions. Even during the ryegrass experiment with shorter chamber closing times, the results from a linear fit are still meaningful (see Fig. 4.2.6).

Subsequently, I scaled the significant flux rates from units of ppb (nmol mol^{-1}) s^{-1}

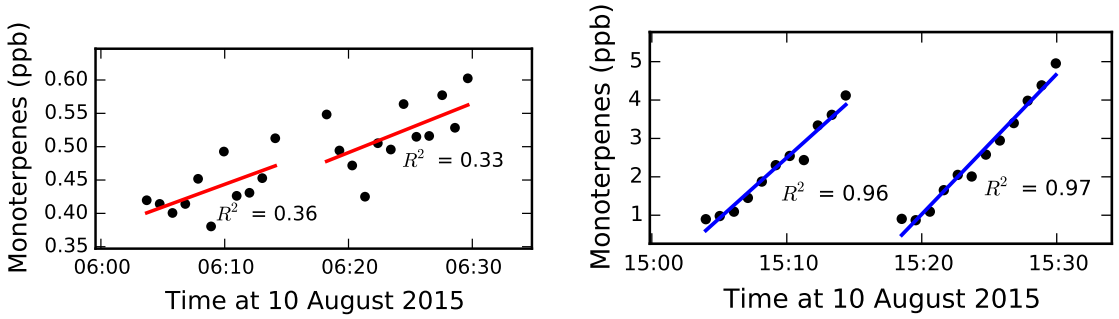

A Early morning insignificant concentration changes

B Significant concentration changes during afternoon

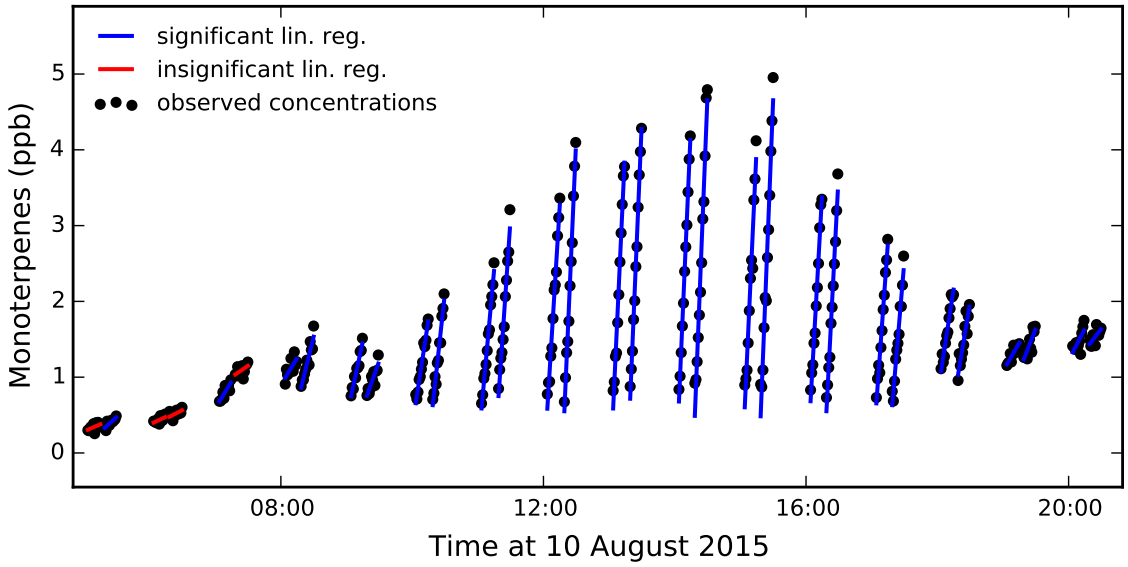

C Entire diurnal cycle

Figure 4.2.4.: Typically observed concentration changes of monoterpenes, as an example of BVOC measurements and flux calculation from maize ecosystem with two chambers during 10 August 2015. For each period of a closed chamber (approx. 12 min), the slope of a linear regression (fitted by ordinary least squares), indicated by blue ($P < 0.05$) and red lines ($P > 0.05$), corresponds to the emission rate in ppb s^{-1}.

($d\mathrm{VOC}_{\mathrm{ppb}}/dt$) to nmol m^{-2} s^{-1} ($d\mathrm{VOC}_{\mathrm{mol\ m^{-2}}}/dt$) by:

$$\frac{d\mathrm{VOC}_{\mathrm{mol\ m^{-2}}}}{dt} = \frac{d\mathrm{VOC}_{\mathrm{ppb}}}{dt} * \frac{V_{\mathrm{Ch}}}{A_{\mathrm{Ch}} * V_m} \tag{4.1}$$

with V_{Ch} as the chamber volume (5.625 m^3), A_{Ch} as base area of the chamber (1.5 m

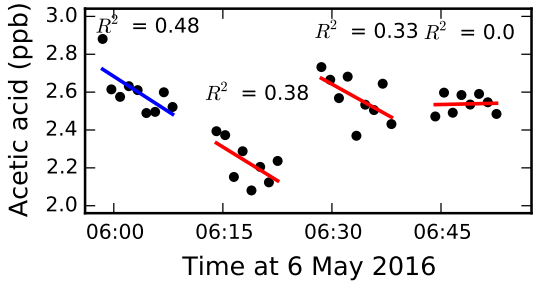

A Early morning significant and insignificant concentration changes

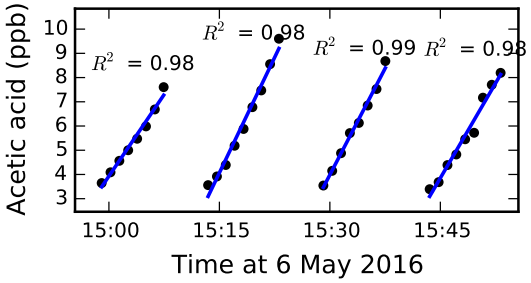

B Significant concentration changes during afternoon

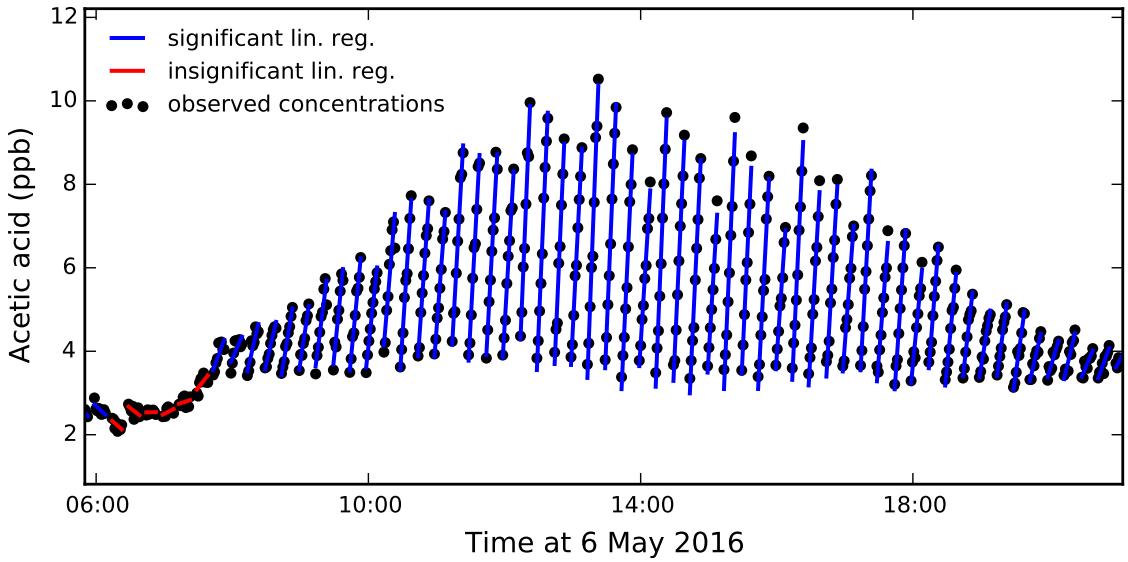

C Entire diurnal cycle

Figure 4.2.5.: Concentration changes and fitted linear regressions of acetic acid from oilseed rape ecosystem with four chambers during 6 May 2016. See Fig. 4.2.4 for a detailed caption.

$\times$ 1.5 m = 2.25 m^2), and V$_m$ as the molar volume calculated by the ideal gas law

$$pV = nR_GT \tag{4.2}$$

rearranged to

$$V_m \equiv \frac{V}{n} = \frac{R_GT}{p} \tag{4.3}$$

with p as the atmospheric pressure, V as the volume of the ideal gas, n as the molar amount of substance, and T as the ambient temperature. All observed chamber

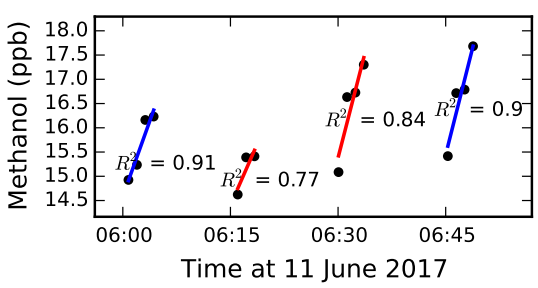

A Early morning significant and insignificant concentration changes

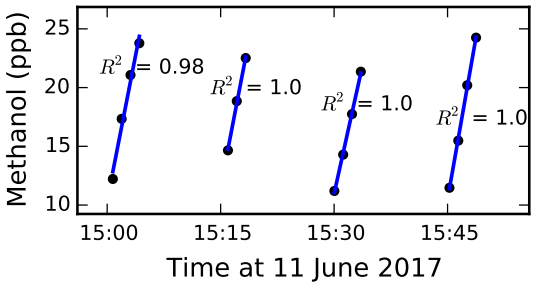

B Significant concentration changes during afternoon

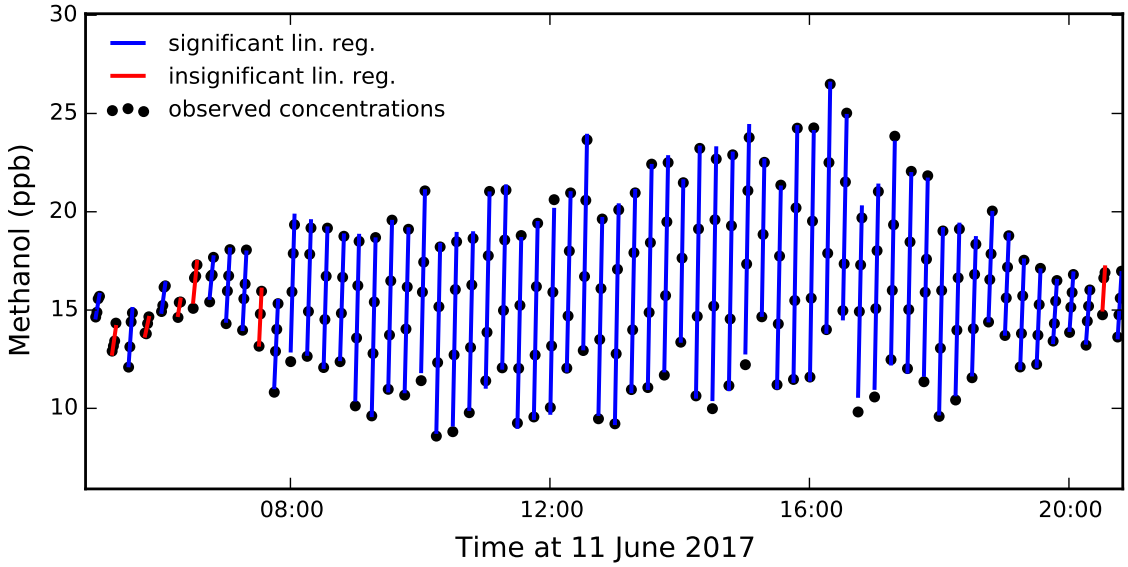

C Entire diurnal cycle

Figure 4.2.6.: Concentration changes of methanol from ryegrass ecosystem with four chambers during 11 June 2017. Note: chambers for ryegrass were closed only for around 4 minutes for half of the entire experiment. See Fig. 4.2.4 for a detailed caption.

fluxes were aggregated to hourly fluxes by averaging calculated fluxes within one hour (2 fluxes for maize and 4 fluxes for oilseed rape and ryegrass campaign). The variability of hourly fluxes is determined by the standard deviation (if there is a minimum of three observed fluxes, thus, the plotted error bars are $2^*\sigma$) as the well as the range of the data (if the observed fluxes are equal to two fluxes only). The variability of daily fluxes is given as the standard error of the mean of all hourly fluxes by $\sigma/\sqrt{N}$ with N as the number of hourly fluxes (normally 24) or as the standard error of the sum by $\sigma * \sqrt{N}$. Generally, positive and negative fluxes indicate net ecosystem emissions and

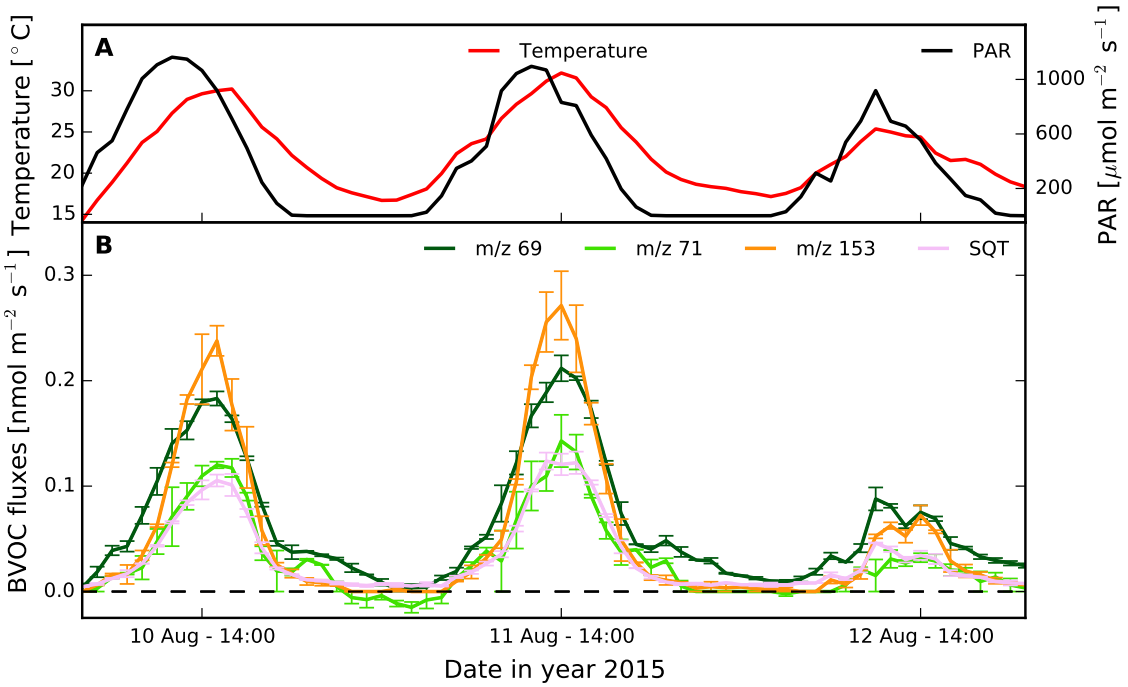

Figure 4.2.7.: Diurnal cycles of maize ecosystem from 10–12 August 2015 of **A** Hourly mean temperature and photosynthetically active radiation (PAR) and **B** hourly mean emission rates of selected BVOCs with similar magnitude, with minimum and maximum values as error bars ($N = 2$).

depositions, respectively. Our observations from all three field experiments show, that the concentrations of many compounds did not significantly change during night, as the examples of hourly flux rates shown in Figs. 4.2.7, 4.2.8, and 4.2.9 demonstrate. This indicates that the production of most of the BVOCs is strongly light-dependent, considering that stomata controls have no effect on highly volatile terpenoids (Niinemets et al., 2004). Also, for water-soluble compounds such as methanol, a stomatal control which would be indicated by an emission burst in the morning, was seldom detected. In contrast, the slopes of concentration changes of all emitted compounds slowly rise during the morning hours until a maximum is reached which generally appears in the early afternoon, and then subsequently decreases again. This diurnal cycle is temperature- and light-dependent, with emission maxima coinciding with the maxima of integrated radiation and temperature. Emission minima can be observed in the night.

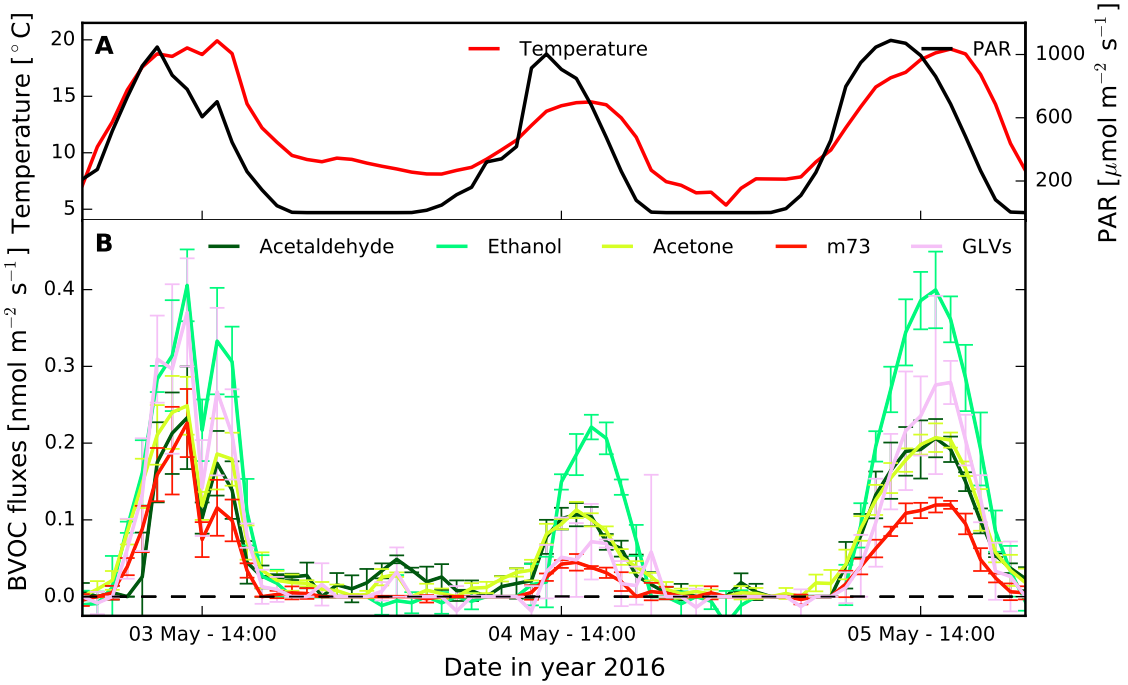

Figure 4.2.8.: Diurnal cycles of oilseed rape ecosystem from 3–5 May 2016 with standard deviation as error bars ($N = 4$). See Fig. 4.2.7 for a detailed caption.

Calculation of standard emission factors

Most of the observational studies provide plant species-specific and BVOC-specific SEFs of the conducted measurements which are used as an input for modeling studies. However, there is no common approach or standardized procedure about the calculation of these factors except that they should relate to 30 °C and 1000 μmol m^{-2} s^{-1} photosynthetic photon flux density (PPFD) (cf. Kesselmeier and Staudt, 1999; Steinbrecher et al., 2009; Karl et al., 2009). Additionally, there is no common sense about the unit the factor should be scaled to. Some studies report scaling to leaf area, to the ground area or to the plant biomass (normally the leaf dry weight) (Kesselmeier and Staudt, 1999; Das et al., 2003; Graus et al., 2013; Bachy et al., 2016). When measurements can be conducted under controlled environmental conditions (either in the laboratory or e.g. by portable gas exchange fluorescence system controlling temperature, radiation and CO_2 conditions of small volume with a basal area of e.g. around 8 cm^2). SEFs can then be directly measured under standard temperature and radiation conditions. However, this approach is only applicable for

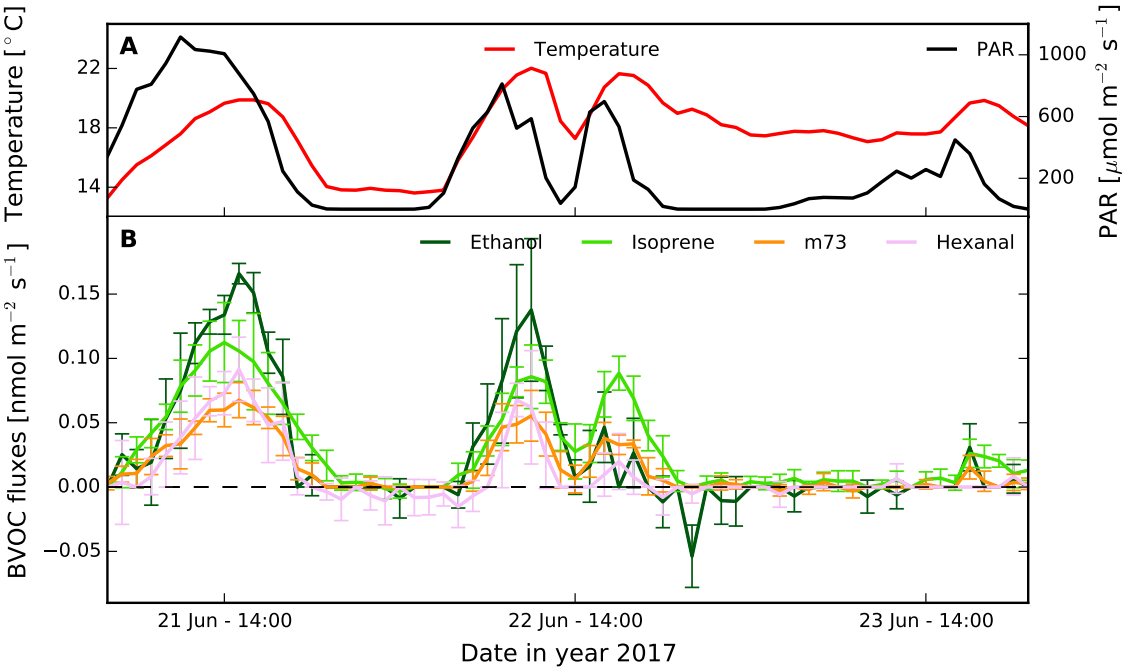

Figure 4.2.9.: Diurnal cycles of ryegrass ecosystem from 21–23 June 2017 with standard deviation as error bars ($N = 4$). See Fig. 4.2.7 for a detailed caption.

field experiments if there are enough measurement points of emissions that cover a sufficiently long period during these conditions (Bachy et al., 2016). From a modeling perspective, it is also possible to fit a given emission model to the observations, which results in a SEF that implicitly considers the assumptions of the chosen model. This however means, that the SEF can substantially vary depending on the choice of emission model (Langford et al., 2017). Most studies use the model from Guenther et al. (1993) and Guenther (1997), as it is relatively simple to be applied (Langford et al., 2017). Thus, I followed this approach and used the model form Guenther et al. (1993) to calculate SEFs from observed hourly mean values (daytime and night-time) during different plant growth stages for compounds with temperature dependence only (pool emissions). Figure 4.2.10 (and Figs. A.2.1 and A.2.2 in the appendix) shows examples of SEF results either during periods with ambient conditions near environmental standard conditions (28–32 °C), or by applying the Guenther et al. (1993) model (see Eq. 2.13) with field observations. Therefore, different methods are applied: (1) rearranging the equation and solving for SEF; (2) curve fitting by adjusting SEF to measurements; and (3) curve fitting by adjusting SEF as well as the β-coefficient (the curvature parameter) to the measurements. The curve fitting

was computed via the Levenburg-Marquardt algorithm with nonlinear least squares which is part of the optimization tool within PYTHON SCIPY library (v0.14.0).

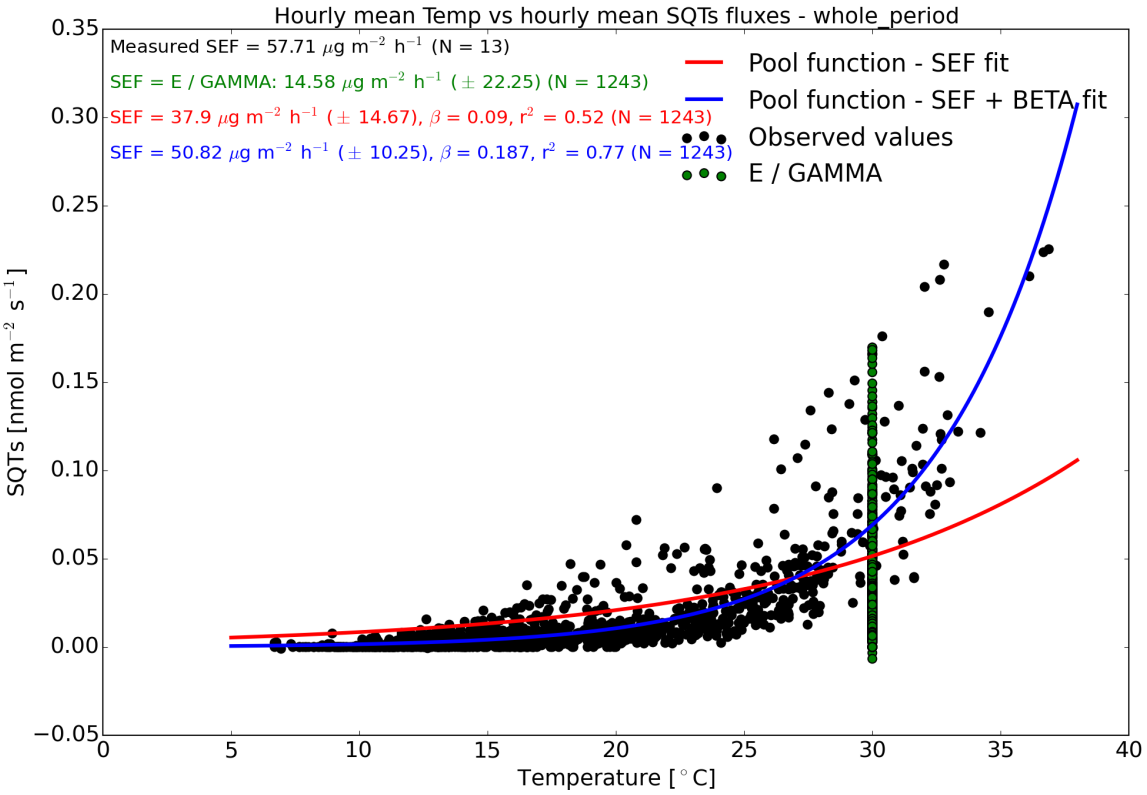

Figure 4.2.10.: Variabilities of standardized emission factors (SEFs) of sesquiterpenes from maize ecosystem by calculating and curve fitting to the Guenther et al. (1993) model from hourly mean temperature and BVOC emission rates of the whole observed growing season as an example from the different crop field experiments.

For the calculation from direct measurements there are only 13 hourly mean values during the maize experiment (zero values during oilseed rape and 5 during ryegrass experiment). Altogether, resulting SEFs vary strongly and their uncertainties are large. By additionally fitting the β-coefficient, I could notably improve the model (compare red and blue line in Fig. 4.2.10 with $R^2 = 0.52$ and 0.77, respectively) in particular for low and high temperatures, with β still being in a range which was reported before (Tarvainen et al., 2005). By fitting both parameters, the SEF as well as the β-coefficient to all my observations from three different crop species (see appendix Tabs. A.1, A.2, and A.3), results improved considerably compared to a fit of the SEF alone. The fraction of explained variance of a linear regression between modeled and observed emissions (R^2) increased by 53.8, 27.0, and 87.6 %, and the

standard error decreased by 19.3, 16.3, and 10.6 % for the maize, oilseed rape, and ryegrass experiment, respectively. It should be noted that increasing the β-coefficient results in lower calculated emission values below the standard temperature of 30 °C. Thus, fitting parameters with data from relatively cold periods tends to derive higher β-coefficients. In Fig. 4.2.10, the resulting graphs of both kinds of fitting are shown for sesquiterpene emissions from maize. Despite considerable different SEFs, the inferiority of the simple SEF fitting is apparent, indicating the importance of β-coefficient adjustment.

I decided to scale the calculated SEFs to the entire plant's aboveground biomass in units of ng g^{-1}DW h^{-1}, instead of scaling to leaf biomass alone, which would be the common approach especially for tree species. The reason is, that field observations of crops rarely distinguish between the aboveground plant compartments as it is done for trees (trunk, branches, leaves). In addition, the distinction between compartments is often not quite clear with crops having green stalks that are also able to photosynthesize and emit trace gases. Especially with respect to modeling, crops are often regarded in terms of biomass or yield (Müller et al., 2017), especially on a regional or global scale (Li et al., 2018). As the biomass of the plants varies over the experiment period, observed emissions are related to the biomass value obtained by linearly interpolating between two biomass measurement points.

Statistical significances

The Kruskal-Wallis H-test examines if the null hypothesis that samples originate from the same population is true. It is used in this study to detect significant differences ($P < 0.05/0.01$) between BVOC emission rates, ambient temperature, and radiation in specific meteorological and plant physiological periods. This non-parametric version of an analysis of variance (ANOVA) procedure is preferred over a parametric test because the assumption of normally distributed samples with equal standard deviations (homoscedasticity) (Kruskal and Wallis, 1952) could not always be fulfilled. All statistical tests for significance were performed using Python Library SciPy (v0.14.0).

4.3. Analyses in the laboratory

BVOCs emitted into the headspace of the closed chambers were also collected for offline GC-MS analyses to chemically identify the specific compounds. The whole laboratory analyses were done by the project partner at the Helmholtz Zentrum München (execution by Dr. Andrea Ghirardo), which is why it is only briefly described in this section. The results from this work are incorporated in Tabs. 4.3, 4.4, and 4.5.

In the field, air samples were taken with a constant flow of 150 cm^3 min^{-1} from the closed chambers for exactly 56 minutes. The samples were stored in glass cartridges filled with 40 mg TENAX-TA 60/80 and 10 mg carbopack X 40/60. The offline analysis was carried out by thermal desorption (TD, Gerstel) and GC-MS (GC type: 7890A; MS type: 5975C; both from Agilent Technologies, Palo Alto, CA, USA) (see Ghirardo et al., 2012, 2016; Weikl et al., 2016, for details). Thereby the samples were thermally desorbed by increasing the temperature at a rate of 280 ℃ min^{-1} to 270 ℃, subsequently cryo-refocused on TENAX-TA at -50 ℃ for 19 s and reinjected by increasing the temperature again at a rate of 12 ℃ min^{-1} to 270 ℃.

BVOCs were qualitatively identified by comparing the retention time (RT) and mass spectra with those of liquid calibration standards. Those compounds without a standard were identified by comparing its kovats retention index (a normalized retention time) and mass spectra with those from the National Institute of Standards and Technology Mass Spectral Library (NIST) and Wiley library (v.275). The sampling procedure was repeated at least 4 times and compared to controls from open chambers. Only those compounds with significantly high emissions recorded during closed chambers were considered in the further analyses. The TD-GC-MS data indicate negligible source of polycarbonate compounds originated from the chambers.

4.4. Biogeochemical modeling of the observed processes

After conducting the field measurements, which is the first objective of this thesis, the second task is to simulate a full seasonal cycle of BVOC emissions from the different bioenergy crops by using the process based emission model `JJv` (see Sect. 2.4.2)

within the LandscapeDNDC framework (see Sect. 2.4.3). Therefore, I began with implementing the JJv model into LandscapeDNDC and compiled all necessary input and evaluation data. This includes initializing the two arable sites used for the measurements (one for maize and ryegrass and one for oilseed rape experiments). Finally, I calibrated parameters for plant physiology and BVOC emissions. Furthermore, new modules, functions, and I/O processing needed elaboration for which I further developed LandscapeDNDC (which is written in C++ programming language) and developed solutions in python.

4.4.1. Model setup for field experiment

To set up and run LandscapeDNDC for a particular site, several files need to be created. These are the external driving forces of meteorological input data, information about the site itself (especially about soil characteristics), how the agricultural site was managed during the simulation. The latter also includes the species that is cultivated, the time of planting, and the properties of the plants initial state. Optionally plant and soil specific parameter values my be adjusted in case default parameters are not available or suitable.

Meteorological input and evaluation data

From meteorological measurements conducted in the field during the experiments, I compiled an input txt file containing hourly information on temperature, precipitation, radiation, relative humidity, wind speed, and atmospheric pressure. These data are used by the canopy microclimate module ECM Grote et al. (2009) to alter micrometeorological conditions within the canopy especially radiative transfer (extinction coefficient concept) and temperature distribution within the canopy (depending on leaf area), as well as in the soil (Kraus et al., 2015).

Data of plant growth, physiology, and gas exchange were used to calibrate and evaluate the model. These are measurements of aboveground biomass, and CO_2 as well BVOC concentration, from which NEE, R_{eco}, GPP, and BVOC fluxes were calculated.

Site files

Two sites, with the notation CarboZALF-D14 and CarboZALF-D15, were initialized with soil property characteristics provided from ZALF. The respective `xml` files can be found in the appendix in Sect. E.1. The soil is divided into several vertical layers with different depths and information about the soil type, texture (sand, clay, silt), organic carbon content, pH, and the bulk density. Missing information such as water holding capacity is internally calculated from soil texture. This information is used by the soil chemistry model $MeTr^x$ (see Kraus et al., 2015, 2016, for more information) to simulate the soil carbon and nitrogen cycle mainly by decomposition and mineralization of soil organic matter as well as nitrification and denitrification processes in order to provide the plants with nutrients (i.e. nitrogen as ammonium NH_4^+ and nitrate NO_3^-).

Management files

Based on the three years of meteorological input data, it was decided to repeat each crop simulation experiment three times, which resulted in three years of simulated data from maize, oilseed rape, and ryegrass. Only the results of the year in which the respective crop has actually grown was used for evaluation. The other simulations are used to demonstrate the robustness of the modeling approach and the sensitivity of the BVOC emissions to variations in meteorology and plant growth. In the `xml` management files, also management practices were assumed to be equal in each year. The description of the management procedures (seeding, fertilizing, cutting, harvesting) were taken from the field management protocols provided from ZALF and can be found in the appendix in Sect. E.2 and Ch. C. The only deviation is regarding the ryegrass management, which stopped around one month after the third cutting event at the beginning of September 2017. Following the management guidelines of the ryegrass cultivar Country 2051 (Deutsche Saatveredelung AG, 2015, and personnel communication with Dr. Gernot Verch, ZALF), two additional (fictive) cut events were introduced in 2017.

Species parameter files

In order to simulate plant growth, physiology, and photosynthesis, any model needs parameters to reflect empirically observed responses or genetically determined reactions to the environment. These parameters are generally considered to be species-specific and thus describe differences between plant species.

Some databases exist that provide parameters which are typically used in many models for plant functional types or specific species. However, these values are obtained from various studies and include a considerable uncertainty. In order to simulate BVOC emissions from plants that represent observed vegetation properties as close as possible, sensitive parameters thus need to be adjusted within the range of reasonable values. Regarding this study, in particular photosynthesis and leaf area (or leaf biomass) have the biggest plant specific impacts on simulating BVOC emissions when using the `JJv` model.

So, I focused on parameter adjustment to represent biomass and photosynthesis as it was observed in the field. The whole set of adjusted parameters within the species-specific parameter `xml` files can be found the appendix in Sect. E.3. Parameter adjustment (excluding BVOC emission-related parameters) for all three crop species was carried out with the help of colleagues at KIT/IMK-IFU Rüdiger Grote (also supervisor of this thesis) and David Kraus.

For the simulation of plant growth and physiology, the model PlaMo^{x} (used in Kraus et al., 2015, 2016) was used as a module within `LandscapeDNDC`. Some parameters that are used by this model are directly provided from measurements, i.e. optimum values for specific leaf area, leaf biomass, and plant height. Others such as carbon and nitrogen content as well as senescence processes of the different plant compartments were adjusted so that observed values of LAI and biomass could be reasonably well represented. Furthermore, growing degree days (GDD) related parameters that impact the allocation of assimilated carbon during different growth stages and for different plant compartments have been adjusted based on phenological observations.

For modelling NEE, R_{eco}, and GPP, the process-based approaches for photosynthesis and stomatal conductance of Farquhar et al. (1980) and Ball et al. (1987) modified by Collatz et al. (1992) is applied, which are part of the PlaMo^{x} model. The most important parameters for this approach are describing the activity state of ribulose-

1,5-bisphosphate carboxylase/oxygenase enzyme (Rubisco) at 25 °C (V_{cmax25}), and leaf stomatal conductivity for water as well as CO_2. These were calibrated to represent measured values of gas exchange. It should be noted that this parameterization also affects BVOC emission calculation, as for example V_{cmax25} determines the electron transport rate. Generally, adjusting plant growth and photosynthesis is an iterative process, as e.g. higher leaf biomass leads to higher GPP values, whereas adjusting V_{cmax25} changes photosynthetic capacity and in turn carbon allocation used for plant growth and thus leads to higher values of plant (and leaf) biomass. The results from model parameter adjustments to simulate the aboveground biomass and GPP will be described and discussed in detail for each of the species in sections 5.1.2, 5.2.2, and 5.3.2.

Furthermore, the species specific BVOC emission parameters SEF, light dependent fraction (LDF), and β-coefficient, are also given in the species parameter file. These were determined by fitting the `JJv` stand-alone model (see Sect. 4.4.2) to emission measurements which will be explained in more detail in Sect. 4.4.3.

4.4.2. Implementation and development of the BVOC emission model (`JJv`)

The `JJv` model (also called energetic status model) as a process based semi-mechanistic approach for simulating light dependent BVOC emissions and is described in Harrison et al. (2013), Morfopoulos et al. (2013, 2014), and Grote et al. (2014).

In order to test the sensitivity and simplify parameterization, I firstly wrote a stand-alone version, which was modular enough to be later implemented into other ecosystem- or land-use models such as the `LandscapeDNDC` framework. The implementation into `LandscapeDNDC` has then enabled to investigate the seasonal development of emissions considering crop management and plant phenology.

`JJv` as a stand-alone

The stand-alone model accurately follows Grote et al. (2014) especially by using the proposed photosynthesis functions from Collatz et al. (1991) as implemented in the Community Land Model `CLM` version 4.0 described in Oleson et al. (2010). The model

is written in python and can be found in the appendix in Sect. F.1. However, the model has only been evaluated yet for emissions from trees (poplar, aspen, eucalypt, sweetgum, and oak). Thus, the first task was to test if the model is capable to be also used with the species-specific photosynthesis parameters typically used for crops, i.e. maize, oilseed rape, and ryegrass (see Tab. 4.6).

Table 4.6.: Species specific photosynthesis parameters for maize, oilseed rape, and ryegrass from literature based adjustments to observations. These parameters are also used to simulate the BVOC emission potential.

Parameter description	Abbreviation [Unit]	Values for Maize	Oilseed rape	Ryegrass
Activation energy for J	AEJM [J mol^{-1}]	77900	37000	46270
Michaelis-Menten coefficient for CO_2 at 25 ℃	K_{C25} [μmol mol^{-1}]	650	260	260
Michaelis-Menten coefficient for O_2 at 25 ℃	K_{O25} [mmol mol^{-1}]	450	179	179
Saturated activity state of Rubisco at 25 ℃	V_{cmax25} [μmol m^{-2} s^{-1}]	130	61	60
Ratio between saturated electron transport rate at 25 ℃ and V_{cmax25}	QJVC [/]	2.25	3.07	2.8
Curvature parameter of J	Θ [/]	0.97	0.9	0.9

The resulting emission response curves can be found in Fig. 4.4.1. According to the different parameterizations, oilseed rape and ryegrass emissions respond similarly to increasing PPFD as trees represented by the data from Grote et al. (2014). Maize shows the lowest potential emission increase especially for low light conditions. Regarding temperature, the emission response of maize is smaller in the beginning but considerably higher than those of other species beyond 30 ℃. The responsible parameter for this reaction is the activation energy for electron transport, AEJM (Grote et al., 2014) which is highest for maize (77900 J mol^{-1}) compared to 37000 and 46270 J mol^{-1} from oilseed rape and ryegrass, respectively. In contrast, higher values of the Michaelis-Menten coefficients for CO_2 and O_2 at 25 ℃ (KC25 and KO25), and especially of V_{cmax25} for maize, lead to higher electron consumption by photosynthesis (J_v) at the same electron supply level (J) compared to the other species and thus to a lower emission potential following the model logic that emissions are related to the result from $J - J_v$.

The dimensionless parameters c_1 and c_2 for the calculation of the photosynthetic emission potential (γ_{ph}, see Eq. 2.25) as well as the enzymatic deactivation energy (ΔH_{d_en}) and the enzyme entropy term (ΔS_{en}) for the calculation of the enzymatic emission potential (γ_{en}, see Eq. 2.26) do generally vary between different plant species but were not changed within this thesis. Instead, the value given by Grote et al. (2014) is used, who derived the dimensionless parameters from observations by using a fractional term ($rc = c_2/c_1 = 0.0157$). The study further evaluated the sensitivity of the model to a reasonable range of values ($rc = 0.001$–0.02) and concluded that temperature and radiation responses were not very responsive to these changes. However, the CO_2 response is affected under elevated ambient CO_2 conditions when using a different ratio. As I apply the model only under recent ambient CO_2 mixing ratios of around 400 ppm, I don't expect substantial impacts when using a fixed value for c_1 and c_2. Species specific values for ΔH_{d_en} and ΔS_{en} can be rarely found in literature, and thus are often used as constant values for most of the species or plant functional types in many models (Collatz et al., 1991; Grote et al., 2014).

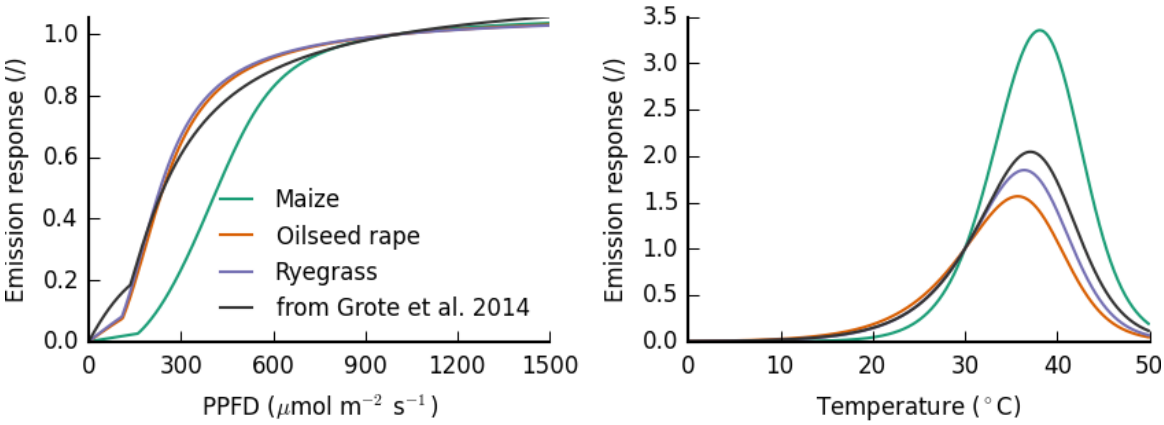

Figure 4.4.1.: BVOC *de novo* emission potentials depending on temperature and PPFD based on `JJv` (see Eq. 2.27) with different parameter sets adjusted to maize, oilseed rape, and ryegrass field experiments and directly from Grote et al. (2014). Left: emission response depending on PPFD only (const. T=30 °C); Right: emission response depending on temperature only (const. PPFD=1000 μmol m^{-2} s^{-1}).

Thus, as these first results from `JJv` stand-alone have shown, plant physiological parameters from bioenergy crop ecosystems may lead to different temperature and PPFD emission responses than those of trees, but are well within an expected range to describe light depend BVOC emissions. In a second step, this model version should serve as a tool to fit species specific BVOC emission parameters from observations

which can then be used for the version which is implemented in `LandscapeDNDC`. So, the implementation is explained in the next paragraph followed by a description of the fitting procedure.

`JJv` implemented in `LandscapeDNDC`

The biggest challenge of implementing `JJv` into `LandscapeDNDC` was to translate it to `C++` and couple it to `LandscapeDNDC` so that all meteorological and physiological variables are correctly provided. Thereby, it is important to follow the general simulation strategy of `LandscapeDNDC`, as it divides the plant canopy into different layers, representing varying micrometeorological conditions (especially radiation, temperature, and water vapor) and biomass distribution. All plant-gas exchange-related processes are calculated separately for each canopy layer. The number and height of the layers dynamically change with plant height. Photosynthesis and BVOC emissions are calculated twice for each layer because leaf area of each canopy layer is dynamically partitioned into sunlit and shaded leaves. The consideration of canopy structure enables the scaling from the leaf-level, reflected by the stand-alone model, to a dynamic ecosystem approach. The structure is thus used to calculate an input pattern of environmental variables in any specific point in time, i.e. the amount of absorbed PPFD and the leaf temperature. Thus, enzyme activities (after Long, 1991), and electron transport rates (after Pury and Farquhar, 1997; von Caemmerer et al., 2009) are calculated twice for each canopy layer for each time step. Apart from the implementation into the ecosystem model structure, photosynthetic variables that were needed for the BVOC calculations to operate needed to be produced and transferred to the `JJv` module. These were in particular several variables that reflect standard conditions for BVOC production regarding temperature, PPFD, and CO_2 (note: for photosynthesis the standard temperature is defined at 25 ℃ whereas for BVOC emissions at 30 ℃). Additionally, I implemented the following variables in their standardized form into the photosynthesis model structure: the Michaelis-Menten coefficients for CO_2 and O_2 reactions of Rubisco (K_{C_std}, K_{O_std}), the saturated activity state of Rubisco (V_{cmax_std}), the saturated electron transport rate (J_{max_std}), the photosynthetic CO_2 compensation (Γ^*_{std}), and the leaf intercellular CO_2 and O_2 mole fraction. The implemented model can be found in the appendix in Sect. F.2.

4.4.3. Fitting of BVOC emission parameters to the joint JJv–pool emission model

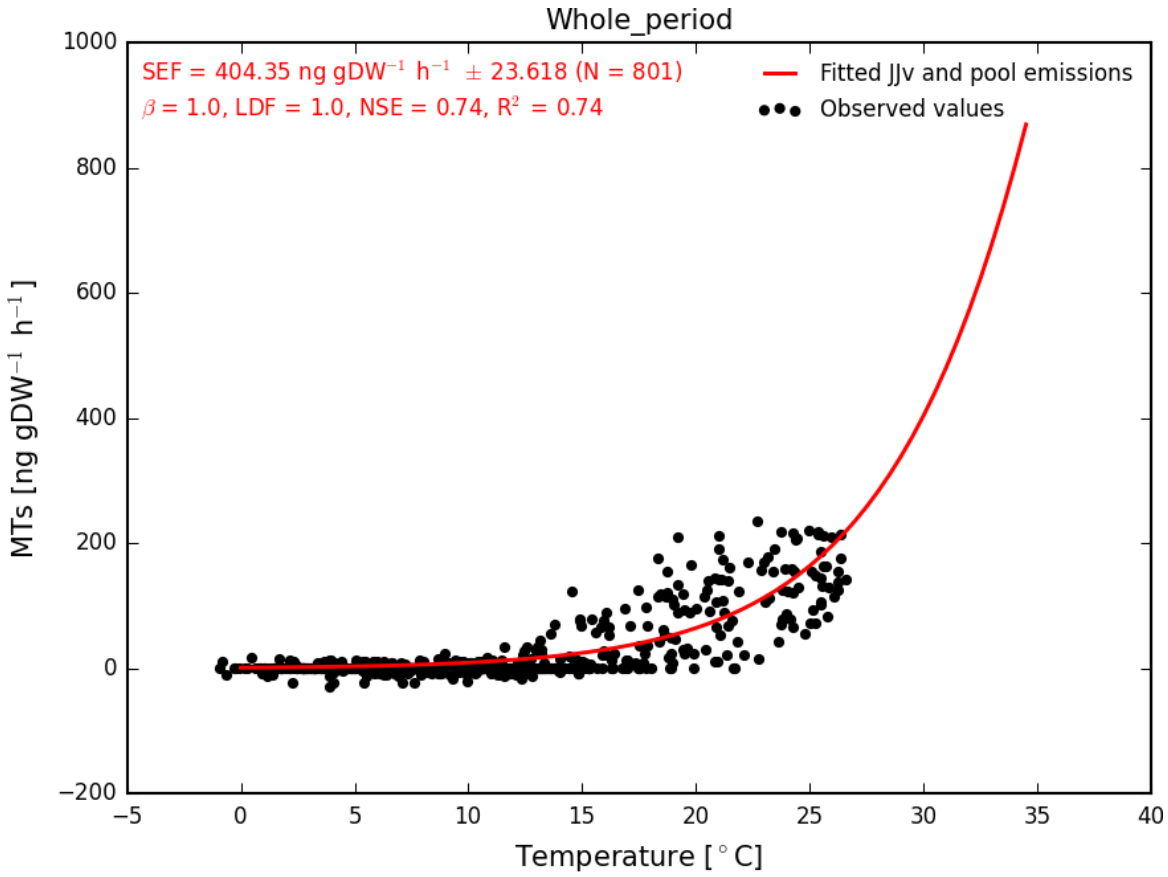

Figure 4.4.2.: Example of fitting SEF, β-coefficient and LDF from houlry observed oilseed rape monoterpenes emissions to the joint JJv–pool emission stand-alone. As the best LDF according to Nash-Sutcliffe modeling efficiency (NSE) resulted in 1, JJv stand-alone without pool emissions was used for the emission response curve.

The procedure to fit SEFs from observed BVOCs emissions from different plant species is the crucial step from observations to modeling. In most cases SEF and other important parameters depending on the chosen emission model, are selected from literature. Here, observations are exclusively available so that relevant parameters could be developed from data. As already mentioned before, the fitted parameter values can strongly vary depending on the chosen model approach (Langford et al., 2017), and also with different fitting procedures (see Sect. 4.2.4).

Additionally, as already pointed out in Sect. 2.4.1, many BVOCs can be emitted

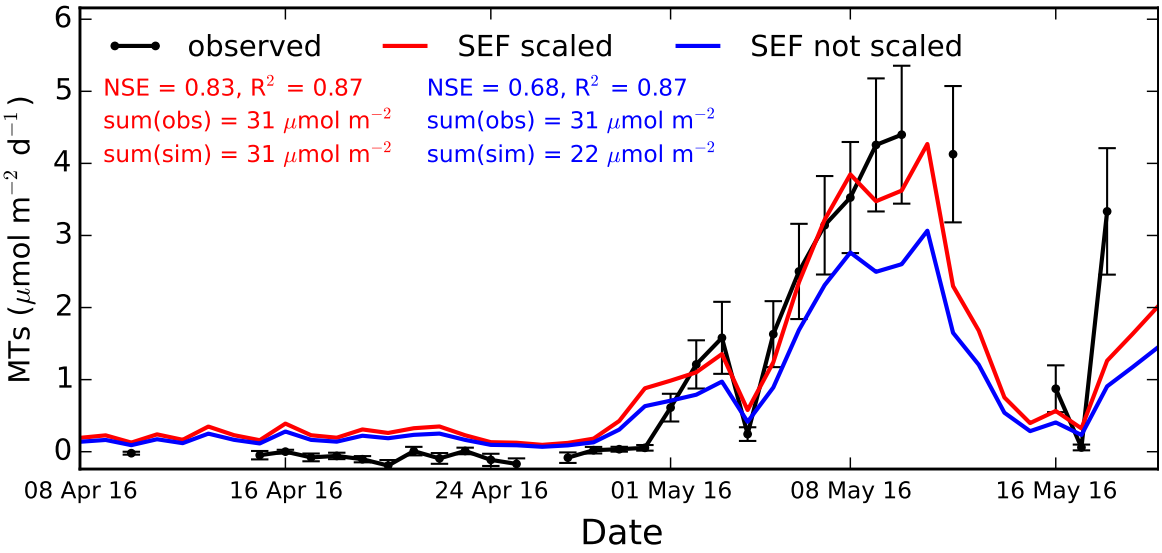

Figure 4.4.3.: Observed and simulated daily sum monoterpenes emissions from oilseed rape as a showcase of fitted (blue line) as well as fitted and scaled (red line) standardized emission factor (SEF) within `LandscapeDNDC`. The NSE, coefficient of determination (R^2) and sum of coinciding observed and simulated values are also given in the respective color. Error bars of observed emissions indicate the standard error of the daily sum with $N = 24$.

from storages and from *de novo* biosynthesis at the same time. Thus, some BVOC emissions can be more mechanistically calculated by fractioning each compound emission into a light dependent fraction (LDF) term considering *de novo* synthesized emissions and a light independent term (1− LDF) considering pool emissions, and thereby significantly improve the simulation result (Ghirardo et al., 2010; Stavrakou et al., 2011; Guenther et al., 2012; Mozaffar et al., 2017). The emission model `MEGAN` v2.1 from Guenther et al. (2012) already proposes LDF values for a number of BVOCs. However, to my knowledge, there is no reference or description of how to derive LDF values. The study of Ghirardo et al. (2010) calculated an LDF value for monoterpene emissions from Scots pine based on laboratory experiments by stable isotope $^{13}CO_2$ labeling. Stavrakou et al. (2011) arbitrarily set an LDF for methanol to the value of 0.8 and Mozaffar et al. (2017) used that value with slight improvements by empirically derived changes of ±0.1. My first analyses of night-time hourly flux rates from maize, oilseed rape, and ryegrass did also indicate that the production of most of the BVOCs is strongly light-dependent. Thus, I also decided to divide BVOC emissions into *de novo* and pool emission by using the `JJv` model for the LDF and the pool emission

algorithm of Guenther et al. (1993) for temperature dependent evaporation, following

$$E_{\text{bvoc}} = \text{SEF}_{\text{bvoc}} * [\text{LDF} * \gamma_{\text{ph\_rel}} * \gamma_{\text{en\_rel}} + (1 - \text{LDF}) * \exp\{\beta(T - T_S)\}] \quad (4.4)$$

However, it is difficult to separate between light dependent *de novo* and light independent pool emissions, using data from field observations where PPFD and temperature are correlated (Ghirardo et al., 2010). A first approach was to fit the pool emission function to night emissions only and subsequently fit the `JJv` model to the deviation between daylight observations and daylight simulations from pool emissions. However, part of the emissions were also influenced by decreased stomatal conductance during the night leading to negligible emissions which should be dedicated to pools. Therefore, BVOC emissions were calculated with a large number of LDFs and the one which fitted the results best were chosen for further simulations. The procedure required a-priori fitting of SEFs and β-coefficients and is described in more detail in Sect. 4.2.4. For the calculations, the joint `JJv`–pool emission approach as stand-alone was used. The decision about the best-fit was done using the Nash-Sutcliffe modeling efficiency (NSE) which is one of the most widely used goodness of fit test statistic between modeled and observed data (Niinemets et al., 2013; Krause et al., 2005) and is defined as

$$\text{NSE} = 1 - \frac{\sum_{i=1}^{n}(O_i - P_i)^2}{\sum_{i=1}^{n}(O_i - \bar{O})^2} \quad (4.5)$$

with O_i as the observed values and P_i as the predicted values, resulting in values of NSE between 1 (perfect fit) and $-\infty$. Values lower than zero indicate that the average of the observations would be a better predictor than the model itself. In contrast to R^2, the NSE is sensitive to systematic model over- or underestimation. All calculated parameters for the three crop species are reported in Tab. 5.2, 5.5, and 5.8 and discussed in Sects. 5.1.1, 5.2.1, and 5.3.1. I am using LDFs for all measured compounds except for isoprene (LDF= 1), which is too volatile to be stored in any specific structure.

Additionally, I scaled the SEFs so that the sum of all simulated emissions by `JJv` in `LandscapeDNDC` equals the sum of all coinciding observed emissions for each compound. The purpose of scaling the SEF is to better represent the sum of emitted BVOCs during the period of the field experiment. Reasons for short-term deviations

could be related to changing emission pattern due to the development and retreat of different plant tissues since each of the three field experiments was conducted during a minimum of two different plant development stages. Also, potentially changing plant metabolism as a result of plant development, can lead to different BVOC compositions. A linear scaling to the observed overall sum of emissions is thus not only ensuring more reliable multi-year estimates but also enable to detect deviations that are caused by periodically occurring processes that are not considered to affect BVOC emissions in the ecosystem model. Scaling the SEFs increased the NSE of daily mean emissions on average by 21.2, 15.1, 64.0 % for the maize, oilseed rape, and ryegrass experiment respectively (see Tabs. 5.3, 5.6, and 5.9 for SEF values before and after scaling). The values of R^2 did not change as this measure is insensitive to linear changes of the magnitude of the simulated emissions. Figure 4.4.2 shows an example of fitting SEF, LDF, and β-coefficient to the joint `JJv`–pool emission stand-alone, and its application with additional scaling of SEF within `LandscapeDNDC` in Fig. 4.4.3.

Nonetheless, as this procedure is extremely dependent on the coupling of the `JJv` model to the model which represents photosynthesis and plant physiology, the transfer of the resulting final SEF values to other ecosystem models is subject to further uncertainties depending on the differences between model frameworks. Hence, comparing SEFs in a broader context, especially with reported values from other studies and other crops, will be based only on the fitted SEF values without scaling.

5. Results of observed and simulated BVOC fluxes

This chapter describes and discusses the results which were obtained by employing the measurement and modeling techniques explained and discussed in the preceding chapter.

5.1. BVOC fluxes from maize

The following sections are divided into observations (Sect. 5.1.1) and simulations (Sect. 5.1.2) from the maize experiment.

5.1.1. Magnitude and composition of observed BVOCs

Some parts of the results of observed BVOC emissions from the maize ecosystem were already shown in my publication Wiß et al. (2017). However, this section will go into more detail and also present a different calculation of SEFs and β-coefficients that were adapted to the joint JJv–pool emission model instead of the pool emission model alone.

Figure 5.1.1 shows the meteorological situation during the BVOC emission experiment 2015. Five periods of temperature, PAR, and precipitation were distinguished: (1) late July with declining temperatures and PAR values until around 15 ℃ and well below 200 μmol m^{-1} s^{-1}, as well as frequent precipitation events, (2) first half of August with fluctuating warm temperatures (> 20 ℃ and daily maximum around 35 ℃), high PAR and mostly dry conditions (few maximum daily sums of 5 mm), (3) second half of August with slightly cooler temperatures than during the first half and

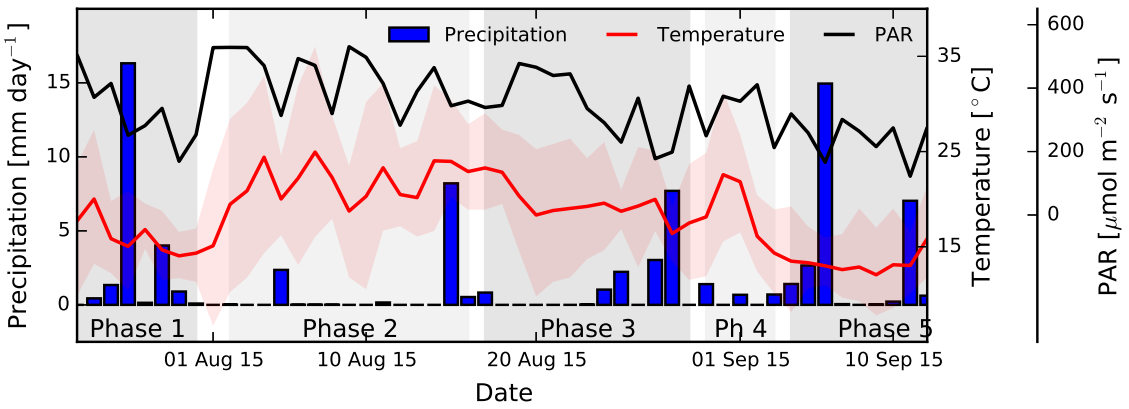

Figure 5.1.1.: Environmental conditions at the CarboZALF field site in Dedelow during the maize field experiment 2015. Precipitation is given as daily sums, air temperature at 2 m aboveground as daily means and daily range, and photosynthetically active radiation (PAR) as daily means. The meteorological phases described in the main text are depicted in gray.

decreasing PAR, particularly during the second week PAR, (4) a short period in the beginning of September with a sudden warming followed by a cooling which is not that much pronounced in the PAR, and (5) cooler days (12–16 ℃), low PAR, and moist conditions until the campaign ended in mid-September. Generally, the months of July, August, and September 2015 were drier (−24 mm, −13 %) and warmer (+1.3 ℃) compared to the 1992–2015 observations at the field site in Dedelow. While July was slightly warmer but wetter, August was notably warmer (+3 ℃) and drier (−23 mm, −50 %) than the long-term mean. September 2015 does not deviate from the long term observations.

GPP is generally following the temperature and PAR tendencies during the meteorological phases (see Fig. 5.1.2). Starting from higher values due to high PAR, GPP declines to low values during phase 1 with a subsequent sharp increase between phase 1 and phase 2 up to the maximum values of 25–30 gC m^{-2} d^{-1}. From around mid of phase 2, GPP gradually decreases following the temperature and PAR fluctuations until values of 5–15 gC m^{-2} d^{-1} at the end of the experiment. The short but characteristic temperature jump in phase 4 with higher mean and maximum values compared to phase 3 is not that sharply expressed in GPP, which may be attributed to the stronger PAR influence than by that of temperature. The maize plants are continuously growing during the whole field campaign with a decline in growth rate in the middle of the the first half of the experiment, leading to aboveground biomass

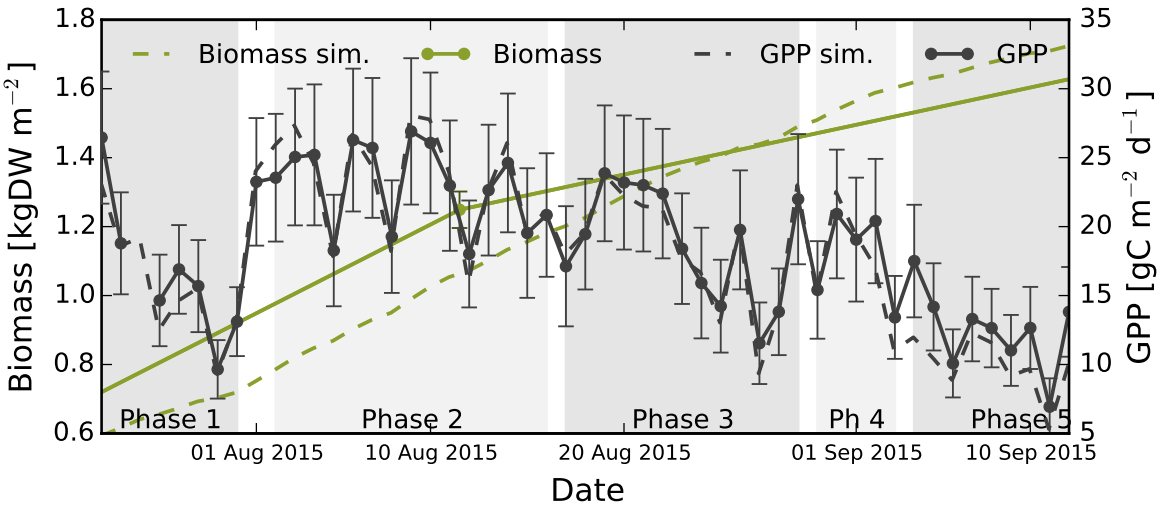

Figure 5.1.2.: Observed and simulated biomass and daily sums of gross primary production (GPP) (calculated from observed CO_2 measurements) from maize ecosystem field experiment 2015. The green line links two biomass observation points linearly. Error bars are given as ± the standard error of the sum. The meteorological phases depicted in gray are described in the main text.

values ranging from 0.7–1.6 kgDW m^{-2}.

Regarding the plant phenological stages, during phase 1, the maize plants were mostly in the reproductive growth and the inflorescence emerged (see Fig. 5.1.3). In phase 2 the plants were flowering, in phase 3 and 4 the fruit developed, and finally during phase 5 the plants were ripening.

Daily mean BVOC fluxes from the maize ecosystem can be divided into three groups according to their flux magnitude (see Fig. 5.1.3). Highest daily mean (∼ 0.2 nmol m^{-2} s^{-1}) as well highest mean values over the entire investigation period (0.075–0.10 nmol m^{-2} s^{-1}) were observed for GLVs (18.0 %), methanol (16.9 %), monoterpenes (15.1 %), acetone (14.2 %), and acetaldehyde (13.0 %) (see Tab. 5.1). These compounds contribute 77.2 % of all observed compounds during the experiment. Generally, the seasonal pattern of all compounds appear to be closely related to meteorology with low values phase 1, a strong emission increase between phase 1 and phase 2 in which daily mean emission rates were highest for all compounds, except for ethanol. Finally, starting in phase 2, a subsequent gradually decline of absolute emissions occured. Comparing phase 2 and 4, mean temperature and PAR values are similar ($P > 0.13$, Kruskal-Wallis H-test) but all BVOC emissions were significantly lower ($P < 0.05$) in phase 4 than in phase 2, suggesting that plant phenology could

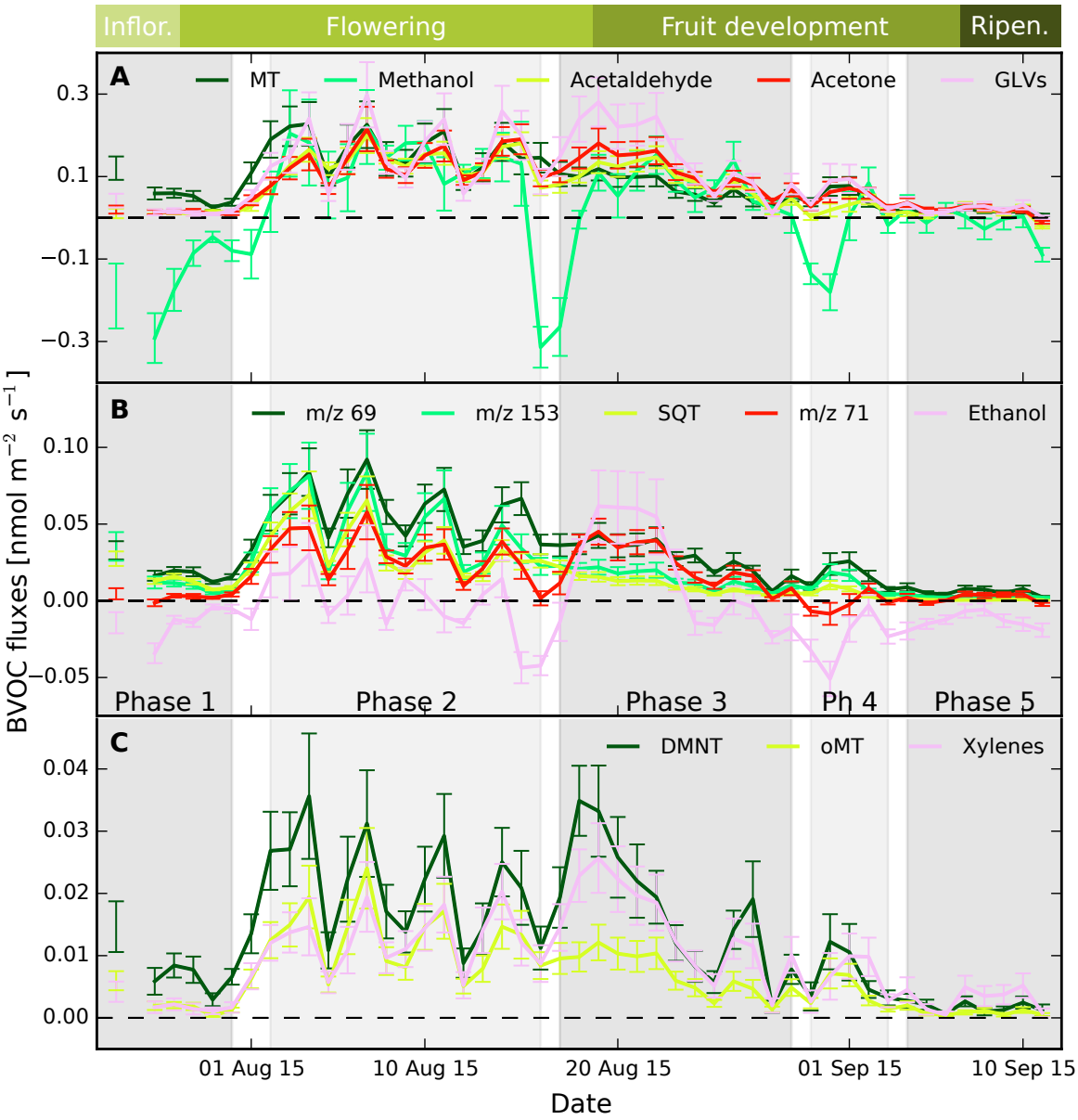

Figure 5.1.3.: Maize plant phenological stages according to BBCH (above **A**; Inflor.: inflorescence emergence; Ripen.: ripening) and daily mean BVOC emissions during the field experiment 2015. Error bars are given as ± the standard error of the mean. BVOCs are grouped according to their flux magnitude with decreasing fluxes from **A** to **C**. Only daily values with more than 75 % of flux data (36 values) are shown. The meteorological phases depicted in gray (**B**) are described in the main text.

be a key factor in controlling emissions. This could also be related to a decline in the biomass of leaves, tassels (the male flower), and the stigmata of the corn. In addition, changing root emissions may also be considered (cf. Wiß et al., 2017).

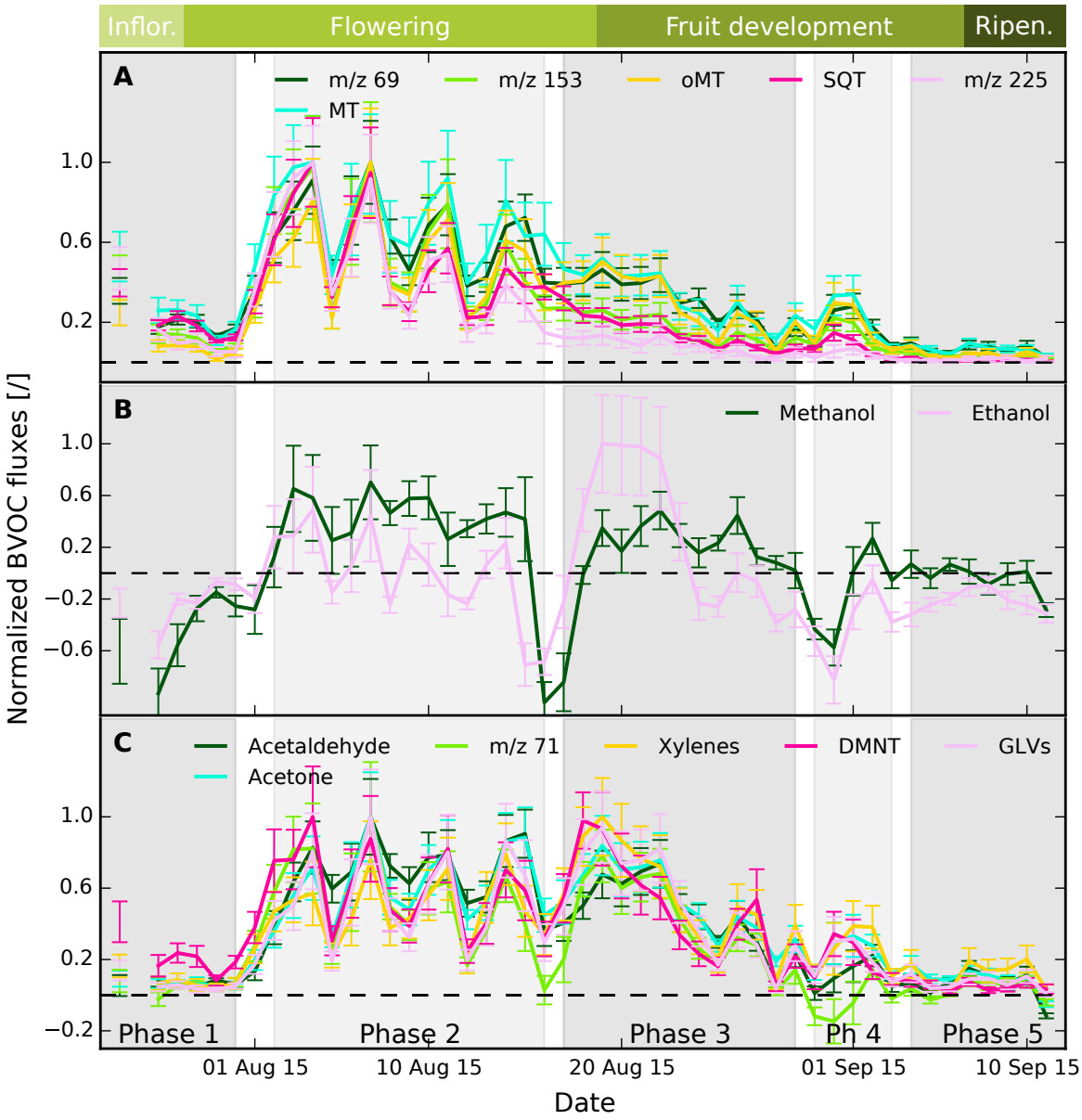

Figure 5.1.4.: Daily mean normalized BVOC emissions from maize ecosystem (emission rates scaled to each compound's maximum value throughout the measurement period) during the field experiment 2015. BVOCs are grouped according to their seasonal flux pattern. The meteorological phases depicted in gray (**C**) are described in the main text

In order to better compare the course of fluxes of different magnitudes, daily mean BVOC fluxes of each compound were normalized by division with the compound's daily mean maximum of the whole season (see Fig. 5.1.4). Thereby, further separation of compounds into three different groups with distinct seasonal flux patterns was possible. The compound group in 5.1.4A mainly consists of volatile terpenoids and

Table 5.1.: Mean molar emissions from maize ecosystem during field experiment 2015 in pmol m^{-2} ground area s^{-1} (negative fluxes set to zero). The fraction of each compound to the total BVOC emission in % is given in brackets. All values are calculated for the two phenological growth stages of flowering as well as fruit development and ripening, and the whole observed period.

Compound	Flowering (24 days)	Fruit dev. and Ripening (28 days)	Whole period (53 days)
Methanol	134.84 (17.7)	69.06 (16.2)	98.57 (16.9)
Acetaldehyde	97.86 (12.8)	56.7 (13.3)	76.17 (13.0)
Ethanol	12.59 (1.7)	16.37 (3.8)	14.64 (2.5)
Acetone	95.39 (12.5)	71.09 (16.7)	83.1 (14.2)
m/z 69	46.52 (6.1)	18.55 (4.4)	31.74 (5.4)
m/z 71	23.72 (3.1)	14.08 (3.3)	18.63 (3.2)
GLVs	118.04 (15.5)	92.05 (21.6)	105.34 (18.0)
Xylenes	9.57 (1.3)	9.27 (2.2)	9.52 (1.6)
MTs	132.25 (17.4)	48.4 (11.4)	88.06 (15.1)
DMNT	17.11 (2.2)	10.23 (2.4)	13.58 (2.3)
m/z 153	36.52 (4.8)	9.57 (2.2)	22.21 (3.8)
oMTs	9.3 (1.2)	4.39 (1.0)	6.75 (1.2)
SQTs	28.37 (3.7)	5.69 (1.3)	16.43 (2.8)
Total	**762.09 (100.0)**	**425.45 (100.0)**	**584.72 (100.0)**

their derivatives. The group in 5.1.4B summarizes the C_1–C_2 alcohols methanol and ethanol. Compounds from the third group in 5.1.4C are defined as other VOCs and include GLVs, acetaldehyde, *m/z* 71, xylenes, acetone, and also the homoterpene DMNT, which originates from the terpenoid biosynthetic pathway (Richter et al., 2016).

Again, all BVOCs show highest normalized emissions (~ 1.0) during phase 2, when temperature as well as PAR were highest, the maize plants were flowering and the fruit development began. However, compounds within Fig. 5.1.4C do still emit at similar high rates during phase 3 ($P > 0.2$) especially at the beginning of phase 3, indicating a close relationship to meteorological conditions only, whereas the compounds within the group of Fig. 5.1.4A (*m/z* 69, *m/z* 153, monoterpenes, oxygenated monoterpenes, sesquiterpenes, and *m/z* 225) significantly vary between both periods ($P < 0.05$). It can thus be hypothesized that the emission of these compounds is additionally influenced by phenological developments.

Methanol and ethanol, and to some degree also acetaldehyde and acetone, are difficult to put in any group because they show considerable net deposition rates coinciding with precipitation events. Thus, deposition is very likely related to the high water solubility of these compounds due to their low Henry's law constant of < 10 Pa m^3 mol^{-1} (e.g., compared to isoprene with 7,780 Pa m^3 mol^{-1}) or α-pinene with 10,840 Pa m^3 mol^{-1} at 25 ℃ (Harley et al., 2007; Niinemets and Reichstein, 2003)).

Insights from standard emission factors

The SEF is defined at fixed conditions of temperature, PPFD, and CO_2 mixing ratio. In Tab. 5.2, it is scaled to the plant's biomass in order to investigate if BVOC emission intensities are different between plant developmental stages. Generally, highest SEF (> 58 ng g^{-1}DW h^{-1}) for the whole period were obtained for monoterpenes, GLVs, acetone, *m/z* 153, and sesquiterpenes (arranged in decreasing order). Although methanol yields amongst the highest emission rates, its SEF is rather low due to the impact of negative fluxes which are fitted to a model that simulates positive fluxes only. All SEFs for the group of terpenoids and their deriviatives (see Fig. 5.1.4A) decreased by more than 50 % (e.g. 67.8 to 29.6 ng g^{-1}DW h^{-1} for sesquiterpenes), between flowering and the joint stage of fruit development and ripening. At the same time, optimal β values increase (+0.04 to +0.06) also reflecting lower emission rates during fruit development and ripening (at least for temperatures below 30 ℃, see Fig. 4.2.10 followed by a brief discussion of β-coefficients). Thus, it is supported that not only temperature and PPFD but rather plant ontogenesis determines the emission seasonality. In contrast, the SEFs from the group of other VOCs (see Fig. 5.1.4C) increase (e.g., hexanal 111.7 to 178.6 ng g^{-1}DW h^{-1}) between flowering and the fruit development and ripening stage. Additionally, the increase of β values is also lower (+0.02 to +0.05) compared to the terpenoids and their derivatives.

Table 5.2.: BVOC emission parameter for maize, fitted to the joint JJv–pool emission stand-alone modeling approach used in this study (see Eq. 4.4). The parameters are the standardized emission factor (SEF) with corresponding standard errors of the estimate (SE) both in ng g^{-1}DW aboveground biomass h^{-1}, the light dependent fraction (LDF) for partitioning between the JJv and pool emission algorithm, β-coefficient as a curvature parameter for the pool emission equation and the Nash-Sutcliffe modeling efficiency (NSE). All values are calculated for three growth periods flowering ($N = 529$), fruit development and ripening (Fr. dev. + Rip., $N = 601$), and the whole measurement period ($N = 1153$).

Compound	**Period**	**SEF (± SE)**	**LDF**	β	**NSE**
m/z 69	Flowering	33.5 (± 6.1)	0.2	0.1	0.81
	Fr. dev. + Rip.	26.3 (± 2.6)	0.3	0.15	0.77
	Whole period	30.7 (± 5.2)	0.2	0.13	0.78
MTs	Flowering	207.1 (± 57.5)	0.2	0.11	0.67
	Fr. dev. + Rip.	172.0 (± 15.9)	0.4	0.16	0.78
	Whole period	190.8 (± 43.7)	0.3	0.13	0.68
m/z 153	Flowering	74.6 (± 20.2)	0.4	0.12	0.72
	Fr. dev. + Rip.	36.5 (± 2.7)	0.4	0.16	0.85
	Whole period	66.3 (± 15.2)	0.5	0.14	0.7
oMTs	Flowering	18.9 (± 3.7)	0.3	0.13	0.83
	Fr. dev. + Rip.	19.0 (± 2.0)	0.4	0.17	0.74
	Whole period	18.2 (± 3.0)	0.3	0.15	0.82
SQTs	Flowering	67.8 (± 16.3)	0.3	0.11	0.73
	Fr. dev. + Rip.	29.6 (± 2.7)	0.3	0.17	0.8
	Whole period	58.9 (± 13.3)	0.3	0.15	0.69
Acetaldehyde	Flowering	45.1 (± 8.3)	0.1	0.12	0.81
	Fr. dev. + Rip.	47.3 (± 7.1)	0.0	0.17	0.65
	Whole period	44.1 (± 7.9)	0.1	0.14	0.77
Acetone	Flowering	65.1 (± 11.3)	0.3	0.12	0.85
	Fr. dev. + Rip.	89.3 (± 10.0)	0.3	0.16	0.73
	Whole period	67.7 (± 11.0)	0.2	0.13	0.8
m/z 71	Flowering	21.2 (± 5.4)	0.3	0.15	0.76
	Fr. dev. + Rip.	23.1 (± 4.1)	0.3	0.18	0.52
	Whole period	20.9 (± 4.8)	0.2	0.17	0.7
Hexenal	Flowering	43.9 (± 8.1)	0.2	0.15	0.85
	Fr. dev. + Rip.	62.2 (± 8.5)	0.3	0.17	0.64
	Whole period	46.2 (± 8.6)	0.2	0.15	0.77

Table continues on the next page

Table 5.2.: *Continued from previous page.*

Compound	Period	SEF (± SE)	LDF	β	NSE
Hexanal	Flowering	111.7 (± 21.0)	0.2	0.15	0.85
	Fr. dev. + Rip.	178.6 (± 23.4)	0.4	0.17	0.65
	Whole period	119.5 (± 23.5)	0.2	0.15	0.75
Xylenes	Flowering	12.5 (± 3.2)	0.2	0.13	0.74
	Fr. dev. + Rip.	22.1 (± 3.5)	0.3	0.16	0.59
	Whole period	13.9 (± 3.5)	0.2	0.13	0.63
DMNT	Flowering	30.1 (± 8.7)	0.2	0.12	0.66
	Fr. dev. + Rip.	29.2 (± 7.2)	0.2	0.15	0.38
	Whole period	29.3 (± 8.0)	0.2	0.13	0.59
Methanol	Flowering	45.1 (± 38.5)	0.4	0.19	0.3
	Fr. dev. + Rip.	58.7 (± 14.9)	0.8	0.18	0.3
	Whole period	44.3 (± 29.1)	0.5	0.19	0.28
Ethanol	Flowering	6.0 (± 6.9)	0.0	0.28	0.27
	Fr. dev. + Rip.	20.4 (± 7.6)	0.4	0.22	0.2
	Whole period	8.1 (± 7.5)	0.0	0.23	0.18

In addition, the LDF values have been statistically fitted and results vary between 0 and 0.5 with the majority of compounds between 0.2–0.3. This means that most of the emissions from the maize ecosystem are better described by the pool emission model instead of the model of *de novo* biosynthesis. This can help in representing emission responses but does not necessary prove that emissions are indeed originating from pools. Generally, results from fitting BVOC parameters, except for methanol and ethanol with high deposition rates, could represent observed emission rates reasonably well (NSE > 0.6). BVOC emission parameters for methanol and ethanol are hardly meaningful since a deposition model was not included in the analysis and thus the fit was necessarily poor (NSE < 0.3).

Hexenal and hexanal from the group of GLVs are fitted separately but have the same LDF and β-value (at similar NSE values), indicating a very similar seasonality, which is why they are shown as summed up values in Sect. 5.1.1.

5.1.2. Simulated seasonality

The following results are obtained with the joint `JJv`–pool emission model coupled to `LandscapeDNDC`. For this purpose, the BVOC emission parameters from Tab. 5.2 are applied for the whole period that had been obtained from fitting observations to the joint `JJv`–pool emission stand-alone, with SEFs scaled to the sum of all observed values (see Sect. 4.4.3 for more details).

Evaluation of the model results

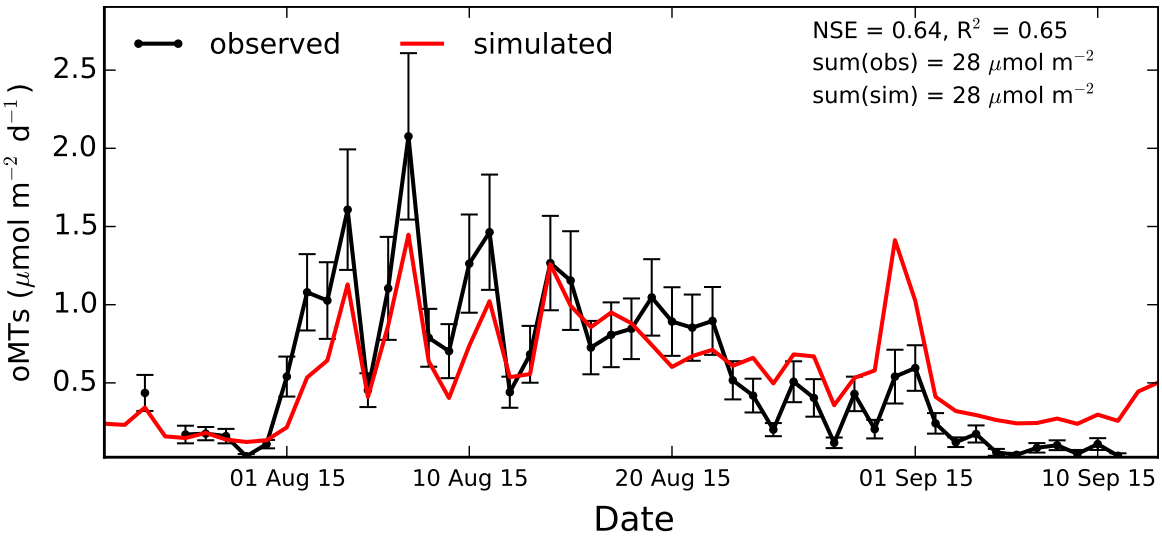

Figure 5.1.5.: Daily sums of observed and simulated oxygenated monoterpenes emissions (LDF= 0.3) from maize ecosystem as a compound example of the group in Fig. 5.1.4A. Error bars indicate ± the standard error of the sum.

Simulations of biomass and GPP during the BVOC observation period had been already shown in Fig. 5.1.2. The simulated biomass is slightly smaller than observations until the end of August when it gets slightly higher. In contrast, simulated daily sums of GPP are almost indistinguishable from observations, at least, during the period of observed BVOC emissions.

The figures 5.1.5, 5.1.6, and 5.1.7 show selected emission compounds as simulated for the observation period. Thereby one compound from each of the groups is presented which were distinguished according to their distinct seasonal pattern. Simulated emissions of oxygenated monoterpenes, representing the group of terpenoids

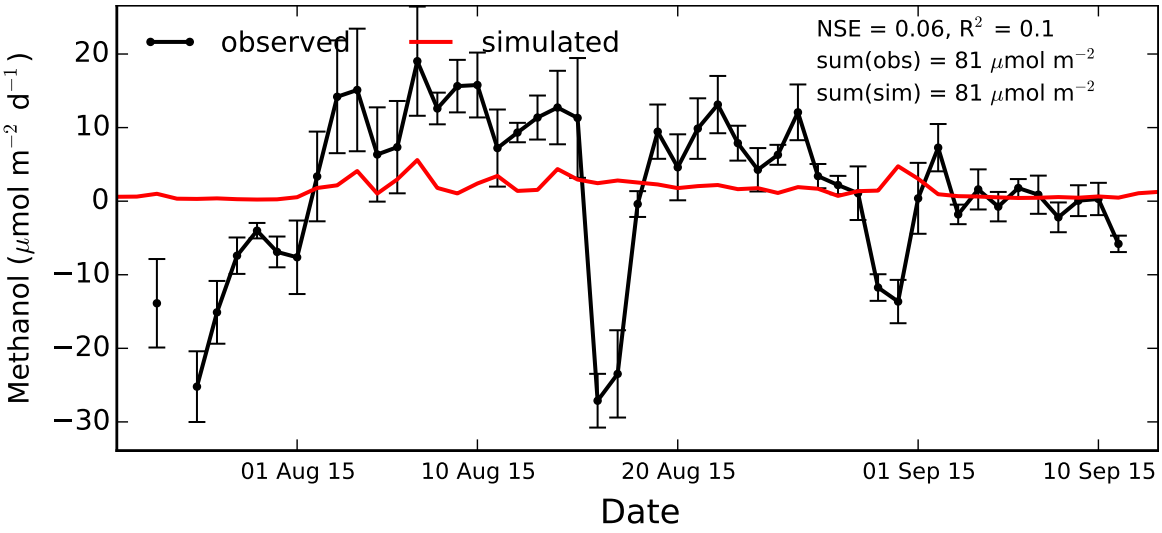

Figure 5.1.6.: Daily sums of observed and simulated methanol emissions (LDF= 0.5) from maize ecosystem as a compound example of the group in Fig. 5.1.4B. Error bars indicate ± the standard error of the sum.

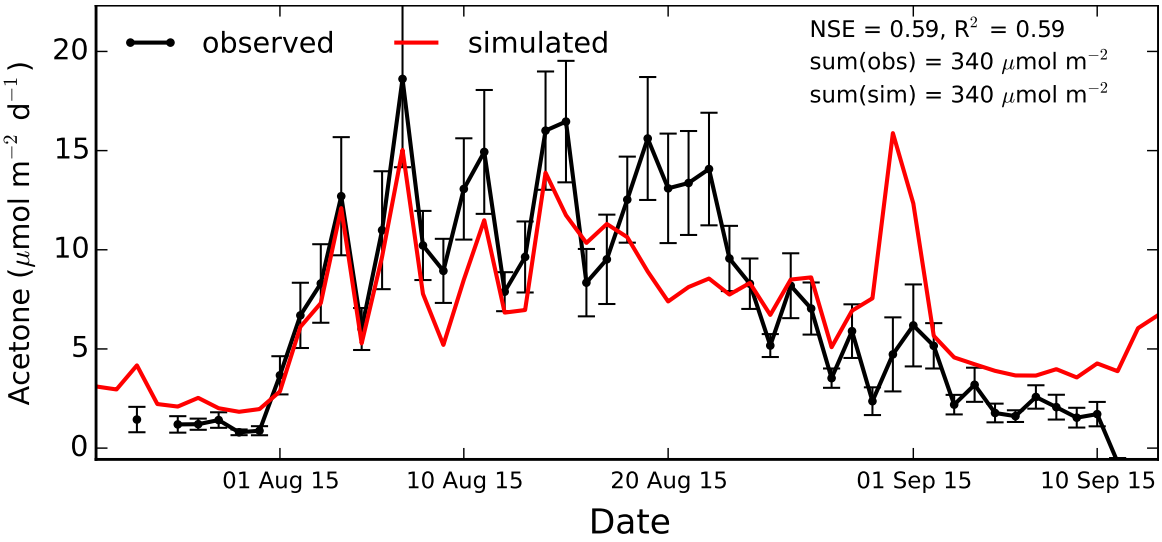

Figure 5.1.7.: Daily sums of observed and simulated acetone emissions (LDF= 0.2) from maize ecosystem as a compound example of the group in Fig. 5.1.4C. Error bars indicate ± the standard error of the sum.

and their derivatives, agree very well with the observed pattern although the early emission increase has not been fully captured by the model. While the subsequent fluctuations of the emission rates until around the 20 August are in line with observations and their measurement range. The model overestimates emissions during fruit development and ripening starting end of August, and is not capable to fully

Table 5.3.: Evaluation of simulated BVOC emissions (daily sums) from maize ecosystem by NSE with (w/) and without (w/o) scaling of SEFs to summed up observations, coefficient of determination (R^2), and the ratio between the sum of all observed and their coinciding simulated values.

Compound	NSE w/	NSE w/o	R^2	$\frac{\sum_{i=1}^{n(\text{obs})} \text{obs}_i}{\sum_{i=1}^{n(\text{obs})} \text{sim}_i}$
Methanol	0.06	-0.0	0.1	0.33
Acetaldehyde	0.44	0.39	0.44	0.86
Ethanol	-0.05	-0.21	0.04	-0.28
Acetone	0.58	0.52	0.59	0.84
m/z 69	0.43	0.32	0.43	0.83
m/z 71	0.33	0.28	0.33	0.86
Hexenal	0.56	0.49	0.56	0.86
Hexanal	0.57	0.54	0.59	0.85
Xylenes	0.45	0.36	0.45	0.85
MTs	0.39	0.25	0.4	0.82
DMNT	0.44	0.32	0.44	0.81
m/z 153	0.42	0.41	0.43	0.88
oMTs	0.64	0.61	0.65	0.86
SQTs	0.36	0.32	0.36	0.85

reproduce the strong emission decrease which has been observed along with a physiological maturity in the ripening stage. It should be noted that the adjusted (higher) β-coefficient from this growth stage instead of medium values for the whole period would have improved model results during this specific period substantially. In contrast, increasing the LDF to increase the importance of photosynthesis for emission could not improve simulation results, (data not shown). Thus, possibly the photosynthesis model calculates high J values with decreasing J_v (as GPP also decreases at the same time), leading to a high photosynthetic emission potential for the `JJv` model and consequently higher emissions. It should be noted that physiology effects on BVOC emissions might not be related only to photosynthesis. For example senescent leaves may have a much lower potential to produce chemical energy from the same amount of incoming radiation than younger leaves. This has been supported by the study of Mozaffar et al. (2018) who observed a strong reduction in BVOC emissions in mature and senescent compared to young leaves for the same environmental conditions.

The simulation results of acetone representing the group of other VOCs show similar deficits at the end of the observed period than that of terpenoids (see Fig. 5.1.7). Additionally, the distinct high emissions around the 20 August are not fully represented by the model as temperature and PPFD were already significantly lower as during the first half of August. Nevertheless, the simulated emission increase at the beginning of the period is in good accordance with observations, and strictly follows temperature and PPFD during this time. This is a difference to the responses of terpenoids and their derivatives where emission increases around 2 days earlier, possibly related to additional emission sources from flowers and tassels. The third group of emissions cannot be simulated with our approach since it is dominated by deposition during some periods, as can be seen by the example of methanol (see Fig. 5.1.6).

The problem of simulating BVOCs which show deposition fluxes (methanol, ethanol, etc.) is even worsened by the scaling of the SEF to observed sums, which decreases each simulated emission peak to a minimum. Nevertheless, scaling the SEF to simulate the observed emission sums has improved the simulated seasonality with higher NSE values for all emitting BVOCs (see Tab. 5.3). In particular, the simulations overestimated emissions before scaling, resulting from exceptionally high emission rates simulated during the ripening stage of maize plants although observed emissions were much lower. This overestimation is also the main reason for the overall moderate fit between simulations and measurements as expressed in NSE (0.33–64) and R^2 (0.33–0.65) values.

Model application for three years

Finally, simulations from three consecutive years are shown, to draw conclusions about average BVOC emissions and their dependece on inter-annual meteorological differences during a growing season of maize crops.

Figure 5.1.8 shows simulated aboveground biomass for three seasons (2015–2017) together with one year of observations (2015). Simulated aboveground biomass is modeled as the sum of stem, leaf, and fruit (fruit or grain, depending on the plant) biomass. The observed biomass can be well represented by the model. During seasons without observations, the plants grow relatively similar to the year 2015 with only small sensitivity to meteorological conditions.

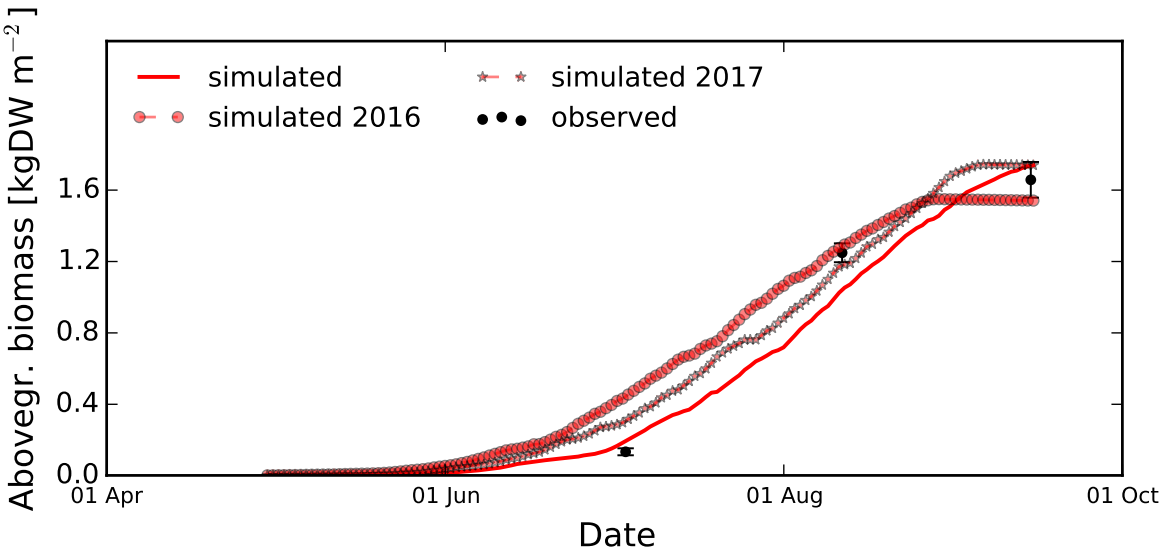

Figure 5.1.8.: Aboveground biomass of maize plants from simulations (red) and observations (black dots for measurements outside the chambers and black stars for measurements inside the chamber; the error bars indicate ± the standard deviation). 2015 is the measurement period, whereas the years 2016 (red circles) and 2017 (red stars) are simulations only.

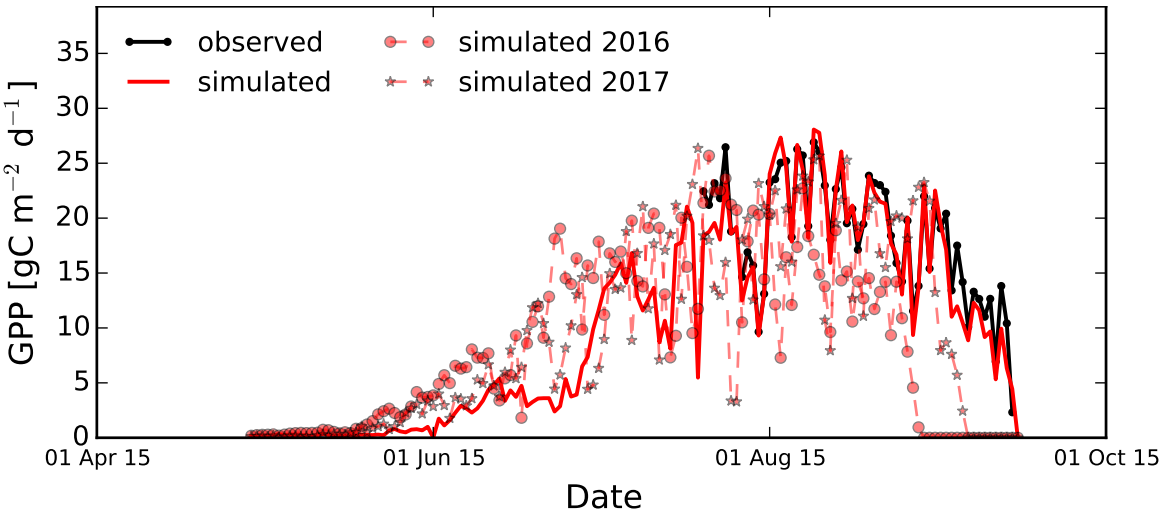

Figure 5.1.9.: Daily sums of GPP from maize ecosystem from simulations over three seasons (red lines) and calculated based on continuous CO_2 measurements during the season 2015 (black dotted line).

Figure 5.1.9 shows daily sums of simulated and observed GPP, which show a very good agreement. During season 2016 (red circles), GPP starts earlier compared to the simulations of 2015 and 2017 due to exceptional warm early summer conditions,

which also leads to higher values of biomass until the beginning of August. In the end of August, the stage of fruit development and ripening is also reached very early, compared to 2015 and assimilation finally drops to zero indicating fully ripened and senescent plants. As a result, simulated biomass remains constant afterwards. Generally, the simulated development of biomass and GPP values of maize during season 2017 is in between the development of 2015 and 2016. At the beginning GPP values (triangle) are between 2015 and 2016 but increase to the level of 2015 dropping to zero several days later than 2016 but earlier than 2015. This variability between years leading to phase shifts of half a month to one month is well within the reported range at this site. These simulations of biomass and GPP over the course of three years can thus serve to provide as reasonable background conditions for simulating BVOC emissions

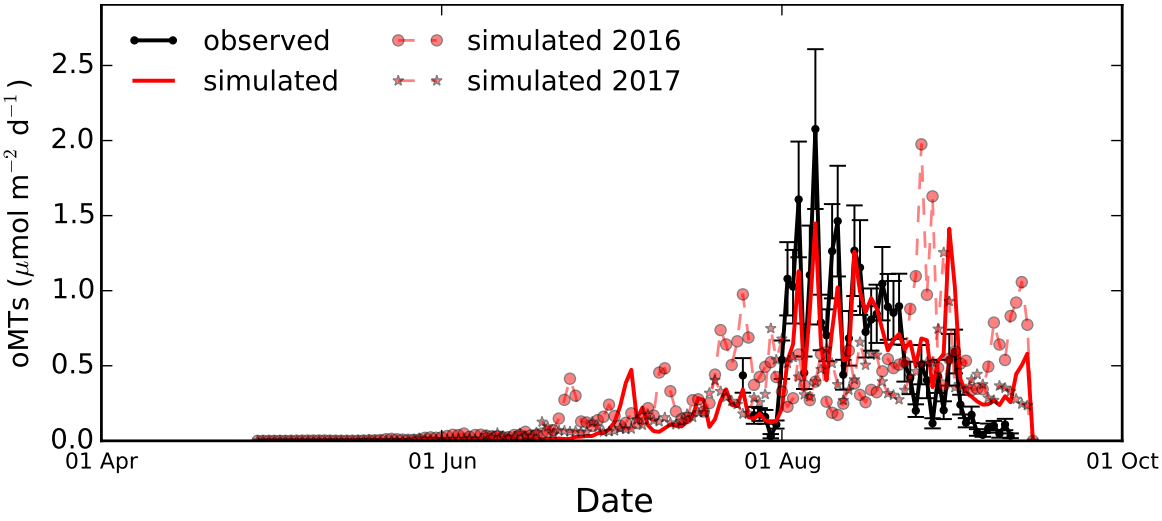

Figure 5.1.10.: Daily sums of observed and simulated oxygenated monoterpenes emissions from maize ecosystem. Similar to Fig. 5.1.5 but for three seasons.

The figures 5.1.10, 5.1.11, and 5.1.12 show simulated BVOC emissions during the course of the selected three years for three compounds which are exemplary for their group. Regarding 2015, there are no major simulated emission events outside the observed period since the observation period already covers a considerably long period. During August 2016 and 2017, emissions are much lower compared to the high simulated and observed values of 2015, which mainly results from the high August 2015 mean temperature of +3 ℃ above the long-term mean (mean temperatures (mean PAR) for August were 20.6 (389.6), 17.1 (342.6), and 18.2 ℃ (352.0 μmol m^{-2} s^{-1})

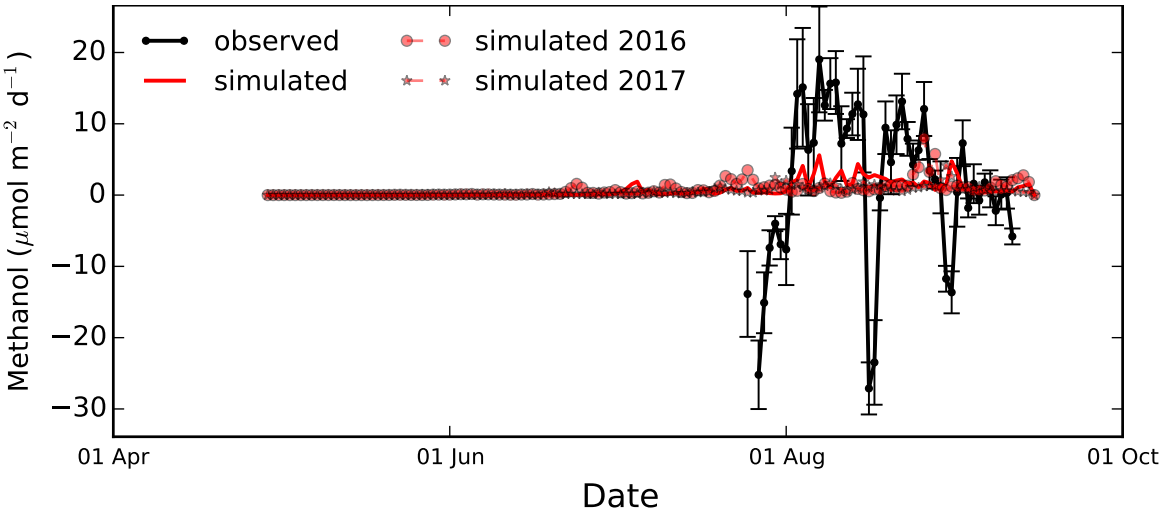

Figure 5.1.11.: Daily sums of observed and simulated methanol emissions from maize ecosystem. Similar to Fig. 5.1.6 but for three seasons.

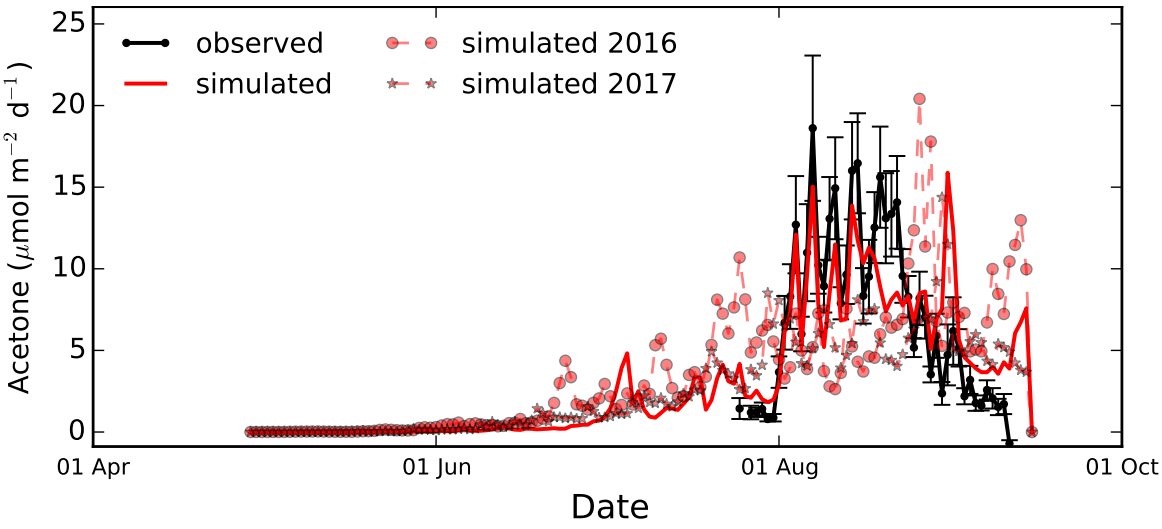

Figure 5.1.12.: Daily sums of observed and simulated acetone emissions from maize ecosystem. Similar to Fig. 5.1.7 but for three seasons.

for 2015, 2016, and 2017, respectively). In contrast, during June, July, and September 2016, simulated emissions are higher than in the preceding year. Again, the main reason is the temperature difference between the years as one of the major drivers of emissions (mean temperatures in June were 14.3, 17.8, and 16.9 for 2015, 2016, and 2017, respectively). Additionally, the biomass from 2016 and 2017 is higher compared to 2015. The emissions during 2017 are generally lower or at most similar to what was simulated in 2015. Simulated emissions notably increase at the end of the growing

seasons of each year, which is probably overestimating field emissions due to reasons already discussed in the analyses of the observations.

5.2. BVOC fluxes from oilseed rape

The following two sections report and discuss observations (Sect. 5.2.1) and simulations (Sect. 5.2.2) from the oilseed rape experiment.

5.2.1. Magnitude and composition from observations

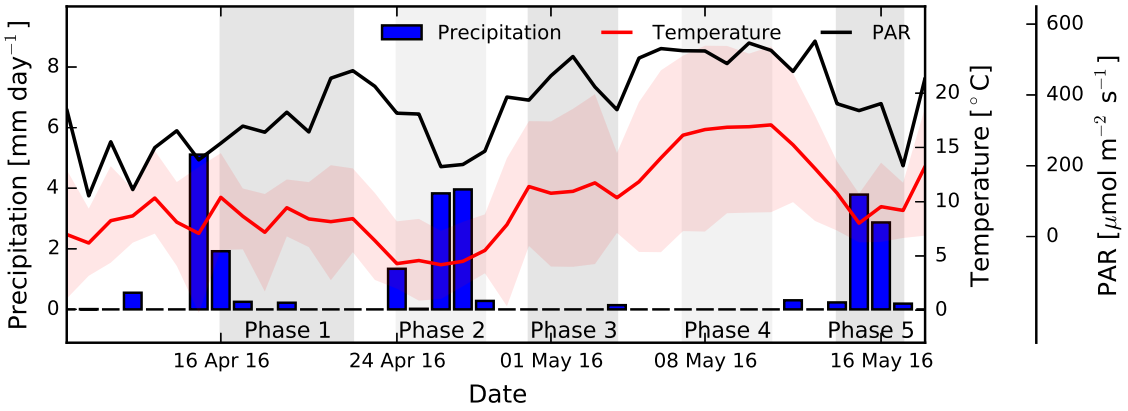

Figure 5.2.1.: Temperature, PAR, and precipitation during the oilseed rape field experiment 2016. The meteorological phases described in the main text are depicted in gray. See 5.1.1 for a detailed caption.

Figure 5.2.1 shows the meteorological conditions during the oilseed rape BVOC experiment in 2016. Similar to the observational period of maize, the whole experiment can be divided into five phases: (1) the third week of April with slightly increasing daily mean temperatures still below 10 °C, rising PAR from 263.5 to 468.4 μmol m^{-2} s^{-1} and precipitation sum of 2.4 mm, (2) end of April with cooler temperatures ($<$ 5 °C), less average PAR ($\sim$ 270 μmol m^{-2} s^{-1}), and higher precipitation sums (9.4 mm), (3) beginning of May after a temperature and PAR increase to almost 12 °C and 508 μmol m^{-2} s^{-1} without any rainfall at all, (4) a period within the first half of May with highest temperature and PAR values during the observation period of about 17 °C and 546 μmol m^{-2} s^{-1} without any rainfall at all, and finally (5) mid May,

when temperature and PAR decreases to 9.4 ℃ and 326.6 μmol m^{-2} s^{-1}, respectively, and precipitation sum is 7.1 mm. Generally, the growing season 2016 was exceptionally dry with a precipitation sum of only 157 mm during the 5 months from May to September in contrast to a long-term mean from 1992–2015 of 295 mm. Additionally, the months May, June, and September with +2.1–2.8 ℃ were notably warmer compared to the long-term mean.

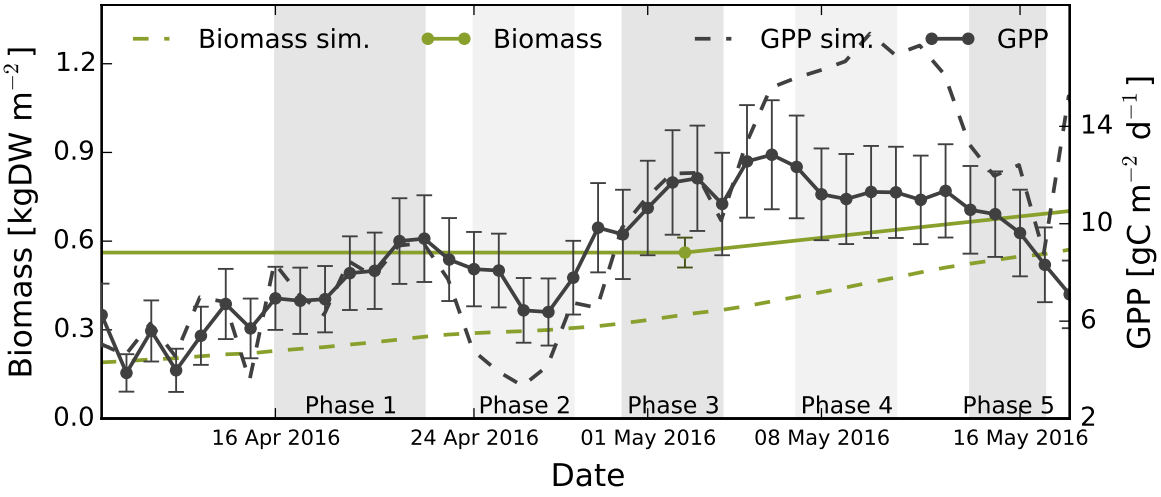

Figure 5.2.2.: Observed biomass and daily sums of gross primary production (GPP) from oilseed rape ecosystem field experiment 2016. See Fig. 5.1.2 for a detailed caption.

The observed aboveground biomass increased only slightly from ∼ 0.55 to 0.72 kgDW m^{-2} during the experiment (see Fig. 5.2.2). In contrast, simulated GPP varies stronger showing values of around 7 gC m^{-2} d^{-1} during the first half (until phase 2 included) and 11 gC m^{-2} d^{-1} during the second half of the campaign. This development generally follows that of temperature and PAR, but exceptions can be detected. For example, the magnitude of GPP of phase 3 and phase 4 was very similar, although mean temperature and PAR were significantly higher during phase 4 (+5.7 ℃ and +96 μmol m^{-2} s^{-1}) than in phase 3. Thus, based on these data, any kind of stress reaction during phase 4, especially drought stress, cannot be excluded.

The plant phenology developed from inflorescence emergence during the first half (phase 1 and phase 2) to the flowering stage in the second half of the experiment (phase 3–5) (see Fig. 5.2.3). Thus, the oilseed rape plants were already in their reproductive growth period at the start of the BVOC measurement campaign.

Similar to observations of maize, BVOC fluxes can be divided into three groups.

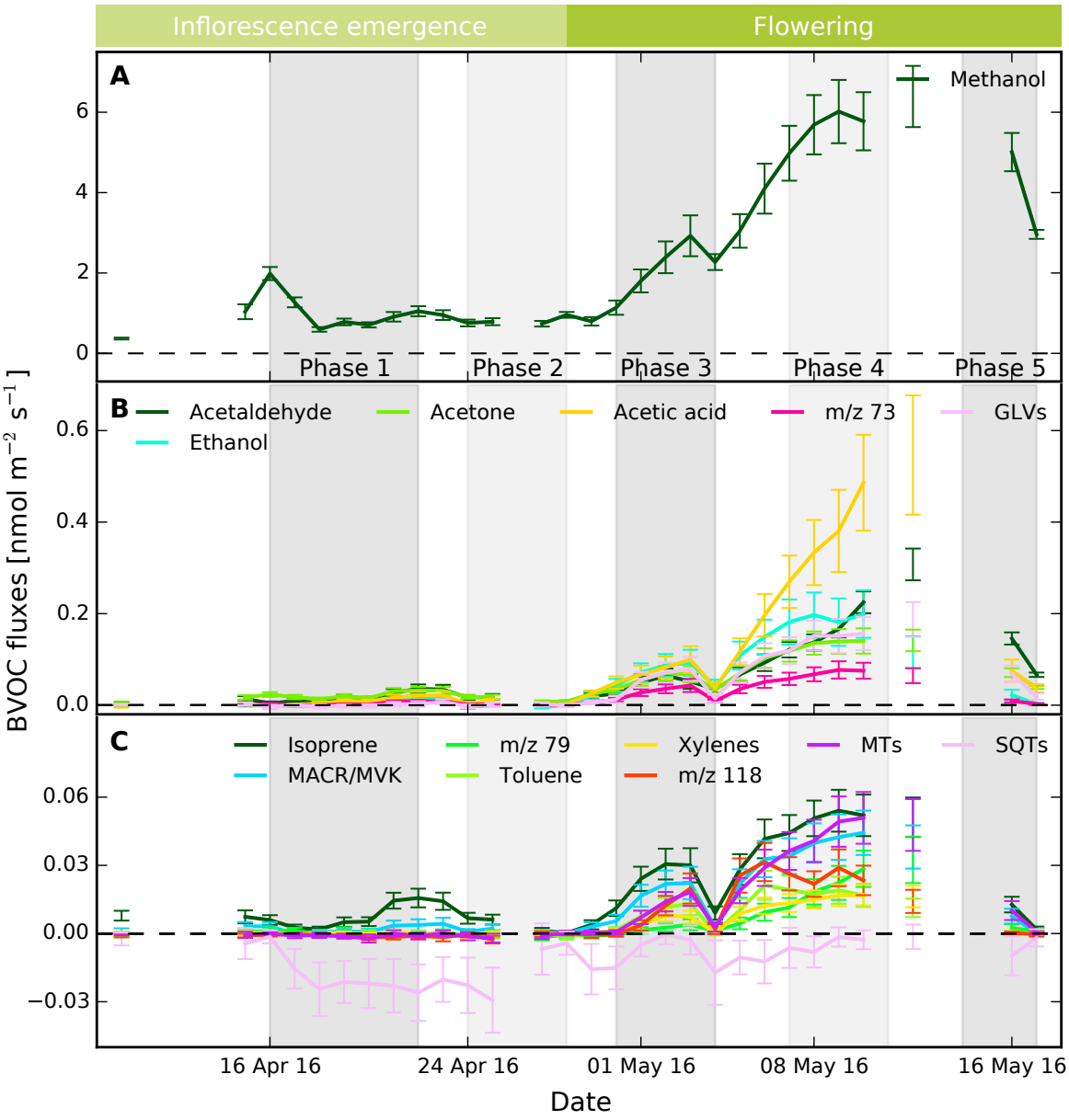

Figure 5.2.3.: Oilseed rape plant phenological stages (above **A**) and daily mean BVOC emissions during the field experiment 2016. Only daily values with more than 75% of flux data (72 values) are shown. The meteorological phases depicted in gray (**A**) are described in the main text. See Fig. 5.1.3 for a detailed caption.

Basically based on their seasonal characteristics (see Figs. 5.2.3, 5.2.4). Methanol was by far the major emitted compound from the oilseed rape ecosystem with highest daily mean emission rates up to 6 nmol m^{-2} s^{-1} and a share of 84.9 % of mean molar emissions during the whole observational period (see Tab. 5.4). It is followed

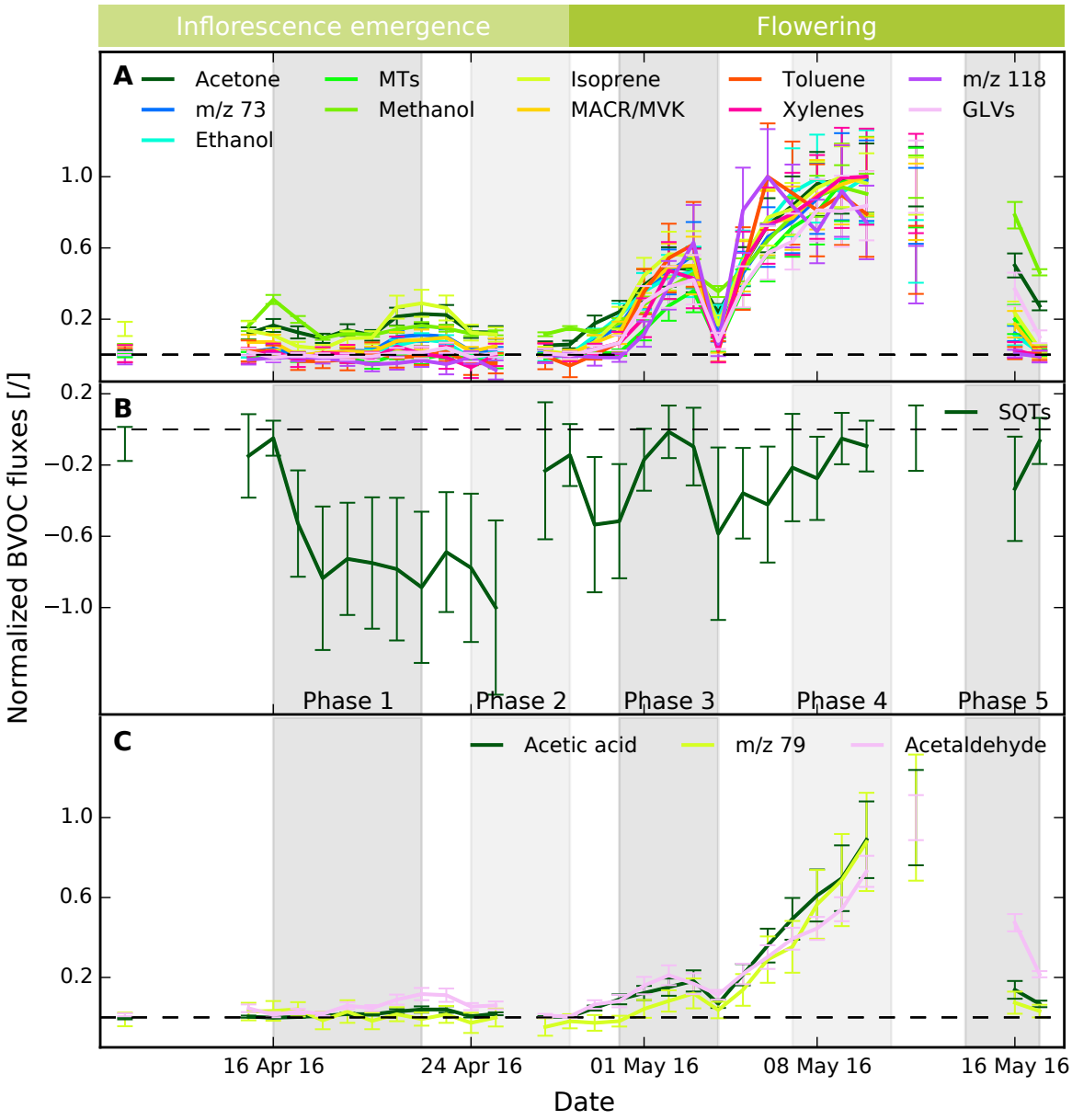

Figure 5.2.4.: Daily mean normalized BVOC emissions from oilseed rape ecosystem (emission rates scaled to each compound's maximum value throughout the measurement period) during the field experiment 2016. BVOCs are grouped according to their seasonal flux pattern. The meteorological phases depicted in gray (**B**) are described in the main text.

by acetaldehyde, acetone, acetic acid, GLVs, and ethanol with maximum daily mean emission rates of 0.1–0.6 nmol m^{-2} s^{-1} and fractions of total ecosystem emissions between 1.7–3.9 %. Generally, all observed compounds are emitted at relatively low rates until the end of phase 2 when emissions start to increase until highest values

Table 5.4.: Mean molar emissions from oilseed rape ecosystem in pmol m^{-2} ground area s^{-1} (negative fluxes set to zero) and fraction of each compound to the total BVOC emission in % in brackets for the two phenological growth stages of inflorescence emergence and flowering as well as for the whole observed growth period.

Compound	Inflorescence emergence (19 days)	Flowering (20 days)	Whole period (40 days)
Methanol	900.2 (92.2)	3901.87 (83.3)	2437.98 (84.9)
Acetaldehyde	17.95 (1.8)	118.4 (2.5)	68.91 (2.4)
Ethanol	5.85 (0.6)	108.71 (2.3)	58.36 (2.0)
Acetone	20.12 (2.1)	87.42 (1.9)	54.24 (1.9)
Acetic acid	9.25 (0.9)	207.69 (4.4)	110.62 (3.9)
Isoprene	8.49 (0.9)	30.99 (0.7)	19.78 (0.7)
MACR+MVK	2.78 (0.3)	23.98 (0.5)	13.57 (0.5)
m/z 73	3.52 (0.4)	40.57 (0.9)	22.4 (0.8)
m/z 79	0.7 (0.1)	10.71 (0.2)	5.81 (0.2)
Toluene	0.47 (0.0)	10.41 (0.2)	5.55 (0.2)
GLVs	4.26 (0.4)	92.47 (1.9)	49.37 (1.7)
Xylenes	0.52 (0.1)	8.77 (0.2)	4.73 (0.2)
m/z 118	0.22 (0.0)	14.25 (0.3)	7.4 (0.3)
MTs	0.41 (0.0)	24.6 (0.5)	12.8 (0.4)
SQTs	1.47 (0.2)	1.32 (0.0)	1.35 (0.0)
Total	**976.22 (100.0)**	**4682.16 (100.0)**	**2872.87 (100.0)**

are reached in phase 4 which is followed by a strong decline in phase 5. This emission pattern follows the main temperature and PAR development at the field site. The emission increase between the meteorological phases 2 and 3 (temperature and PAR increase) also coincides with a growth stage change from inflorescence emergence to flowering. As an approach to disentangle between both dependencies SEFs are calculated which are shown in Tab. 5.5 and discussed in the next paragraph. During the observed growth stages, total daily mean BVOC emissions increased from 0.98 (19 days of inflorescence emergence) to 4.68 nmol m^{-2} s^{-1} (20 days of flowering) which is potentially driven by higher temperatures and PAR as well as the change in plant phenology with fully developing flowers. Concerning the seasonality, the compounds show no distinct change in their absolute emissions between phase 1 and 2, although meteorological conditions changed to significantly cooler days and less PAR. During phase 3, emissions of all compounds increase considerable but fall back to the previous level at the very end of the period. The large group of BVOCs within Fig.

5.2.4A increase to normalized values of 0.3–0.6 whereas the group of BVOCs within Fig. 5.2.4C does not emit beyond 0.2. The emission pattern of increase followed by sudden decrease can also be detected in PAR and—lagged by one day—in daily mean temperatures and (even more pronounced) in maximum daily temperatures. After phase 3, the compounds within group A begin to increase and approach a saturation level of maximum values according to PAR and temperature development with varying light and temperature dependences. This saturation was not observed in the emissions of group C which were rising up to normalized values of 1 after phase 4 although PAR and especially temperature already started to decrease again. Fluxes of sesquiterpenes are constantly below zero. Therefore, it can be assumed that they are either deposited to the oilseed rape plants or have undergone chemical reactions with O_3, NO_3, or OH within the headspace of the chambers. The large standard errors compared to the other compounds indicate that the measured magnitudes of fluxes strongly vary during the course of a day or between the chambers. Other than for the maize experiment, isoprene could be detected at m/z 69 for the oilseed rape ecosystem, and thus it is likely that also the isoprene oxidation products methacrolein (MACR) and methyl vinyl ketone (MVK) can be derived from the detection results at m/z 71 (Brilli et al., 2012; Yuan et al., 2017a).

Unfortunately, there are some missing data due to leakages caused by a tube connection problem at the beginning of the observation period, an outage of the engine which opens and closes the chambers end of April, and unspecified problems caused by PTR-MS outages in May. Therefore, potentially interesting informations are lost that could indicate when and how emissions started to decrease until the end of phase 5.

Insights from standard emission factors

As expected, methanol has the highest SEF with 6241 ng g^{-1}DW h^{-1}, followed by acetic acid, GLVs, ethanol, acetone, and monoterpenes (due to its high molar mass) with SEFs of 1388–403 ng g^{-1}DW h^{-1} for the whole period (see Tab. 5.5). The SEFs of group A significantly increase between inflorescence emergence and flowering and are smaller for the inflorescence emergence and the whole period. This indicates a substantial seasonal emission dependence on the plant growth stages in addition to temperature and PAR. All compounds except for methanol and GLVs can be

simulated best with high LDFs (0.8–1.0) for all different plant phenological stages, leading to the presumption that most of the emitted compounds from the oilseed rape ecosystem originate from *de novo* instead of pool emissions. As also indicated by the insensitivity of emissions to decreasing temperatures during inflorescence emergence, it is possible that the oilseed rape ecosystem is less sensitive to temperature changes in that growth stage than assumed in the `JJv` model.

Consequently, statistical correlation between simulations and measurements for this period are less good (NSE of −0.01–0.74) than the emissions during flowering and the whole period (NSE of 0.34–0.84). For hexenal, toluene, and sesquiterpenes the NSE becomes negative, which means that the mean of observed emission data describes the observed emissions better than the joint `JJv`-pool emission model (Niinemets et al., 2013). Both models, `JJv` and the pool emission model, do not include deposition processes of any kind, which is why observed negative fluxes that have occurred in particular for sesquiterpenes (and monoterpenes, toluene, *m/z* 79, and 118 for some days) are fitted very poorly. Thus, I will neglect emissions of sesquiterpenes for the simulation study.

Table 5.5.: BVOC emission parameter for oilseed rape, fitted to the joint `JJv`–pool emission stand-alone modeling approach used in this study. SEF given in ng g^{-1}DW aboveground biomass h^{-1}. See caption of Tab. 5.2 for more details. All values are calculated for three growth periods inflorescence emergence (Infl. emerg., $N = 368$), flowering ($N = 410$), and the whole measurement period (WS, $N = 801$).

Compound	**Period**	**SEF (± SE)**	**LDF**	β	**NSE**
Methanol	Infl. emerg.	4667.2 (± 188.1)	0.7	0.07	0.36
	Flowering	6043.7 (± 638.6)	0.6	0.05	0.64
	Whole period	6241.2 (± 527.1)	0.5	0.08	0.68
Ethanol	Infl. emerg.	315.2 (± 9.5)	1.0	1.0	0.32
	Flowering	651.7 (± 37.4)	1.0	1.0	0.83
	Whole period	645.3 (± 28.0)	1.0	1.0	0.84
Acetone	Infl. emerg.	984.0 (± 9.6)	1.0	1.0	0.74
	Flowering	419.5 (± 25.7)	0.8	0.07	0.83
	Whole period	435.0 (± 20.5)	0.8	0.08	0.84
Isoprene	Infl. emerg.	493.4 (± 7.7)	1.0	1.0	0.53
	Flowering	213.1 (± 16.0)	1.0	1.0	0.65

Table continues on the next page

Table 5.5.: *Continued from previous page.*

Compound	Period	SEF (± SE)	LDF	β	NSE
	Whole period	218.2 (± 13.2)	1.0	1.0	0.66
MACR/MVK	Infl. emerg.	186.0 (± 4.9)	1.0	1.0	0.33
	Flowering	178.0 (± 13.4)	0.9	0.07	0.76
	Whole period	182.5 (± 10.4)	0.9	0.1	0.77
m/z 73	Infl. emerg.	252.8 (± 5.2)	1.0	1.0	0.46
	Flowering	324.9 (± 22.7)	0.9	0.08	0.78
	Whole period	333.3 (± 17.0)	0.9	0.11	0.8
Toluene	Infl. emerg.	-7.0 (± 3.1)	1.0	1.0	-0.01
	Flowering	128.6 (± 10.3)	1.0	1.0	0.72
	Whole period	126.0 (± 7.9)	1.0	1.0	0.72
Hexenal	Infl. emerg.	-21.1 (± 7.9)	1.0	1.0	-0.01
	Flowering	211.2 (± 18.8)	1.0	1.0	0.67
	Whole period	206.8 (± 14.9)	1.0	1.0	0.66
Hexanal	Infl. emerg.	526.1 (± 11.4)	0.5	0.3	0.22
	Flowering	711.1 (± 56.6)	0.8	0.09	0.75
	Whole period	748.6 (± 44.1)	0.8	0.12	0.77
Xylenes	Infl. emerg.	20.3 (± 2.8)	1.0	1.0	0.02
	Flowering	122.3 (± 9.1)	1.0	1.0	0.74
	Whole period	120.4 (± 7.0)	1.0	1.0	0.75
m/z 118	Infl. emerg.	-68.5 (± 4.3)	1.0	1.0	0.03
	Flowering	192.8 (± 21.8)	0.9	0.09	0.59
	Whole period	204.3 (± 16.4)	1.0	1.0	0.61
MTs	Infl. emerg.	-2.2 (± 5.6)	0.0	0.03	0.0
	Flowering	380.4 (± 30.8)	0.9	0.09	0.73
	Whole period	404.4 (± 23.6)	1.0	1.0	0.74
SQTs	Infl. emerg.	-2121.8 (± 70.2)	1.0	1.0	0.12
	Flowering	-80.3 (± 52.7)	1.0	1.0	-0.06
	Whole period	-118.2 (± 67.9)	1.0	1.0	-0.13
Acetaldehyde	Infl. emerg.	710.1 (± 10.9)	1.0	1.0	0.56
	Flowering	225.0 (± 42.8)	0.6	0.04	0.34
	Whole period	245.6 (± 34.2)	0.5	0.08	0.44
Acetic acid	Infl. emerg.	584.0 (± 12.5)	1.0	1.0	0.45
	Flowering	1348.6 (± 121.4)	0.9	0.08	0.69

Table continues on the next page

Table 5.5.: *Continued from previous page.*

Compound	Period	SEF (± SE)	LDF	β	NSE
	Whole period	1388.2 (± 89.7)	0.9	0.12	0.72
m/z 79	Infl. emerg.	-12.0 (± 3.1)	1.0	1.0	0.01
	Flowering	114.2 (± 13.2)	1.0	1.0	0.56
	Whole period	111.8 (± 9.8)	1.0	1.0	0.57

5.2.2. Simulated seasonality

In this Section, I will evaluate simulation results with the joint `JJv`-pool emission model within `LandscapeDNDC` for the observed period, and apply the model for three consecutive growing seasons.

Evaluation of the model results

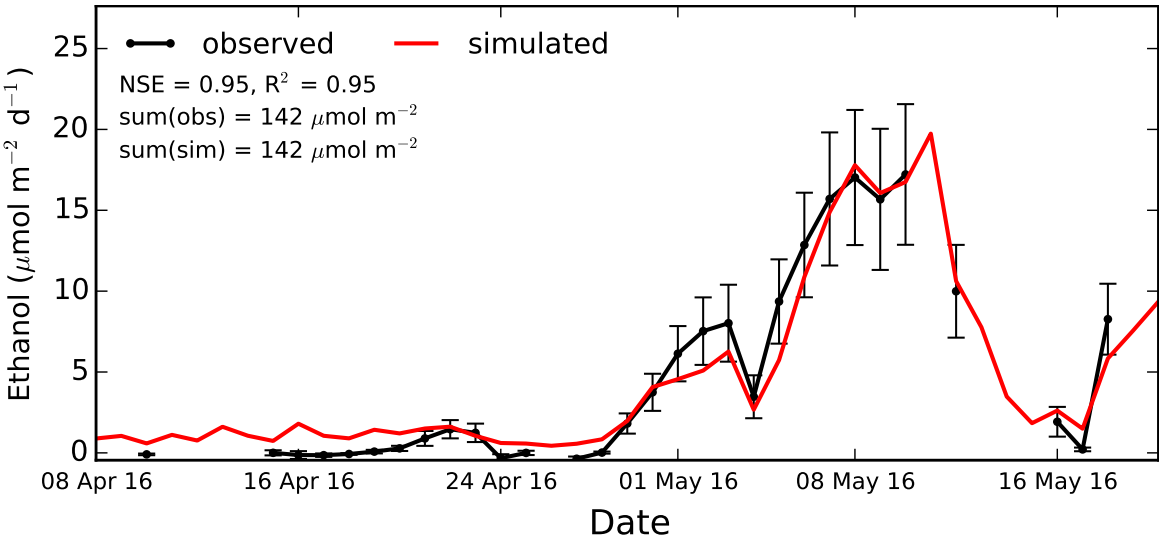

Figure 5.2.5.: Daily sums of observed and simulated (LDF= 1.0) ethanol emissions from oilseed rape ecosystem as a compound example of the group in Fig. 5.2.4A. Error bars indicate ± the standard error of the sum.

The results of simulated biomass and GPP are shown in Fig. 5.2.2. Biomass is underestimated throughout the whole BVOC observation period. However, the modeled negative bias declines towards the end of the period. Variability and magnitude

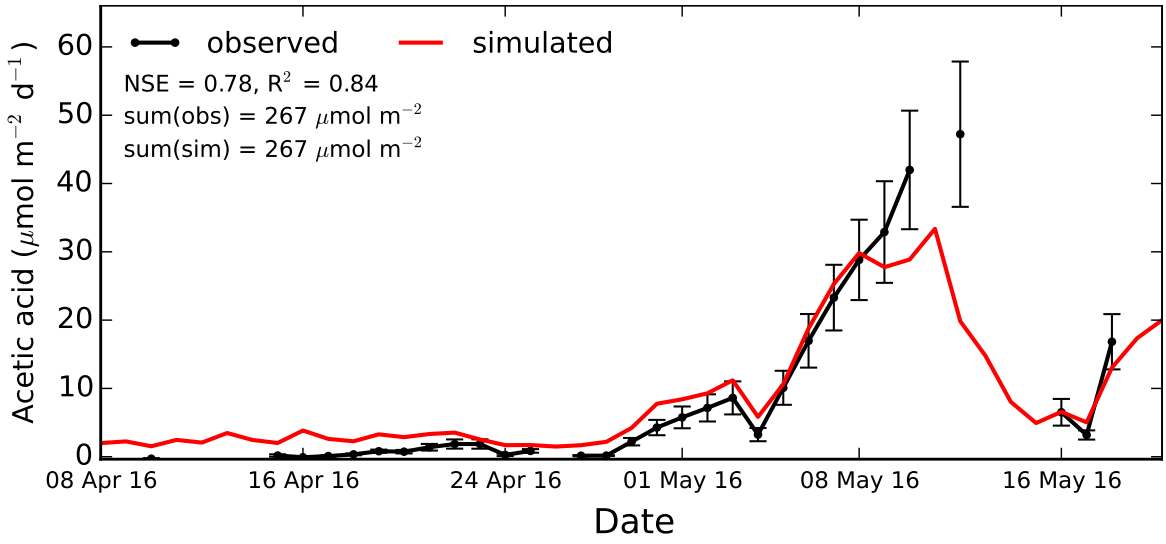

Figure 5.2.6.: Daily sums of observed and simulated (LDF= 0.9) acetic acid emissions from oilseed rape ecosystem as a compound example of the group in Fig. 5.2.4C. Error bars indicate ± the standard error of the sum.

of GPP is simulated well until the end of phase 1 and during phase 3. Phase 2 was significantly cooler (−5 ℃) with less PAR than in phase 1 and was thus simulated to perform a relatively low photosynthetical activity although observations of GPP indicate comparable levels between both periods. Similarly, higher GPP was expected in phase 3 compared to phase 4 because of significantly higher temperature and PAR values, but such a difference between phases could not be observed. Thus, it is hypothesized that plant stress occurred, e.g. due to drought which was not appropriately simulated by the model.

Despite the problems with GPP, BVOC emissions were very well simulated. Figures 5.2.5 and 5.2.6 show exemplary simulated BVOC emissions and observations of one compound from the group within Fig. 5.2.4A and 5.2.4C, respectively. Modeling results from sesquiterpenes as the only representative within the deposition flux group of Fig. 5.2.4B are not shown as explained earlier.

With an NSE of 0.95, ethanol emissions are represented very well by the `JJv` within `LandscapeDNDC` approach (LDF of 1.0), besides a small overestimation until the end of April and the slight underestimation (still within the observational standard error) during phase 3 (see Fig. 5.2.5). Emissions of acetic acid as a representative of group C, are also simulated reasonably well (NSE = 0.78), although, the observed increase after

Table 5.6.: Evaluation of simulated BVOC emissions (daily sums) from oilseed rape ecosystem by NSE with (w/) and without (w/o) scaling of SEFs to summed up observations, coefficient of determination (R^2), and the ratio between the sum of all observed and their coinciding simulated values.

Compound	NSE w/	NSE w/o	R^2	$\frac{\sum_{i=1}^{n(\text{obs})} \text{obs}_i}{\sum_{i=1}^{n(\text{obs})} \text{sim}_i}$
Methanol	0.89	0.89	0.92	0.95
Acetaldehyde	0.66	0.69	0.78	0.88
Ethanol	0.95	0.81	0.95	1.36
Acetone	0.95	0.94	0.96	1.02
Acetic acid	0.78	0.72	0.84	1.18
Isoprene	0.81	0.45	0.89	2.08
MACR/MVK	0.9	0.83	0.93	1.17
m/z 73	0.91	0.84	0.94	1.19
m/z 79	0.69	0.61	0.74	1.23
Toluene	0.83	0.71	0.86	1.32
Hexenal	0.83	0.75	0.87	1.2
Hexanal	0.84	0.8	0.88	1.1
Xylenes	0.89	0.76	0.92	1.31
m/z 118	0.75	0.61	0.78	1.38
MTs	0.83	0.68	0.87	1.39

8 May is not captured by the model (see Fig. 5.2.6). Similarly as for the deviation in GPP, a possible explanation for thus underestimation could be the occurrence of some kind of stress. For example drought stressed ecosystems have been occasionally shown to increase their oxygenated BVOCs emissions (Loreto and Schnitzler, 2010). During the oilseed rape experiment, these high emissions could be observed for methanol, acetaldehyde, acetic acid, *m/z* 79, and hexanal (not shown).

Generally, the simulation results are very satisfying for all observed BVOCs with NSE values of 0.66–0.95 (see Tab. 5.6). Again, the model skill could be improved by scaling SEFs to the sum of observed emissions. Due to a potential (drought) stress induced emission response of all compounds within group C, a lower model efficiency (acetaldehyde, *m/z* 79, and acetic acid with values of 0.66, 0.69, and 0.78, respectively) was achieved compared to the compounds within group A.

Model application for three years

In the following, simulation results for three consecutive years with planted oilseed rape are shown.

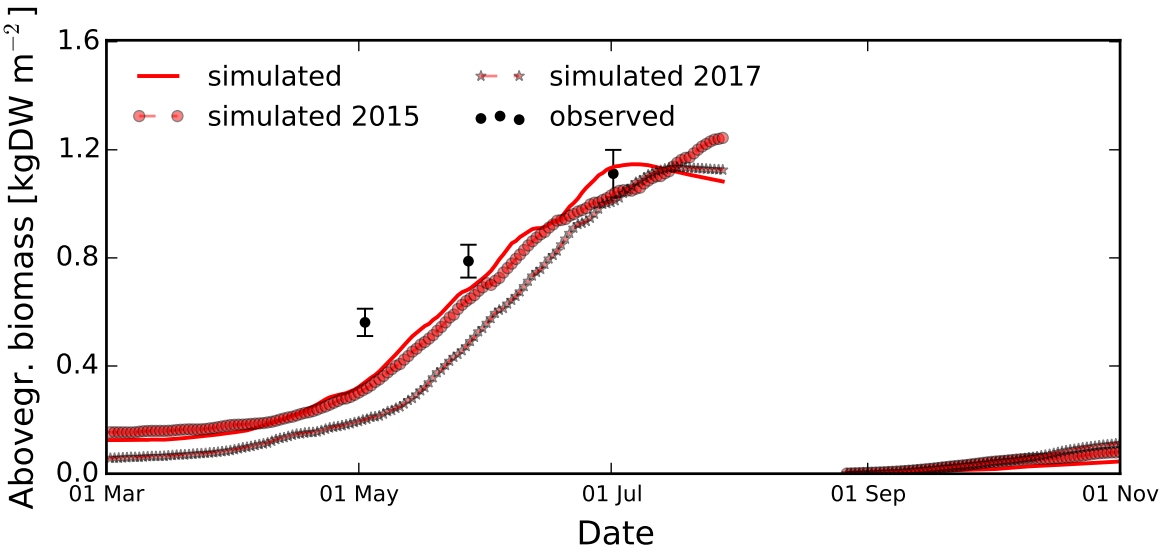

Figure 5.2.7.: Aboveground biomass of oilseed rape plants. 2016 is the measurement period, whereas the years 2015 (dashed red circles) and 2017 (dashed red stars) are simulations only. See Fig. 5.1.8 for a detailed caption.

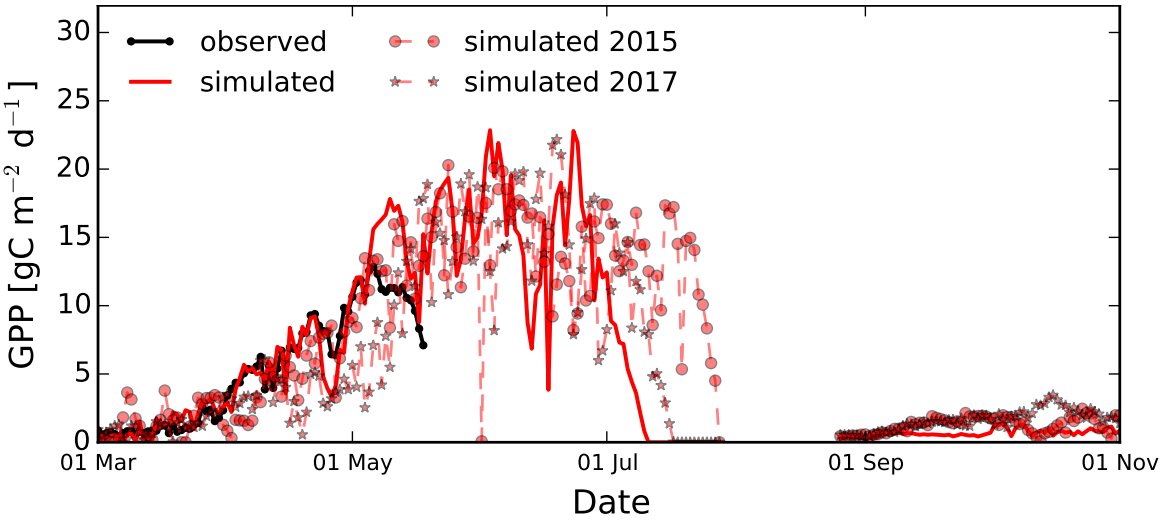

Figure 5.2.8.: Daily sums of GPP from oilseed rape ecosystem from simulations over three seasons (red lines) and calculated based on continuous CO_2 measurements during the season 2016 (black dotted line).

The simulated biomass of the oilseed rape plants is somewhat underestimated dur-

ing the first half of its development in 2016. It seems that the model has difficulties to sustain the high biomass increase particularly at the start of the growing season in 2016, so that the first observation point is simulated around 40 % below the observed one (see Fig. 5.2.7). Nevertheless, the simulation achieves to meet the measured final biomass beginning of July. The simulated season 2015 is very similar to 2016, whereas the development of the biomass during 2017 is apparently lower compared to the other seasons, but again reaching similar values in the end. It is likely that the lower monthly mean temperatures in the growing season 2017 (Nov 2016: 3.6 ℃, Dez 2016: 3.3 ℃, Jan 2017: -1.0 ℃, Feb 2017: 1.4 ℃, Mar 2017: 6.7 ℃) compared to that in 2016 (Nov 2015: 6.0 ℃, Dez 2015: 5.5 ℃, Jan 2016: 0.3 ℃, Feb 2016: 3.4 ℃, Mar 2016: 4.4 ℃) are responsible for this lesser plant growth.

The simulated magnitude and seasonal development of GPP of the oilseed rape plants resembles the measurements of 2016, with short and low periods of under- and overestimation before and after the beginning of May (see Fig. 5.2.8). During the years with no observations, the variability of GPP is well within a range that can be expected from different meteorological boundary conditions. Similar to maize, the plants reached senescence earliest during season 2016, and latest in 2015 with a temporal difference of around half a month to one month.

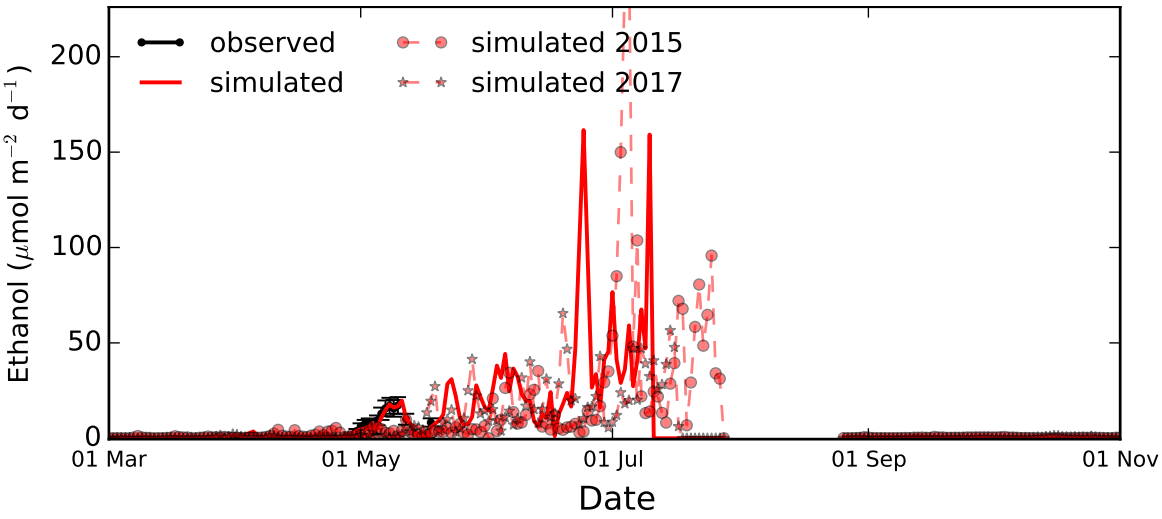

Figure 5.2.9.: Daily sums of observed and simulated ethanol emissions from oilseed rape ecosystem. Similar to Fig. 5.2.5 but for three seasons.

Figures 5.2.9 and 5.2.10 show simulated BVOC fluxes for three entire growth periods, exemplary for ethanol and acetic acid from seasonality group A and C (see

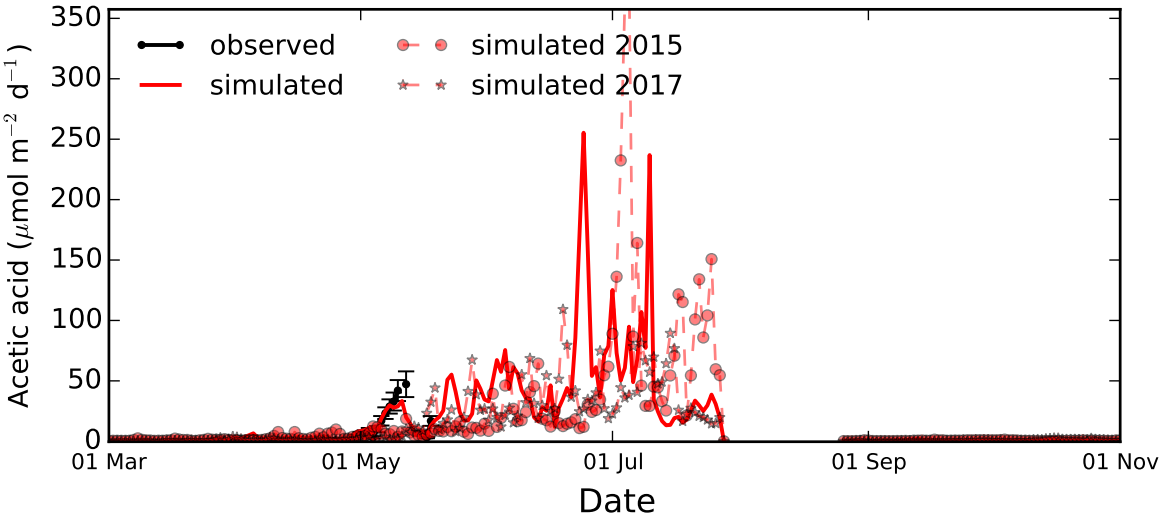

Figure 5.2.10.: Daily sums of observed and simulated acetic acid emissions from oilseed rape ecosystem. Similar to Fig. 5.2.6 but for three seasons.

Fig. 5.2.4), respectively (again sesquiterpenes from group B with deposition fluxes only, are not considered). The simulated emissions of both compounds increase after the observation period which is linked to a simultaneous increase in temperature and PAR as well as growing biomass and increasing GPP. Especially the peaks around 1 July 2015 and 2016 exceed the observed emissions in April and May by far (the peak throughout two days in the simulation results for 2015 is cut for a better readability of the overall emission rates). Ethanol reaches a maximum value of 256 μmol m^{-2} d^{-1} and acetic acid reaches 391 μmol m^{-2} d^{-1}. These strong emission rates are due to the observed daily maximum temperatures of 34.5 and 34.8 ℃. At the end of the growing season, when the oilseed rape plants are fully ripened and do not assimilate carbon anymore (simulated GPP = 0, between mid July and start of August 2015–2017), also the simulated ethanol emissions (LDF = 1.0) drop to zero. Acetic acid emissions (LDF = 0.9) are simulated until the start of August for all years, though at smaller rates in 2016 and 2017 than in 2015, more or less corresponding to monthly mean temperatures in August (2015: 20.6 ℃, 2016: 17.2 ℃, 2017: 18.2 ℃).

5.3. BVOC fluxes from ryegrass

The next two sections describe and discuss observations (Sect. 5.3.1) and simulations (Sect. 5.3.2) from the ryegrass campaign.

5.3.1. Magnitude and composition from observations

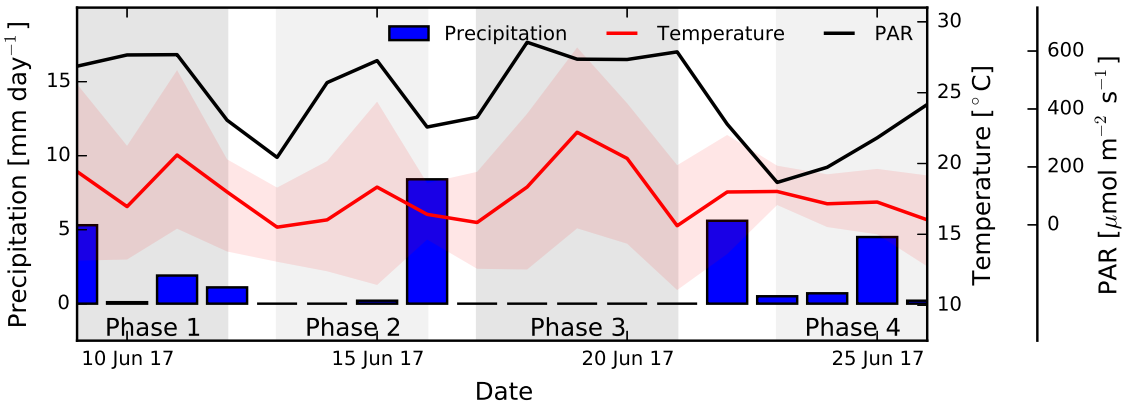

Figure 5.3.1.: Temperature, PAR, and precipitation during the ryegrass field experiment 2017. The meteorological phases described in the main text are depicted in gray. See 5.1.1 for a detailed caption.

The oscillating meteorological conditions during the ryegrass campaign in 2017 are divided into four different phases (see Fig. 5.3.1): (1) temperature increase and decrease of around 3 °C and PAR decrease from 587–361 μmol m^{-2} s^{-1} within four days, (2) a similar pattern at 2 °C lower average temperature and increase and decrease of PAR of 233–567–338 μmol m^{-2} s^{-1}, (3) warmest conditions with a temperature oscillation of around 6 °C around an average temperature of 18.5 °C and with highest PAR during the measurement period increasing from 371 to 630 μmol m^{-2} s^{-1}, and (4) after a strong radiative drop, again increasing PAR from 146 to 415 μmol m^{-2} s^{-1} at almost constant temperatures of around 17 °C. During all phases except of phase 3 (where no rainfall occurred), precipitation sums were between 5.9 and 8.6 mm. Generally, June and July 2017 were relatively wet with 270 mm of rainfall compared to a long term mean of 132 mm (1992–2015). However, August and September were substantially drier with a sum of 70 mm instead of 113 mm during the long term mean. Mean temperatures were well in line with long-term mean with a maximum

deviation of +1.3 ℃ in June.

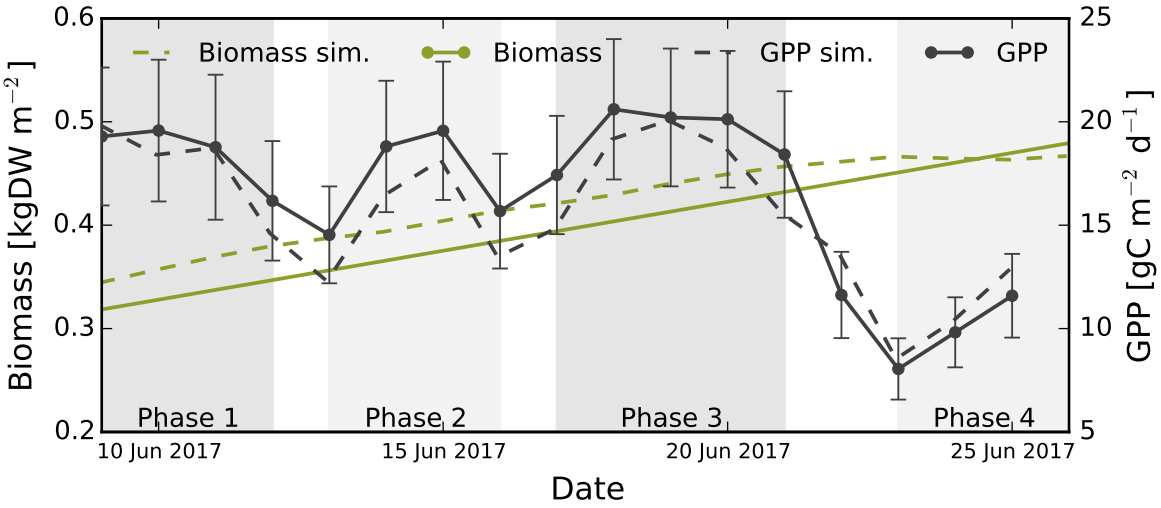

Figure 5.3.2.: Observed biomass and daily sums of gross primary production (GPP) from ryegrass ecosystem field experiment 2017. See Fig. 5.1.2 for a detailed caption.

During the whole measurement period, the observed aboveground biomass increased from 0.32–0.48 kgDW m^{-2} which was fairly well met by the model (see Fig. 5.3.2). Observed and simulated GPP strictly follows the development of temperature and PAR during phases 1–3 until the cooling and radiation decrease from phase 3 to phase 4.

The ryegrass plants were mainly in the heading stage during our BVOC field campaign (see Fig. 5.3.3). Heading, as a plant development stage of perennial grasses is similar to the emerging of inflorescences in annual crops (Gustavsson, 2011). Only during the very last days of our measurements, the plants developed to the flowering stage. Hence, due to the small observational sample size during flowering, specific plant phenological emission pattern related to this stage are not very meaningful.

According to the magnitude and seasonal characteristics, BVOC emissions can be divided again into three different groups (see Fig. 5.3.3 and 5.3.4). Similar to oilseed rape, methanol was the dominating compound emitted from the ryegrass ecosystem with daily mean emission rates up to 2.8 nmol m^{-2} s^{-1} (see Fig. 5.3.3) and a fraction of 80.2 % of all molar compounds considering the whole observational period (see Tab. 5.7). It is followed by maximum daily mean emission rates of 0.12–0.77 nmol m^{-2} s^{-1} for the compounds acetaldehyde, acetone, and ethanol, that represent total ecosystem emission fractions between 2.2–8.9 %. The differentiation by seasonal development of

emitted BVOCs shows that most of the compounds follow an emission pattern that generally corresponds to temperature and PAR development (see Fig. 5.3.4A).

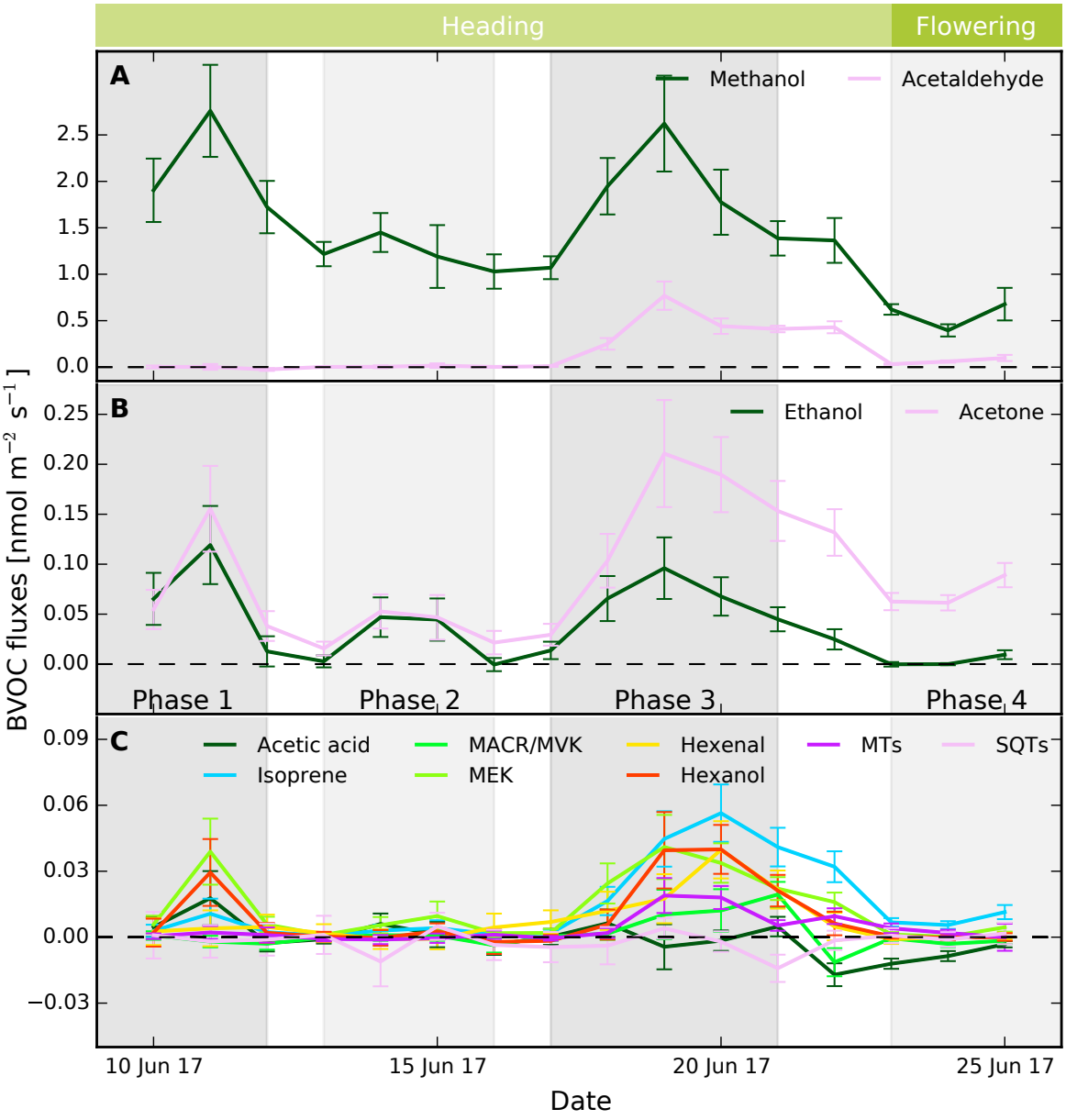

Figure 5.3.3.: Ryegrass plant phenological stages (above **A**) and daily mean BVOC emissions during the field experiment 2017. Only daily values with more than 75% of flux data (72 values) are shown. See Fig. 5.1.3 for a detailed caption.

Nevertheless, emissions in phase 2 seem to be less intense compared to phase 1 and 3, considering that temperatures are only moderately lower, especially for acetone, MEK, and hexanol, where normalized values decrease from around 0.8 to values well below

0.4. However, since the PTR-MS failed for 4 hours at the afternoon of 15 Jun 2017 (12:50–17:15 o'clock) due to excessive heat, emissions are likely underrepresented.

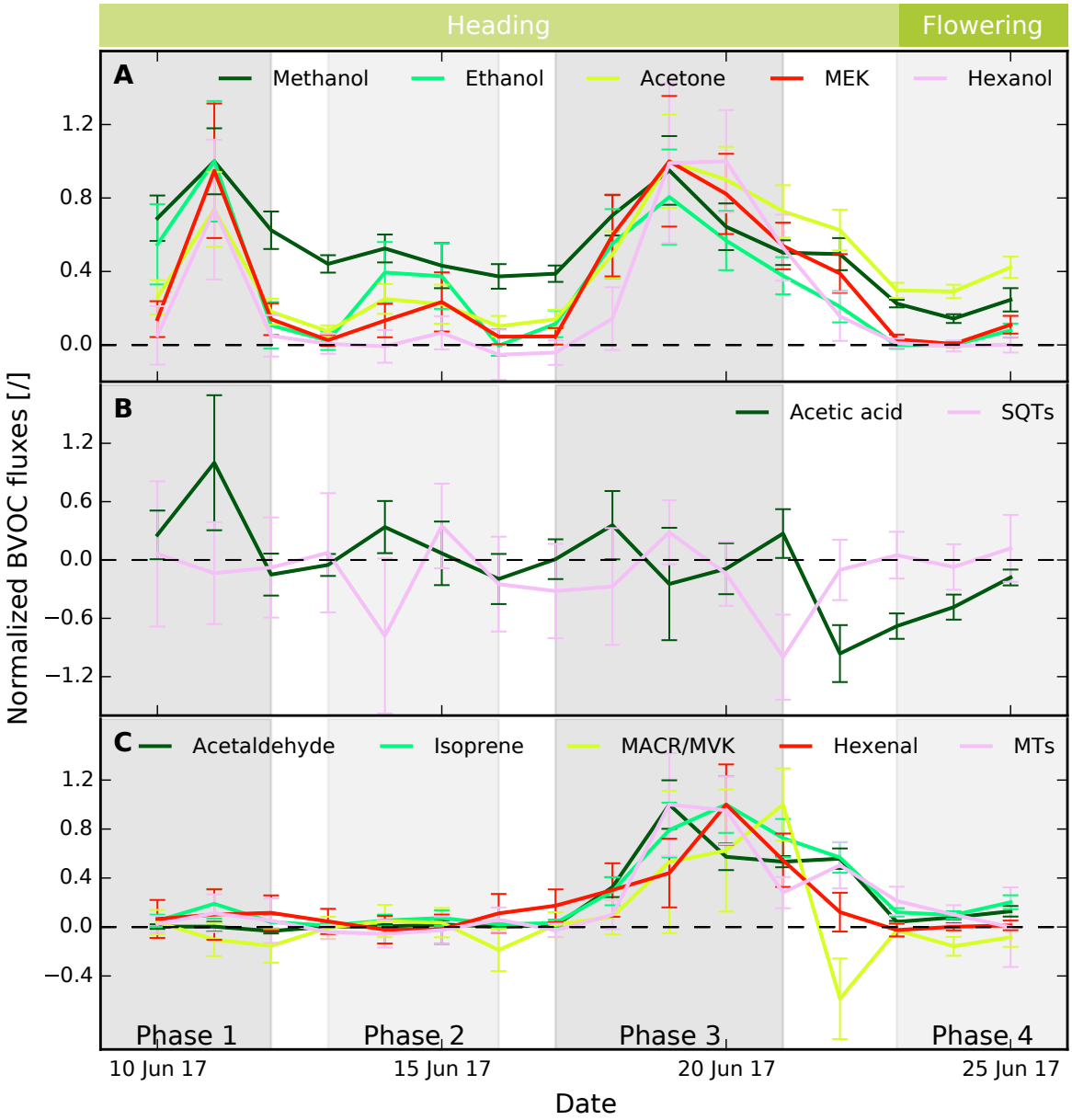

Figure 5.3.4.: Daily mean normalized BVOC emissions (emission rates scaled to each compound's maximum value throughout the measurement period) and ± standard error of the mean. Only daily values with more than 75% of flux data (72 values) are shown. The meteorological phases described in the main text are depicted in gray and named in **C** (as in Fig. 5.1.4 and Fig. 5.2.4 but for ryegrass field campaign).

In phase 3, all compounds of group A except ethanol, reach the highest emission rates

Table 5.7.: Mean molar emissions from ryegrass ecosystem in pmol m^{-2} ground area s^{-1} (negative fluxes set to zero) and fraction of each compound to the total BVOC emission in % in brackets for the two phenological growth stages of inflorescence emergence and flowering as well as for the whole observed growth period.

Compound	Heading (14 days)	Flowering (4 days)	Whole period (18 days)
Methanol	1647.98 (80.4)	558.39 (78.3)	1416.47 (80.2)
Acetaldehyde	184.8 (9.0)	58.45 (8.2)	157.92 (8.9)
Ethanol	48.01 (2.3)	4.31 (0.6)	38.75 (2.2)
Acetone	91.98 (4.5)	71.72 (10.1)	87.77 (5.0)
Acetic acid	6.14 (0.3)	0.03 (0.0)	4.84 (0.3)
Isoprene	17.19 (0.8)	8.16 (1.1)	15.28 (0.9)
MACR+MVK	6.22 (0.3)	0.37 (0.1)	4.98 (0.3)
MEK	16.07 (0.8)	2.68 (0.4)	13.23 (0.7)
Hexenal	11.3 (0.6)	1.32 (0.2)	9.19 (0.5)
Hexanal	13.03 (0.6)	0.69 (0.1)	10.42 (0.6)
MTs	4.75 (0.2)	2.86 (0.4)	4.36 (0.2)
SQTs	2.49 (0.1)	4.4 (0.6)	2.9 (0.2)
Total	**2049.97 (100.0)**	**713.4 (100.0)**	**1766.11 (100.0)**

at the hottest days during the field experiment. Only emissions of hexanol were still high one day later, when all other compounds of group A already declined. BVOCs of the group within Fig. 5.3.4C showed only low normalized emission rates (< 0.4) during both phase 1 and 2 but increased emissions in phase 3 reaching maximum rates when the temperature already decreased but PAR was still at a high level. Thus, it seems that especially isoprene, hexenal, MACR/MVK, and monoterpenes are more sensitive to radiation than temperature alone, assuming that the ryegrass ecosystem was not stressed at that time. Acetic acid and sesquiterpenes, which are pooled to one group shown in Fig. 5.3.4B, are emitted and deposited with similar rates but do not show a distinct seasonality that can be linked to the predominant meteorological situation. Interestingly. deposition and emission of these two compounds develop in the opposite direction to each other. Hexenal and hexanal showed very similar seasonal emission patterns for maize and oilseed rape ecosystem, and were thus summed up into the group of GLVs as it is commonly done. However, for the ryegrass ecosystem, hexenal ($C_6H_{10}O$) emitted at relatively low rates at the beginning of the observation period during phase 1 (group C), whereas hexanal ($C_6H_{12}O$) emitted already at relatively

high rates during this phase (group A).

Insights from standard emission factors

The SEFs are highest for methanol with 2698 ng g^{-1}DW h^{-1}, followed by acetaldehyde, acetone, and ethanol with values ranging from 796–192 ng g^{-1}DW h^{-1} for the whole period (see Tab. 5.8). Most of the compounds have LDFs of 1.0 except for acetone (0.9), methanol (0.8), and acetaldehyde, where the best results for the period of heading and the whole observation period are obtained when only pool emissions are considered. The LDF values for the flowering stage alone should be regarded with care because the sample size for the calculation of parameters has been very small. Nevertheless, some compounds such as methanol, ethanol, acetone, acetaldehyde, and isoprene, yield reasonable NSE values. Interestingly, the SEFs of compounds with similar LDF between different growth stages (ethanol, acetone, isoprene) are smallest during flowering which is contrary to what has been observed from maize and oilseed rape ecosystems. This is also counter intuitive, because one would expect an emission potential increase from emerging flowers as attractors for insects.

Generally, the goodness of fit as derived with the stand-alone model for the whole observation period performs reasonably well with NSE of 0.47–0.71 for BVOCs that do not show negative emission rates.

Table 5.8.: BVOC emission parameter for ryegrass, fitted to the joint JJv–pool emission stand-alone modeling approach used in this study. SEF given in ng g^{-1}DW aboveground biomass h^{-1}. See caption of Tab. 5.2 for more details. All values are calculated for three growth periods heading ($N = 312$), flowering ($N = 85$), and the whole measurement period (WS, $N = 397$).

Compound	Period	SEF (± SE)	LDF	β	NSE
Methanol	Heading	2541.5 (± 314.9)	0.7	0.07	0.54
	Flowering	3413.7 (± 82.0)	0.5	0.26	0.61
	Whole period	2697.9 (± 298.5)	0.8	0.06	0.54
Ethanol	Heading	180.7 (± 30.2)	0.9	0.09	0.4
	Flowering	46.3 (± 3.3)	1.0	1.0	0.35
	Whole period	192.6 (± 27.3)	1.0	1.0	0.41
Acetone	Heading	440.6 (± 38.8)	0.9	0.09	0.71

Table continues on the next page

Table 5.8.: *Continued from previous page.*

Compound	Period	SEF (± SE)	LDF	β	NSE
	Flowering	399.0 (± 10.0)	0.9	0.06	0.75
	Whole period	439.1 (± 34.8)	0.9	0.09	0.71
MEK	Heading	120.7 (± 15.5)	1.0	1.0	0.52
	Flowering	36.9 (± 2.6)	1.0	1.0	0.29
	Whole period	117.7 (± 14.0)	1.0	1.0	0.52
Hexanal	Heading	149.7 (± 19.3)	1.0	1.0	0.56
	Flowering	5.2 (± 3.0)	1.0	1.0	0.01
	Whole period	144.6 (± 17.7)	1.0	1.0	0.54
Acetic acid	Heading	23.5 (± 11.7)	1.0	1.0	0.09
	Flowering	-38.0 (± 4.1)	1.0	1.0	-0.44
	Whole period	21.3 (± 10.6)	1.0	1.0	0.08
SQTs	Heading	-12.0 (± 31.9)	0.3	0.05	0.0
	Flowering	-110.9 (± 22.1)	1.0	1.0	0.08
	Whole period	-17.3 (± 30.3)	0.6	0.08	0.01
Acetaldehyde	Heading	784.1 (± 84.5)	0.0	0.25	0.57
	Flowering	669.0 (± 22.1)	0.5	0.3	0.47
	Whole period	795.8 (± 75.9)	0.0	0.26	0.58
Isoprene	Heading	113.9 (± 11.9)	1.0	1.0	0.62
	Flowering	102.8 (± 3.4)	1.0	1.0	0.62
	Whole period	113.5 (± 10.7)	1.0	1.0	0.63
MACR+MVK	Heading	44.9 (± 11.4)	1.0	1.0	0.28
	Flowering	-4.2 (± 2.4)	1.0	1.0	-0.11
	Whole period	43.1 (± 10.3)	1.0	1.0	0.26
Hexenal	Heading	101.1 (± 18.7)	1.0	1.0	0.36
	Flowering	22.9 (± 3.9)	1.0	1.0	0.11
	Whole period	98.3 (± 16.8)	1.0	1.0	0.36
MTs	Heading	78.5 (± 11.1)	1.0	1.0	0.52
	Flowering	58.9 (± 9.7)	0.2	0.3	0.01
	Whole period	76.8 (± 10.9)	1.0	1.0	0.47

5.3.2. Simulated seasonality

In the following, I will evaluate results from the joint JJv-pool emission model within LandscapeDNDC for the observed period, and subsequently apply the model for three consecutive growing seasons.

Evaluation of the model results

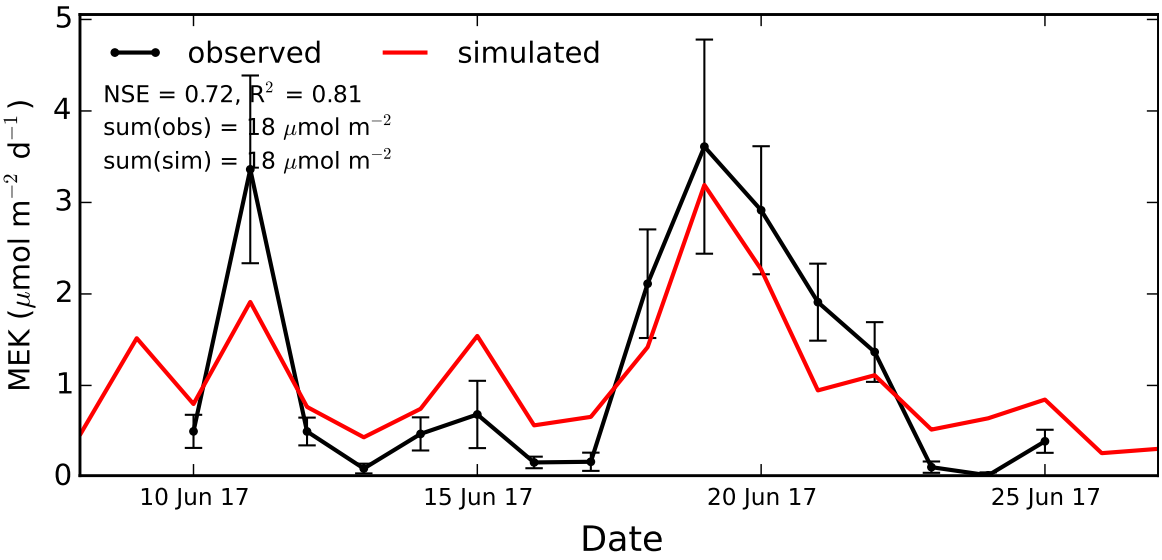

Figure 5.3.5.: Daily sums of observed and simulated (LDF= 1.0) methyl ethyl ketone (MEK) emissions from ryegrass ecosystem as a compound example of the group in Fig. 5.3.4A. Error bars indicate ± the standard error of the sum.

The magnitude of simulated aboveground biomass during the period of the field experiment is generally in good agreement with observations (see Fig. 5.3.2). The simulated growth rate in that phase remains constant until the end of phase 3. Afterwards it declines, which can be linked to a strong reduction in simulated GPP at the same time. Also GPP is generally well represented by the model with respect to variability and magnitude, including the strong GPP decrease between phase 3 and 4 that has been observed.

Simulated BVOC emissions during the observation period are shown exemplary in Figs. 5.3.5 and 5.3.6 for the emission pattern group A and C, respectively. For methyl ethyl ketone, the general seasonal variability that is simulated by the model based on leaf development could be reasonably captured, resulting in an NSE with 0.72. Yet,

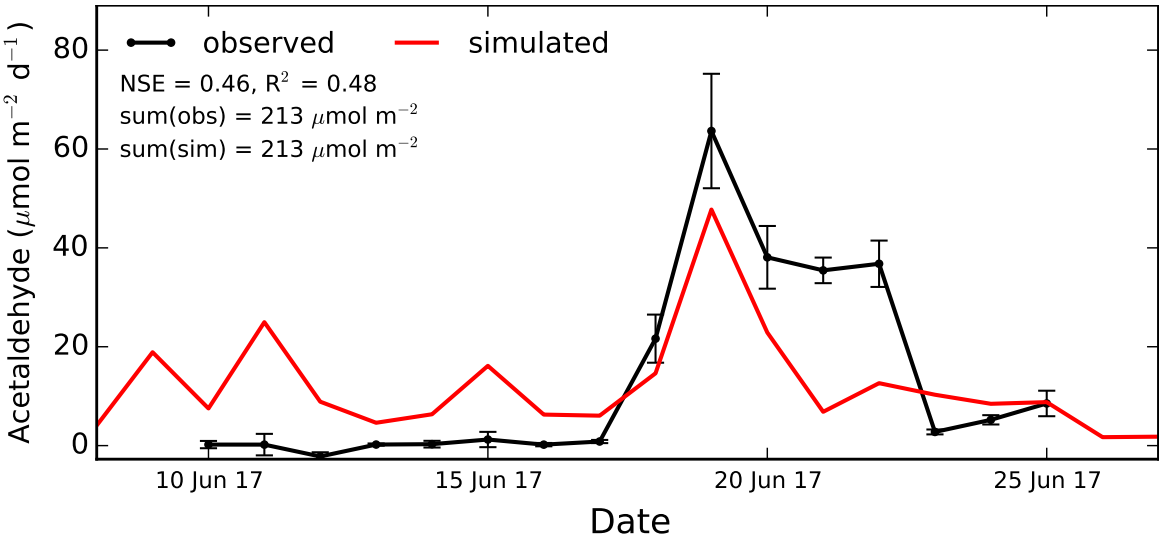

Figure 5.3.6.: Daily sums of observed and simulated (LDF= 0.0) acetaldehyde emissions from ryegrass ecosystem as a compound example of the group in Fig. 5.3.4C. Error bars indicate ± the standard error of the sum.

simulated emissions are not as high as the observed emission peak in phase 1 and overestimates the (negligible) emission increase during phase 2. However, the emission pattern of phase 3 is in accordance to observations with rates mostly within the range of the standard error. In phase 4 simulated emissions are again overestimated since measured emissions drop to practically zero. Simulated acetaldehyde emissions (see Fig. 5.3.6) strictly follow the temperature variability (LDF= 0.0) during phases 1 and 2, although measurements did not show such a dependency but rather constant emissions with very low rates. Additionally, after the emission burst of one very warm day (19 June), observed emissions remain several days on a plateau at rates which are not justified by temperature and radiation conditions. Also, a clear distinction between major growth stages is not apparent, leading to the assumption that physiological changes that happen within a growth stage could be responsible drivers, e.g. the proportion of the inflorescence during the heading stage. Similar to the emissions from maize and oilseed rape, the compounds within the group from Fig. 5.3.4B (acetic acid and sesquiterpenes) are mostly deposited and thus, are not captured by the applied model as already discussed for methanol exchange rates from the maize ecosystem (see Figs. 5.1.6, 5.1.11).

For all other BVOCs simulation by the joint `JJv`–pool emission model within `LandscapeDNDC` are within a reasonable range of NSE 0.34–72. This statement is

Table 5.9.: Evaluation of daily summed simulated vs observed BVOC emissions from ryegrass ecosystem by Nash-Sutcliffe efficiency (NSE), coefficient of determination (R^2), and the ratio between the sum of all observed and their coinciding simulated values.

Compound	NSE w/	NSE w/o	R^2	$\frac{\sum_{i=1}^{n(\text{obs})} \text{obs}_i}{\sum_{i=1}^{n(\text{obs})} \text{sim}_i}$
Methanol	0.34	-0.14	0.36	0.78
Acetaldehyde	0.46	0.47	0.48	0.99
Ethanol	0.61	0.6	0.62	0.87
Acetone	0.68	0.59	0.69	0.83
Acetic acid	-0.03	-0.27	0.05	-0.2
Isoprene	0.46	0.47	0.49	0.87
MACR/MVK	0.09	-0.29	0.2	0.21
MEK	0.72	0.73	0.81	0.8
Hexenal	0.34	0.28	0.36	0.72
Hexanal	0.55	0.55	0.77	0.61
MTs	0.46	0.46	0.6	0.65

only partly true for the emission pattern of group C, which was represented with an average NSE of 0.41 (in group A it is 0.60), probably due to internal changes in metabolite production that is not covered by the model.

Model application for three years

The simulated biomass growth could represent observed yields for repeated cuttings during the season 2017 quite well (see Fig. 5.3.7), despite a slight overestimation of the first growth period. Based on this evaluation, the simulated season 2016 yields lower biomass values than 2015 and 2017, which is more pronounced before the third cutting event. The main reason is assumed to be the dry July 2016 with a precipitation sum of only 21 mm, compared to 88 and 130 mm during 2015 and 2017, respectively.

Also GPP of ryegrass during 2017 could be very well reproduced by simulations, except for a short period of overestimation for several days around beginning of April and directly after the first cut (see Fig. 5.3.8). Generally, the grass cutting events, which occurred twice during GPP observations and reduced leaf biomass for photosyntheis, are also clearly visible in the simulations for all three years. Similar to maize

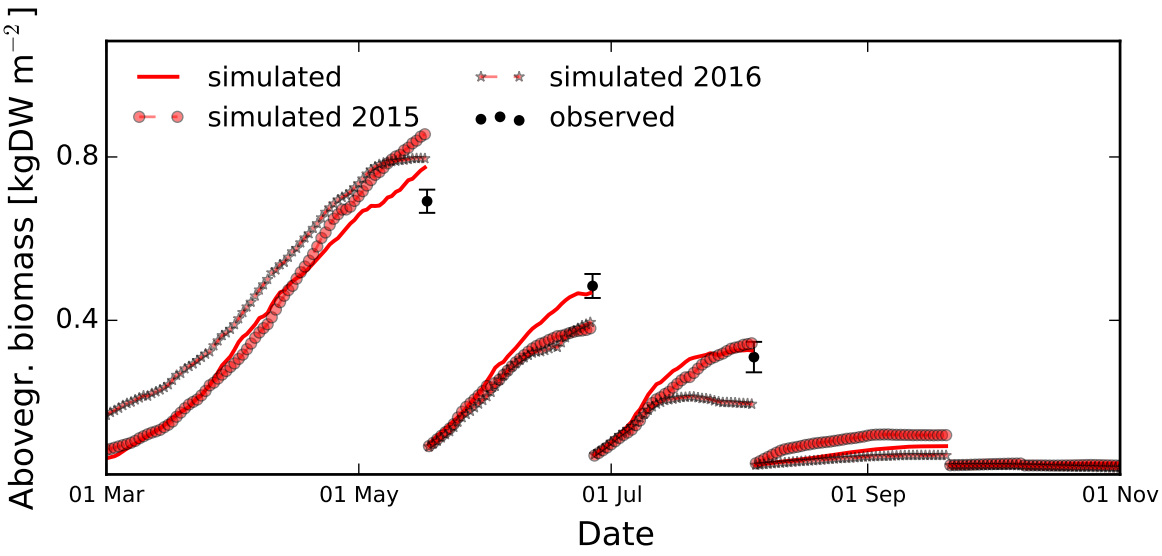

Figure 5.3.7.: Aboveground biomass of ryegrass plants. 2017 is the measurement period, whereas the years 2015 (dashed red circles) and 2016 (dashed red stars) are simulations only. See Fig. 5.1.8 for a detailed caption.

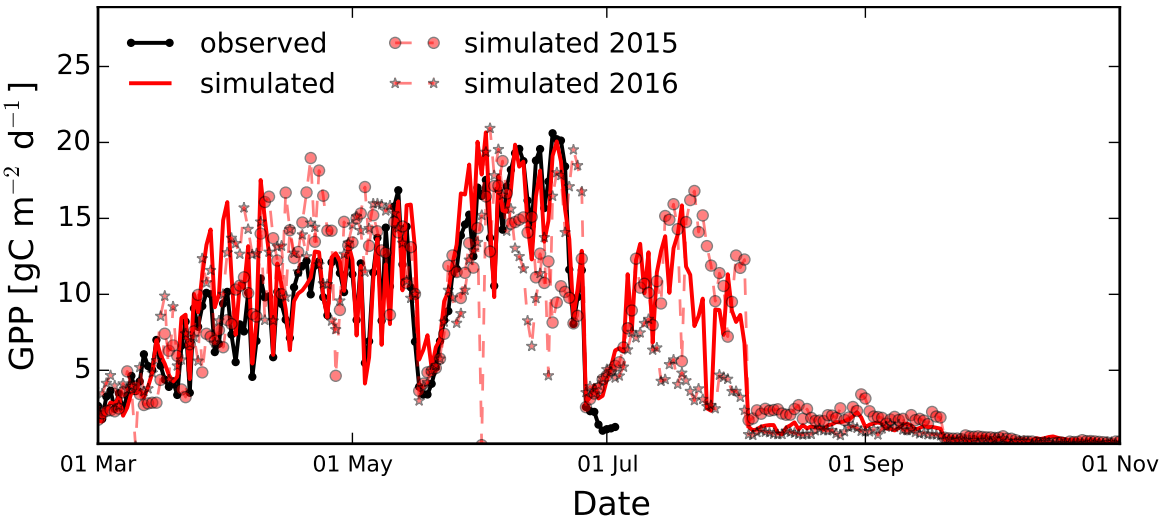

Figure 5.3.8.: Daily sums of GPP from ryegrass ecosystem from simulations over three seasons (red lines) and calculated based on continuous CO_2 measurements during the season 2017 (black dotted line).

and oilseed rape simulations, GPP in 2016 remains lower in the beginning of June compared to the other years. After this decrease GPP cannot recover anymore to the high values of 2015 and 2017, which also lead to considerably lower values in the aboveground biomass.

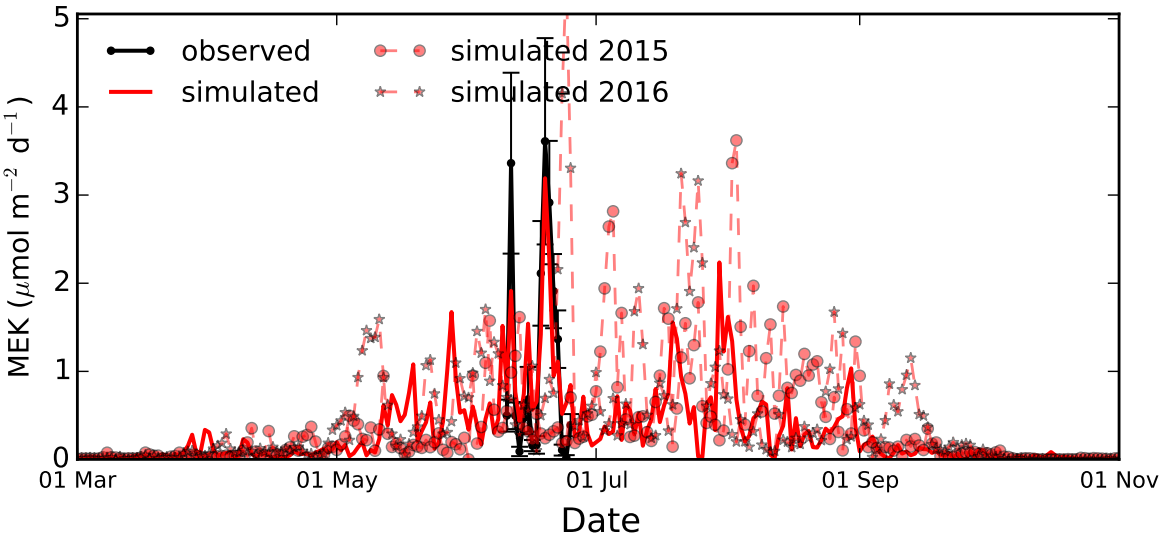

Figure 5.3.9.: Daily sums of observed and simulated methyl ethyl ketone emissions from ryegrass ecosystem. Similar to Fig. 5.3.5 but for three seasons.

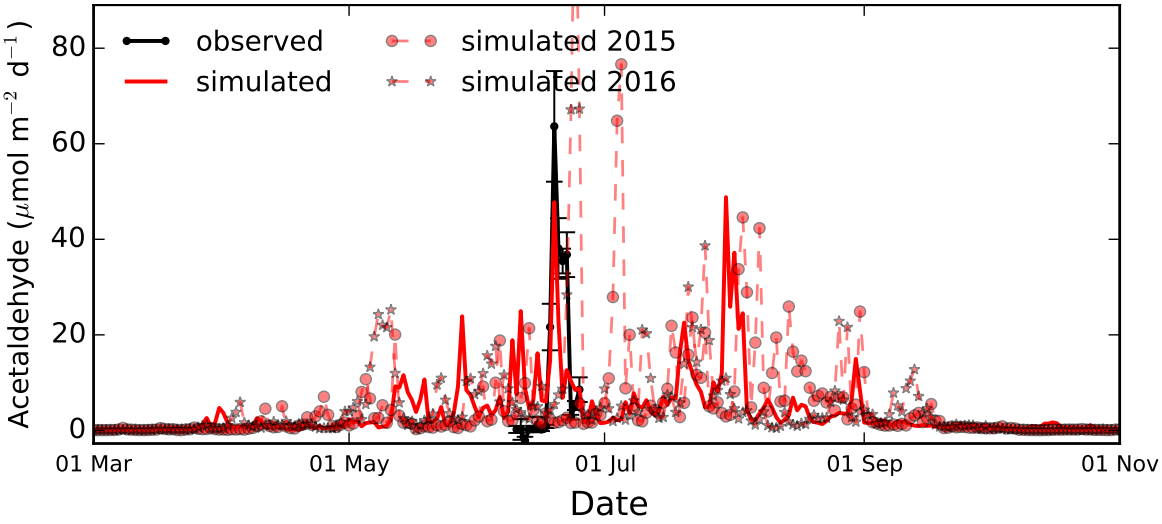

Figure 5.3.10.: Daily sums of observed and simulated acetaldehyde emissions from ryegrass ecosystem. Similar to Fig. 5.3.6 but for three seasons.

The Figs. 5.3.9 and 5.3.10 show methyl ethyl ketone and acetaldehyde emissions for three entire growth seasons. Interestingly, the five simulated cutting events which decrease the ryegrass plants to around 10–20 % of their initial biomass, do not visibly decrease emissions. Instead, emissions are much more related to temperature (and PAR) so that the decrease in leaf area is of minor importance. However, methyl ethyl ketone emissions, which are strongly coupled to photosynthesis (LDF= 1.0), show

more intensive peaks during these warm days than emissions of acetaldehyde which is simulated as pool emissions only (with a very high β-coefficient of 0.26). Thus, example shows, that simulated emission rates can be more sensitive to temperature (exponential relation) and PAR than to the biomass (linear relation).

5.4. Annual BVOC fluxes and potential impact on air chemistry

Finally, the simulations described in sections 5.1, 5.2, and 5.3 which are based on the same meteorological conditions, are now used to compare the annual magnitude and composition of BVOC emissions between the three different bioenergy crops. Additionally, by considering BVOC–OH reaction rate coefficients, the plant specific impacts on the atmospheric chemistry is estimated.

5.4.1. Total annual BVOC fluxes from maize, oilseed rape, and ryegrass

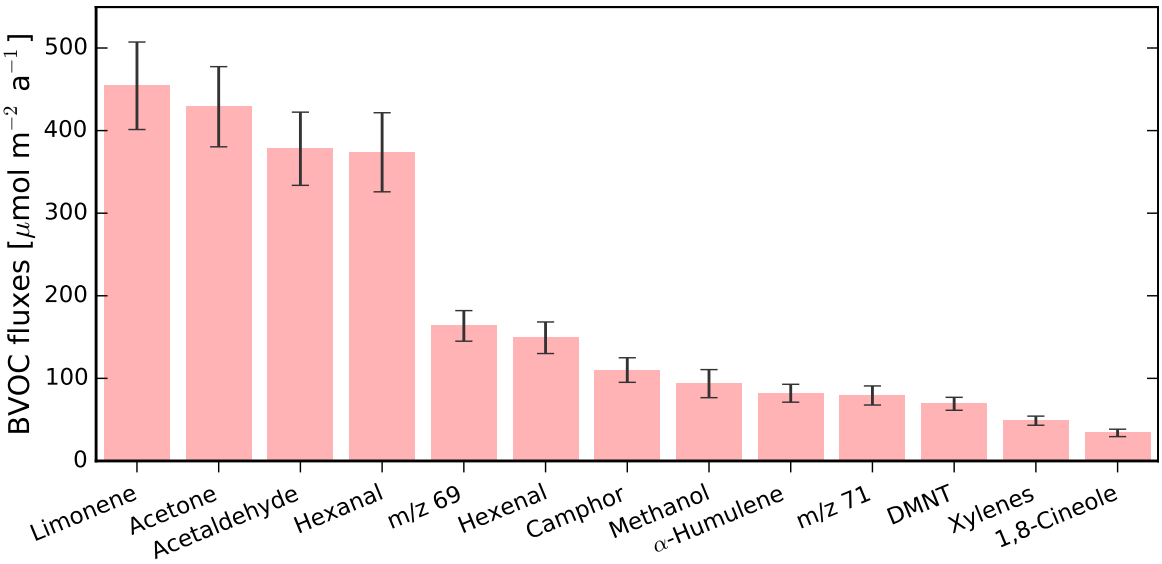

Figure 5.4.1.: Simulated annual BVOC fluxes from the maize ecosystem for three consecutive years (2015–2017). The error bars indicate ± the standard deviation of three yearly sums.

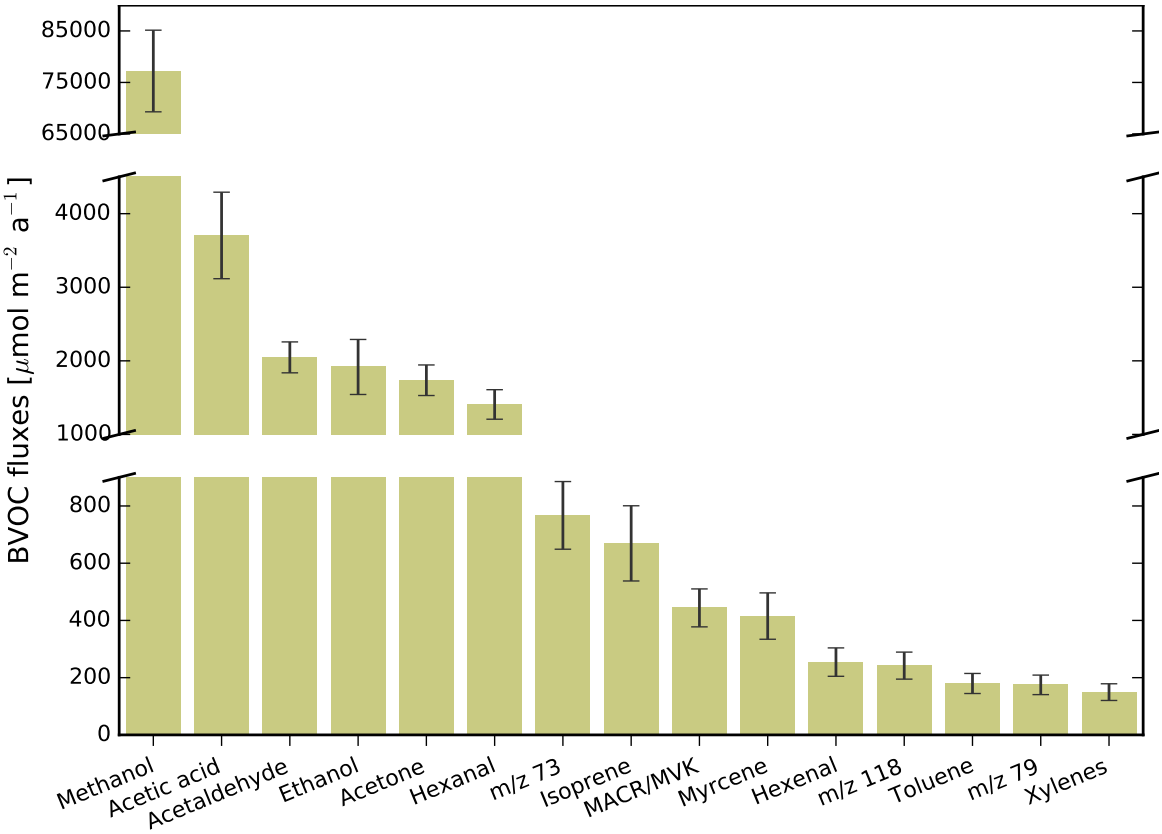

Figure 5.4.2.: Simulated annual BVOC fluxes from the oilseed rape ecosystem. See 5.4.1 for a detailed caption.

Figures 5.4.1, 5.4.2 and 5.4.3 show simulated average annual emission rates from 2015–2017 of all detected BVOCs from maize, oilseed rape, and ryegrass, respectively (see Appendix Tab. B for actual values). Generally, with 91,328.5 ± 7,966.8 μmol m^{-2}, oilseed rape emits the highest amount of total BVOCs per year followed by the ryegrass (15,742.8 ± 645.5 μmol m^{-2}, 17.2 % of total emissions from oilseed rape) and maize (2,464.5 ± 104.9 μmol m^{-2}, 2.7 % of total emissions from oilseed rape) ecosystem. Whereas the variation between the different compounds is relatively small for the maize ecosystem (34–454 μmol m^{-2}) it is much higher for oilseed rape which shows a more than 500-fold difference between measured BVOCs (149–77,220 μmol m^{-2}). In ryegrass the variation is even higher (10–13,220 μmol m^{-2}) with a factor of more than 1,300 between mean annual emissions of the lowest and highest simulated compound. Thereby, mainly non-terpenoid oxygenated compounds are among the highest fractions of total BVOC emissions for oilseed rape and ryegrass, with methanol by far the most dominating compound. In contrast to the maize ecosystem, where

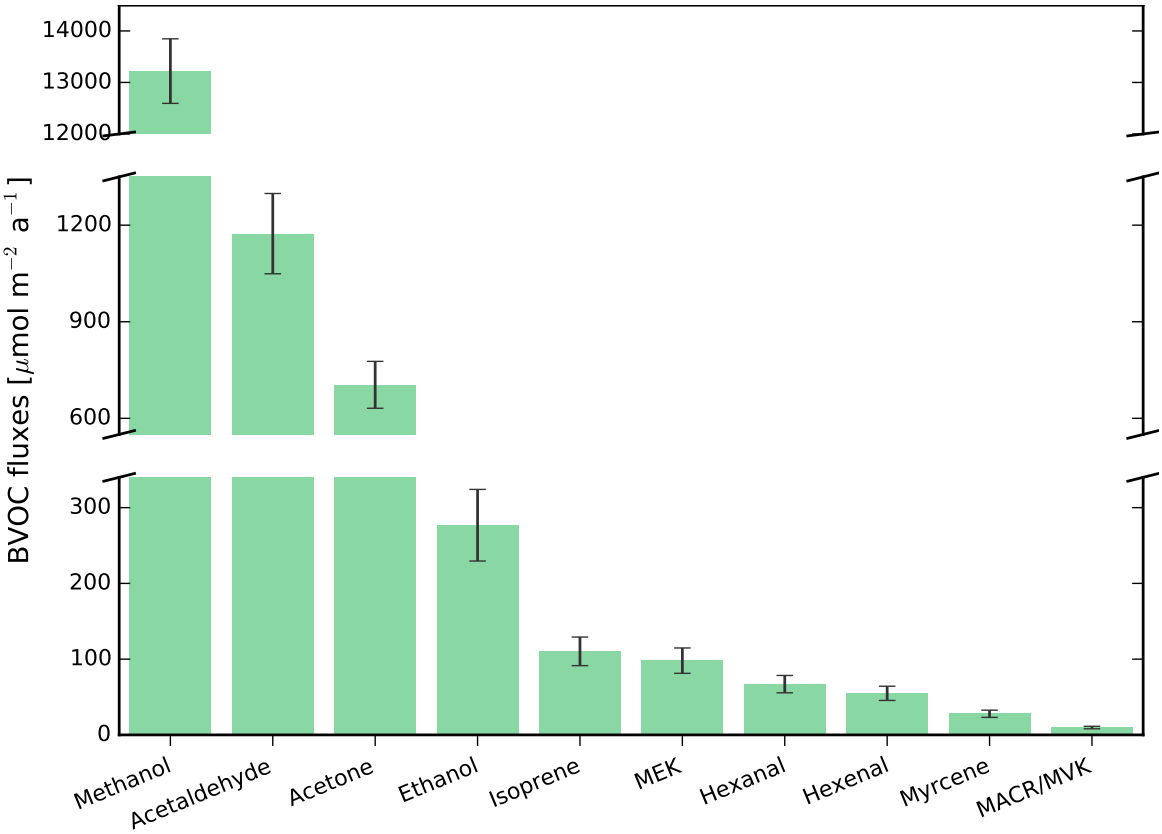

Figure 5.4.3.: Simulated annual average BVOC fluxes from the ryegrass ecosystem. See 5.4.1 for a detailed caption.

the monoterpene limonen is the highest emitted compound during the whole year. However, summing up hexenal and hexanal (523 μmol m^{-2} a^{-1}), the group of GLVs would exceed limonene emissions from maize.

5.4.2. Comparison of potential impacts on air chemistry

In the following, the potential impacts of emissions from all three crops on air chemistry should be estimated. This is approached by weighting the annual emission amounts with the corresponding BVOC–OH reaction rate coefficients that are shown in Tab. 5.10. Generally, the degradation with OH is the dominant primary BVOC reaction in the atmosphere leading to the formation of O_3 and SOA, as well as indirectly increasing radiative forcing. Compared to BVOC–O_3, BVOC–NO_3 reactions, and the photolysis of BVOCs, most of the BVOC rate coefficients are higher for reac-

Table 5.10.: BVOC–OH reaction rate coefficients (k-rates) for those compounds I detected during the three field experiments from maize, oilseed rape, and ryegrass. The k-rates are given at a temperature of 298.15 K in units of cm^3 $molecule^{-1}$ s^{-1}. If not additionally indicated, the values were taken from the Master Chemical Mechanism, MCM v3.2, via website: `http://mcm.leeds.ac.uk/MCM`, where also the references for each rate can be found.

m/z	Detected compound	OH k-rate
33	Methanol	8.96×10^{-13}
45	Acetaldehyde	1.49×10^{-11}
47	Ethanol	3.21×10^{-12}
59	Acetone	1.75×10^{-13}
61	Acetic acid	8.00×10^{-13}
69	Isoprene	1.00×10^{-10}
71	MVK	2.01×10^{-11}
	MACR	2.86×10^{-11}
73	MEK	1.11×10^{-12}
93	Toluene	5.63×10^{-12}
99	Hexenal[1]	3.85×10^{-11}
101	Hexanal	2.88×10^{-11}
107	o-Xylenes	1.36×10^{-11}
137	Myrcene[1]	2.15×10^{-10}
	Limonene	1.64×10^{-10}
	Thujene[3]	9.06×10^{-11}
	Trans-β-Ocimene[1]	2.52×10^{-10}
151	DMNT[3]	2.32×10^{-10}
153	Camphor[3]	9.88×10^{-12}
	Methyl salicylate[3]	1.11×10^{-11}
155	1,8-Cineole[3]	2.26×10^{-11}
205	Isolongifolene[2]	9.6×10^{-11}
	α-Humulene[1]	2.93×10^{-10}
	Junipene[3]	6.21×10^{-11}

[1]Values taken from Peeters et al. (2007)

[2]Values taken from Hakola et al. (2012)

[3]Values taken from `AopWin v1.92`™ module of the `EPI`™ software suite (www.epa.gov, EPA, USA)

tions with OH (see Tab. 2.1 and Sect. 2.2.2). Also, O_3 molecules are consumed quite fast by reactions with NO to form $NO_2 + O_2$ and are thus not available for reactions with BVOCs ($k = 1.9 \times 10^{-14}$ cm^3 $molecule^{-1}$ s^{-1} leading to a lifetime of < 2 min at

an ambient O_3 concentration of 7×10^{11} molecule cm^{-3}) (Atkinson and Arey, 2003; Burkholder et al., 2015). Using the total BVOC–OH reactivity for impact estimation has already been done in several studies (Hu et al., 2018; Hakola et al., 2017; Sarkar et al., 2016; Ghirardo et al., 2016; Graus et al., 2013).

Generally, reactions of BVOCs with OH can be described by

$$\text{BVOC} + \text{OH} \longrightarrow \text{first-generation products} \tag{5.1}$$

where the total BVOC–OH ($R_{\text{BVOC–OH}}$) reactivity in units of s^{-1} is calculated by

$$R_{\text{BVOC–OH}} = \sum_i k_{\text{BVOC}_i+\text{OH}}[\text{BVOC}_i] \tag{5.2}$$

with $k_{\text{BVOC}_i+\text{OH}}$ as the reaction rate coefficient of the specific compound i and OH (cm^3 $molecule^{-1}$ s^{-1}) and [BVOC_i] as the ambient concentration of the specific compound i (molecule cm^{-3}) (Hakola et al., 2012; Burkholder et al., 2015; Sarkar et al., 2016; Sinha et al., 2012; Atkinson and Arey, 2003). In order to be able to use plant emissions or, from another point of view, immissions into an air parcel instead of concentrations (similar to the studies of Graus et al. (2013) and Hu et al. (2018)), a couple of simplifying assumptions are necessary (see below). I calculated a potential BVOC–OH reactivity for every compound from each of the three crops and then scaled to the total potential BVOC–OH reactivity from maize ($Rp_{\text{BVOC–OH}}(c,\text{maize})$) by:

$$Rp_{\text{BVOC–OH}}(c) = \sum_i k_{\text{BVOC}_i+\text{OH}} \frac{\partial \text{BVOC}_i(c)}{\partial t} \tag{5.3a}$$

$$Rp_{\text{BVOC–OH}}(c,\text{maize}) = \frac{Rp_{\text{BVOC–OH}}(c)}{Rp_{\text{BVOC–OH}}(\text{maize})} \tag{5.3b}$$

with $\text{BVOC}_i(c)$ as the specific compound i from crop type c which is basically maize, oilseed rape, or ryegrass. Although, this very basic approach lacks the consideration of several important physical and chemical processes, it is still possible to draw meaningful conclusions by defining the following assumptions: (1) The emission rates from the different ecosystems are linearly proportional to the BVOC concentration change within the boundary layer above the crop ecosystem. This definition of a linear scaling enables the comparison of different ecosystem fluxes since it is independent on meteorological and air chemical boundary conditions (e.g. the boundary layer

height). Thus, by scaling with the total potential reactivity from maize (1.4×10^{-7} *arbitrary unit*), this factor will be canceled out. (2) I neglect any turbulent transport processes into and out of the respective boundary layer volume, as well as any other chemical degradation processes than that with OH molecules. (3) The potential OH reactivity is only affected by BVOC fluxes ($\partial \mathrm{BVOC}_i(c)/\partial t$). Thus, the OH molecule concentration does not constrain the reaction rates during the entire year and OH molecules are unlimited available during day- and nighttime. Under natural conditions, at least the relative magnitude of BVOC fluxes is similar to the OH mixing ratios, with higher values during daytime and lower values during the night. (4) The k-rate is set constant assuming a constant air temperature of 25 ℃ during the whole year. (5) Reactions between BVOCs and O_3 as well as with the NO_3 radical are neglected.

As k-rates are only defined for BVOCs with known molecular structure, I could calculate the potential BVOC–OH reactivity only for those compounds which were identified by GC-MS analysis. That is, *m/z* 69 (163.5 μmol m^{-2}, 6.6 % of total BVOC emissions) and *m/z* 71 (79.2 μmol m^{-2} a^{-1}, 3.2 %) from maize ecosystem, and *m/z* 73 (767.1 μmol m^{-2}, 0.8 %), *m/z* 79 (174.9 μmol m^{-2}, 0.2 %), and *m/z* 118 (242.1 μmol m^{-2}, 0.3 %) for the oilseed rape ecosystem were not considered. Regarding the ryegrass ecosystem, I could detect all measured compounds. As I can not differentiate between MACR and MVK by means of PTR-MS measurements, I used a mean k-rate of both compounds.

The results of the weighting procedure indicate that in contrast to the huge variability of total annual BVOC emission fluxes (37-fold between oilseed rape and maize), the difference between the potential annual impact on air chemistry of the investigated plants is relatively small (6-fold between oilseed rape and ryegrass, see Fig. 5.4.4). The highest impact on atmospheric chemistry is expected to originate from oilseed rape BVOC emissions (scaling factor 2.4), which is followed by maize (1.0) and ryegrass (scaling factor 0.4). As the composition of BVOCs emitted from oilseed rape is similar to that of ryegrass (mainly oxygenated compounds such as methanol, acetaldehyde, ethanol, and acetone with k-rates between 1.75×10^{-13} and 1.49×10^{-11} cm^3 $molecule^{-1}$ s^{-1}), the difference between their total emissions (5.8-fold) is similar to the difference between their impacts on atmospheric reactivity (6.0-fold). In contrast to these two plants, maize, emits relatively large amounts of terpenes (limonene, α-humulene) as well as the homoterpene DMNT, which are highly reactive (k-rates

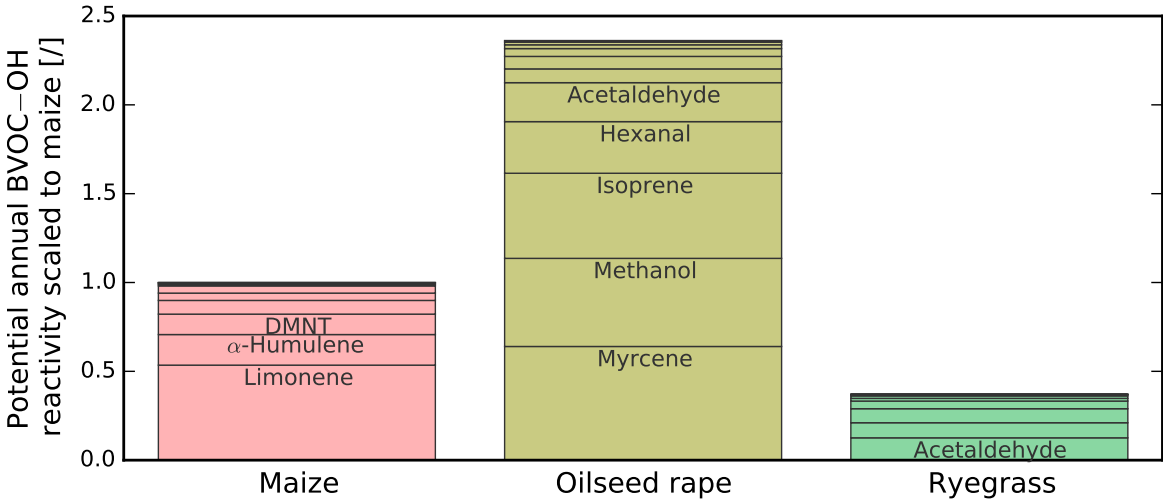

Figure 5.4.4.: Potential mean annual BVOC–OH reactivity from three simulated years 2015–2017 from maize, oilseed rape, and ryegrass ecosystem. All values are scaled to the total potential BVOC–OH reactivity of maize (for the calculation see Eq. 5.3). For a better readability, only those compounds with values > 0.1 are named in the bars.

between 1.64×10^{-10} and 2.93×10^{-10} cm^3 molecule^{-1} s^{-1}). Thus, despite the relatively small amount of annual BVOC emissions compared to oilseed rape and ryegrass (approximately 3 and 16 % of the oilseed rape and ryegrass emissions), the difference of potential impact on air chemistry strongly reduces from 37-fold to 2.4-fold between maize and oilseed rape, and from 6.4-fold to 0.4-fold between maize and ryegrass.

6. Discussion and Conclusions

6.1. Suitability of applied methods

This section deals with the methodological goals of this thesis, which are (1) to test the applicability of using large automatic chambers to detect BVOC emissions from crop canopies; and (2) to develop and evaluate an BVOC model that considers *de novo* as well as pool emissions and can be applied to investigate trace gas exchanges from bioenergy plants.

6.1.1. Advantages and limitations of BVOC measurements with large automatic chambers

As to my knowledge, this is the first time that large automatic chambers with a flow-through non-steady-state approach were used to detect BVOC exchanges at an experimental field site. This technique enabled to detect a multitude of different BVOCs from the whole ecosystem (all plant compartments and soil) of three bioenergy crops under field conditions. Especially for maize, significant fluxes of highly reactive compounds were detected. These include methyl salicylate, oxygenated monoterpenes, and sesquiterpenes (strong SOA forming potential), which were not observed or at least not quantified in previous field experiments (Sakulyanontvittaya et al., 2008; Hallquist et al., 2009; Li et al., 2011; Xu et al., 2018). Particularly sesquiterpenes which strongly adhere to any walls within a measurement setup (tubes, chamber walls) (Pagonis et al., 2017; Aaltonen et al., 2013) were hardly detectable at the canopy scale before (Ciccioli et al., 1999; Jardine et al., 2011). Technically, it has been evaluated that measuring fluxes of sesquiterpenes with the presented setup is possible when flushing the tubes with ambient air during a non-measuring period of 48 minutes

(which increased the measurement precision for all compounds). The measurements also benefit from a long PTR-MS dwell time of 10 seconds for *m/z* 205. The chamber technique has many advantages but some precautions also need to be accounted for to correctly interpret the collected data set which are briefly summarized in Tab. 6.1 and will be discussed in the following, as has partly also done in my publication Wiß et al. (2017).

Table 6.1.: Brief summary list of advantages and limitations resulting from my conducted measurement of BVOC fluxes with large automatic chambers.

Advantages	Limitations
⊕ ecosystem patch can be exactly determined	⊖ change of temperature, CO_2 concentration, and humidity at days with strong radiation
⊕ meteorological quantities and trace gas concentrations are measured within a defined headspace	⊖ simultaneous reactions between BVOCs–NO_x–O_3
⊕ basic statistical approach to detect fluxes	⊖ increase of ambient BVOC concentrations

A particular advantage of the large chamber approach is that the measured ecosystem patch is clearly defined (e.g., in terms of crop species, number of individuals, crop height, leaf area index, and phenological stages). In contrast, in open systems such as eddy covariance a horizontal flux footprint analysis is needed to define the size and properties of the area, which is the source of the measured compounds. The process of determining the properties of the BVOC emitting and non-emitting plants that determine the measurement results is further complicated by the fact that this area changes with wind speed and direction (Fuentes et al., 2000). Furthermore, all meteorological drivers, which are important for vegetation processes and BVOC emissions (e.g., temperature, radiation, humidity, precipitation) as well as the concentrations of trace gases (BVOCs, CO_2, and others) are measured directly for the whole canopy headspace. Finally, the basic statistical approach of a linear regression fitted by ordinary least squares to calculate the fluxes has been shown to be relatively robust and easy to compute whereas open micrometeorological measurement systems require extensive post processing (see Sect. 2.3.1 for more information about the calculations) procedure as for example using the (disjunct) eddy covariance techniques.

Nevertheless, the following limitations need to be carefully considered when applying the new methodology. At hot days with intense radiation, the chamber construction has a distinct greenhouse effect leading to rising temperatures and a CO_2

concentration decrease due to ecosystem C assimilation. Additionally, increased transpiration leads to higher relative humidity. All these changes may potentially affect BVOC emissions and deposition leading to emission estimates that are different than those occurring under natural conditions close by. To be safe of directly damaging temperatures, the chambers open automatically when a threshold of 40 ℃ is exceeded, which has however never been reached during the investigations (observed maximum headspace temperature of 38.6, 33.9, and 33.0 ℃ for the maize, oilseed rape, and ryegrass campaign, respectively). The potential systematic error due to elevated temperatures below this threshold is regarded as small because the closure period of 12 min is too short to affect the *de novo* synthesis of BVOCs (Noe et al., 2010; Calfapietra et al., 2013b). Thus, only pool emissions which depend on storage size and evaporation resistance can be significantly increased (Ghirardo et al., 2010; Peñuelas and Staudt, 2010). However, as there were no strong non-linearities of BVOC concentration changes within the chambers, I assume that the share of pool emissions is either small (see light dependent fraction values of Tabs. 5.2, 5.5, and 5.8, as well as Köllner et al. (2004a)) or that the headspace temperature change was not significant enough to increase leaf temperature during chamber closure.

Generally, BVOC degradation processes triggered by O_3, OH, and NO_3 radical have the potential to reduce the observed emissions. Due to fast photolysis rates of the NO_3 radical, BVOC–NO_3 reactions mainly occur during nighttime when measured BVOC fluxes were negligible. Concerning reactions with O_3, additional measurements of O_3, NO, and NO_2 concentrations were made during the oilseed rape and ryegrass field experiments. Concentration decreases of O_3 and NO, and NO_2 increases of similar magnitude were detected (data not shown). Thus, it is reasonable to assume that NO reacts with O_3 to form NO_2 and depleting O_3 quickly. This reaction likely dominates over potential BVOCs–O_3 reactions which is also supported by observed higher k-rates of NO–O_3 than for most of the BVOCs–O_3 reactions (Atkinson and Arey, 2003; Burkholder et al., 2015). It is also not likely that O_3 forms within the chamber headspace because NO emissions from the soil are expected to be relatively high (Pilegaard, 2013; Molina-Herrera et al., 2017) compared to BVOC emissions resulting in a low VOC:NO_x ratio (see Sect. 2.2.2).

Another process that can potentially lead to flux underestimation is that an increase in the BVOC concentration of the chamber headspace leads to a decrease of the concentration gradient relative to the BVOC source. Principally, this results in

smaller diffusive gas fluxes which are also part of the emission process especially from pool emissions. However, the gradient decrease is small due to the relatively small concentrations and the time interval for any feedback to the diffusion process is also small. In addition, we assume only a minor proportion of diffusive BVOC emission so that the overall bias is also supposed to be small.

It should also be noted, that four custom-made automatic chambers were used during the oilseed rape and ryegrass campaigns but only two chambers were available for the measurements at the maize field. This may increase the uncertainty due to ecosystem heterogeneity. However, since the enclosure system is relatively large, it already includes a large number of plants which should require fewer replicates than measuring just one specific leaf, flower, or plant. Heterogeneity may be introduced to variations of soil conditions within the whole field, which however are mostly small at agricultural fields. Nevertheless, I admit that hourly flux calculations from four chambers are more robust than from only two and should be used whenever available.

6.1.2. The joint JJv–pool emission model as a tool for BVOC crop emission estimates

Environmental modeling studies can have different objectives, which can be structured according to Smith and Smith (2007) into (i) quantify the results of a process with varying inputs which are not possible to be measured (e.g., changing temperature and radiation as input); (ii) explain how underlying processes may contribute to an observed result; (iii) close gaps in measurement periods; (iv) estimate responses at other places with different environmental conditions; and (v) estimate the impact of events under past and/or future conditions.

To improve the general applicability of BVOC emission models also under changing environmental conditions, there is growing need to develop process-based mechanistic instead of empirical approaches (Laffineur et al., 2012; Seco et al., 2015; Brilli et al., 2016). Therefore, the model approach in this study explicitly links BVOC emissions to photosynthesis and leaf development, which I parameterized with observational data to represent the emissions per unit ground area throughout the whole vegetation period. Thus, internal (i.e. biomass, leaf area) as well es external (temperature, radiation, water availability) driving forces are explicitly considered (aim (i) and (v)).

Concerning the parameterization of the BVOC model, the consideration of empirically derived light dependent fractions (LDFs), fitting of standardized emission factors (SEFs) and β-coefficients lead to an overall good agreement between observed and simulated values. By fitting SEFs to observations during different periods, potential impacts from specific plant development stages could be determined (aim (ii); see Sect. 6.2.1 for further discussion). Indeed, the results indicate that the explicit link between plant development and BVOC emission parameters would be suitable for some compounds although not for all. Concerning aim (iv) and (v), this model approach and its parameterization can arguably be used for different periods, on larger spatial scales, or implemented into other models. This includes the implementation into global earth system models as far as a Farquhar-type description is used to represent photosynthesis, e.g. the Community Earth System Model (`CESM`) and its Community Land Model (`CLM`) (Lawrence et al., 2018).

The joint `JJv`–pool emission model, which was re-coded, parameterized and coupled to `LandscapeDNDC` within this study, represents observed emission rates reasonably well. Scaling the SEFs to the observed emission sums of each compound additionally significantly improved model results (increase of Nash-Sutcliffe modeling efficiency (NSE)). The respective scaling sactor is < 1.0 for most simulated BVOCs of the maize and ryegrass ecosystems and > 1.0 for the oilseed rape ecosystem (see Tabs. 5.3, 5.6, and 5.9 for values per compound). It mainly compensates for the over- (ryegrass) or under- (oilseed rape) estimation of simulated biomass. In case of maize, the picture is more complex because the change of emissions due to different plant development phases is more expressed here, leading the model to overestimate BVOC emissions during ripening and senescence phases. Improving the simulation results in order to decrease emissions during plant ripening can be approached from two sides. First, the photosynthesis model which calculates J (total electron supply) and J_v should account for potentially decreased values of J during ripening, which is also supported by literature finding that the efficiency to convert incoming radiation into electron supply declines during ripening of leaves (Tanaka and Yamaguchi, 1972; Campbell et al., 2019). Second, SEFs can be explicitly linked to ontogenetic phases, potentially reducing *de novo* synthesis during the ripening of the plants as argued by Brilli et al. (2016).

During the field measurements with different bioenergy crops, negative net fluxes of some compounds were detected (methanol, ethanol, acetic acid, and sesquiterpenes).

BVOC deposition, however, is not yet included in the model, The underlying processes at the biosphere-atmosphere interface are still matter of debate and more than one mechanism is likely to be responsible (Niinemets et al., 2014; Wohlfahrt et al., 2015; Spielmann et al., 2017). Especially, as there are fundamental differences between compounds of varying hydrophilic and lipophilic characteristics (see Sect. 6.2.1 for further discussion). While practically all empirical and process-based modeling approaches such as e.g., `MEGAN` (Guenther et al., 2012), `BEIS` (Pierce et al., 1998; Bash et al., 2016), Martin et al. (2000) model, `SIM-BIM` (Zimmer et al., 2000; Lehning et al., 2001), and `SIM-BIM2` (Grote et al., 2006) lack algorithms representing deposition processes (cf. Niinemets et al. (2014)), there are suggestions to include wet and dry deposition into models which mostly concentrate on oxygenated compounds with high water solubility, in particular methanol (Seco et al., 2015). One approach is to calculate deposition velocities explicitly in dependce on multiple path resistances (Bamberger et al., 2011; Wohlfahrt et al., 2015; Kelly et al., 2019). However, major uncertainties, are connected to this suggestion, e.g. specific resistance terms can be highly variable leading to the conclusion that this approach is only meaningful for gap filling and not for incorporation into mechanistic modeling frameworks (Bamberger et al., 2011). A promising mechanism has been suggested by Laffineur et al. (2012), which describes absorption/desorption processes of methanol in water films and their further degradation. However, the applicability of the model to other BVOCs remains unexplored.

6.2. Comparison between the observed bioenergy plants

Within the following section, I will revisit the scientific objectives of the thesis, which are (1) to determine the composition and amount of seasonal changing BVOC emission fluxes from the most important bioenergy plants in Germany throughout their major growth periods under field conditions; (2) to evaluate the impact of meteorological factors (in particular temperature and radiation), as well as phenological stages on the source strength of BVOC emissions; and (3) to compare simulated total annual BVOC fluxes between the observed bioenergy crops and evaluate their impact on air chemistry per energy yield yield based on the example investigation.

6.2.1. Differences in BVOC composition and fluxes

Flux differences between bioenergy crops

During the field experiments, a similar number of compounds were measured between the mass boundaries m/z 33 and m/z 225. Thereby, it could be shown that the oilseed rape ecosystem emits the largest number of BVOCs with 16 different compounds (without considering different isomers and nominally isobaric ions) followed by maize with 15 and ryegrass with 12 different BVOCs (see Tabs. 4.3, 4.4, and 4.5 for the specific compounds). For maize, there are 5 compounds with each being emitted by more than 10 % (13 % – 18 %) of the total BVOC emissions and all other detected compounds contribute by at least 1 % each. In contrast, oilseed rape and ryegrass emissions are dominated by methanol with 84.9 % and 80.2 %, respectively, From oilseed rape, only 6 other compounds contribute by more than 1 % to the total emissions and only 4 compounds from ryegrass (see Tabs. 5.1, 5.4, and 5.7 for a detailed overview of the three bioenergy crops).

The change of BVOC composition between different growth stages is more expressed in oilseed rape than in maize or ryegrass. During the flowering growth stage, 6 compounds from oilseed rape each contribute more than 1 % of total BVOC emissions, while this is true for only 3 compounds during the earlier growth stage of inflorescence emergence. The share of emitted compounds from maize and ryegrass does not change considerably between growth stages.

Seasonal flux magnitudes

The magnitude of total BVOC fluxes strongly differs between bioenergy crops with oilseed rape being the highest emitter followed by ryegrass and maize. During the full field observation periods, the mean emission rates are 2.87, 1.77, and 0.59 nmol m^{-2} s^{-1} for oilseed rape, ryegrass, and maize, respectively (as the length of the observation periods differ, the mean value instead of the sum is used here). Due to different observation periods (duration and growth stages) annual emission amounts can better be taken from simulations, which indicate total emissions of 91.3 (± 8.0), 15.7 (± 0.6), and 2.5 (± 0.1) mmol m^{-2} a^{-1} for oilseed rape, ryegrass, and maize, respectively (see Tab. B.1 for detailed numbers). Thus, direct observations suggest

an overall emission of oilseed rape that is 4.9-fold higher than that of maize, whereas simulations over three entire growth periods indicate a 37-fold difference. This large discrepancy underlines the vast importance of representing such processes by a modeling approach for upscaling, especially when observations are not available during a complete growing season.

Observed bidirectional fluxes

Besides emissions, also deposition fluxes could be observed at all examined bioenergy crops. For maize, bidirectional fluxes were especially observed from methanol and ethanol, in particular during wet periods. This implies a distinct wet deposition e.g. by absorption into water films on (leaf) surfaces (Seco et al., 2015; Wohlfahrt et al., 2015), which is controlled by very low gas-aqueous phase partitioning equilibrium defined by low values of Henry's law constant (H) of 0.461 and 0.507 Pa m^3 mol^{-1} (Niinemets and Reichstein, 2003), respectively. Additionally, deposition may be enhanced by high stomatal conductance (Kesselmeier, 2001; Seco et al., 2007; Mozaffar, 2017), which I assume to be present during periods of high GPP when deposition fluxes could be observed. The importance of uptake could be better determined following Fick's law (concentration gradient directed to the substomatal cavities) investigating the compensation point (Kesselmeier, 2001; Harley et al., 2007; Hörtnagl et al., 2014) but, unfortunately, no compensation point measurements have been conducted in this study. Fluxes of acetone and acetaldehyde, compounds with the next smallest H values (3.88 and 7.00 Pa m^3 mol^{-1}), were already only observed as net emissions. However, bidirectional fluxes of acetaldehyde from maize were observed by Graus et al. (2013), who detected ambient acetaldehyde concentration above its compensation point resulting in net depositions. Another study on maize (Bachy et al., 2016) indicated bidirectional fluxes of many compounds (acetic acid, acetone, methanol, methacrolein + methy vinyl ketone, methy ethyl ketone, monoterpenes, benzene, and toluene), but hypothesized that the soil may have acted as the main sink. Interestingly, the study of Bachy et al. (2016) found relatively low net emissions (except for methanol) which may thus be due to high gross deposition, decreasing net fluxes.

For the oilseed rape ecosystem, sesquiterpenes showed a net deposition over the entire observation period while net fluxes of monoterpenes, toluene, m/z 79, and 118

were observed to act in both directions. When net sesquiterpenes deposition decreased a coinciding increase in GPP and thus stomatal conductance could be observed at the same time. Hence, a potential plant or stomatal uptake is very unlikely. It rather seems that the soil may act as a major sink for sesquiterpenes that is not often compensated by emissions (cf. Bachy et al., 2016; Spielmann et al., 2017). The net deposition decline of sesquiterpenes may thus be due to increasing emissions from the oilseed rape plants, especially from appearing flowering tissues (Jakobsen et al., 1994; McEwan and Smith, 1998; Veromann et al., 2013). To the author's knowledge, there is no oilseed rape study on bidirectional BVOC fluxes, which may be due to the fact that mostly branch enclosure techniques were applied (Jakobsen et al., 1994; König et al., 1995; McEwan and Smith, 1998; Müller et al., 2002; Veromann et al., 2013; Morrison et al., 2016), which did not include deposition processes into the soil. This underlines the need to measure the whole soil–plant–atmosphere ecosystem to be able to correctly account for bidirectional fluxes as well.

From the ryegrass ecosystem, bidirectional fluxes of acetic acid and sesquiterpenes could be observed with opposed flux pattern of emission and deposition between both compounds. The opposed flux pattern indicates two different deposition processes. Since there is no distinct correlation between GPP/stomatal conductance and deposition of acetic acid, it seems that it may be solely absorbed in water films after rain events by partitioning into the aqueous phase ($H = 0.0133$ Pa m^3 mol^{-1}). In contrast, daily sesquiterpene fluxes correlate well with daily mean temperatures, and only show deposition fluxes when temperatures decrease. I thus hypothesize that (similar to the results from the oilseed rape ecosystem) sesquiterpenes may be emitted by the plants with a strong temperature dependence and deposited to the soil at a more constant rate. This assumption is supported by results from Bamberger et al. (2011), who also detected bidirectional fluxes of sesquiterpenes, besides others, from a grassland site. Nevertheless, it is still not known which of the deposition processes are dominant (chemical loss, scavenging to the soil ...).

6.2.2. Impact of phenology on flux seasonality

During the field campaigns, the general seasonal bidirectional flux pattern of all BVOCs could be clearly linked to the external environmental drivers, i.e. temperature and radiation. Also, precipitation affected fluxes of some compounds, especially

wet deposition. Comparing mean molar emissions, it could be deduced, however, that several processes differ in importance in different growth stages. For maize and oilseed rape, emissions are higher during flowering (762 and 4682 pmol m^{-2} s^{-1}) than during fruit development (maize: 425 pmol m^{-2} s^{-1}) and inflorescence emergence (oilseed rape: 976 pmol m^{-2} s^{-1}). The flower as an additional plant tissue is a strong BVOC source with a large variety of compounds, also for maize and oilseed rape plants (McEwan and Smith, 1998; Köllner et al., 2004a,b; Knudsen et al., 2006; Veromann et al., 2013; Muhlemann et al., 2014; Wiß et al., 2017). However, environmental conditions can override the influences of plant development stage, which is why mean emissions of ryegrass are lower during a relatively cooler period despite the grass was in its flowering period. Nevertheless, by normalizing the fluxes, comparing observed standardized emission factors (SEFs) between different growth stages, and analyzing deviations between simulated and observed fluxes, I could detect a pronounced impact of plant ontogenesis on BVOC composition and fluxes for all three bioenergy crops. It should be noted, however, that this differentiation is particular apparent in some, but not in all compound groups.

From the maize ecosystem, emissions of the group terpenoids and their derivatives (Fig. 5.1.4A) show a steep increase at the beginning of the flowering period, which could not be fully explained by environmental developments that are represented by the model (see Fig. 5.1.5 for observed and simulated oxygenated monoterpenes). Furthermore, the SEFs of all compounds within this group are reduced by half between the flowering and the fruit development and ripening stage, which is again a development too steep to be explained solely by meteorology (see Tab. 5.2 for exact values). The emissions of the group in Fig. 5.1.4C are particularly high between the end of the flowering and beginning of fruit development, whereas declining temperatures and radiation indicate declining emissions (see Fig. 5.1.7). In this group too, the SEFs increase between the flowering and the fruit development and ripening stage. Both groups additionally show a slight emission increase during a rise of temperature and radiation at the end of the growing season whereas simulated emissions are estimated to be much higher, indicating that enzyme activity is considerably lower than during the plant growth phase. A seasonal changing emission regime caused by the development of maize leaves was also previously shown by Mozaffar et al. (2017, 2018) and for poplar trees as well (Brilli et al., 2016). Thus, the observed seasonal flux pattern from the maize ecosystem originate from a complex mixture of effects from instantaneous

and cumulative temperature, radiation, and precipitation, plant developmental stage, and the appearance and disappearance of specific tissues.

All compounds from the oilseed rape ecosystem, except methanol, are emitted at very low rates during the inflorescence emergence, despite a well-developed biomass and medium values of GPP. Emission rates rise when flowering starts. As this is valid for the SEFs of a majority of compounds (see Tab. 5.5 for values), this development can be also strongly related to the plant growth stage with additional flowering tissues. The intense development cannot be explained by the moderately rising temperature and radiation. Generally, differences in seasonal flux pattern between the group in Fig. 5.2.4A and 5.2.4C are small compared to those from the maize field. Nevertheless, a special characteristic of the group in Fig. 5.2.4A is the distinct emission increase at the beginning of flowering, whereas the compounds of the group in Fig. 5.2.4C show higher emissions in mid flowering stage. Both phenomena, however, cannot be explained by the development of temperature, radiation, or biomass regime as indicated by model results (see Figs. 5.2.5 and 5.2.6). Following McEwan and Smith (1998), I speculate that an additional emission source occurs related to the formation of flowering tissues during this time that is responsible for the altered BVOC composition.

The decrease of most SEFs from heading of the ryegrass to the flowering growth stage needs to be handled with care, since the sample size for their calculation during flowering is quite small (85 measurements) compared to the heading stage (312) (see Tab. 5.8 for values). Nevertheless, besides acetic acid and sesquiterpenes that show bidirectional fluxes, two compound groups with specific emission pattern can be identified within the heading growth stage. The characteristic differences are oscillating emissions during the first half of the measurement period of the group in Fig. 5.3.4A, while almost no emissions could be detected for the BVOC group in Fig. 5.3.4C. However, both pattern cannot be represented by the model, neither by the `JJv` model (LDF = 1, see Fig. 5.3.5) nor by the pool emission model only (LDF = 0, see Fig. 5.3.6). Thus, potential intra growth stage developments are assumed to lead to these diverging pattern which cannot be described by environmental driving forces.

6.2.3. Deviations of OH-reactivity between the bioenergy crops

OH-reactivity per energy yield from bioenergy plants

The reaction with OH is the dominant primary atmospheric BVOC degradation pathway, compared to reactions with O_3 and NO_3 (Atkinson and Arey, 2003; Burkholder et al., 2015). Thus, I used the potential annual BVOC–OH reactivity to compare impacts on atmospheric chemistry between the investigated bioenergy plants. These impacts on air chemistry include the formation of O_3 and SOA, as well as an indirect radiative forcing by prolonging the CH_4 lifetime (Atkinson, 2000; Carslaw et al., 2010; Kaplan et al., 2006).

Although simulated total annual BVOC emissions from the maize ecosystem comprise only 2.7 % of the total emissions from oilseed rape, the reactivity of its emission is about 42 %. This is because a large fraction of maize emission consits of the monoterpene limonene, the sesquiterpene α-humulene, and the homoterpene DMNT, all compounds with high OH-reactivity. The compound with the highest OH-reactivity from oilseed rape is the monoterpene myrcene, although it only accounts for 0.45 % of the total emission mass as the majority of emitted compounds are non-terpenoids (methanol, acetic acid, acetaldehyde, ethanol, acetone). Similarly, ryegrass emissions consist mainly of methanol, acetaldehyde, and acetone—components with a relatively low OH-reactivity. Consequently, the total annual emissions from ryegrass compared to the emissions from oilseed rape (17.2 %) are very similar to the OH-reactivity (15.7 %). The study of Graus et al. (2013) found higher potential OH-reactivity of maize compared to switchgrass, which could also be related to higher terpenoid emissions from maize. When comparing the OH-reactivity between willow and the C_4-perennial grass *Miscanthus*, Hu et al. (2018) even found an 8-fold difference in reactivity between both crops. As the calculations were based on isoprene and a joint group of other VOCs, *Miscanthus* as a non-isoprene emitter was found to have a low potential impact on atmospheric chemistry. Investigations, from a Norway spruce forest corroborated that terpenoids (isoprene, monoterpenes, and sesquiterpenes) had the major contribution to the OH-reactivity compared to other VOCs (Hakola et al., 2017). Thus, even relatively small emissions of terpenoids often dominate potential impacts on air chemistry over a higher quantity of emissions form less reactive compounds. As all aforementioned studies calculated relative values of OH-reactivity a direct comparison

with the current investigations is not possible.

In order to judge various crops against each other, emission quantity and quality needs to be related to a reference quantity. Plants, however, are quite different regarding the kind of tissue they produce. Since energy crops are investigated here, I relate emissions not only to yield but to the theoretical potential of electricity that can be produced by burning the harvested biomass in a combined heat and power plant (18,731, 13,900, and 9,549 kWh ha^{-1} a^{-1} from maize, oilseed rape, and ryegrass respectively, see Chapter 3). Based on this calculation, oilseed rape has a 3.2-fold larger potential OH-reactivity per energy yield than maize and maize an 1.4-fold larger impact than ryegrass. Thus, if only these three energy crops are compared, planting ryegrass instead of oilseed rape would decrease the potential impact on atmospheric chemistry per kWh to less than 22 %.

Comparison to OH-reactivity per energy yield from poplar

It may be worth comparing atmospheric chemistry impacts from bioenergy crops with that of other plants that are grown to produce energy, e.g. short rotation coppices. For this end, detailed studies have been carried out about woody biomass production from poplar short rotation plantations and their impact on ground level O_3 concentration (Beltman et al., 2013; Ashworth et al., 2013, 2015; Zenone et al., 2016). The potential impact from a poplar plantation on OH-reactivity can be estimated from a recent study of Portillo-Estrada et al. (2018). Here, 148.1 mol isoprene are emitted per ha and year, which further needs to be multiplied by the isoprene k-rate and scaled to the total potential BVOC–OH reactivity of maize. The result is a 10-times higher potential impact on air chemistry of poplar plantations compared to maize. Even if the energy potential of 30,000 to 50,000 kWh ha^{-1} a^{-1} from poplar plantations is considered, the potential impact on atmospheric chemistry per energy yield is still 3.7 to 6.2 times higher than that of maize, and is therefore still higher than that of oilseed rape. These results suggest the use of ryegrass or maize instead of oilseed rape or even poplar, as a principal future bioenergy source when only impacts on atmospheric chemistry by the potential OH-reactivity are accounted for.

6.3. Differences to other BVOC emissions studies

In the following section, I compare the BVOC composition and emissions with other studies on the investigated bioenergy crops and other plant types as well. Insight into bidirectional fluxes, especially deposition was already examined in Sect. 6.2.1.

6.3.1. Comparison with studies on maize, oilseed rape, and ryegrass

The subsequent paragraphs summarize and compare main results between the measured bioenergy crops. For more details, e.g., about measurement techniques in the cited literature see Chapter 3.

Maize

To be able to compare my results with those from various other studies about maize, only observed emissions during the flowering period are considered. The highest emissions within this period were that of methanol, monoterpenes, GLVs, acetaldehyde, and acetone ranging from 13 % to 18 % of the total molar BVOC fluxes. However, the absolute mean methanol emission rates (4 μg m^{-2} ground area h^{-1} including deposition, 16 μg m^{-2} h^{-1} negative fluxes set to zero) are considerably smaller than what has been found by previous studies (28–3450 μg m^{-2} h^{-1}) (Das et al., 2003; Graus et al., 2013; Bachy et al., 2016; Mozaffar et al., 2018). In these studies, methanol provides by far for the highest fraction ($>$ 50 %) of total BVOC fluxes. There is less difference regarding other compounds: emissions of monoterpenes and acetone (65 and 21 μg m^{-2} h^{-1}, respectively) are more than one order of magnitude lower compared to Das et al. (2003) (661 and 425 μg m^{-2} h^{-1}, respectively) but higher than those from other studies (2–50 μg m^{-2} h^{-1}) (Graus et al., 2013; Bachy et al., 2016; Mozaffar et al., 2018). Thus, in this case the detected emission rates can be regarded within the large range of what has been reported before. This range may be explained by the use of different cultivars, drought periods during the measurements, or different availability of nutrients, especially mineral nitrogen (Gouinguené et al., 2001; Oluwafemi et al., 2012). The lower rates of methanol net emissions that had been observed here clearly result from co-occurring deposition fluxes. This means, that total

fluxes of methanol and also ethanol can easily be overestimated when observations are collected during particularly dry periods where no considerable deposition occurs. My results are also in line with recent observations about decreasing temperature sensitivity (smaller SEF during senescence compared to flowering) of methanol emissions from maize leaves (Mozaffar et al., 2017). Additionally, previous genetic and physiological investigations on maize leaves could be confirmed that found that maize plants should be able to emit both, sesquiterpenes and oxygenated monoterpenes in considerable quantities (Schnee et al., 2002, 2006; Köllner et al., 2004a,b; Fontana et al., 2011). Both compound groups could not be quantified in field measurements before.

Oilseed rape

Most of the preceding oilseed rape measurements were conducted with branch enclosure techniques only, while information on the whole plant biomass or leaf area index was lacking. So, the measured emission rates could hardly be scaled to the ground area or entire plant biomass. Hence, a quantitative comparison of the results presented here with these studies is not possible. However, regarding the emitted BVOC composition, it can be stated that fluxes of methanol, have not been indicated before although they dominated the emissions in the current study (85 % of total molar emissions). Possibly, this is because the focus of most of the previous studies was on terpenoid emissions only (Müller et al., 2002; Himanen et al., 2009; Morrison et al., 2016) and in some cases also the applied analytical procedures were not suitable to detect methanol (König et al., 1995).

In order to compare laboratory measurements with my study, I calculated emissions under laboratory environmental conditions based on the standardized emission factors (SEFs) that I derived from the field campaign. Veromann et al. (2013) observed under laboratory conditions of 300 μmol m^{-2} s^{-1} PPFD and 24 °C mean BVOC emissions of acetic acid and monoterpenes (750 and 130.2 pmol m^{-2} flower projected area s^{-1}) that are similar to my simulation results (851.8 and 105.0 pmol m^{-2} ground area s^{-1}), assuming that the projected flower area is not larger than the ground area. The GLV emission rate based on the field measurements of 362.9 pmol m^{-2} ground area s^{-1} is however much higher than the 36.2 pmol m^{-2} flower projected area s^{-1}, reported by Veromann et al. (2013).

The study of König et al. (1995) conducted field measurements during daytime at flowering stage. Results can therefore be compared with aforementioned values by scaling to aboveground biomass (600 gDW m^{-2}). Again, monoterpene emission rates are very similar (85.69 ng g^{-1}DW aboveground biomass h^{-1}) while those of GLVs are higher (296.1 ng g^{-1}DW aboveground biomass h^{-1}) than what was measured by König et al. (1995) (monoterpenes 74.6–108.7 ng g^{-1}DW leaf h^{-1}, GLVs: 30.5–47.2 ng g^{-1}DW leaf h^{-1}). The uncertainty of the measured emission rates is underlined by the study of Müller et al. (2002) who found lower monoterpene emissions of 30–60 ng g^{-1}DW plant h^{-1} and that of Jakobsen et al. (1994), McEwan and Smith (1998), and Himanen et al. (2009), who indicated that monoterpene emissions represent the highest fraction among all measured BVOCs, while Morrison et al. (2016) could not report any monoterpene emissions at all. Among all monoterpenes, I detected myrcene as the most abundant compound which is confirmed by the measurements of Jakobsen et al. (1994). Other compounds are also detected in very varying amounts. In my study, sesquiterpene fluxes were dominated by deposition while Veromann et al. (2013) measured small average emissions of 0.51 pmol m^{-2} flower projected area s^{-1}. Similarly, the studies of Jakobsen et al. (1994) and McEwan and Smith (1998) also detected small amounts of sesquiterpene emissions. In only few studies, also oxygenated monoterpenes were observed (König et al., 1995; McEwan and Smith, 1998) which were not found during the field measurements presented here. In contrast, I detected high emissions of acetone, acetaldehyde, and ethanol, which was previously only reported to occur in small amounts by McEwan and Smith (1998).

Regional modeling studies that tried to estimate the overall impact of oilseed rape on air chemistry over Saxony found a small but noticeably effect on O_3 production as a result from terpenoid emission (Münzenberg-St.Denis and Renner, 1999; Renner and Münzenberg, 2003). These studies additionally pointed out, that there is a large uncertainty in BVOC emission measurements and thus on the applied parameterization. The measurements and simulations presented here that support a relatively high emission potential of monoterpenes and acetic acid, corroborate and intensify the notion that impacts on air chemistry can be expected when oilseed rape is extensively planted.

Ryegrass

There are only few direct measurements of ryegrass (*Lolium multiflorum* or *Lolium perenne*) emissions in the literature. From these, Custer and Schade (2007) focused on fluxes of methanol and acetaldehyde from *Lolium multiflorum* but only detected small amounts of net deposition. I also measured bidirectional fluxes although the substantial emissions led to an overall net emission. Custer and Schade (2007) also reported net methanol emissions which reached a maximum of around 10 μmol m^{-2} h^{-1}. This is less than half the maximum hourly emissions that could be observed in mid-June (23.4 μmol m^{-2} h^{-1}) in the field. BVOC emissions from *Lolium perenne* were measured by Pańka et al. (2013) under laboratory conditions by concentrating on pathogen infection. For non-infected plants they detected high emission amounts of GLVs and the sesquiterpene β-caryophyllene, besides minor emissions of monoterpenes and oxygenated monoterpenes. This is in contrast to results of the present study where these compounds formed less than 1 % of the total BVOC emission. However, results cannot be compared quantitatively because leaf area or plant biomass were not provided.

Other studies examined BVOC emissions from grasslands including different graminoid and forb species. The study of Ruuskanen et al. (2011) reports 24 h mean values from 1 day of measurements which can be compared to 24 h mean values at 19 June 2017 in the present study. Only methanol net emissions were observed by Ruuskanen et al. (2011) (5.89 nmol m^{-2} s^{-1}) which were more than double than indicted by my measurements (2.62 nmol m^{-2} s^{-1}). Fluxes of monoterpenes (-3.39 nmol m^{-2} s^{-1}), oxygenated monoterpenes (-0.19 nmol m^{-2} s^{-1}), acetic acid (-0.18 nmol m^{-2} s^{-1}) and sesquiterpenes (-0.03 nmol m^{-2} s^{-1}) were considered as net depositions. In my measurements, emission and deposition fluxes of acetic acid were balanced during the selected day, whereas monoterpenes showed a small amount of net emissions (0.02 nmol m^{-2} s^{-1}). Average daytime fluxes from 19 June 2017 of methanol, acetaldehyde, and acetone are 5.08, 1.04, and 0.44 nmol m^{-2} s^{-1}, respectively. These are in the lower range of what was observed by Davison et al. (2008) for methanol (8.7–38 nmol m^{-2} s^{-1}), acetaldehyde (0.6–8.4 nmol m^{-2} s^{-1}), acetone (0.3–5.1 nmol m^{-2} s^{-1}), and 2-butanone (0.3–2.2 nmol m^{-2} s^{-1}). The large range from Davison et al. (2008) results from measurements averaged over 4 days including a cutting event at the first day which induced a strong emission increase. Other grassland studies detected

emission bursts of methanol, GLVs, acetaldehyde, acetone, and isoprene that last for some hours to few days after cutting (Bamberger et al., 2010, 2011; Ruuskanen et al., 2011; Brilli et al., 2012; Hörtnagl et al., 2014). Since in my study, cut induced emissions from the managed ryegrass field were not considered, modeling results of annual BVOC emissions from ryegrass can be judged as rather conservative estimates.

Additionally, I could not detect any significant fluxes of highly reactive oxygenated monoterpenes from the ryegrass and oilseed rape ecosystem as well, which had been reported in previous studies (König et al., 1995; McEwan and Smith, 1998; Himanen et al., 2009; Pańka et al., 2013). Assuming that these are related to conditions that may occur frequently but not under all environmental conditions and that I thus have missed them by chance, the potential impact on atmospheric chemistry from these species may be higher on a larger spatial and temporal scale than has been calculated here.

6.3.2. Differences to other vegetation types

Herein, I compare BVOC standardized emission factors (SEFs) from the three observed bioenergy plants with SEFs from other vegetation types (see Tab. 6.2). Many studies report SEFs of isoprene and some also provide information about monoterpenes and sesquiterpenes, but information about the occurrence and sensitivity of other BVOCs is still very scarce (Kesselmeier and Staudt, 1999). More recent emission inventories such as that by Karl et al. (2009), use only one emission value to describe the large group of OVOCs and even this values is not based on dedicated studies but represents a default SEF of 2.0 μg g^{-1}DW h^{-1}.

The observed bioenergy crops from this study are in a similar range of emitted terpenoids compared to other arable crops which are used for food production such as wheat (*Triticum*) and rice (*Oryza*) (see Tab. 6.2). Other crops, which are used for bioenergy production can emit significantly higher amounts of highly reactive compounds (e.g. isoprene from giant reed (*Arundo donax*)) or relatively low amounts, at least of terpenoids as from elephant grass (*Miscanthus*). Fast growing tree species such as poplar (*Populus*), willow (*Salix*), and eucalyptus (*Eucalyptus*) are also a preferred source of woody biomass for bioenergy production (Beltman et al., 2013). These species have a strong potential to emit large amounts of isoprene and monoterpenes,

Table 6.2.: Overview of terpenoid BVOC standardized emission factors (SEFs) from maize, oilseed rape, and ryegrass ecosystems compared to selected other bioenergy-related vegetation types. The values are scaled to PPFD of 1000 μmol m^2 s^{-1} and 30 °C in units of μg compound g^{-1}DW h^{-1}. The dry weight of leaf or plant biomass density used for scaling is also given in g m^{-2}. n.def., not defined in the reference.

Vegetation type	Biomass density	Isoprene	Monoterpenes	Sesquiterpenes	Reference
Maize	1200	0	0.19	0.059	This study
Oilseed rape	600	0.218	0.404	0	This study
Ryegrass	400	0.114	0.077	0	This study
Wheat	n.def.	0.01–0.5	n.def.	n.def.	a, b
Rice	n.def.	n.def.	0.4–0.5	n.def.	a, c
Giant reed	n.def.	34–142	n.def.	n.def.	a, c
Elephant grass	n.def.	0–0.01	n.def.	n.def.	a, b
Oil palm	n.def.	0–172.9	1	n.def.	a, c
Eucalyptus	400	15–57	0.7–9.2	n.def.	a, c, d, e
Willow	150	0.1–115	0.1–10	0.1	a, b, d, e, f
Poplar	320	0–70	0	0	d, e

a: Rosenkranz et al. (2015); b: Morrison et al. (2016); c: Kesselmeier and Staudt (1999); d: Beltman et al. (2013); e: Karl et al. (2009); f: Copeland et al. (2012)

indicating a high impact on O_3 and SOA forming potential. As I could show for the estimated annual OH-reactivity scaled to the energy yield from a poplar plantation, the high energy density of trees cannot compensate for the surplus of emitted reactive compounds, putting ryegrass, maize, and even oilseed rape in a better position for the bioenergy production.

7. Summary of Conclusions

Bioenergy production using agricultural plants is rapidly expanding in Europe and is likely to change the emissions of highly reactive biogenic volatile organic compounds (BVOCs). This might have the capability to impact air quality and regional climate but accurate field observations that are needed to evaluate these impacts are lacking. I thus investigated the emissions of as many as 16 BVOCs by field observations of the most prominent bioenergy plants in Germany (maize, oilseed rape, and ryegrass). The investigation included at least two plant developmental stages and a wide range of environmental conditions. Subsequently, the results were used to parameterize a mechanistic process-based BVOC model, which considers *de novo* as well as pool emissions, that was evaluated and coupled to an ecosystem model within the scope of this study. From observations and modeling, I conclude the following:

The impact on air chemistry by potential BVOC–OH reactivity varies substantially by crop species and is largest with oilseed rape. Simulated total annual BVOC emissions deviate by a factor of 37 between the investigated bioenergy plants. By combining these results with potential BVOC–OH reaction rates and scaling to the respective energy yields, however only a 4.5-fold difference has been found which is caused by the large range of OH-reactivity rates between the different BVOCs. Thus, from the viewpoint of potential air chemistry impact, ryegrass and maize are to be preferred above oilseed rape as well as poplar, willow, and eucalyptus (based on literature values).

The temporal dynamics of BVOC emissions can only be captured with long-term measurements considering bidirectional fluxes and plant development. Seasonal bidirectional BVOC flux patterns could be generally explained by instantaneous and cumulative temperature, radiation, and precipitation regimes. However, the sensitivity of BVOC emissions towards temperature and radiation did significantly change on time scales larger than a week which could be clearly linked to different plant development stages. Emerging plant tissues such as flowers can act as additionally BVOC sources and therefore impact the composition and amount of fluxes as well. Observed net deposition processes were explained by wet deposition and fluxes into the soil.

Overall BVOC emissions from bioenergy plants in Germany are small compared to woody bioenergy plants but are similar to that of cereals. The amount of BVOC emissions from maize, oilseed rape and ryegrass, which are important bioenergy plants in Germany, are several times lower compared to fast growing tree species, which are a preferred source of woody biomass for bioenergy production. In contrast, the emission amounts from crops which are used for food production such as wheat and rice have a similar magnitude when compared to the investigated bioenergy plants.

Large non-steady state chambers are suitable for long-term BVOC flux measurements. This is the first time that large automatic chambers with a flow-through non-steady-state approach were used to detect BVOC exchanges. By carefully considering few limitations, this technique enabled to quantify a multitude of different BVOCs including methyl salicylate, oxygenated monoterpenes as well as sesquiterpenes which have the characteristic to adhere to many kinds of surfaces within a measurement setup. Other advantages are that the ecosystem patch can be exactly determined, meteorological quantities and trace gas concentrations are measured within a defined headspace, and a basic statistical approach can be used to detect BVOC fluxes.

The process-based `JJv` BVOC emission model is well working in combination with a biogeochemical ecosystem model but needs additional consideration of specific development phases such as flowering. I simulated an explicit link of BVOC emissions to photosynthesis and plant development by coupling the state-of-the-art process-based BVOC emission model `JJv` and a pool emission approach to the biogeochemical ecosystem model `LandscapeDNDC`. By parameterizing the models with data from my field campaigns, simulated BVOC emissions could represent observed emission rates throughout the whole vegetation period reasonably well. However, deposition processes of any kind are not included in the model. Generally, it should be considered to include emissions during specific plant development stages or from plant tissues other than leaves as for examples flowers. Nevertheless, this model approach and its parameterization can now be used for other periods, on larger spatial scales, or implemented into other simulation frameworks such as earth system models, when a Farquhar-type description is used to simulate photosynthesis.

Bibliography

Aaltonen, H., and Coauthors, 2013: Continuous VOC flux measurements on boreal forest floor. *Plant and Soil*, **369 (1)**, 241–256, DOI:10.1007/s11104-012-1553-4.

Arbeitsgemeinschaft Energiebilanzen, 2015: *Auswertungstabellen zur Energiebilanz Deutschland. 1990 bis 2014*. URL http://www.ag-energiebilanzen.de/.

Arneth, A., and Coauthors, 2007: Process-based estimates of terrestrial ecosystem isoprene emissions: incorporating the effects of a direct CO_2-isoprene interaction. *Atmospheric Chemistry and Physics*, **7 (1)**, 31–53, DOI:10.5194/acp-7-31-2007.

Arneth, A., and Coauthors, 2010a: From biota to chemistry and climate: towards a comprehensive description of trace gas exchange between the biosphere and atmosphere. *Biogeosciences*, **7 (1)**, 121–149.

Arneth, A., and Coauthors, 2010b: Terrestrial biogeochemical feedbacks in the climate system. *Nature Geoscience*, **3 (8)**, 525.

Ashworth, K., O. Wild, A. S. D. Eller, and C. N. Hewitt, 2015: Impact of biofuel poplar cultivation on ground-level ozone and premature human mortality depends on cultivar selection and planting location. *Environmental Science & Technology*, **49 (14)**, 8566–8575, DOI:10.1021/acs.est.5b00266.

Ashworth, K., O. Wild, and C. Hewitt, 2013: Impacts of biofuel cultivation on mortality and crop yields. *Nature Climate Change*, **3 (5)**, 492–496.

Atkinson, R., 2000: Atmospheric chemistry of VOCs and NO_x. *Atmospheric Environment*, **34 (12-14)**, 2063 – 2101, DOI:10.1016/S1352-2310(99)00460-4.

Atkinson, R., and J. Arey, 2003: Gas-phase tropospheric chemistry of biogenic volatile organic compounds: a review. *Atmospheric Environment*, **37**, 197 – 219, DOI: 10.1016/S1352-2310(03)00391-1.

Bachy, A., M. Aubinet, N. Schoon, C. Amelynck, B. Bodson, C. Moureaux, and B. Heinesch, 2016: Are BVOC exchanges in agricultural ecosystems overestimated? Insights from fluxes measured in a maize field over a whole growing season. *Atmospheric Chemistry and Physics*, **16 (8)**, 5343–5356, DOI:10.5194/acp-16-5343-2016.

Baldwin, I. T., R. Halitschke, A. Paschold, C. C. von Dahl, and C. A. Preston, 2006: Volatile Signaling in Plant-Plant Interactions: "Talking Trees" in the Genomics Era. *Science*, **311 (5762)**, 812–815, DOI:10.1126/science.1118446.

Ball, J. T., I. E. Woodrow, and J. A. Berry, 1987: A model predicting stomatal conductance and its contribution to the control of photosynthesis under different environmental conditions. *Progress in photosynthesis research*, Springer, 221–224.

Baltensperger, U., and Coauthors, 2005: Secondary organic aerosols from anthropogenic and biogenic precursors. *Faraday Discuss.*, **130**, 265–278, DOI:10.1039/B417367H.

Bamberger, I., and Coauthors, 2010: BVOC fluxes above mountain grassland. *Biogeosciences*, **7 (5)**, 1413–1424, DOI:10.5194/bg-7-1413-2010.

Bamberger, I., and Coauthors, 2011: Deposition fluxes of terpenes over grassland. *Journal of Geophysical Research: Atmospheres*, **116 (D14)**, DOI:10.1029/2010JD015457.

Bash, J. O., K. R. Baker, and M. R. Beaver, 2016: Evaluation of improved land use and canopy representation in BEIS v3.61 with biogenic VOC measurements in California. *Geoscientific Model Development*, **9 (6)**, 2191–2207, DOI:10.5194/gmd-9-2191-2016.

Beltman, J. B., C. Hendriks, M. Tum, and M. Schaap, 2013: The impact of large scale biomass production on ozone air pollution in europe. *Atmospheric Environment*, **71**, 352 – 363, DOI:10.1016/j.atmosenv.2013.02.019.

Bentsen, N. S., and C. Felby, 2012: Biomass for energy in the European Union - a review of bioenergy resource assessments. *Biotechnology for Biofuels*, **5 (1)**, 1–10, DOI:10.1186/1754-6834-5-25.

BHKW Infozentrum GbR, 2018: Pflanzenöle-BHKW. URL http://www.pflanzenoel-bhkw.de/pflanzenoel-bhkw_pflanzenoele.html, accessed 08 May 2018.

Bonn, B., and G. K. Moortgat, 2003: Sesquiterpene ozonolysis: Origin of atmospheric new particle formation from biogenic hydrocarbons. *Geophysical Research Letters*, **30(11) (11)**, DOI:10.1029/2003GL017000.

Brilli, F., L. Hörtnagl, I. Bamberger, R. Schnitzhofer, T. M. Ruuskanen, A. Hansel, F. Loreto, and G. Wohlfahrt, 2012: Qualitative and quantitative characterization of volatile organic compound emissions from cut grass. *Environmental Science & Technology*, **46 (7)**, 3859–3865, DOI:10.1021/es204025y.

Brilli, F., and Coauthors, 2016: Rapid leaf development drives the seasonal pattern of volatile organic compound (VOC) fluxes in a 'coppiced' bioenergy poplar plantation. *Plant, Cell & Environment*, **39 (3)**, 539–555, DOI:10.1111/pce.12638.

Burkholder, J., and Coauthors, 2015: Chemical kinetics and photochemical data for use in atmospheric studies: evaluation number 18. Tech. rep., Pasadena, CA: Jet Propulsion Laboratory, National Aeronautics and Space.

Butterbach-Bahl, K., and Coauthors, 2019: Landscapedndc v1.29.0. a process model for simulating biosphere-atmosphere-hydrosphere exchange processes. Users guide, Karlsruhe Institute for Technology. Institute of Meteorology and Climate Research – Atmospheric Environmental Research, Garmisch-Partenkirchen, Bavaria, Germany.

Calfapietra, C., S. Fares, F. Manes, A. Morani, G. Sgrigna, and F. Loreto, 2013a: Role of Biogenic Volatile Organic Compounds (BVOC) emitted by urban trees on ozone concentration in cities: A review. *Environmental Pollution*, **183**, 71 – 80, DOI:10.1016/j.envpol.2013.03.012.

Calfapietra, C., E. Pallozzi, I. Lusini, and V. Velikova, 2013b: Modification of BVOC Emissions by Changes in Atmospheric [CO_2] and Air Pollution. *Biology, Controls and Models of Tree Volatile Organic Compound Emissions*, Ü. Niinemets, and R. K. Monson, Eds., Springer Netherlands, Dordrecht, 253–284, DOI: 10.1007/978-94-007-6606-8_10.

Campbell, P. K. E., and Coauthors, 2019: Diurnal and Seasonal Variations in Chlorophyll Fluorescence Associated with Photosynthesis at Leaf and Canopy Scales. *Remote Sensing*, **11 (5)**, DOI:10.3390/rs11050488.

Carlton, A. G., C. Wiedinmyer, and J. H. Kroll, 2009: A review of Secondary Organic Aerosol (SOA) formation from isoprene. *Atmospheric Chemistry and Physics*, **9 (14)**, 4987–5005.

Carslaw, K. S., O. Boucher, D. V. Spracklen, G. W. Mann, J. G. L. Rae, S. Woodward, and M. Kulmala, 2010: A review of natural aerosol interactions and feedbacks within the earth system. *Atmospheric Chemistry and Physics*, **10 (4)**, 1701–1737, DOI:10.5194/acp-10-1701-2010.

Ciais, C. S., P., and Coauthors, 2013: Carbon and Other Biogeochemical Cycles. *Climate Change 2013: The Physical Science Basis. Contribution of Working Group I to the Fifth Assessment Report of the Intergovernmental Panel on Climate Change*, T. Stocker, G.-K. P. D. Qin, M. Tignor, S. Allen, J. Boschung, Y. X. A. Nauels, V. Bex, and P. Midgley, Eds., Cambridge University Press, Cambridge, United Kingdom and New York, NY, USA, Chap. 6, 465–570, DOI: 10.1017/CBO9781107415324.015.

Ciccioli, P., and Coauthors, 1999: Emission of reactive terpene compounds from orange orchards and their removal by within-canopy processes. *Journal of Geophysical Research: Atmospheres*, **104 (D7)**, 8077–8094, DOI:10.1029/1998JD100026.

Collatz, G., J. Ball, C. Grivet, and J. A. Berry, 1991: Physiological and environmental regulation of stomatal conductance, photosynthesis and transpiration: a model that includes a laminar boundary layer. *Agricultural and Forest Meteorology*, **54 (2)**, 107 – 136, DOI:https://doi.org/10.1016/0168-1923(91)90002-8.

Collatz, G. J., M. Ribas-Carbo, and J. Berry, 1992: Coupled photosynthesis-stomatal

conductance model for leaves of c4 plants. *Functional Plant Biology*, **19 (5)**, 519–538.

Copeland, N., J. N. Cape, and M. R. Heal, 2012: Volatile organic compound emissions from miscanthus and short rotation coppice willow bioenergy crops. *Atmospheric Environment*, **60**, 327 – 335, DOI:10.1016/j.atmosenv.2012.06.065.

Crutzen, P. J., A. R. Mosier, K. A. Smith, and W. Winiwarter, 2008: N_2O release from agro-biofuel production negates global warming reduction by replacing fossil fuels. *Atmospheric Chemistry and Physics*, **8 (2)**, 389–395, DOI:10.5194/acp-8-389-2008.

Custer, T., and G. Schade, 2007: Methanol and acetaldehyde fluxes over ryegrass. *Tellus B: Chemical and Physical Meteorology*, **59 (4)**, 673–684, DOI:10.1111/j.1600-0889.2007.00294.x.

Das, M., D. Kang, V. Aneja, W. Lonneman, D. Cook, and M. Wesely, 2003: Measurements of hydrocarbon air–surface exchange rates over maize. *Atmospheric Environment*, **37 (16)**, 2269 – 2277, DOI:10.1016/S1352-2310(03)00076-1.

Davison, B., A. Brunner, C. Ammann, C. Spirig, M. Jocher, and A. Neftel, 2008: Cut-induced voc emissions from agricultural grasslands. *Plant Biology*, **10 (1)**, 76–85, DOI:10.1055/s-2007-965043.

Degenhardt, J., T. G. Köllner, and J. Gershenzon, 2009: Monoterpene and sesquiterpene synthases and the origin of terpene skeletal diversity in plants. *Phytochemistry*, **70 (15–16)**, 1621–1637, DOI:10.1016/j.phytochem.2009.07.030.

Deming, B. L., and Coauthors, 2019: Measurements of delays of gas-phase compounds in a wide variety of tubing materials due to gas–wall interactions. *Atmospheric Measurement Techniques*, **12 (6)**, 3453–3461, DOI:10.5194/amt-12-3453-2019.

Deutsche Saatveredelung AG, 2015: Country 2051 Feldgras ein- bis zweijährig. Lippstadt, Germany, URL https://www.dsv-saaten.de/zwischenfruechte/zwischenfruechte_futter/mischungen/country2051.html, accessed 12 April 2017.

Dicke, M., and F. Loreto, 2010: Induced plant volatiles: from genes to climate change. *Trends in Plant Science*, **15**, 115–117, DOI:10.1016/j.tplants.2010.01.007.

Dislich, C., and Coauthors, 2017: A review of the ecosystem functions in oil palm plantations, using forests as a reference system. *Biological Reviews*, **92 (3)**, 1539–1569, DOI:10.1111/brv.12295.

Dudareva, N., A. Klempien, J. K. Muhlemann, and I. Kaplan, 2013: Biosynthesis, function and metabolic engineering of plant volatile organic compounds. *New Phytologist*, **198 (1)**, 16–32.

Dudareva, N., F. Negre, D. A. Nagegowda, and I. Orlova, 2006: Plant Volatiles: Recent Advances and Future Perspectives. *Critical Reviews in Plant Sciences*, **25 (5)**, 417–440, DOI:10.1080/07352680600899973.

EEA, European Environment Agency, 2011: Agriculture. Copenhagen, Denmark, URL https://www.eea.europa.eu/themes/agriculture/intro, accessed 10 May 2017.

EEA, 2013: *EU bioenergy potential from a resource-efficiency perspective*. Luxembourg: Publications Office of the European Union, European Environment Agency.

Emmerson, K. M., M. E. Cope, I. E. Galbally, S. Lee, and P. F. Nelson, 2017: Isoprene and monoterpene emissions in australia: comparison of a multi-layer canopy model with megan and with atmospheric concentration observations. *Atmospheric Chemistry and Physics Discussions*, **2017**, 1–21, DOI:10.5194/acp-2017-911.

Erneuerbare-Energien-Gesetz, 2014: *Erneuerbare-Energien-Gesetz - EEG 2014*. Gesetz füFr den Ausbau erneuerbarer Energien.

European Commission, 2014: *EU energy, transport and GHG emissions trends to 2050 – Reference scenario 2013*. Luxemburg, European Union, URL http://ec.europa.eu/clima/policies/strategies/2030/docs/eu_trends_2050_en.pdf.

European Commission, 2014b: *State of play on the sustainability of solid and gaseous biomass used for electricity, heating and cooling in the EU*. Brussels, European Union, URL http://ec.europa.eu/transparency/regdoc/rep/10102/2014/EN/10102-2014-259-EN-F1-1.PDF.

FAO, Food and Agriculture Organization of the United Nations Statistics Division (FAOSTAT), 2019: Food and agriculture data. URL http://www.fao.org/faostat/en/#home, accessed 08 February 2019.

Farquhar, G. D., and T. D. Sharkey, 1982: Stomatal conductance and photosynthesis. *Annual review of plant physiology*, **33 (1)**, 317–345.

Farquhar, G. D., S. von Caemmerer, and J. A. Berry, 1980: A biochemical model of photosynthetic co2 assimilation in leaves of c3 species. *Planta*, **149 (1)**, 78–90, DOI:10.1007/BF00386231.

Filella, I., and Coauthors, 2018: A MODIS Photochemical Reflectance Index (PRI) as an Estimator of Isoprene Emissions in a Temperate Deciduous Forest. *Remote Sensing*, **10 (4)**, 557.

FNR, Fachagentur für Nachwachsende Rohstoffe e.V., 2018a: Ackergras. URL https://pflanzen.fnr.de/energiepflanzen/ackergras/, accessed 08 May 2018.

FNR, Fachagentur für Nachwachsende Rohstoffe e.V., 2018b: Daten und Fakten. URL https://mediathek.fnr.de/grafiken/daten-und-fakten.html, accessed 28 July, 2018.

FNR, Fachagentur für Nachwachsende Rohstoffe e.V., 2018c: Mais. *Zea mays* L. URL https://pflanzen.fnr.de/energiepflanzen/mais/, accessed 08 May 2018.

FNR, Fachagentur für Nachwachsende Rohstoffe e.V., 2018d: Raps. *Brassica lapus* L. URL https://pflanzen.fnr.de/energiepflanzen/raps/, accessed 08 May 2018.

Fontana, A., M. Held, C. A. Fantaye, T. C. Turlings, J. Degenhardt, and J. Gershenzon, 2011: Attractiveness of Constitutive and Herbivore-Induced Sesquiterpene Blends of Maize to the Parasitic Wasp *Cotesia marginiventris* (cresson). *Journal of Chemical Ecology*, **37 (6)**, 582, DOI:10.1007/s10886-011-9967-7.

Fuentes, J. D., and Coauthors, 2000: Biogenic hydrocarbons in the atmospheric boundary layer: A review. *Bulletin of the American Meteorological Society*, **81**, 1537 – 1575.

Ghirardo, A., W. Heller, M. Fladung, J.-P. Schnitzler, and H. Schroeder, 2012: Function of defensive volatiles in pedunculate oak (*Quercus robur*) is tricked by the moth *Tortrix viridana*. *Plant, cell & environment*, **35 (12)**, 2192–2207.

Ghirardo, A., K. Koch, R. Taipale, I. Zimmer, J.-P. Schnitzler, and J. Rinne, 2010: Determination of *de novo* and pool emissions of terpenes from four common boreal/alpine trees by $^{13}CO_2$ labelling and PTR-MS analysis. *Plant, Cell & Environment*, **33 (5)**, 781–792, DOI:10.1111/j.1365-3040.2009.02104.x.

Ghirardo, A., and Coauthors, 2016: Urban stress-induced biogenic VOC emissions and SOA-forming potentials in Beijing. *Atmospheric Chemistry and Physics*, **16 (5)**, 2901–2920, DOI:10.5194/acp-16-2901-2016.

Gouinguené, S., T. Degen, and T. C. J. Turlings, 2001: Variability in herbivore-induced odour emissions among maize cultivars and their wild ancestors (teosinte). *CHEMOECOLOGY*, **11 (1)**, 9–16, DOI:10.1007/PL00001832.

Graus, M., A. Eller, R. Fall, B. Yuan, Y. Qian, P. Westra, J. de Gouw, and C. Warneke, 2013: Biosphere-atmosphere exchange of volatile organic compounds over C4 biofuel crops. *Atmospheric Environment*, **66**, 161–168, DOI:10.1016/j.atmosenv.2011.12.042.

Grote, R., T. Keenan, A.-V. Lavoir, and M. Staudt, 2010: Process-based simulation of seasonality and drought stress in monoterpene emission models. *Biogeosciences*, **7 (1)**, 257–274.

Grote, R., R. Kiese, T. Grünwald, J.-M. Ourcival, and A. Granier, 2011: Modelling forest carbon balances considering tree mortality and removal. *Agricultural and Forest Meteorology*, **151 (2)**, 179 – 190, DOI:http://dx.doi.org/10.1016/j.agrformet.2010.10.002.

Grote, R., A.-V. Lavoir, S. Rambal, M. Staudt, I. Zimmer, and J.-P. Schnitzler, 2009: Modelling the drought impact on monoterpene fluxes from an evergreen Mediterranean forest canopy. *Oecologia*, **160 (2)**, 213–223, DOI:10.1007/s00442-009-1298-9.

Grote, R., S. Mayrhofer, R. J. Fischbach, R. Steinbrecher, M. Staudt, and J.-P. Schnitzler, 2006: Process-based modelling of isoprenoid emissions from evergreen leaves of *Quercus ilex* (L.). *Atmospheric Environment*, **40**, 152–165.

Grote, R., R. K. Monson, and U. Niinemets, 2013: Leaf-level Models of Constitutive and Stress-Driven Volatile Organic Compound Emissions. *Biology, Controls and Models of Tree Volatile Organic Compound Emissions*, U. Niinemets, and R. K. Monson, Eds., Springer Netherlands, Dordrecht, 315–355, DOI:10.1007/978-94-007-6606-8_12, URL https://doi.org/10.1007/978-94-007-6606-8_12.

Grote, R., C. Morfopoulos, Ü. Niinemets, Z. Sun, T. F. Keenan, F. Pacifico, and T. Butler, 2014: A fully integrated isoprenoid emissions model coupling emissions to photosynthetic characteristics. *Plant, Cell & Environment*, **37 (8)**, 1965–1980.

Grote, R., and U. Niinemets, 2008: Modeling volatile isoprenoid emissions – a story with split ends. *Plant Biology*, **10 (1)**, 8–28, DOI:10.1055/s-2007-964975.

Guenther, A., 1997: Seasonal and spatial variations in natural volatile organic compound emissions. *Ecological Applications*, **7 (1)**, 34–45, DOI:10.1890/1051-0761(1997)007[0034:SASVIN]2.0.CO;2.

Guenther, A., T. Karl, P. Harley, C. Wiedinmyer, P. I. Palmer, and C. Geron, 2006: Estimates of global terrestrial isoprene emissions using megan (model of emissions of gases and aerosols from nature). *Atmospheric Chemistry and Physics*, **6 (11)**, 3181–3210, DOI:10.5194/acp-6-3181-2006.

Guenther, A. B., X. Jiang, C. L. Heald, T. Sakulyanontvittaya, T. Duhl, L. K. Emmons, and X. Wang, 2012: The model of emissions of gases and aerosols from nature version 2.1 (MEGAN2.1): an extended and updated framework for modeling biogenic emissions. *Geoscientific Model Development*, **5 (6)**, 1471–1492, DOI:10.5194/gmd-5-1471-2012.

Guenther, A. B., R. K. Monson, and R. Fall, 1991: Isoprene and monoterpene emission rate variability: Observations with eucalyptus and emission rate algorithm development. *Journal of Geophysical Research: Atmospheres*, **96 (D6)**, 10 799–10 808, DOI:10.1029/91JD00960.

Guenther, A. B., P. R. Zimmerman, P. C. Harley, R. K. Monson, and R. Fall, 1993: Isoprene and monoterpene emission rate variability: model evaluations and sensitivity analyses. *Journal of Geophysical Research*, **98 (D7)**, 12 609–12 617.

Gustavsson, A.-M., 2011: A developmental scale for perennial forage grasses based on the decimal code framework. *Grass and Forage Science*, **66 (1)**, 93–108.

Haas, E., and Coauthors, 2013: LandscapeDNDC: a process model for simulation of biosphere–atmosphere–hydrosphere exchange processes at site and regional scale. *Landscape Ecology*, **28 (4)**, 615–636, DOI:10.1007/s10980-012-9772-x.

Hakola, H., H. Hellén, M. Hemmilä, J. Rinne, and M. Kulmala, 2012: In situ measurements of volatile organic compounds in a boreal forest. *Atmospheric Chemistry and Physics*, **12 (23)**, 11 665–11 678, DOI:10.5194/acp-12-11665-2012.

Hakola, H., V. Tarvainen, A. P. Praplan, K. Jaars, M. Hemmilä, M. Kulmala, J. Bäck, and H. Hellén, 2017: Terpenoid and carbonyl emissions from norway spruce in finland during the growing season. *Atmospheric Chemistry and Physics*, **17 (5)**, 3357–3370, DOI:10.5194/acp-17-3357-2017.

Hallquist, M., and Coauthors, 2009: The formation, properties and impact of secondary organic aerosol: current and emerging issues. *Atmospheric Chemistry and Physics*, **9 (14)**, 5155–5236, DOI:10.5194/acp-9-5155-2009.

Hansel, A., A. Jordan, C. Warneke, R. Holzinger, A. Wisthaler, and W. Lindinger, 1999: Proton-transfer-reaction mass spectrometry (PTR-MS): on-line monitoring of volatile organic compounds at volume mixing ratios of a few pptv. *Plasma Sources Science and Technology*, **8 (2)**, 332.

Hantson, S., W. Knorr, G. Schurgers, T. A. Pugh, and A. Arneth, 2017: Global isoprene and monoterpene emissions under changing climate, vegetation, CO2 and land use. *Atmospheric Environment*, **155**, 35 – 45, DOI:https://doi.org/10.1016/j.atmosenv.2017.02.010.

Harley, P., J. Greenberg, U. Niinemets, and A. Guenther, 2007: Environmental controls over methanol emission from leaves. *Biogeosciences*, **4 (6)**, 1083–1099, DOI:10.5194/bg-4-1083-2007.

Harper, K. L., and N. Unger, 2018: Global climate forcing driven by altered BVOC fluxes from 1990 to 2010 land cover change in maritime Southeast Asia. *Atmospheric Chemistry and Physics*, **18 (23)**, 16 931–16 952, DOI:10.5194/acp-18-16931-2018.

Harrison, S. P., and Coauthors, 2013: Volatile isoprenoid emissions from plastid to planet. *New Phytologist*, **197 (1)**, 49–57, DOI:10.1111/nph.12021.

Heald, C. L., and Coauthors, 2008: Predicted change in global secondary organic aerosol concentrations in response to future climate, emissions, and land use change. *Journal of Geophysical Research: Atmospheres*, **113 (D5)**, n/a–n/a, DOI:10.1029/2007JD009092.

Heimann, M., and M. Reichstein, 2008: Terrestrial ecosystem carbon dynamics and climate feedbacks. *Nature*, **451 (7176)**, 289, DOI:10.1038/nature06591.

Himanen, S. J., A. Nerg, A. Nissinen, D. M. Pinto, C. N. Stewart, G. M. Poppy, and J. K. Holopainen, 2009: Effects of elevated carbon dioxide and ozone on volatile terpenoid emissions and multitrophic communication of transgenic insecticidal oilseed rape (*Brassica napus*). *New Phytologist*, **181 (1)**, 174–186, DOI:10.1111/j.1469-8137.2008.02646.x.

Hoffmann, M., N. Jurisch, E. A. Borraz, U. Hagemann, M. Drösler, M. Sommer, and J. Augustin, 2015: Automated modeling of ecosystem CO_2 fluxes based on periodic closed chamber measurements: A standardized conceptual and practical approach. *Agricultural and Forest Meteorology*, **200**, 30 – 45, DOI:http://dx.doi.org/10.1016/

j.agrformet.2014.09.005.

Hoffmann, M., M. Schulz-Hanke, J. Garcia Alba, N. Jurisch, U. Hagemann, T. Sachs, M. Sommer, and J. Augustin, 2017: A simple calculation algorithm to separate high-resolution ch_4 flux measurements into ebullition- and diffusion-derived components. *Atmospheric Measurement Techniques*, **10 (1)**, 109–118, DOI:10.5194/amt-10-109-2017.

Hoffmann, M., and Coauthors, 2018: Maize carbon dynamics are driven by soil erosion state and plant phenology rather than nitrogen fertilization form. *Soil and Tillage Research*, **175**, 255 – 266, DOI:https://doi.org/10.1016/j.still.2017.09.004.

Holopainen, J. K., and J. Gershenzon, 2010: Multiple stress factors and the emission of plant VOCs. *Trends in Plant Science*, **15 (3)**, 176–184, DOI:10.1016/j.tplants.2010.01.006.

Hörtnagl, L., and Coauthors, 2014: Acetaldehyde exchange above a managed temperate mountain grassland. *Atmospheric Chemistry and Physics*, **14 (11)**, 5369–5391, DOI:10.5194/acp-14-5369-2014.

Houska, T., D. Kraus, R. Kiese, and L. Breuer, 2017: Constraining a complex biogeochemical model for CO_2 and N_2O emission simulations from various land uses by model–data fusion. *Biogeosciences*, **14 (14)**, 3487–3508, DOI:10.5194/bg-14-3487-2017.

Hu, B., A.-M. Jarosch, M. Gauder, S. Graeff-Hönninger, J.-P. Schnitzler, R. Grote, H. Rennenberg, and J. Kreuzwieser, 2018: VOC emissions and carbon balance of two bioenergy plantations in response to nitrogen fertilization: A comparison of *Miscanthus* and *Salix*. *Environmental Pollution*, **237**, 205 – 217, DOI:https://doi.org/10.1016/j.envpol.2018.02.034.

Immerzeel, D. J., P. A. Verweij, F. van der Hilst, and A. P. C. Faaij, 2014: Biodiversity impacts of bioenergy crop production: a state-of-the-art review. *GCB Bioenergy*, **6 (3)**, 183–209, DOI:10.1111/gcbb.12067.

Inomata, S., H. Tanimoto, S. Kameyama, U. Tsunogai, H. Irie, Y. Kanaya, and Z. Wang, 2008: Technical note: Determination of formaldehyde mixing ratios in air with ptr-ms: laboratory experiments and field measurements. *Atmospheric Chemistry and Physics*, **8 (2)**, 273–284, DOI:10.5194/acp-8-273-2008.

International Energy Agency, 2015: *Excerpt From Renewables Information – IEA Statistics: Key Renewables Trends*.

International Energy Agency, F., 2017: *How2Guide for Bioenergy: Roadmap Development and Implementation*. IEA, FAO.

IONICON, 2011: *IONICON High-Sensitivity PTR-QMS 500 product factsheet*. Innsbruck, Austria, IONICON Analytik GmbH, URL http://www.ionicon.com/sites/

default/files/uploads/doc/factsheet_ionicon_hs_ptr_qms_500.pdf.

IONICON, 2013: *Technologies overview: Proton transfer reaction - mass spectrometry*. Innsbruck, Austria, IONICON Analytik GmbH, URL http://www.ionicon.com/sites/default/files/uploads/downloads/flyer_2013_IONICON_PTR-MS_technology_overview.pdf.

IONICON, 2016: *Hands-on PTR-MS 2016. Training documentation*. Innsbruck, Austria, IONICON Analytik GmbH.

IUPAC, 1997: *Compendium of Chemical Terminology (the "Gold Book")*. 2nd ed., Blackwell Scientific, Oxford, DOI:10.1351/goldbook.

Jakobsen, H. B., P. Friis, J. K. Nielsen, and C. E. Olsen, 1994: Emission of volatiles from flowers and leaves of brassica napus in situ. *Phytochemistry*, **37 (3)**, 695 – 699, DOI:http://dx.doi.org/10.1016/S0031-9422(00)90341-8.

Jardine, K., and Coauthors, 2011: Within-canopy sesquiterpene ozonolysis in Amazonia. *Journal of Geophysical Research: Atmospheres*, **116 (D19)**, n/a–n/a, DOI: 10.1029/2011JD016243.

Jordan, A., and Coauthors, 2009: A high resolution and high sensitivity proton-transfer-reaction time-of-flight mass spectrometer (PTR-TOF-MS). *International Journal of Mass Spectrometry*, **286 (2)**, 122 – 128, DOI:https://doi.org/10.1016/j.ijms.2009.07.005.

June, T., A. Meijide, C. Stiegler, A. P. Kusuma, and A. Knohl, 2018: The influence of surface roughness and turbulence on heat fluxes from an oil palm plantation in Jambi, Indonesia. *IOP Conference Series: Earth and Environmental Science*, IOP Publishing, Vol. 149, 012048.

Kaiser, J., and Coauthors, 2018: High-resolution inversion of OMI formaldehyde columns to quantify isoprene emission on ecosystem-relevant scales: application to the southeast US. *Atmospheric Chemistry and Physics*, **18 (8)**, 5483–5497, DOI: 10.5194/acp-18-5483-2018.

Kaplan, J. O., G. Folberth, and D. A. Hauglustaine, 2006: Role of methane and biogenic volatile organic compound sources in late glacial and Holocene fluctuations of atmospheric methane concentrations. *Global Biogeochemical Cycles*, **20 (2)**, DOI: 10.1029/2005GB002590.

Karl, M., A. Guenther, R. Köble, A. Leip, and G. Seufert, 2009: A new european plant-specific emission inventory of biogenic volatile organic compounds for use in atmospheric transport models. *Biogeosciences*, **6 (6)**, 1059–1087, DOI:10.5194/bg-6-1059-2009.

Karl, T. G., C. Spirig, J. Rinne, C. Stroud, P. Prevost, J. Greenberg, R. Fall, and A. Guenther, 2002: Virtual disjunct eddy covariance measurements of or-

ganic compound fluxes from a subalpine forest using proton transfer reaction mass spectrometry. *Atmospheric Chemistry and Physics*, **2 (4)**, 279–291, DOI: 10.5194/acp-2-279-2002.

Kegge, W., and R. Pierik, 2010: Biogenic volatile organic compounds and plant competition. *Trends in Plant Science*, **15 (3)**, 126 – 132, DOI:https://doi.org/10.1016/j.tplants.2009.11.007.

Kelly, J. M., R. M. Doherty, F. M. O'Connor, G. W. Mann, H. Coe, and D. Liu, 2019: The roles of volatile organic compound deposition and oxidation mechanisms in determining secondary organic aerosol production: a global perspective using the UKCA chemistry–climate model (vn8.4). *Geoscientific Model Development*, **12 (6)**, 2539–2569, DOI:10.5194/gmd-12-2539-2019.

Kesselmeier, J., 2001: Exchange of Short-Chain Oxygenated Volatile Organic Compounds (VOCs) between Plants and the Atmosphere: A Compilation of Field and Laboratory Studies. *Journal of Atmospheric Chemistry*, **39 (3)**, 219–233, DOI: 10.1023/A:1010632302076.

Kesselmeier, J., and M. Staudt, 1999: Biogenic Volatile Organic Compounds (VOC): An Overview on Emission, Physiology and Ecology. *Journal of Atmospheric Chemistry*, **33 (1)**, 23–88, DOI:10.1023/A:1006127516791.

Klatt, S., and Coauthors, 2017: Exploring impacts of vegetated buffer strips on nitrogen cycling using a spatially explicit hydro-biogeochemical modeling approach. *Environmental Modelling & Software*, **90**, 55 – 67, DOI:https://doi.org/10.1016/j.envsoft.2016.12.002.

Knote, C., and Coauthors, 2014: Simulation of semi-explicit mechanisms of SOA formation from glyoxal in aerosol in a 3-D model. *Atmospheric Chemistry and Physics*, **14 (12)**, 6213–6239, DOI:10.5194/acp-14-6213-2014.

Knudsen, J. T., R. Eriksson, J. Gershenzon, and B. Stå hl, 2006: Diversity and distribution of floral scent. *The Botanical Review*, **72 (1)**, 1, DOI:10.1663/0006-8101(2006)72[1:DADOFS]2.0.CO;2.

Köllner, T. G., C. Schnee, J. Gershenzon, and J. Degenhardt, 2004a: The sesquiterpene hydrocarbons of maize (*Zea mays*) form five groups with distinct developmental and organ-specific distributions. *Phytochemistry*, **65 (13)**, 1895 – 1902, DOI:http://dx.doi.org/10.1016/j.phytochem.2004.05.021.

Köllner, T. G., C. Schnee, J. Gershenzon, and J. Degenhardt, 2004b: The Variability of Sesquiterpenes Emitted from Two *Zea mays* Cultivars Is Controlled by Allelic Variation of Two Terpene Synthase Genes Encoding Stereoselective Multiple Product Enzymes. *The Plant Cell*, **16 (5)**, 1115–1131, DOI:10.1105/tpc.019877.

König, G., M. Brunda, H. Puxbaum, C. Hewitt, S. Duckham, and J. Rudolph, 1995: Relative contribution of oxygenated hydrocarbons to the total biogenic VOC emis-

sions of selected mid-European agricultural and natural plant species. *Atmospheric Environment*, **29 (8)**, 861 – 874, DOI:https://doi.org/10.1016/1352-2310(95)00026-U.

Kraus, D., S. Weller, S. Klatt, E. Haas, R. Wassmann, R. Kiese, and K. Butterbach-Bahl, 2015: A new LandscapeDNDC biogeochemical module to predict CH_4 and N_2O emissions from lowland rice and upland cropping systems. *Plant and Soil*, **386 (1)**, 125–149, DOI:10.1007/s11104-014-2255-x.

Kraus, D., and Coauthors, 2016: How well can we assess impacts of agricultural land management changes on the total greenhouse gas balance (CO_2, CH_4 and N_2O) of tropical rice-cropping systems with a biogeochemical model? *Agriculture, Ecosystems & Environment*, **224**, 104 – 115, DOI:https://doi.org/10.1016/j.agee.2016.03.037.

Krause, P., D. P. Boyle, and F. Bäse, 2005: Comparison of different efficiency criteria for hydrological model assessment. *Advances in Geosciences*, **5**, 89–97, DOI:10.5194/adgeo-5-89-2005.

Kreuzwieser, J., and Coauthors, 2014: The venus flytrap attracts insects by the release of volatile organic compounds. *Journal of Experimental Botany*, DOI:10.1093/jxb/ert455.

Kruskal, W. H., and W. A. Wallis, 1952: Use of Ranks in One-Criterion Variance Analysis. *Journal of the American Statistical Association*, **47 (260)**, 583–621, DOI:10.1080/01621459.1952.10483441.

Laffineur, Q., and Coauthors, 2011: Isoprene and monoterpene emissions from a mixed temperate forest. *Atmospheric Environment*, **45 (18)**, 3157 – 3168, DOI:http://dx.doi.org/10.1016/j.atmosenv.2011.02.054.

Laffineur, Q., and Coauthors, 2012: Abiotic and biotic control of methanol exchanges in a temperate mixed forest. *Atmospheric Chemistry and Physics*, **12 (1)**, 577–590, DOI:10.5194/acp-12-577-2012.

Langford, B., and Coauthors, 2017: Isoprene emission potentials from european oak forests derived from canopy flux measurements: an assessment of uncertainties and inter-algorithm variability. *Biogeosciences*, **14 (23)**, 5571–5594, DOI:10.5194/bg-14-5571-2017.

Lawrence, D., R. Fisher, C. Koven, K. Oleson, S. Swenson, and M. Vertenstein, 2018: Clm5 documentation. technical description of version 5.0 of the community land model (clm). Tech. rep., National Center for Atmospheric Research (NCAR), Boulder, Colorados.

Lehning, A., W. Zimmer, I. Zimmer, and J.-P. Schnitzler, 2001: Modeling of annual variations of oak (quercus robur l.) isoprene synthase activity to predict isoprene emission rates. *Journal of Geophysical Research: Atmospheres*, **106 (D3)**, 3157–

3166.

Leppik, E., T. Tammaru, and B. Frérot, 2014: A view of diel variation of maize odorscape. *American Journal of Plant Sciences*, **5**, 811–820.

Li, C., J. Aber, F. Stange, K. Butterbach-Bahl, and H. Papen, 2000: A process-oriented model of N_2O and no emissions from forest soils: 1. Model development. *Journal of Geophysical Research: Atmospheres*, **105 (D4)**, 4369–4384, DOI:10.1029/1999JD900949.

Li, W., C. Yue, P. Ciais, J. Chang, D. Goll, D. Zhu, S. Peng, and A. Jornet-Puig, 2018: ORCHIDEE-MICT-BIOENERGY: an attempt to represent the production of lignocellulosic crops for bioenergy in a global vegetation model. *Geoscientific Model Development*, **11 (6)**, 2249–2272, DOI:10.5194/gmd-11-2249-2018.

Li, Y. J., Q. Chen, M. I. Guzman, C. K. Chan, and S. T. Martin, 2011: Second-generation products contribute substantially to the particle-phase organic material produced by β-caryophyllene ozonolysis. *Atmospheric Chemistry and Physics*, **11 (1)**, 121–132, DOI:10.5194/acp-11-121-2011.

Li, Z., and T. D. Sharkey, 2013: Molecular and Pathway Controls on Biogenic Volatile Organic Compound Emissions. *Biology, Controls and Models of Tree Volatile Organic Compound Emissions*, Ü. Niinemets, and R. K. Monson, Eds., Springer Netherlands, Dordrecht, 119–151, DOI:10.1007/978-94-007-6606-8_5, URL https://doi.org/10.1007/978-94-007-6606-8_5.

Lindinger, W., A. Hansel, and A. Jordan, 1998: On-line monitoring of volatile organic compounds at pptv levels by means of proton-transfer-reaction mass spectrometry (PTR-MS) medical applications, food control and environmental research. *International Journal of Mass Spectrometry and Ion Processes*, **173 (3)**, 191 – 241, DOI:10.1016/S0168-1176(97)00281-4.

Livingston, G. P., and G. L. Hutchinson, 1995: Enclosure-based measurement of trace gas exchange: applications and sources of error. *Methods in Ecology. Biogenic Trace Gases: Measuring Emissions from Soil and Water*, Vol. 51, Blackwell Science Oxford, Chap. 2, 14–51.

Lloyd, J., and J. A. Taylor, 1994: On the temperature Dependence of Soil Respiration. *Functional Ecology*, **8 (3)**, 315–323.

Long, S. P., 1991: Modification of the response of photosynthetic productivity to rising temperature by atmospheric CO2 concentrations: Has its importance been underestimated? *Plant, Cell & Environment*, **14 (8)**, 729–739, DOI:10.1111/j.1365-3040.1991.tb01439.x.

Loreto, F., M. Dicke, J.-P. Schnitzler, and T. C. J. Turlings, 2014: Plant volatiles and the environment. *Plant, Cell & Environment*, **37 (8)**, 1905–1908, DOI:10.1111/pce.12369.

Loreto, F., and J.-P. Schnitzler, 2010: Abiotic stresses and induced BVOCs. *Trends in Plant Science*, **15 (3)**, 154 – 166, DOI:http://dx.doi.org/10.1016/j.tplants.2009.12.006.

Makkonen, R., A. Asmi, V.-M. Kerminen, M. Boy, A. Arneth, A. Guenther, and M. Kulmala, 2012: BVOC-aerosol-climate interactions in the global aerosol-climate model ECHAM5.5-HAM2. *Atmospheric Chemistry and Physics*, **12 (21)**, 10 077–10 096, DOI:10.5194/acp-12-10077-2012.

Maleknia, S. D., T. L. Bell, and M. A. Adams, 2007: PTR-MS analysis of reference and plant-emitted volatile organic compounds. *International Journal of Mass Spectrometry*, **262 (3)**, 203 – 210, DOI:https://doi.org/10.1016/j.ijms.2006.11.010.

Manoli, G., A. Meijide, N. Huth, A. Knohl, Y. Kosugi, P. Burlando, J. Ghazoul, and S. Fatichi, 2018: Ecohydrological changes after tropical forest conversion to oil palm. *Environmental Research Letters*.

Martin, M., C. Stirling, S. Humphries, and S. Long, 2000: A process-based model to predict the effects of climatic change on leaf isoprene emission rates. *Ecological Modelling*, **131 (2)**, 161 – 174, DOI:https://doi.org/10.1016/S0304-3800(00)00258-1.

McCalmont, J. P., A. Hastings, N. P. McNamara, G. M. Richter, P. Robson, I. S. Donnison, and J. Clifton-Brown, 2015: Environmental costs and benefits of growing Miscanthus for bioenergy in the UK. *GCB Bioenergy*, DOI:10.1111/gcbb.12294.

McEwan, M., and W. H. M. Smith, 1998: Identification of volatile organic compounds emitted in the field by oilseed rape (brassica napus ssp. oleifera) over the growing season. *Clinical & Experimental Allergy*, **28 (3)**, 332–338, DOI:10.1046/j.1365-2222.1998.00234.x.

McKinney, K. A., and Coauthors, 2019: A sampler for atmospheric volatile organic compounds by copter unmanned aerial vehicles. *Atmospheric Measurement Techniques*, **12 (6)**, 3123–3135, DOI:10.5194/amt-12-3123-2019.

Meier, U., Ed., 2001: *Growth stages of mono-and dicotyledonous pants. BBCH Monograph.* 2nd ed., Federal Biological Research Center for Agriculture and Forestry.

Mentel, T. F., and Coauthors, 2013: Secondary aerosol formation from stress-induced biogenic emissions and possible climate feedbacks. *Atmospheric Chemistry and Physics*, **13 (17)**, 8755–8770, DOI:10.5194/acp-13-8755-2013.

Misztal, P., and Coauthors, 2015: Atmospheric benzenoid emissions from plants rival those from fossil fuels. *Scientific Reports*, **5**, 12 064–.

Molina-Herrera, S., and Coauthors, 2016: A modeling study on mitigation of N_2O emissions and NO_3 leaching at different agricultural sites across europe using LandscapeDNDC. *Science of The Total Environment*, **553**, 128 – 140, DOI:https://doi.org/10.1016/j.scitotenv.2015.12.099.

Molina-Herrera, S., and Coauthors, 2017: Importance of soil NO emissions for the total atmospheric NO_x budget of Saxony, Germany. *Atmospheric Environment*, **152**, 61 – 76, DOI:https://doi.org/10.1016/j.atmosenv.2016.12.022.

Monson, R. K., R. Grote, Ü. Niinemets, and J.-P. Schnitzler, 2012: Modeling the isoprene emission rate from leaves. *New Phytologist*, **195 (3)**, 541–559, DOI:10.1111/j.1469-8137.2012.04204.x.

Morfopoulos, C., I. C. Prentice, T. F. Keenan, P. Friedlingstein, B. E. Medlyn, J. Peñuelas, and M. Possell, 2013: A unifying conceptual model for the environmental responses of isoprene emissions from plants. *Annals of Botany*, **112 (7)**, 1223–1238, DOI:10.1093/aob/mct206.

Morfopoulos, C., and Coauthors, 2014: A model of plant isoprene emission based on available reducing power captures responses to atmospheric CO_2. *New Phytologist*, **203 (1)**, 125–139.

Morrison, E. C., J. Drewer, and M. R. Heal, 2016: A comparison of isoprene and monoterpene emission rates from the perennial bioenergy crops short-rotation coppice willow and Miscanthus and the annual arable crops wheat and oilseed rape. *GCB Bioenergy*, **8 (1)**, 211–225, DOI:10.1111/gcbb.12257.

Mozaffar, A., 2017: Exchanges of biogenic volatile organic compounds between the atmosphere and agricultural plants/ecosystems in controlled and field conditions. Ph.D. thesis, University of Liege, Belgium.

Mozaffar, A., and Coauthors, 2017: Methanol emissions from maize: Ontogenetic dependence to varying light conditions and guttation as an additional factor constraining the flux. *Atmospheric Environment*, **152**, 405–417, DOI:http://dx.doi.org/10.1016/j.atmosenv.2016.12.041.

Mozaffar, A., and Coauthors, 2018: Biogenic volatile organic compound emissions from senescent maize leaves and a comparison with other leaf developmental stages. *Atmospheric Environment*, **176**, 71 – 81, DOI:https://doi.org/10.1016/j.atmosenv.2017.12.020.

Muhlemann, J. K., A. Klempien, and N. Dudareva, 2014: Floral volatiles: from biosynthesis to function. *Plant, Cell & Environment*, **37 (8)**, 1936–1949, DOI:10.1111/pce.12314.

Müller, C., and Coauthors, 2017: Global gridded crop model evaluation: benchmarking, skills, deficiencies and implications. *Geoscientific Model Development*, **10 (4)**, 1403–1422, DOI:10.5194/gmd-10-1403-2017.

Müller, K., and Coauthors, 2002: Monoterpene emissions and carbonyl compound air concentrations during the blooming period of rape (brassica napus). *Chemosphere*, **49 (10)**, 1247 – 1256, DOI:http://dx.doi.org/10.1016/S0045-6535(02)00610-0.

Münzenberg-St.Denis, A., and E. Renner, 1999: Numerical investigation of the influence of biogenic emissions on ozone over saxony (Germany). *Physics and Chemistry of the Earth, Part C: Solar, Terrestrial & Planetary Science*, **24 (5)**, 487 – 490, DOI:https://doi.org/10.1016/S1464-1917(99)00076-8.

Myhre, G., and Coauthors, 2013: Anthropogenic and Natural Radiative Forcing. *Climate Change 2013: The Physical Science Basis. Contribution of Working Group I to the Fifth Assessment Report of the Intergovernmental Panel on Climate Change*, T. Stocker, G.-K. P. D. Qin, M. Tignor, S. Allen, J. Boschung, Y. X. A. Nauels, V. Bex, and P. Midgley, Eds., Cambridge University Press, Cambridge, United Kingdom and New York, NY, USA, Chap. 8, 659–740, DOI: 10.1017/CBO9781107415324.018.

Niinemets, Ü., 2010: Mild versus severe stress and BVOCs: thresholds, priming and consequences. *Trends in Plant Science*, **15 (3)**, 145–153, DOI:10.1016/j.tplants.2009.11.008.

Niinemets, Ü., 2018: What Are Plant-Released Biogenic Volatiles and How They Participate in Landscape- to Global-Level Processes? *Ecosystem Services from Forest Landscapes: Broadscale Considerations*, A. H. Perera, U. Peterson, G. M. Pastur, and L. R. Iverson, Eds., Springer International Publishing, Cham, 29–56, DOI:10.1007/978-3-319-74515-2_3, URL https://doi.org/10.1007/978-3-319-74515-2_3.

Niinemets, Ü., P. Ciccioli, S. M. Noe, and M. Reichstein, 2013: Scaling BVOC Emissions from Leaf to Canopy and Landscape: How Different Are Predictions Based on Contrasting Emission Algorithms? *Biology, Controls and Models of Tree Volatile Organic Compound Emissions*, Ü. Niinemets, and R. K. Monson, Eds., Springer Netherlands, Dordrecht, 357–390, DOI:10.1007/978-94-007-6606-8_13, URL https://doi.org/10.1007/978-94-007-6606-8_13.

Niinemets, Ü., S. Fares, P. Harley, and K. J. Jardine, 2014: Bidirectional exchange of biogenic volatiles with vegetation: emission sources, reactions, breakdown and deposition. *Plant, Cell & Environment*, **37 (8)**, 1790–1809, DOI:10.1111/pce.12322.

Niinemets, Ü., F. Loreto, and M. Reichstein, 2004: Physiological and physicochemical controls on foliar volatile organic compound emissions. *Trends in Plant Science*, **9 (4)**, 180–186, DOI:10.1016/j.tplants.2004.02.006.

Niinemets, Ü., and M. Reichstein, 2003: Controls on the emission of plant volatiles through stomata: Differential sensitivity of emission rates to stomatal closure explained. *Journal of Geophysical Research: Atmospheres*, **108 (D7)**, DOI:10.1029/2002JD002620.

Niinemets, Ü., G. Seufert, R. Steinbrecher, and J. D. Tenhunen, 2002: A model coupling foliar monoterpene emissions to leaf photosynthetic characteristics in mediterranean evergreen quercus species. *New Phytologist*, **153 (2)**, 257–275, DOI: 10.1046/j.0028-646X.2001.00324.x.

Niinemets, Ü., J. D. Tenhunen, P. C. Harley, and R. Steinbrecher, 1999: A model of isoprene emission based on energetic requirements for isoprene synthesis and leaf photosynthetic properties for liquidambar and quercus. *Plant, Cell & Environment*, **22 (11)**, 1319–1335, DOI:10.1046/j.1365-3040.1999.00505.x.

Niinemets, Ü., and Coauthors, 2010: The leaf-level emission factor of volatile isoprenoids: caveats, model algorithms, response shapes and scaling. *Biogeosciences*, **7 (6)**, 1809–1832, DOI:10.5194/bg-7-1809-2010.

Nikièma, P., D. E. Rothstein, and R. O. Miller, 2012: Initial greenhouse gas emissions and nitrogen leaching losses associated with converting pastureland to short-rotation woody bioenergy crops in northern Michigan, USA. *Biomass and Bioenergy*, **39**, 413 – 426, DOI:http://dx.doi.org/10.1016/j.biombioe.2012.01.037.

Noe, S., Ü. Niinemets, and J.-P. Schnitzler, 2010: Modeling the temporal dynamics of monoterpene emission by isotopic labeling in *Quercus ilex* leaves. *Atmospheric Environment*, **44 (3)**, 392 – 399, DOI:http://dx.doi.org/10.1016/j.atmosenv.2009.10.023.

OECD, 2013: *Energy supply*. OECD Publishing, DOI:10.1787/factbook-2013-41-en.

Oleson, K. W., and Coauthors, 2010: Technical description of version 4.0 of the community land model (clm). Tech. rep., National Center for Atmospheric Research (NCAR), Boulder, Colorado, USA.

Oluwafemi, S., M. Birkett, J. Caulfield, and J. Pickett, 2012: Variability of Volatile Organic Compounds Emitted by Seedlings of Seven African Maize Varieties When Infested by Adult Cicadulina Storeyi China Leafhopper Vectors of Maize Streak Virus. *African Crop Science Journal*, **20**, 117–124.

Pagonis, D., J. E. Krechmer, J. de Gouw, J. L. Jimenez, and P. J. Ziemann, 2017: Effects of gas–wall partitioning in teflon tubing and instrumentation on time-resolved measurements of gas-phase organic compounds. *Atmospheric Measurement Techniques*, **10 (12)**, 4687–4696, DOI:10.5194/amt-10-4687-2017.

Pańka, D., D. Piesik, M. Jeske, and A. Baturo-Cieśniewska, 2013: Production of phenolics and the emission of volatile organic compounds by perennial ryegrass (*Lolium perenne* L.)/*Neotyphodium lolii* association as a response to infection by *Fusarium poae*. *Journal of plant physiology*, **170 (11)**, 1010–1019.

Peñuelas, J., D. Asensio, D. Tholl, K. Wenke, M. Rosenkranz, B. Piechulla, and J. Schnitzler, 2014: Biogenic volatile emissions from the soil. *Plant, Cell & Environment*, **37 (8)**, 1866–1891, DOI:10.1111/pce.12340.

Peñuelas, J., J. Llusià, D. Asensio, and S. Munneé-Bosch, 2005: Linking isoprene with plant thermotolerance, antioxidants and monoterpene emissions. *Plant, Cell & Environment*, **28 (3)**, 278–286, DOI:10.1111/j.1365-3040.2004.01250.x.

Peñuelas, J., G. Marino, J. LLusia, C. Morfopoulos, G. Farré-Armengol, and I. Filella, 2013: Photochemical reflectance index as an indirect estimator of foliar isoprenoid emissions at the ecosystem level. *Nature communications*, **4**.

Peñuelas, J., and M. Staudt, 2010: BVOCs and global change. *Trends in Plant Science*, **15 (3)**, 133 – 144, DOI:10.1016/j.tplants.2009.12.005.

Peeters, J., W. Boullart, V. Pultau, S. Vandenberk, and L. Vereecken, 2007: Structure-Activity Relationship for the Addition of OH to (Poly)alkenes: Site-Specific and Total Rate Constants. *The Journal of Physical Chemistry A*, **111 (9)**, 1618–1631, DOI:10.1021/jp066973o.

Piccot, S. D., J. J. Watson, and J. W. Jones, 1992: A global inventory of volatile organic compound emissions from anthropogenic sources. *Journal of Geophysical Research: Atmospheres*, **97 (D9)**, 9897–9912, DOI:10.1029/92JD00682.

Pichersky, E., and J. Gershenzon, 2002: The formation and function of plant volatiles: Perfumes for pollinator attraction and defense. *Current Opinion in Plant Biology*, **5 (3)**, 237–243, DOI:10.1016/S1369-5266(02)00251-0.

Pierce, T., C. Geron, L. Bender, R. Dennis, G. Tonnesen, and A. Guenther, 1998: Influence of increased isoprene emissions on regional ozone modeling. *Journal of Geophysical Research: Atmospheres*, **103 (D19)**, 25 611–25 629.

Pierik, R., C. L. Ballaré, and M. Dicke, 2014: Ecology of plant volatiles: taking a plant community perspective. *Plant, Cell & Environment*, **37 (8)**, 1845–1853, DOI:10.1111/pce.12330.

Pilegaard, K., 2013: Processes regulating nitric oxide emissions from soils. *Philosophical Transactions of the Royal Society of London B: Biological Sciences*, **368 (1621)**, 1–8, DOI:10.1098/rstb.2013.0126.

Pope III, C. A., R. T. Burnett, M. Thun, E. E. Calle, D. Krewski, K. Ito, and G. D. Thurston, 2002: Lung cancer, cardiopulmonary mortality, and long-term exposure to fine particulate air pollution. *JAMA*, **287 (9)**, 1132–1141, DOI:10.1001/jama.287.9.1132.

Porter, W. C., K. C. Barsanti, E. C. Baughman, and T. N. Rosenstiel, 2012: Considering the Air Quality Impacts of Bioenergy Crop Production: A Case Study Involving *Arundo donax*. *Environmental Science & Technology*, **46 (17)**, 9777–9784, DOI:10.1021/es3013084.

Porter, W. C., T. N. Rosenstiel, A. Guenther, J.-F. Lamarque, and K. Barsanti, 2015: Reducing the negative human-health impacts of bioenergy crop emissions through region-specific crop selection. *Environmental Research Letters*, **10 (5)**, 054 004.

Portillo-Estrada, M., T. Kazantsev, E. Talts, T. Tosens, and Ü. Niinemets, 2015: Emission Timetable and Quantitative Patterns of Wound-Induced Volatiles Across

Different Leaf Damage Treatments in Aspen (*Populus tremula*). *Journal of Chemical Ecology*, 1–13, DOI:10.1007/s10886-015-0646-y.

Portillo-Estrada, M., T. Zenone, N. Arriga, and R. Ceulemans, 2018: Contribution of volatile organic compound fluxes to the ecosystem carbon budget of a poplar short-rotation plantation. *GCB Bioenergy*, **0 (0)**, DOI:10.1111/gcbb.12506.

Pury, D. G. G., and G. D. Farquhar, 1997: Simple scaling of photosynthesis from leaves to canopies without the errors of big-leaf models. *Plant, Cell & Environment*, **20 (5)**, 537–557, DOI:10.1111/j.1365-3040.1997.00094.x.

REN21, 2015: *Renewables 2015 Global Status Report*. Paris: REN21 Secretariat, Renewable Energy Policy Network for the 21st Century.

Renner, E., and A. Münzenberg, 2003: Impact of Biogenic Terpene Tmissions from *Brassica napus* on Tropospheric Ozone over Saxony (Germany). *Environmental Science and Pollution Research*, **10 (3)**, 147–153, DOI:10.1065/espr2003.05.154.

Richter, A., and Coauthors, 2016: Characterization of biosynthetic pathways for the production of the volatile homoterpenes DMNT and TMTT in *Zea mays*. *The Plant Cell*, DOI:10.1105/tpc.15.00919.

Rosenkranz, M., T. Pugh, J.-P. Schnitzler, and A. Arneth, 2015: Effect of land-use change and management on biogenic volatile organic compound emissions – selecting climate-smart cultivars. *Plant, Cell & Environment*, **38 (9)**, 1896–1912, DOI:10.1111/pce.12453.

Rosenkranz, M., and J.-P. Schnitzler, 2016: Plant Volatiles. *eLS*, John Wiley & Sons, Ltd, Chichester, DOI:10.1002/9780470015902.a0000910.pub3, URL http://dx.doi.org/10.1002/9780470015902.a0000910.pub3.

Ruuskanen, T. M., and Coauthors, 2011: Eddy covariance VOC emission and deposition fluxes above grassland using PTR-TOF. *Atmospheric Chemistry and Physics*, **11 (2)**, 611–625, DOI:10.5194/acp-11-611-2011.

Sakulyanontvittaya, T., A. Guenther, D. Helmig, J. Milford, and C. Wiedinmyer, 2008: Secondary organic aerosol from sesquiterpene and monoterpene emissions in the united states. *Environmental Science & Technology*, **42 (23)**, 8784–8790, DOI:10.1021/es800817r.

Sarkar, C., and Coauthors, 2016: Overview of voc emissions and chemistry from ptr-tof-ms measurements during the suskat-abc campaign: high acetaldehyde, isoprene and isocyanic acid in wintertime air of the kathmandu valley. *Atmospheric Chemistry and Physics*, **16 (6)**, 3979–4003, DOI:10.5194/acp-16-3979-2016.

Schnee, C., T. G. Köllner, J. Gershenzon, and J. Degenhardt, 2002: The Maize Gene terpene synthase 1 Encodes a Sesquiterpene Synthase Catalyzing the Formation of (*E*)-β-Farnesene, (*E*)- Nerolidol, and (*E,E*)-farnesol after Herbivore Damage. *Plant*

Physiology, **130 (4)**, 2049–2060, DOI:10.1104/pp.008326.

Schnee, C., T. G. Köllner, M. Held, T. C. J. Turlings, J. Gershenzon, and J. Degenhardt, 2006: The products of a single maize sesquiterpene synthase form a volatile defense signal that attracts natural enemies of maize herbivores. *Proceedings of the National Academy of Sciences of the United States of America*, **103 (4)**, 1129–1134, DOI:10.1073/pnas.0508027103.

Schultz, M. G., and Coauthors, 2015: The Global Atmosphere Watch reactive gases measurement network. *Elementa: Science of the Anthropocene*, **3 (67)**.

Schurgers, G., A. Arneth, R. Holzinger, and A. H. Goldstein, 2009: Process-based modelling of biogenic monoterpene emissions combining production and release from storage. *Atmospheric Chemistry and Physics*, **9 (10)**, 3409–3423, DOI:10.5194/acp-9-3409-2009.

Seco, R., J. Peñuelas, and I. Filella, 2007: Short-chain oxygenated VOCs: Emission and uptake by plants and atmospheric sources, sinks, and concentrations. *Atmospheric Environment*, **41 (12)**, 2477 – 2499, DOI:https://doi.org/10.1016/j.atmosenv.2006.11.029.

Seco, R., and Coauthors, 2015: Ecosystem-scale volatile organic compound fluxes during an extreme drought in a broadleaf temperate forest of the Missouri Ozarks (central USA). *Global Change Biology*, **21 (10)**, 3657–3674, DOI:10.1111/gcb.12980.

Sharkey, T. D., A. E. Wiberley, and A. R. Donohue, 2008: Isoprene Emission from Plants: Why and How. *Annals of Botany*, **101 (1)**, 5–18, DOI:10.1093/aob/mcm240.

Sharkey, T. D., and S. Yeh, 2001: Isoprene emission from plants. *Annual review of plant biology*, **52 (1)**, 407–436.

Sindelarova, K., and Coauthors, 2014: Global data set of biogenic voc emissions calculated by the megan model over the last 30 years. *Atmospheric Chemistry and Physics*, **14 (17)**, 9317–9341, DOI:10.5194/acp-14-9317-2014.

Sinha, V., and Coauthors, 2012: Constraints on instantaneous ozone production rates and regimes during DOMINO derived using in-situ OH reactivity measurements. *Atmospheric Chemistry and Physics*, **12 (15)**, 7269–7283, DOI:10.5194/acp-12-7269-2012.

Smith, J., and P. Smith, 2007: *Environmental modelling: an introduction*. Oxford University Press.

Sommer, M., J. Augustin, and M. Kleber, 2016: Feedbacks of soil erosion on SOC patterns and carbon dynamics in agricultural landscapes—The CarboZALF experiment. *Soil and Tillage Research*, **156**, 182 – 184, DOI:10.1016/j.still.2015.09.015.

Spielmann, F. M., S. Langebner, A. Ghirardo, A. Hansel, J.-P. Schnitzler, and

G. Wohlfahrt, 2017: Isoprene and α-pinene deposition to grassland mesocosms. *Plant and Soil*, **410 (1)**, 313–322, DOI:10.1007/s11104-016-3009-8.

Stavrakou, T., and Coauthors, 2011: First space-based derivation of the global atmospheric methanol emission fluxes. *Atmospheric Chemistry and Physics*, **11 (10)**, 4873–4898, DOI:10.5194/acp-11-4873-2011.

Steinbrecher, R., and Coauthors, 2009: Intra- and inter-annual variability of VOC emissions from natural and semi-natural vegetation in europe and neighbouring countries. *Atmospheric Environment*, **43 (7)**, 1380 – 1391, DOI:http://dx.doi.org/10.1016/j.atmosenv.2008.09.072.

Szogs, S., A. Arneth, P. Anthoni, J. C. Doelman, F. Humpenöder, A. Popp, T. A. Pugh, and E. Stehfest, 2017: Impact of LULCC on the emission of BVOCs during the 21st century. *Atmospheric Environment*, **165**, 73 – 87, DOI:https://doi.org/10.1016/j.atmosenv.2017.06.025.

Tanaka, A., and J. Yamaguchi, 1972: Dry matter production, Yield Components and Grain yield of the Maize Plant. *Journal of the Faculty of Agriculture, Hokkaido University*, **57 (1)**, 71–132.

Tani, A., S. Hayward, A. Hansel, and C. N. Hewitt, 2004: Effect of water vapour pressure on monoterpene measurements using proton transfer reaction-mass spectrometry (PTR-MS). *International Journal of Mass Spectrometry*, **239 (2–3)**, 161 – 169, DOI:10.1016/j.ijms.2004.07.020.

Tarvainen, V., H. Hakola, H. Hellén, J. Bäck, P. Hari, and M. Kulmala, 2005: Temperature and light dependence of the VOC emissions of Scots pine. *Atmospheric Chemistry and Physics*, **5 (4)**, 989–998, DOI:10.5194/acp-5-989-2005.

Tingey, D. T., M. Manning, L. C. Grothaus, and W. F. Burns, 1979: The influence of light and temperature on isoprene emission rates from live oak. *Physiologia Plantarum*, **47 (2)**, 112–118, DOI:10.1111/j.1399-3054.1979.tb03200.x.

Tingey, D. T., M. Manning, L. C. Grothaus, and W. F. Burns, 1980: Influence of Light and Temperature on Monoterpene Emission Rates from Slash Pine. *Plant Physiology*, **65 (5)**, 797–801, DOI:10.1104/pp.65.5.797.

Tiwari, S., R. Grote, G. Churkina, and T. Butler, 2016: Ozone damage, detoxification and the role of isoprenoids–new impetus for integrated models. *Functional plant biology*, **43 (4)**, 324–336.

Vanzo, E., and Coauthors, 2015: Facing the future - Effects of short-term climate extremes on isoprene-emitting and non-emitting poplar. *Plant Physiology*, DOI:10.1104/pp.15.00871.

Vanzo, E., and Coauthors, 2016: Modulation of protein s-nitrosylation by isoprene emission in poplar. *Plant Physiology*, pp–01 842.

Veromann, E., and Coauthors, 2013: Effects of nitrogen fertilization on insect pests, their parasitoids, plant diseases and volatile organic compounds in brassica napus. *Crop Protection*, **43**, 79 – 88, DOI:http://dx.doi.org/10.1016/j.cropro.2012.09.001.

Vickers, C. E., J. Gershenzon, M. T. Lerdau, and F. Loreto, 2009: A unified mechanism of action for volatile isoprenoids in plant abiotic stress. *Nat Chem Biol*, **5**, 283–291.

Vlasenko, A., A. M. Macdonald, S. J. Sjostedt, and J. P. D. Abbatt, 2010: Formaldehyde measurements by proton transfer reaction – mass spectrometry (ptr-ms): correction for humidity effects. *Atmospheric Measurement Techniques*, **3 (4)**, 1055–1062, DOI:10.5194/amt-3-1055-2010.

von Caemmerer, S., G. Farquhar, and J. Berry, 2009: Biochemical model of c3 photosynthesis. *Photosynthesis in silico: Understanding Complexity from Molecules to Ecosystems*, A. Laisk, L. Nedbal, and Govindjee, Eds., Springer Netherlands, Dordrecht, 209–230, DOI:10.1007/978-1-4020-9237-4_9, URL https://doi.org/10.1007/978-1-4020-9237-4_9.

Weikl, F., A. Ghirardo, J.-P. Schnitzler, and K. Pritsch, 2016: Sesquiterpene emissions from *Alternaria alternata* and *Fusarium oxysporum*: Effects of age, nutrient availability, and co-cultivation. *Scientific reports*, **6**, DOI:10.1038/srep22152.

Whiting, D., M. Roll, and L. Vickerman, 2014: Plant Physiology: Photosynthesis, Respiration, and Transpiration. CMG GardenNotes 141, Colorado Master Gardener. URL www.cmg.colostate.edu.

Williams, J., C. Stönner, J. Wicker, N. Krauter, B. Derstroff, E. Bourtsoukidis, T. Klüpfel, and S. Kramer, 2016: Cinema audiences reproducibly vary the chemical composition of air during films, by broadcasting scene specific emissions on breath. *Scientific Reports*, **6**, 25 464, DOI:10.1038/srep25464.

Wink, M., 2003: Evolution of secondary metabolites from an ecological and molecular phylogenetic perspective. *Phytochemistry*, **64 (1)**, 3 – 19, DOI:https://doi.org/10.1016/S0031-9422(03)00300-5.

Wiß, F., A. Ghirardo, J.-P. Schnitzler, C. Nendel, J. Augustin, M. Hoffmann, and R. Grote, 2017: Net ecosystem fluxes and composition of biogenic volatile organic compounds over a maize field – interaction of meteorology and phenological stages. *GCB Bioenergy*, **9 (11)**, 1627–1643, DOI:10.1111/gcbb.12454.

Wohlfahrt, G., and Coauthors, 2015: An ecosystem-scale perspective of the net land methanol flux: synthesis of micrometeorological flux measurements. *Atmospheric Chemistry and Physics*, **15 (13)**, 7413–7427, DOI:10.5194/acp-15-7413-2015.

Xu, H., and T. C. Turlings, 2018: Plant Volatiles as Mate-Finding Cues for Insects. *Trends in Plant Science*, **23 (2)**, 100 – 111, DOI:https://doi.org/10.1016/j.tplants.2017.11.004.

Xu, L., H. O. T. Pye, J. He, Y. Chen, B. N. Murphy, and N. L. Ng, 2018: Large contributions from biogenic monoterpenes and sesquiterpenes to organic aerosol in the southeastern united states. *Atmospheric Chemistry and Physics Discussions*, **2018**, 1–47, DOI:10.5194/acp-2017-1109.

Yeoman, M. M., and C. L. Yeoman, 1996: Manipulating secondary metabolism in cultured plant cells. *New Phytologist*, **134 (4)**, 553–569, DOI:10.1111/j.1469-8137.1996.tb04921.x.

Yuan, B., A. R. Koss, C. Warneke, M. Coggon, K. Sekimoto, and J. A. de Gouw, 2017a: Proton-Transfer-Reaction Mass Spectrometry: Applications in Atmospheric Sciences. *Chemical Reviews*, **117 (21)**, 13 187–13 229, DOI:10.1021/acs.chemrev.7b00325.

Yuan, X., Z. Feng, S. Liu, B. Shang, P. Li, Y. Xu, and E. Paoletti, 2017b: Concentration- and flux-based dose–responses of isoprene emission from poplar leaves and plants exposed to an ozone concentration gradient. *Plant, Cell & Environment*, **40 (9)**, 1960–1971, DOI:10.1111/pce.13007.

Zenone, T., C. Hendriks, F. Brilli, E. Fransen, B. Gioli, M. Portillo-Estrada, M. Schaap, and R. Ceulemans, 2016: Interaction between isoprene and ozone fluxes in a poplar plantation and its impact on air quality at the european level. *Scientific Reports*, **6**, DOI:10.1038/srep32676.

Zheng, Y., N. Unger, M. P. Barkley, and X. Yue, 2015: Relationships between photosynthesis and formaldehyde as a probe of isoprene emission. *Atmospheric Chemistry and Physics*, **15 (15)**, 8559–8576, DOI:10.5194/acp-15-8559-2015.

Ziemann, P. J., and R. Atkinson, 2012: Kinetics, products, and mechanisms of secondary organic aerosol formation. *Chem. Soc. Rev.*, **41**, 6582–6605, DOI:10.1039/C2CS35122F.

Zimmer, W., N. Brüggemann, S. Emeis, C. Giersch, A. Lehning, R. Steinbrecher, and J.-P. Schnitzler, 2000: Process-based modelling of isoprene emission by oak leaves. *Plant, Cell & Environment*, **23 (6)**, 585–595, DOI:10.1046/j.1365-3040.2000.00578.x.

Acknowledgements

This PhD thesis is the result of a valuable supervision and cooperation with several colleagues, some lucky circumstances, a very pleasant and enjoyable time at KIT/IMK-IFU in Garmisch-Partenkirchen, the fortune of having such an inspiring circle of friends, and of course my family, especially my wife Lea, who supported me all the way.

In particular, I want to thank my IFU internal supervisor Rüdiger Grote for his introduction to and guidance within the BVOC topic as well as for our several fruitful discussions about modeling of BVOCs, all fields of politics and society. I also want to thank him explicitly for his calm but precise guidance and super fast text revisions.

Andrea Ghirardo from Helmholtz Zentrum München was kind of my supervisor from the measurement perspective without whom all field campaigns would have failed before they had even started. Additionally, he conducted all GC-MS measurements and introduced me into how setting up and precisely measuring with the PTR-MS instrument. Without his practical and theoretical input, I would have never been in the position to open the treasure of plant volatiles and hydrocarbons. Needless to say that I had a super fun time during our field work in the Uckermark region. How much this means, you will only be able to understand if you have ever been there.

Also Jogi Schnitzler from Helmholtz Zentrum München strongly supported me with my field and laboratory studies, all his equipment and especially with his creativity in paper writing. It was a good moment when he laughed out loud as he read a mail about a speed ticket fine with his institute's car together with a picture of me behind the wheel.

My main supervisors HaPe Schmid from KIT/IMK-IFU and Mark Wenig from LMU Munich nagged me from time to time into the right direction and helped me to focus on the topic and not to lose track so that this study would not get lost too much in details.

A big thank you to all of my colleagues and friends from the IFU in Garmisch-Partenkirchen, without whom I would not have had such a wonderful, sportive, and excessive time during the days of mountain-biking, skiing, bouldering, soccer, lunch breaks, and lab time. Very special shout-outs to Marcus, Baldur, and David. We had fruitful discussions, did the one or the other mountain-bike trip, and enjoyed long evenings with a beer or two until midnight.

I also want to thank my project partners from ZALF in Müncheberg and Dedelow, especially Claas Nendel (project coordination), Gernot Verch (head of the research station in Dedelow), Jürgen Augustin (initiator of the automatic chamber system), Marten Schmidt (build up and maintenance), Peter Rakowski (maintenance), Mathias Hoffmann (calculation of observed CO_2 exchange), Heide-Marie Pankow (biomass measurements), and Ingrid Onasch (LAI measurements). Each of them strongly supported all of the field works during the three years.

I have been in the lucky position to have become part of the Helmholtz Research School *Mechanisms and Interactions of Climate Change in Mountain Regions* (MICMoR), which served me many good times during all the respective activities including long sessions in the numerous courses as well as the fun parts with the fellows. Without this PhD program I could not have afforded all my scientific activities in Obergurgl, Siberia, Colorado, and Oxford. With respect to that I want to thank Elija Bleher for her really great and quick support. After the end of my PhD contract I received an additional three month thesis completion grant from MICMoR.

The following bands helped me remain focused during hours of programming: Thy Art is Murder, After the Burial, Animals as Leaders, Beyond Creation, Meshuggah, Fit for an Autopsy, Humanities last breath, Breakdown of Sanity, Ghost Inside, Car bomb, Emmure, Lamb of God, Parkway Drive.

My biggest gratitude goes to my family: My parents and brothers who believe in my work and gave me the feeling that it may have an impact and is definitely worth to be done and to finish my thesis successfully. My uncles in Berlin gave me home and food, we undertook sailing adventures and generally had a wonderful time during my several weeks of staying in Berlin for not too far remote access during the field campaigns, additional modeling work at IASS in Potsdam, and some Berlin club nights. The greatest gratitude goes to my wife Lea for her humor, open mind, and optimism. Amongst many other things she managed my live next to work and sports, agreed on my time consuming living situation between Munich and Garmisch and was even fine with almost no holiday trips during the past two years. And somebody needed to take care of our dog as well...

A. Standard emission factors calculated by the Guenther, 1997 approach

A.1. Tables with SEF for all compounds and field experiments

Table A.1.: Fitted BVOC standardized emission factor (SEF) for maize ecosystem experiment 2015 with corresponding standard errors of the estimate (SE) both in ng gDW^{-1} aboveground biomass h^{-1}, fitted and standard value of the empirical β-coefficient as a curvature parameter from the equation for temperature-dependent emissions in K^{-1} (see Eq. 2.13 and Guenther et al., 1993; Guenther, 1997) and coefficient of determination (R^2). All values are calculated for three growth periods flowering (FW, $N = 529$), fruit development and ripening (FR, $N = 601$), and the whole season (WS, $N = 1153$).

Compound	**Period**	**SEF (± SE)**	β	R^2	**SEF (± SE)**	β	R^2
m/z 69	FW	29.79 (± 7.25)	0.09	0.73	32.74 (± 6.28)	0.13	0.79
	FR	12.96 (± 3.59)	0.09	0.57	19.1 (± 2.84)	0.148	0.73
	WS	23.23 (± 6.83)	0.09	0.62	29.01 (± 5.36)	0.151	0.77
MTs	FW	180.01 (± 65.13)	0.09	0.57	200.86 (± 59.12)	0.137	0.65
	FR	72.85 (± 23.81)	0.09	0.51	118.46 (± 17.72)	0.163	0.73
	WS	138.57 (± 53.92)	0.09	0.51	177.77 (± 44.93)	0.159	0.66
m/z 153	FW	61.35 (± 26.41)	0.09	0.52	71.04 (± 21.56)	0.17	0.68
	FR	15.7 (± 4.54)	0.09	0.57	25.2 (± 3.12)	0.161	0.79
	WS	43.51 (± 21.22)	0.09	0.42	59.77 (± 16.15)	0.198	0.67
oMTs	FW	15.5 (± 5.61)	0.09	0.61	17.98 (± 4.02)	0.171	0.8
	FR	7.76 (± 2.83)	0.09	0.47	13.01 (± 2.16)	0.168	0.69
	WS	12.52 (± 4.7)	0.09	0.55	16.84 (± 3.18)	0.18	0.79
SQTs	FW	58.15 (± 19.98)	0.09	0.59	65.72 (± 16.98)	0.152	0.71
	FR	12.94 (± 4.08)	0.09	0.53	21.04 (± 2.96)	0.163	0.75
	WS	40.76 (± 17.53)	0.09	0.46	54.41 (± 13.63)	0.186	0.68
Acetaldehyde	FW	39.64 (± 10.14)	0.09	0.72	44.02 (± 8.44)	0.135	0.81

Table continues on the next page

Table A.1.: *Continued from previous page.*

Compound	**Period**	**SEF (± SE)**	β	R^2	**SEF (± SE)**	β	R^2
	FR	24.85 (± 8.64)	0.09	0.47	37.43 (± 7.32)	0.15	0.62
	WS	33.81 (± 9.94)	0.09	0.63	41.84 (± 7.97)	0.146	0.76
Acetone	FW	54.93 (± 16.75)	0.09	0.67	62.81 (± 12.21)	0.157	0.83
	FR	42.78 (± 13.2)	0.09	0.52	64.62 (± 10.63)	0.151	0.69
	WS	50.23 (± 15.19)	0.09	0.63	63.58 (± 11.44)	0.155	0.79
m/z 71	FW	17.25 (± 7.47)	0.09	0.54	20.21 (± 5.56)	0.182	0.75
	FR	9.88 (± 4.85)	0.09	0.34	16.49 (± 4.25)	0.165	0.49
	WS	14.27 (± 6.47)	0.09	0.47	19.45 (± 4.92)	0.185	0.69
Hexenal	FW	36.0 (± 12.93)	0.09	0.63	42.05 (± 8.44)	0.176	0.84
	FR	28.12 (± 10.68)	0.09	0.44	44.59 (± 8.93)	0.158	0.61
	WS	32.97 (± 11.9)	0.09	0.56	43.32 (± 8.76)	0.168	0.76
GLVs	FW	91.5 (± 33.37)	0.09	0.62	107.44 (± 21.68)	0.174	0.84
	FR	74.51 (± 29.95)	0.09	0.42	123.29 (± 24.61)	0.165	0.61
	WS	84.97 (± 31.96)	0.09	0.55	112.12 (± 23.88)	0.168	0.75
Xylenes	FW	10.49 (± 3.99)	0.09	0.58	12.06 (± 3.27)	0.157	0.72
	FR	10.52 (± 4.1)	0.09	0.42	15.99 (± 3.58)	0.152	0.56
	WS	10.51 (± 4.05)	0.09	0.51	13.09 (± 3.56)	0.147	0.62
DMNT	FW	25.96 (± 9.9)	0.09	0.56	29.17 (± 8.91)	0.141	0.64
	FR	15.83 (± 7.69)	0.09	0.3	22.2 (± 7.3)	0.139	0.37
	WS	22.07 (± 9.05)	0.09	0.47	27.52 (± 8.09)	0.149	0.58
Methanol	FW	31.04 (± 42.43)	0.09	0.15	42.42 (± 38.73)	0.213	0.29
	FR	15.4 (± 16.56)	0.09	0.13	34.11 (± 15.26)	0.198	0.26
	WS	23.52 (± 32.26)	0.09	0.12	39.7 (± 29.33)	0.222	0.27
Ethanol	FW	3.4 (± 7.92)	0.09	0.04	5.98 (± 6.92)	0.279	0.27
	FR	5.22 (± 8.21)	0.09	0.07	13.77 (± 7.67)	0.206	0.19
	WS	3.92 (± 8.11)	0.09	0.05	7.76 (± 7.54)	0.233	0.18

Table A.2.: Fitted BVOC standardized emission factor (SEF) for oilseed rape ecosystem experiment 2016 All values are calculated for three growth periods inflorescence emergence (IE, $N = 368$), flowering (FW, $N = 410$), and the whole measurement period (WS, $N = 801$). See Tab. A.1 for a detailed caption.

Compound	**Period**	**SEF (± SE)**	β	R^2	**SEF (± SE)**	β	R^2
Methanol	IE	1969.37 (± 205.87)	0.09	0.23	1484.66 (± 206.69)	0.076	0.22
	FW	4619.23 (± 680.41)	0.09	0.59	4803.21 (± 684.2)	0.094	0.59
	WS	4108.46 (± 561.33)	0.09	0.63	5448.52 (± 553.71)	0.116	0.64
Ethanol	IE	21.7 (± 11.02)	0.09	0.09	2022.15 (± 9.65)	0.331	0.3
	FW	254.4 (± 58.04)	0.09	0.58	566.57 (± 46.77)	0.183	0.73
	WS	208.87 (± 48.45)	0.09	0.52	618.8 (± 34.96)	0.2	0.75
Acetone	IE	95.18 (± 15.37)	0.09	0.33	504.61 (± 13.46)	0.178	0.49
	FW	223.71 (± 33.62)	0.09	0.71	349.14 (± 30.18)	0.14	0.77
	WS	198.43 (± 28.87)	0.09	0.68	369.08 (± 23.81)	0.149	0.78
Isoprene	IE	47.46 (± 9.82)	0.09	0.24	395.07 (± 8.74)	0.203	0.4
	FW	94.17 (± 15.37)	0.09	0.68	141.17 (± 14.23)	0.135	0.73
	WS	84.79 (± 13.59)	0.09	0.64	148.21 (± 12.02)	0.142	0.72
MACR/MVK	IE	15.85 (± 5.66)	0.09	0.12	300.7 (± 5.23)	0.247	0.25
	FW	81.14 (± 17.33)	0.09	0.59	149.73 (± 15.19)	0.159	0.69
	WS	68.31 (± 14.55)	0.09	0.54	162.98 (± 11.68)	0.175	0.71
m/z 73	IE	21.3 (± 6.42)	0.09	0.16	381.93 (± 5.74)	0.244	0.33
	FW	144.09 (± 31.19)	0.09	0.59	282.31 (± 26.63)	0.167	0.7
	WS	120.02 (± 25.92)	0.09	0.54	308.59 (± 19.94)	0.184	0.73
Toluene	IE	-1.4 (± 3.1)	0.09	-0.0	6492.41 (± 3.11)	0.669	-0.01
	FW	49.85 (± 13.65)	0.09	0.5	118.72 (± 11.51)	0.192	0.64
	WS	39.77 (± 11.36)	0.09	0.42	132.7 (± 8.78)	0.214	0.66
Hexenal	IE	-4.66 (± 7.84)	0.09	0.0	6515844.09 (± 7.89)	1.897	-0.01
	FW	80.95 (± 24.25)	0.09	0.46	198.01 (± 20.95)	0.196	0.59
	WS	64.14 (± 20.3)	0.09	0.38	223.0 (± 16.36)	0.219	0.6
GLVs	IE	23.23 (± 12.45)	0.09	0.07	1537.07 (± 11.53)	0.316	0.2
	FW	354.36 (± 70.03)	0.09	0.62	617.15 (± 62.25)	0.152	0.7
	WS	289.73 (± 61.09)	0.09	0.55	703.01 (± 48.11)	0.177	0.72
Xylenes	IE	1.21 (± 2.78)	0.09	0.01	87.79 (± 2.76)	0.309	0.02
	FW	47.53 (± 12.46)	0.09	0.52	110.07 (± 10.46)	0.188	0.66
	WS	38.47 (± 10.29)	0.09	0.45	121.4 (± 7.9)	0.207	0.68
m/z 118	IE	-7.7 (± 4.28)	0.09	0.02	50479685.25 (± 4.52)	10.296	-0.09
	FW	83.2 (± 25.58)	0.09	0.43	160.47 (± 23.71)	0.164	0.51
	WS	65.49 (± 20.82)	0.09	0.37	184.74 (± 17.93)	0.192	0.53
MTs	IE	-5.78 (± 5.57)	0.09	-0.0	1823516.77 (± 5.67)	1.238	-0.04
	FW	164.49 (± 40.45)	0.09	0.53	341.8 (± 35.11)	0.174	0.65
	WS	131.29 (± 34.12)	0.09	0.46	390.49 (± 26.64)	0.2	0.67
SQTs	IE	-226.96 (± 72.62)	0.09	0.06	671309410.85 (± 84.14)	73.569	-0.26
	FW	-47.96 (± 51.44)	0.09	-0.01	-30.08 (± 51.06)	0.044	0.01
	WS	-82.07 (± 65.24)	0.09	-0.05	-35.47 (± 63.73)	0.023	0.0
Acetaldehyde	IE	65.33 (± 14.45)	0.09	0.23	498.71 (± 13.05)	0.197	0.37
	FW	183.25 (± 44.1)	0.09	0.3	172.89 (± 43.88)	0.084	0.31
	WS	159.91 (± 34.99)	0.09	0.42	213.14 (± 34.76)	0.116	0.43
Acetic acid	IE	47.15 (± 15.49)	0.09	0.15	1369.32 (± 13.53)	0.27	0.35
	FW	602.34 (± 148.79)	0.09	0.53	1203.45 (± 131.71)	0.169	0.63
	WS	493.79 (± 121.13)	0.09	0.48	1339.71 (± 97.29)	0.19	0.67

Table continues on the next page

Table A.2.: *Continued from previous page.*

Compound	**Period**	**SEF (± SE)**	β	R^2	**SEF (± SE)**	β	R^2
m/z 79	IE	-0.24 (± 3.08)	0.09	0.0	2054659.3 (± 3.08)	3.7	-0.0
	FW	42.57 (± 15.96)	0.09	0.35	119.31 (± 14.26)	0.215	0.48
	WS	34.18 (± 12.44)	0.09	0.31	130.55 (± 10.52)	0.233	0.51

Table A.3.: Fitted BVOC standardized emission factor (SEF) for ryegrass ecosystem experiment 2017 All values are calculated for three growth periods heading (HD, $N = 312$), flowering (FW, $N = 85$), and the whole measurement period (WS, $N = 397$). See Tab. A.1 for a detailed caption.

Compound	**Period**	**SEF (± SE)**	β	R^2	**SEF (± SE)**	β	R^2
Methanol	HD	1428.06 (± 359.17)	0.09	0.4	1781.47 (± 349.5)	0.116	0.43
	FW	463.64 (± 116.57)	0.09	0.22	10964.43 (± 92.98)	0.359	0.5
	WS	1280.57 (± 352.02)	0.09	0.37	1879.49 (± 333.62)	0.134	0.43
Ethanol	HD	66.5 (± 34.61)	0.09	0.22	120.53 (± 32.9)	0.163	0.29
	FW	4.61 (± 4.04)	0.09	0.05	58239.58 (± 3.38)	0.943	0.33
	WS	57.08 (± 32.01)	0.09	0.19	124.84 (± 29.94)	0.18	0.29
Acetone	HD	160.59 (± 56.75)	0.09	0.37	322.32 (± 48.81)	0.178	0.53
	FW	104.01 (± 16.57)	0.09	0.31	636.95 (± 13.99)	0.242	0.51
	WS	152.07 (± 51.63)	0.09	0.36	324.29 (± 43.84)	0.179	0.54
MEK	HD	37.53 (± 19.5)	0.09	0.24	84.62 (± 17.59)	0.191	0.38
	FW	4.75 (± 3.04)	0.09	0.06	984.94 (± 2.79)	0.555	0.2
	WS	32.52 (± 17.98)	0.09	0.21	86.95 (± 15.94)	0.205	0.38
Hexanol	HD	40.74 (± 25.92)	0.09	0.2	125.7 (± 22.27)	0.235	0.41
	FW	0.25 (± 2.97)	0.09	0.0	237898218.37 (± 2.87)	1.971	0.07
	WS	34.55 (± 23.75)	0.09	0.17	128.79 (± 20.09)	0.248	0.41
Acetic acid	HD	4.13 (± 12.13)	0.09	0.02	-30.76 (± 12.18)	1.397	0.01
	FW	-10.36 (± 3.21)	0.09	0.11	1049478.21 (± 4.65)	4.983	-0.88
	WS	1.91 (± 11.06)	0.09	0.0	-30.76 (± 11.02)	1.397	0.01
SQTs	HD	-12.18 (± 31.92)	0.09	0.0	33.47 (± 32.26)	1.323	-0.02
	FW	-1.0 (± 23.01)	0.09	-0.0	7965843.0 (± 23.02)	3.712	-0.0
	WS	-10.47 (± 30.32)	0.09	0.01	33.49 (± 30.56)	1.323	-0.01
Acetaldehyde	HD	231.3 (± 109.78)	0.09	0.27	761.12 (± 84.7)	0.259	0.57
	FW	70.39 (± 28.16)	0.09	0.15	36377.96 (± 18.97)	0.64	0.61
	WS	206.67 (± 101.01)	0.09	0.25	770.91 (± 76.08)	0.264	0.57
Isoprene	HD	35.05 (± 16.47)	0.09	0.28	86.51 (± 14.14)	0.206	0.47
	FW	14.93 (± 4.92)	0.09	0.18	2027.98 (± 3.32)	0.515	0.63
	WS	31.99 (± 15.08)	0.09	0.26	88.01 (± 12.72)	0.212	0.47
MACR/MVK	HD	7.83 (± 13.07)	0.09	0.05	41.56 (± 12.25)	0.302	0.16
	FW	-2.39 (± 2.29)	0.09	-0.0	8.85363679315e+16 (± 2.41)	4.257	-0.11
	WS	6.26 (± 11.74)	0.09	0.04	42.33 (± 10.96)	0.314	0.16
Hexenal	HD	29.37 (± 21.65)	0.09	0.15	76.05 (± 20.2)	0.211	0.26
	FW	1.23 (± 4.07)	0.09	0.01	8294.43 (± 3.91)	0.82	0.09
	WS	25.1 (± 19.71)	0.09	0.13	78.44 (± 18.18)	0.226	0.26
MTs	HD	20.26 (± 14.57)	0.09	0.17	98.09 (± 11.58)	0.331	0.48
	FW	5.74 (± 9.69)	0.09	0.01	422.76 (± 9.65)	0.467	0.01
	WS	18.09 (± 13.84)	0.09	0.14	97.98 (± 11.2)	0.331	0.44

A.2. Example plots for fitting SEF

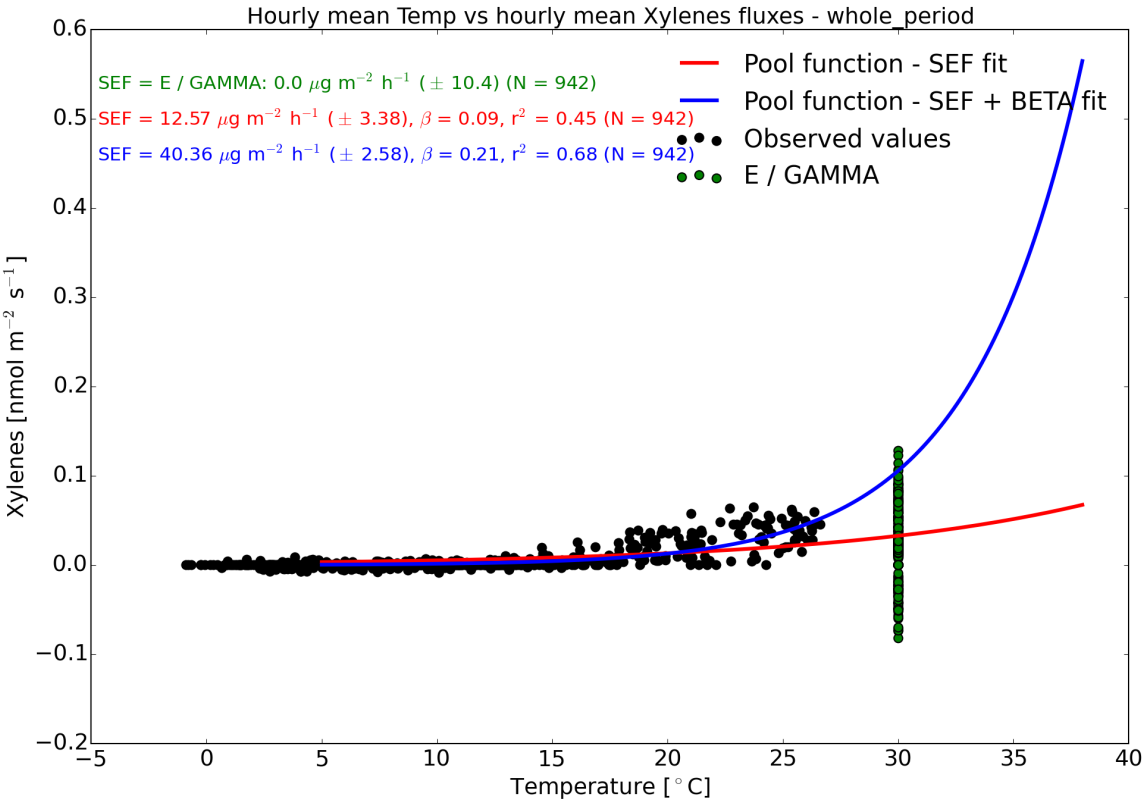

Figure A.2.1.: Variabilities of standardized emission factors (SEFs) of xylene from oilseed rape ecosystem by calculating and curve fitting from hourly mean temperature and BVOC emission rates of the whole observed growing season as an example from the different crop field experiments.

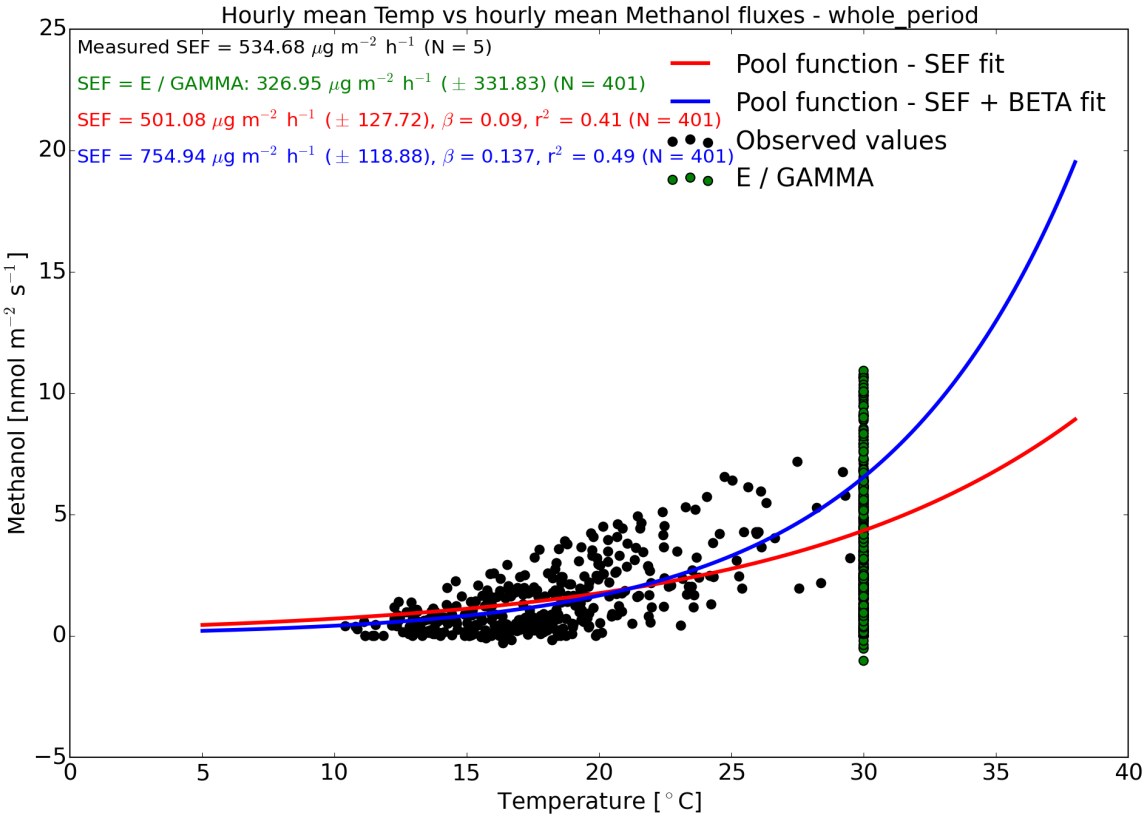

Figure A.2.2.: Variabilities of standardized emission factors (SEFs) of methanol from ryegrass ecosystem by calculating and curve fitting from hourly mean temperature and BVOC emission rates of the whole observed growing season as an example from the different crop field experiments.

B. Simulated annual BVOC emission sums

Table B.1.: Simulated average yearly BVOC emission rates and standard deviation in brackets from maize, oilseed rape, and ryegrass ecosystem during 2015–2017 at the CarboZALF field site in Dedelow in μmol m^{-2} a^{-1}. See Figs. 5.4.1, 5.4.2, and 5.4.3 for an overview by bar plots.

Biogenic volatile organic compound	**Maize**	**Oilseed rape**	**Ryegrass**
Hemiterpene			
Isoprene	0 (0)	669.3 (131.4)	110.3 (18.9)
(oxygenated) Monoterpenes			
Limonene	454.3 (53.0)	0 (0)	0 (0)
Myrcene	0 (0)	415.2 (81.0)	27.9 (4.8)
Camphor	110.1 (14.9)	0 (0)	0 (0)
1,8-Cineole	34.0 (4.5)	0 (0)	0 (0)
Homoterpene			
DMNT	69.2 (7.8)	0 (0)	0 (0)
Sesquiterpene			
α-Humulene	82.0 (10.8)	0 (0)	0 (0)
other VOCs			
Methanol	93.6 (17.0)	77220.8 (7925.1)	13220.3 (626.7)
Ethanol	0 (0)	1916.7 (373.9)	276.8 (47.3)
Acetaldehyde	378.0 (44.3)	2047.2 (210.1)	1173.7 (124.7)
Acetone	428.9 (48.5)	1736.4 (207.7)	704.1 (72.8)
Acetic acid	0 (0)	3704.1 (587.9)	0 (0)
m/z 69	163.5 (18.5)	0 (0)	0 (0)
MACR/MVK	0 (0)	443.8 (66.3)	9.7 (1.7)
m/z 71	79.3 (11.6)	0 (0)	0 (0)
MEK	0 (0)	0 (0)	98.0 (16.7)
m/z 73	0 (0)	767.1 (118.2)	0 (0)
m/z 79	0 (0)	174.9 (34.1)	0 (0)
Toluene	0 (0)	179.7 (35.0)	0 (0)
Hexenal	149.2 (19.1)	254.4 (49.6)	54.9 (9.4)
Hexanal	373.7 (47.9)	1407.3 (200.6)	67.0 (11.4)
Xylenes	48.8 (5.5)	149.5 (29.2)	0 (0)
m/z 118	0 (0)	242.1 (47.2)	0 (0)
Total	2464.5 (104.9)	91328.5 (7966.8)	15742.8 (645.5)

C. Protocols of plant development and field management

Leibniz-Zentrum für Agrarlandschaftsforschung (ZALF) e.V.

Forschungsstation Dedelow
Steinfurther Straße 14
17291 Dedelow
Tel.: 039853/6090 Fax: 039853/60924
email: verch@zalf.de

Carbo-ZALF – VOCE – Projekt = Streifen 13 – 15 WW und Silomais 2015

Standort:	Carbo	Str. 13-14 Str.15	WW WW grün/SM
Vorfrucht:	Zwischenfrucht Senf/SM		
Sorte:	WW„Tiger“ Mais“Zoey“	Aussaat: 07.10.14 Aufgang:18.10.14 Aussaat: 29.04.15 Aufgang:14.05.15	300 K/m² WW Fe13= 256 Pfl./m²WW Fe14= 286 Pfl./m²WW Fe15= 250 Pfl./m²WW 11 Kö/m² SM Fe15 Fe15= 11 Pfl./m² Mais

Bodenbearbeitung :

-30.09.14: Saatfurche nach Silomais;
-07.10.14: Aussaat WW mit Amazone/Kreiselgrubber-Kombination
-29.04.15: Bodenbearbeitung nach abgestorbenem WW mit Schwergrubber in Feld 15, Saatbettbereitung mit Kreiselbrubber; Aussaat mit Becker-Maisdrille

Anbau VOCE im Feld 13 – 15 ab 2015

Jahr	Feld 15	Feld 14	Feld 13
2015	Silomais	WW	WW
2016	Grünroggen/Silomais	Raps	Wintergerste
2017	Grünroggen/Silomais	WW	Raps

Pflanzenentwicklung:

Datum:	**16.10.**	**21.10.**	**03.11.**	**17.11.**	**27.11.**	**17.02.**	**17.03.**	**07.04.**	**13.04.**	**20.04.**	**28.04.**
EC:											
WW	9	11	12	21	21/22	23/24	23/24	25	30	31	31
Mais											

Datum:	**04.05.**	**11.05.**	**18.05.**	**26.05.**	**01.06.**	**08.06.**	**15.06.**	**22.06.**	**28.06.**	**06.07.**	**13.07.**
EC:											
WW	31/32	33	37	41	47/51	59/61	69	69	71	73	77
Mais			12	13	14	15/16	17/18	18/30	31	33	37

Datum:	**17.07.**	**24.07.**	**28.07.**	**03.08.**	**18.08.**	**14.09.**			
EC:									

WW	85	87	87/89	89					
Mais	51	55	63	65	71	89			

Anbaumaßnahmen:

Herbizid:	0,8 l/ha Bacara Forte Feld 13 - 15	am 29.10.2014
	3,0 l/ha Round up zum Abtöten des WW Feld 15	am 19.03.2015
	TM: 3,0 l/ha Gardo Gold + 0,5 l/ha Callisto im Mai Feld 15	am 26.05.2015
Fungizid:	1,5 l/ha Capalo in WW Feld 13+14	am 15.04.2015
	1,5 l/ha Adexar Feld 13+14 WW	am 11.05.2015
MBP:	TM: 1,2 l/ha CCC + 0,1 l/ha Moddus in WW Feld 13 + 14	am 15.04.2015
Insektizid:	0,075 l/ha Karate Zeon Feld 13 - 15	am 29.10.2014
	125 g/ha Steward zu Mais Fe 15	am 08.07.2015
Düngung:	1 dt/ha Kieserit Feld 13-15	am 23.03.2015
	80 kgN/ha KAS Feld 13+14 WW	am 23.03.2015
	80 kgN/ha Harnstoff Feld 13+14 WW	am 22.04.2015
	300 kg/ha K_2O = 249 k/ha K als K60 Feld 15	am 24.04.2015
	110 kg/ha P_2O_5 = 48,4 kg/ha P als P40 Feld 15	am 27.04.2015
	160 kg N/ha Harnstoff Feld 15 Mais	am 29.04.2015

Bemerkungen:

- infolge der günstigen Witterung ist WW zügig aufgelaufen mit normalen Pflanzenbeständen
- 13.11.: N_{min}-Proben mit Maschine aus Müncheberg 0 – 60 cm
- 17.11.:durch milden und feuchten Herbst gute Bestandesentwicklung, infolge anhaltend warmer und feuchter Witterung ist der WW pilzbelastet mit Erysiphe graminis
- 22.11.14: Vegetationsende; der WW geht wenig bestockt in die Winterruhe
- 16.12.14: nach der ersten Frostperiode folgt milde Witterung bis Ende Januar
- Wintereinbruch am 29.01.15 mit Schnee(5cm) und Frost, am Tag Temperaturen ≥ Null, aber immer wieder Neuschnee bis 10 cm, ab 04.02. Nachtfröste bei -9 bis -11°C und auch am Tag Dauerfrost, geschlossene Schneedecke bis 08.02., danach Tauwetter und Wechsel von Frost in der Nacht und Plusgraden am Tag, kein erneuter Winter mehr
- 04.03.15: Bodenproben 0 – 30 cm an festen Punkten(Dr.Verch)
- 05.03.15:Bodenproben N_{min} mit Maschine 0 – 90 cm
- wegen Veränderung im Versuchsprogramm von EVA zu VOCE wird der WW Feld 15 abgetötet, weil als Nachfrucht Silomais geplant ist
- Vegetationsbeginn: 28.03.15, das Frühjahr geht einher mit kalten Nächten, Trockenheit, viel Wind und durchschnittlichen Temperaturen, so dass die Pflanzenentwicklung eher verhalten erfolgt
- endlich 9 mm Regen am 26./27.04.!

- 04.05.: WW auf Feld 13-14zeigt sich als gleichmäßiger geschlossener Bestand, kein Virusbefall
- 11.05.: noch kein Aufgang Mais, beginnt aber vereinzelt zu spitzen
- Monat Mai ist insgesamt kühler als in Durchschnittsjahren und dazu auch sehr trocken, so dass das Wachstum eher verhalten war
- Monat Juni ist ebenso kühl und trocken, ab Monatsmitte kommen nur sehr verhalten Niederschläge und die Natur braucht dringend Regen!
- Maissorte „Zoay“ nimmt eine zügige Entwicklung, bleibt am Ende aber eher kurz, nur sehr wenig Zünslerbefall
- 25.09.2015: Ernte der Restfläche Mais

Leibniz-Zentrum für Agrarlandschaftsforschung (ZALF) e.V.

Forschungsstation Dedelow
Steinfurther Straße 14
17291 Dedelow
Tel.: 039853/6090 Fax: 039853/60924
email: verch@zalf.de

Carbo-ZALF – VOCE – Projekt = Streifen 14 Raps 2016

Standort:	Carbo	Str. 14	Raps
Vorfrucht:	Str.14 = WW		
Sorte:	Raps „PR44D06“	Aussaat: 26.08.15 Aufgang: 03.09.15	50 K/m² Raps 39 Pfl./m² Raps

Bodenbearbeitung :

14.08.15: Ernte Restfläche WW Feld 14 mit Mähdrescher
17.08.15: Stoppelsturz mit Scheibenegge Fe 14
25.08.15: Saatfurche Feld 14 zu Raps
26.08.15: Aussaat Raps mit Amazone/Kreiselgrubber-Kombination

Anbau VOCE im Feld 13 – 15 ab 2015

Jahr	Feld 15	Feld 14	Feld 13
2015	WWgrün/Silomais	WW	WW
2016	Grünroggen/Silomais	Raps	Wintergerste
2017	Weidelgras	WR	WR

Pflanzenentwicklung:

Datum:	**07.09.**	**18.09.**	**16.10.**	**26.10.**	**11.11.**	**07.12.**	**09.03.**	**31.03.**	**18.04.**	**25.04.**	**02.05.**
EC:											
Raps WH cm	11	14	16	17	18	19	19	B.30	53/55	57/59 24 - 45	59/63 49-77

Datum:	**09.05.**	**17.05.**	**23.05.**	**30.05.**	**06.06.**	**14.06.**	**20.06.**	**27.06.**	**18.07.**	**25.07.**	**01.08.**
EC:											
Raps WH cm	65 56-88	67 63-101	69 69-103	71 72-115	77 64-96	79 56-94	81 58-98	83 65-100	89	92	-

Anbaumaßnahmen:

Herbizid:	2,0 l/ha Butisan Gold Feld 14 Raps	am 08.09.2015
	0,5 l/ha Gallant Super Feld 14 Raps	am 08.09.2015
Fungizid:	ohne	
MBP:	0,4 l/ha Toprex Feld 14 Raps	am 02.10.2015
Insektizid:	0,075 l/ha Karate Zeon Feld 14 Raps	am 02.10.2015
	TM: 0,075 l/ha Karate + 150 g/ha Plenum Feld14 Raps	am05.04.2016
Düngung:	30 kg N/ha KAS Feld 14 Raps	am 03.09.2015
	TM: 400 g/ha Bor + 5 kg/ha Bittersalz Feld 14 Raps	am 02.10.2015
	100 kg/ha K_2O= 167kg/ha 60erKali Feld13-14	am 05.10.2015
	90 kg/ha P_2O_5 = 250 kg/ha P40 Feld 13-14	am 06.10.2015
	2 dt/ha Kieserit Feld 14 Raps per Hand	am 01.03.2016
	80 kg N/ha Harnstoff Feld 14 Raps	am 01.03.2016
	60 kg N/ha KAS Feld 14 Raps	am 06.04.2016

Bemerkungen:

- Hauben stehen Feld 14 Raps
- Raps normal aufgelaufen
- mit einsetzenden Niederschlägen im Oktober/November normale Entwicklung im Raps, im November sind bezüglich der Tagestemperaturen noch immer Wachstumsbedingungen, aber es findet kaum noch Entwicklung statt,
- Dezember noch immer mild und kein Winter in Sicht! Weit überdurchschnittliche Temperaturen von 15°C bis Ende des Monats mit Wachstum
- Vegetationsende: 02.01.2016
- dann Temperatursturz, Anfang Januar -15°C als Kahlfrost mit starkem Ostwind, nach 4 Tagen Schnee und Regen mit Tauwetter und weiter um den Gefrierpunkt, 18.01. 2 cm Neuschnee und Temperaturen bis -10°C, 23.01. nochmals 2 cm Neuschnee, anschließend Regen und durchgreifendes Tauwetter mit Temperaturen bis 10°C
- 08.02.: 1m² oberirdische Biomasse Raps auf Feld 14 per Hand geerntet und eingefroren (WH 4 bis 5 cm; 48 Pflanzen; 574,5 g),
- weiter milde Witterung, ab 2.Februarhälfte leichter Frost und kurzes Schneeintermezzo, danach Wechselfröste, mild und nass
- Wechselfröste gehen weiter bis in den März und Tagestemperaturen im einstelligen Bereich, Erwärmung in 2. Märzhälfte
- Vegetationsbeginn: 29.03.2016
- 25.04.: Raps ist insgesamt sehr differenziert und dünn, EC 57/59, in den Hauben schon EC 60/61, ab diesem Termin Wuchshöhemessung, diese ist auch sehr differenziert
- Monat April durchgehend kühl und trocken mit viel Wind, am Ende des Monats Niederschläge und nasse Bestände
- 02.05.: Ernte Biomasse 4 x1m² Raps zum Zeitpunkt Blüte und TS-

Bestimmung

- Monat Mai bringt Wärme, aber es bleibt extrem trocken
- 19.05.: Raps in den Hauben ist geerntet und Biomasse bestimmt, damit weitere Messung abgeschlossen, es erfolgt auf Restfläche noch 4 x 1 m² Biomassebestimmung zum Ende der Blüte (27.05.)und zur Ernte (01.07.)
- Trockenheit bleibt bis zur Ernte erhalten
- 28.07.: Ernte Raps Feld 14 mit Mähdrescher ohne Ertragsfeststellung

Leibniz-Zentrum für Agrarlandschaftsforschung (ZALF) e.V.

Forschungsstation Dedelow
Steinfurther Straße 14
17291 Dedelow
Tel.: 039853/6090 Fax: 039853/60924
email: verch@zalf.de

Carbo-ZALF – VOCE – Projekt = 15 Weidelgras 2017

Standort:	Carbo	Str. 15	Weidelgras
Vorfrucht:	Str.15 = WR/SM		
Sorte:	Weidelgras Mischung Country 2051	Aussaat: 12.08./29.08.16 Aufgang: 24.08./05.09.16	30 kg/ha/40 kg/ha Gras

Bodenbearbeitung :

04.08.16: vorzeitige Ernte Silomais Feld15 wegen Nachfrucht Weidelgras
08.08.16: Maisstoppeln Feld 15 gemulcht,
09.08.19: Saatfurche Feld 15 zu Weidelgras
11.08.16: Saatbettbereitung mit Kreiselgrubber Feld 15
12.08.16: Aussaat Weidelgras mit Amazone/Kreiselgrubber-Kombination
29.08.16: weil infolge Trockenheit sehr lückiger Aufgang Weidelgras, Neubestellung mit Amazone/Kreiselgrubber-Kombination

Anbau VOCE im ab 2015

Jahr	**Feld 15**
2015	WWgrün/Silomais
2016	Grünroggen/Silomais
2017	Weidelgras

Pflanzenentwicklung:

1. Schnitt (17.05.)

Datum:	**25.10.**	**28.11.**	**14.12.**	**01.03.**	**15.03.**	**31.03.**	**04.04.**	**20.04.**	**09.05.**	**15.05.**	**22.05.**
EC:											
WH in cm Weidelgras	09-14	10-15	11-16	10-12	12-15	16-22	25-29	29-32	45-52	64-73	9-24

2.Schnitt (26.06. Hauben,Restfläche 28.06.)

3.Schnitt (04.08.,Rest14.08.)

Datum:	**29.05.**	**06.06.**	**12.06.**	**19.06.**	**27.06.**	**03.07.**	**10.07.**	**17.07.**	**24.07.**	**31.07.**	**14.08.**
EC:											
WH in cm Weidelgras	22-35	50-65	67-86	82-98	78-106	10-18	16-24	33-45	41-73	60-92	18-24

Datum:	**24.08.**	**30.08.**	**18.09.**						
EC:									
WH cm Weidelgras	23-48	34-61	41-73						

Anbaumaßnahmen:

Herbizid:	3,5 l/ha Round up Fe 15 Weidelgras		am 19.09.2017
Fungizid:	ohne		
MBP:	ohne		
Insektizid:	ohne		
Düngung:	80 kg N/ha	KAS zu Weidelgras Fe 15	am 14.03.2017
	50 kg N/ha	KAS zu Weidelgras Fe 15	am 23.05.2017
	30 kg N/ha	KAS zu Weidelgras F15(nur Hauben)	am 06.07.2017

Bemerkungen:

- Weidelgras infolge Trockenheit sehr lückenhaft aufgelaufen, darum 2. Aussaat am 29.08., die nach Niederschlägen am 05.09. aufgeht und duchgängige Reihen sichtbar macht
- 14.12.: Pflanzen grüner und weiterentwickelt, Witterung lässt kaum noch Weiterentwicklung erwarten
- Anfang Januar wird es kälter mit Nachtfrösten, etwas Schnee und auch am Tag Temperaturen unter 0°C, 31.1. fast 20 cm Schnee
- Witterung bleibt auch im Februar winterlich, Wechselfröste, teilweise am Tag Temperaturen wenig über Null, aber Schneedecke taut nie ganz weg, Fröste im einstelligen Bereich
- 2.Februarhälfte ohne Nachtfröste und Tauwetter, Tagestemperaturen einstellig, ab 21.2. Regen und Sturm
- Ende des Monats Februar mild, teilweise Tagestemperaturen im 2-stelligen Bereich, Saaten erscheinen grüner und in Wachstumsstimmung,
- Monat März mit milden Temperaturen, teilweise noch Nachtfröste
- 1.N-Gabe wird verwogen und per Hand gestreut am 14.03.2017, weil Hauben stehen und Technik behindern
- im Verlauf des März Regen und Sturm, am Ende des Monats fast sommerlich warm
- April sehr durchwachsen, warm bis 20 °C, Mitte des Monats Schnee, Regen und Frost, auch am Tag kühl, 2. Monatshälfte durchgehend sehr kühl und Nachtfröste, begleitet von Niederschlägen
- Monat Mai beginnt kühl mit Nachtfrösten und Niederschlägen, ab Monatsmitte wärmer, aber trocken

- 17.05.17: 1. Schnitt Weidelgras
- 26.06.17: 2. Schnitt Weidelgras in den Hauben, Restfläche erst am 28.06.; das Weidelgras hat zu dem Zeitpunkt die Rispe geschoben, blüht und geht ins Lager, Restfläche soweit zugänglich gemulcht, Rest mit Sense per Hand und abgetragen,
- Monat Juni durchwachsen, von heiß bis kühl und immer wieder Regen (Gesamt 141 mm im Juni), durchschnittlich kühler
- 3. N - Gabe erfolgt nur unter den Hauben
- Monat Juli weiter sehr durchwachsen, zumeist kühl und viele Niederschläge, am 25/26.07. über 80 mm als Dauerregen
- 04.08.: 3. Schnitt in den Hauben; Restfläche erst am 14.8., weil keine Kapazität war
- Monat August durchwachsen, eher kühl und Niederschläge durchschnittlich,
- am 19.09.17 wird das Weidelgras mit Round up abgetötet, der Versuch ist beendet, die Hauben bleiben aber stehen und messen weiter

D. Item list for Dedelow field experiments

Item list for Dedeliw field experiments – VOCE

F. Havermann, A. Ghirardo

February 11, 2019

General

- Ryegrass (*Lolium perenne* L.) field experiment in Dedelow, from 06 to 30 June, 2017
- Accommodation in "Am Tanger" from 06 to 09 June; at the research center Dedelow from 28 to 30 June

Instruments

- PTR-QMS 500 BVOC measurement device from Ionicon Analytik GmbH, Innsbruck, Austria
- GCU for PTR-QMS calibration from Ionicon Analytik GmbH, Innsbruck, Austria
- O_3 41M O_3 measurement device from Environment S.A. Poissy, France
- CLD 86 YP NO_x measuremnet device from Eco Physics, Duernten, Switzerland
- GFS-3000 Portable Gas Exchange Fluorescence System from Heinz Walz GmbH, Effeltrich, Germany

PTR-MS related stuff

- Repair kit (cleaning the ion-source, cleaning the detector (SEM), changing the diaphragm of the pump ...)
- Mass flow controller, pressure controller, pressure gauges (for maintenance)
- All tools for setting up the machine
- Emergency generator
- Electricity supply
- Laptop & keyboad & mouse

- PTFE tube 1/4″(ca. 90 m)
- PTFE tube 1/8″(ca. 5 m)
- 5 times 3/2 way PTFE valve (1 for safety reasons)
- Fittings for the valves to connect to all tubes (4-5 times each for sample line in, sample line out, flushing line out)
- Items to connect valves to electricity
- 6 times T-piece (connect all sample lines to one line as input for instruments and for flushing the tube)
- 1 time T-piece for the connection of the PTR-MS
- 3 times an air pump, ca. 10 L min^{-1} (1 for PTR-MS inlet, 1 for flushing the tube, 1 for GFS-3000 System)
- Some fittings for 1/4″and a few for 1/8″tubes
- Isolation and heating ("Begleitheizunng/Heizband") for the tubes
- Water for H_3O^+
- VOC standard gas for calibration and testing (incl. pressure reducer)

GCU related stuff

- Standard gas
- zero air (N_2)
- Water
- Mass flow controller
- Electricity supply

O_3 41M related stuff

- 1 time 4 piece (connection of O_3 and NO_x)
- Electricity supply

NO_x related stuff

- 1 time 4 piece (connection of O_3 and NO_x)
- Electricity supply

GFS-3000 and offline GC-MS related stuff

- Double distillate water
- Humidifier material
- Drier material
- CO_2 cartridge
- Netbook
- Glass tubes with PDMS, Tenax, and Carbopacks
- Tweezers
- Medical gloves
- 4 mass flow controller and air pump

Miscellaneous

- Power distribution
- Needle valve
- Bike
- Shovel & hammer
- Folding chairs
- Sunshade
- Cool box
- Knife
- Sun creme
- Swimming trunks
- Blanket
- Music & music boxes
- Rain coat
- Sandals
- Gas flow meter
- Rotameter
- Lighter
- Cutter knife
- USB stick
- Wify stick
- Duct tape
- Cable tie
- Yard stick
- Pencils & marker
- Field book
- Tobacco etc
- Beer & pizza
- BBQ & charcoal

E. LandscapeDNDC model setup files

E.1. Site file

The following lines are content from a `xml` file describing the site characteristics of the CarboZALF-D15 field site. The field site CarboZALF-D14 does only marginally differ and is therefore not shown here.

```
<?xml version="1.0" encoding="UTF-8"?>
<ldndcsite>
    <description>
        <author>Felix Havermann</author>
        <date>2017-06-06</date>
        <dataset>
            CarboZALF field D15 in Dedelow, Brandenburg, Deutschland
        </dataset>
        <source>
            Communiction with Michael Berg, ZALF (abgabe_Berg_lse.xls)
        </source>
    </description>

    <site id="0" >
    <soil>
        <general usehistory="arable" litterheight="0.0" soil="sicl" />
        <layers>
            <layer depth="350" split="12" bd="" clay="0.1"
              corg="0.0058" sand="0.58" ph="7.66" scel="0.058"/>
            <layer depth="120" split="4" bd="" clay="0.1"
              corg="0.0019" sand="0.58" ph="6.22" scel="0.048"/>
            <layer depth="390" split="10" bd="" clay="0.19"
              corg="0.0034" sand="0.50" ph="6.9" scel="0.021"/>
            <layer depth="1140" split="10" bd="" clay="0.13"
              corg="0.0002" sand="0.57" ph="7.76" scel="0.041"/>
        </layers>
    </soil>
    </site>
</ldndcsite>
```

E.2. Management files

In the following, the content of the field management `xml` files is given. The information about the agricultural management (seeding, fertilizing, cutting, harvesting) is taken from the field management protocols provided from the ZALF which are embedded in this work in Ch. C.

E.2.1. Management for maize

```
<?xml version="1.3"?>
<ldndcevent>
    <event  id="0" >
        <comment>
            All 2015 events from the file "VOCE␣Feld13-15WW␣2015.docx";
            Silage Corn/Maize variety ZOEY from advanta seeds;

            The 2016 and 2017 events are the same as for 2015;
        </comment>

        <!-- 2014 -->
        <event type="plant" time="2014-04-29" >
            <plant name="Silage␣Corn" type="SICO" >
                <crop initialbiomass="20.0" />
            </plant>
        </event>

        <event type="fertilize" time="2014-04-30">
            <fertilize type="urea" amount="160.0" />
        </event>

        <event type="harvest" time="2014-09-15" >
            <harvest name="Silage␣Corn" stubbleheight="0.1" />
        </event>

        <!-- 2015 -->
        <event type="plant" time="2015-04-29" >
            <plant name="Silage␣Corn" type="SICO" >
                <crop initialbiomass="20.0" />
            </plant>
        </event>

        <event type="fertilize" time="2015-04-30">
            <fertilize type="urea" amount="160.0" />
        </event>

        <event type="harvest" time="2015-09-15" >
            <harvest name="Silage␣Corn" stubbleheight="0.1" />
        </event>
```

```
        <!-- 2016 -->
        <event type="plant" time="2016-04-29" >
            <plant name="Silage␣Corn" type="SICO" >
                <crop initialbiomass="20.0" seedlingnumber="110000"/>
            </plant>
        </event>

        <event type="fertilize" time="2016-04-30">
            <fertilize type="urea" amount="160.0" />
        </event>

        <event type="harvest" time="2016-09-15" >
            <harvest name="Silage␣Corn" stubbleheight="0.1" />
        </event>

        <!-- 2017 -->
        <event type="plant" time="2017-04-29" >
            <plant name="Silage␣Corn" type="SICO" >
                <crop initialbiomass="20.0" seedlingnumber="110000"/>
            </plant>
        </event>

        <event type="fertilize" time="2017-04-30">
            <fertilize type="urea" amount="160.0" />
        </event>

        <event type="harvest" time="2017-09-15" >
            <harvest name="Silage␣Corn" stubbleheight="0.1" />
        </event>
    </event>
</ldndcevent>
```

E.2.2. Management for oilseed rape

```
<?xml version="1.3"?>
<ldndcevent>
    <global time="2014-08-01" />
    <event  id="0" >
        <comment>
            All management from the file "VOCE␣Feld14Raps2016.docx";
            Rapeseed variety PR44D06 from Pioneer
        </comment>

        <!-- 2015 -->
        <event type="plant" time="2014-08-26" >
            <plant name="Rapeseed" type="RAPE" >
                <crop initialbiomass="20.0" seedlingnumber="390000"/>
            </plant>
```

```
</event>

<event type="fertilize" time="2014-09-03">
    <fertilize type="nh4no3" amount="30.0" />
</event>

<event type="fertilize" time="2015-03-02">
    <fertilize type="urea" amount="80.0" />
</event>

<event type="fertilize" time="2015-04-06">
    <fertilize type="nh4no3" amount="60.0" />
</event>

<event type="harvest" time="2015-07-28" >
    <harvest name="Rapeseed" remains="0" />
</event>


<!-- 2016 -->
<event type="plant" time="2015-08-26" >
    <plant name="Rapeseed" type="RAPE" >
        <crop initialbiomass="20.0" seedlingnumber="390000"/>
    </plant>
</event>

<event type="fertilize" time="2015-09-03">
    <fertilize type="nh4no3" amount="30.0" />
</event>

<event type="fertilize" time="2016-03-02">
    <fertilize type="urea" amount="80.0" />
</event>

<event type="fertilize" time="2016-04-06">
    <fertilize type="nh4no3" amount="60.0" />
</event>

<event type="harvest" time="2016-07-28" >
    <harvest name="Rapeseed" remains="0" />
</event>


<!-- 2017 -->
<event type="plant" time="2016-08-26" >
    <plant name="Rapeseed" type="RAPE" >
        <crop initialbiomass="20.0" seedlingnumber="390000"/>
    </plant>
</event>

<event type="fertilize" time="2016-09-03">
```

```
            <fertilize type="nh4no3" amount="30.0" />
        </event>

        <event type="fertilize" time="2017-03-02">
            <fertilize type="urea" amount="80.0" />
        </event>

        <event type="fertilize" time="2017-04-06">
            <fertilize type="nh4no3" amount="60.0" />
        </event>

        <event type="harvest" time="2017-07-28" >
            <harvest name="Rapeseed" remains="0" />
        </event>

    </event>
</ldndcevent>
```

E.2.3. Management for ryegrass

```
<?xml version="1.3"?>
<ldndcevent>
    <global time="2014-01-01" />
    <event  id="0" >
        <comment>
          All management from the file
          "VOCE_Feld15Weidelgras_2017.docx";
          Ryegrass Country 2051: 85% italian ryegrass
          (Lolium multiflorum, Welsches Weidelgras) and 15%
          hybrid ryegrass (Lolium x hybridum, Bastard Weidelgras)
        </comment>

        <!-- 2015 -->
        <event type="plant" time="2015-01-01" >
            <plant name="Lolium␣Italicum" type="LOIT" >
                <grass initialbiomass="30.0" />
            </plant>
        </event>


        <event type="fertilize" time="2015-03-14">
            <fertilize type="nh4no3" amount="80.0" />
        </event>

        <event type="cut" time="2015-05-17" >
            <cut name="Lolium␣Italicum" remains="400" />
        </event>

        <event type="fertilize" time="2015-05-23">
```

```
    <fertilize type="nh4no3" amount="50.0" />
</event>

<event type="cut" time="2015-06-26" >
    <cut name="Lolium␣Italicum" remains="300" />
</event>

<event type="fertilize" time="2015-07-06">
    <fertilize type="nh4no3" amount="30.0" />
</event>

<event type="cut" time="2015-08-04" >
    <cut name="Lolium␣Italicum" remains="212" />
</event>

<event type="cut" time="2015-09-20" >
    <cut name="Lolium␣Italicum" remains="212" />
</event>

<event type="cut" time="2015-10-8" >
    <cut name="Lolium␣Italicum" remains="212" />
</event>

<!-- 2016 -->
<event type="fertilize" time="2016-03-14">
    <fertilize type="nh4no3" amount="80.0" />
</event>

<event type="cut" time="2016-05-17" >
    <cut name="Lolium␣Italicum" remains="400" />
</event>

<event type="fertilize" time="2016-05-23">
    <fertilize type="nh4no3" amount="50.0" />
</event>

<event type="cut" time="2016-06-26" >
    <cut name="Lolium␣Italicum" remains="300" />
</event>

<event type="fertilize" time="2016-07-06">
    <fertilize type="nh4no3" amount="30.0" />
</event>

<event type="cut" time="2016-08-04" >
    <cut name="Lolium␣Italicum" remains="212" />
</event>

<event type="cut" time="2016-09-20" >
    <cut name="Lolium␣Italicum" remains="212" />
</event>
```

```
        <event type="cut" time="2016-10-8" >
            <cut name="Lolium␣Italicum" remains="212" />
        </event>

        <!-- 2017 -->
        <event type="fertilize" time="2017-03-14">
            <fertilize type="nh4no3" amount="80.0" />
        </event>

        <event type="cut" time="2017-05-17" >
            <cut name="Lolium␣Italicum" remains="400" />
        </event>

        <event type="fertilize" time="2017-05-23">
            <fertilize type="nh4no3" amount="50.0" />
        </event>

        <event type="cut" time="2017-06-26" >
            <cut name="Lolium␣Italicum" remains="300" />
        </event>

        <event type="fertilize" time="2017-07-06">
            <fertilize type="nh4no3" amount="30.0" />
        </event>

        <event type="cut" time="2017-08-04" >
            <cut name="Lolium␣Italicum" remains="212" />
        </event>

        <event type="cut" time="2017-09-20" >
            <cut name="Lolium␣Italicum" remains="212" />
        </event>

        <event type="cut" time="2017-10-8" >
            <cut name="Lolium␣Italicum" remains="212" />
        </event>

    </event>
</ldndcevent>
```

E.3. Species specific parameter files

In the following, the content of the species specific parameter `xml` files is given. That are parameters describing plant growth, physiology, and photosynthesis which were adjusted to meet observations of biomass, NEE, R_{eco}, and GPP. Further, the BVOC emission specific parameters SEF, LDF, and β-coefficient, are given which were de-

termined by fitting the JJv stand-alone model to emission measurements (see Sect. 4.4.3 for details on the calculation procedure).

E.3.1. Species specific parameter for maize

```
<?xml version="1.0" ?>
<ldndcspeciesparameters>
    <speciesparameters id="0" >
        <species mnemonic="SICO" group="crop" name="Silage␣Corn" >

            <!-- Plant growth, physiology and photosynthesis -->
            <par name="h2oref_a" value="0.7" />
            <par name="h2oref_gs" value="0.65" />
            <par name="slope_gsa" value="10.0"/>
            <par name="gdd_base_temperature" value="8.0" />
            <par name="gdd_emergence" value="70.0"/>
            <par name="gdd_stem_elongation" value="200.0"/>
            <par name="gdd_grain_filling" value="500.0" />
            <par name="gdd_maturity" value="1100.0" />
            <par name="mfolopt" value="0.44"/>
            <par name="tlimit" value="0.0"/>
            <par name="sladecline" value="0.0"/>
            <par name="slamax" value="6.5"/>
            <par name="slamin" value="6.5"/>
            <par name="faleaf" value="0.65"/>
            <par name="vcmax25" value="130"/>


            <!-- JJv BVOC emission specific parameters -->
            <par name="ef_methanol" value="0.0443" />
            <par name="ldf_methanol" value="0.5" />
            <par name="beta_methanol" value="0.19" />
            <par name="ef_acetaldehyde" value="0.0441" />
            <par name="ldf_acetaldehyde" value="0.1" />
            <par name="beta_acetaldehyde" value="0.14" />
            <par name="ef_ethanol" value="0.0081" />
            <par name="ldf_ethanol" value="0.0" />
            <par name="beta_ethanol" value="0.23" />
            <par name="ef_acetone" value="0.0677" />
            <par name="ldf_acetone" value="0.2" />
            <par name="beta_acetone" value="0.13" />
            <par name="ef_iso" value="0.0307" />
            <par name="ldf_iso" value="0.2" />
            <par name="beta_iso" value="0.13" />
            <par name="ef_mvk_macr" value="0.0209" />
            <par name="ldf_mvk_macr" value="0.2" />
            <par name="beta_mvk_macr" value="0.17" />
            <par name="ef_hexenal" value="0.0462" />
            <par name="ldf_hexenal" value="0.2" />
```

```
            <par name="beta_hexenal" value="0.15" />
            <par name="ef_hexanal" value="0.1195" />
            <par name="ldf_hexanal" value="0.2" />
            <par name="beta_hexanal" value="0.15" />
            <par name="ef_xylenes" value="0.0139" />
            <par name="ldf_xylenes" value="0.2" />
            <par name="beta_xylenes" value="0.13" />
            <par name="ef_monoterpenes" value="0.1908" />
            <par name="ldf_monoterpenes" value="0.3" />
            <par name="beta_monoterpenes" value="0.13" />
            <par name="ef_dmnt" value="0.0293" />
            <par name="ldf_dmnt" value="0.2" />
            <par name="beta_dmnt" value="0.13" />
            <par name="ef_camphor" value="0.0663" />
            <par name="ldf_camphor" value="0.5" />
            <par name="beta_camphor" value="0.14" />
            <par name="ef_o_monoterpenes" value="0.0182" />
            <par name="ldf_o_monoterpenes" value="0.3" />
            <par name="beta_o_monoterpenes" value="0.15" />
            <par name="ef_sesquiterpenes" value="0.0589" />
            <par name="ldf_sesquiterpenes" value="0.3" />
            <par name="beta_sesquiterpenes" value="0.15" />

        </species>
    </speciesparameters>
</ldndcspeciesparameters>
```

E.3.2. Species specific parameter for oilseed rape

```
<?xml version="1.0" ?>
<ldndcspeciesparameters>
    <speciesparameters id="0" >
        <species mnemonic="rape" group="crop" name="rapeseed" >

        <!-- Plant growth, physiology and photosynthesis -->
        <par name="slamax" value="20.0"/>
        <par name="slamin" value="20.0"/>
        <par name="gdd_base_temperature" value="0.0" />
        <par name="gdd_emergence" value="100.0"/>
        <par name="gdd_stem_elongation" value="920.0"/>
        <par name="gdd_flowering" value="920.0" />
        <par name="gdd_grain_filling" value="1200.0"/>
        <par name="gdd_maturity" value="2600.0"/>
        <par name="tlimit" value="4.0" />
        <par name="sladecline" value="0.8" />
        <par name="nc_fruit_max" value="0.039" source="wofost␣model"/>
        <par name="nc_fruit_min" value="0.015" source="wofost␣model"/>
        <par name="ncfolopt" value="0.05" source="wofost␣model"/>
        <par name="ncfolmin" value="0.01" source="wofost␣model"/>
```

```
<par name="nc_structural_tissue_max" value="0.01"/>
<par name="nc_structural_tissue_min" value="0.0055"/>
<par name="ncfrtopt" value="0.01"/>
<par name="grain" value="0.5"/>
<par name="h2oref_a" value="0.5" />
<par name="tlimit" value="4.0" />
<par name="senescroot"     value="0.02" />
<par name="senescdrought"  value="0.01" />
<par name="senesctemp"     value="0.01" />
<par name="senescage"      value="0.001" />
<par name="sladecline"      value="0.8" />
<par name="chill_units" value="25.0" />
<par name="chill_temp_max" value="5.0" />

<!-- JJv BVOC emission specific parameters -->
<par name="ef_methanol" value="6.2412" />
<par name="ldf_methanol" value="0.5" />
<par name="beta_methanol" value="0.08" />
<par name="ef_acetaldehyde" value="0.2456" />
<par name="ldf_acetaldehyde" value="0.5" />
<par name="beta_acetaldehyde" value="0.08" />
<par name="ef_ethanol" value="0.6453" />
<par name="ldf_ethanol" value="1.0" />
<par name="beta_ethanol" value="1.0" />
<par name="ef_acetone" value="0.435" />
<par name="ldf_acetone" value="0.8" />
<par name="beta_acetone" value="0.08" />
<par name="ef_acetic_acid" value="1.3881" />
<par name="ldf_acetic_acid" value="0.9" />
<par name="beta_acetic_acid" value="0.12" />
<par name="ef_iso" value="0.2182" />
<par name="ldf_iso" value="1.0" />
<par name="beta_iso" value="1.0" />
<par name="ef_mvk_macr" value="0.1825" />
<par name="ldf_mvk_macr" value="0.9" />
<par name="beta_mvk_macr" value="0.1" />
<par name="ef_mek" value="0.3333" />
<par name="ldf_mek" value="0.9" />
<par name="beta_mek" value="0.11" />
<par name="ef_benzene" value="0.1118" />
<par name="ldf_benzene" value="1.0" />
<par name="beta_benzene" value="1.0" />
<par name="ef_toluene" value="0.126" />
<par name="ldf_toluene" value="1.0" />
<par name="beta_toluene" value="1.0" />
<par name="ef_hexenal" value="0.2068" />
<par name="ldf_hexenal" value="1.0" />
<par name="beta_hexenal" value="1.0" />
<par name="ef_hexanal" value="0.7486" />
<par name="ldf_hexanal" value="0.8" />
<par name="beta_hexanal" value="0.12" />
```

```
        <par name="ef_xylenes" value="0.1204" />
        <par name="ldf_xylenes" value="1.0" />
        <par name="beta_xylenes" value="1.0" />
        <par name="ef_indole" value="0.2043" />
        <par name="ldf_indole" value="1.0" />
        <par name="beta_indole" value="1.0" />
        <par name="ef_monoterpenes" value="0.4044" />
        <par name="ldf_monoterpenes" value="1.0" />
        <par name="beta_monoterpenes" value="1.0" />
        <par name="ef_sesquiterpenes" value="0.0" />
        <par name="ldf_sesquiterpenes" value="0.0" />
        <par name="beta_sesquiterpenes" value="0.0" />

        </species>
    </speciesparameters>
</ldndcspeciesparameters>
```

E.3.3. Species specific parameter for ryegrass

```
<?xml version="1.0" ?>
<ldndcspeciesparameters>
    <speciesparameters id="0" >
        <species mnemonic="loit" group="grass" name="lolium␣italicum">

            <!-- Plant growth, physiology and photosynthesis -->
            <par name="grain"           value="0.1" />
            <par name="root"            value="0.4" />
            <par name="vcmax25"         value="68.0" />
            <par name="fyield"          value="0.1" />
            <par name="nfix_rate"       value="0.1" />
            <par name="shoot_stimulation_reprod" value="1.5" />
            <par name="chill_units"      value="0.0" />
            <par name="grain"           value="0.1" />
            <par name="root"            value="0.4" />
            <par name="straw"           value="0.5" />
            <par name="nfix_rate"       value="0.1" />
            <par name="tlimit"          value="0.0" />
            <par name="max_tdd"         value="2000.0" />
            <par name="senescdrought"   value="0.01" />
            <par name="senesctemp"      value="0.01" />
            <par name="senescence_age"       value="0.001" />
            <par name="senescage"       value="0.001" />
            <par name="sladecline"       value="0.8" />
            <par name="slamax" value="15.0" />
            <par name="slamin" value="15.0" />
            <par name="vcmax25" value="60.0" />
            <par name="gddfolstart" value="0.0" />
            <par name="mfolopt" value="1.0" />
            <par name="fyield" value="0.1" />
```

```
            <!-- JJv BVOC emission specific parameters -->
            <par name="ef_methanol" value="2.6979" />
            <par name="ldf_methanol" value="0.8" />
            <par name="beta_methanol" value="0.06" />
            <par name="ef_acetaldehyde" value="0.7958" />
            <par name="ldf_acetaldehyde" value="0.0" />
            <par name="beta_acetaldehyde" value="0.26" />
            <par name="ef_ethanol" value="0.1926" />
            <par name="ldf_ethanol" value="1.0" />
            <par name="beta_ethanol" value="1.0" />
            <par name="ef_acetone" value="0.4391" />
            <par name="ldf_acetone" value="0.9" />
            <par name="beta_acetone" value="0.09" />
            <par name="ef_acetic_acid" value="0.0213" />
            <par name="ldf_acetic_acid" value="1.0" />
            <par name="beta_acetic_acid" value="1.0" />
            <par name="ef_iso" value="0.1135" />
            <par name="ldf_iso" value="1.0" />
            <par name="beta_iso" value="1.0" />
            <par name="ef_mvk_macr" value="0.0431" />
            <par name="ldf_mvk_macr" value="1.0" />
            <par name="beta_mvk_macr" value="1.0" />
            <par name="ef_mek" value="0.1177" />
            <par name="ldf_mek" value="1.0" />
            <par name="beta_mek" value="1.0" />
            <par name="ef_hexenal" value="0.0983" />
            <par name="ldf_hexenal" value="1.0" />
            <par name="beta_hexenal" value="1.0" />
            <par name="ef_hexanal" value="0.1446" />
            <par name="ldf_hexanal" value="1.0" />
            <par name="beta_hexanal" value="1.0" />
            <par name="ef_monoterpenes" value="0.0768" />
            <par name="ldf_monoterpenes" value="1.0" />
            <par name="beta_monoterpenes" value="1.0" />
            <par name="ef_sesquiterpenes" value="0.0" />
            <par name="ldf_sesquiterpenes" value="0.0" />
            <par name="beta_sesquiterpenes" value="0.0" />

        </species>
    </speciesparameters>
</ldndcspeciesparameters>
```

F. The JJv model source code

I wrote the JJv model (Grote et al., 2014) as a stand-alone in PYTHON programming language and implemented the model into the LandscapeDNDC framework written in C++ programming language. Both versions are shown in the following two sections.

F.1. JJv stand-alone

```
#! /usr/bin/env python
# -*- coding: utf-8 -*-

# This script calculates light dependent (de novo) BVOC emissions
# according to the JJv model as described in Grote et al. 2014, PCE

import numpy as np

def jjv( species, temp_c, ppfd, co2):
    """Calculation of BVOC activity factor to scale standard emission
    factors to actual conditions following the JJv approach

    species       :  plant species for calculation
    temp_c        :  actual temperature value(s) in degree C (np.array)
    ppfd          :  actual ppfd in units of umol m-2 s-1
    co2           :  ambient co2 mole fraction (umol mol-1; or ppm)
    """

    # CHECK FOR MASKED VALUES
    if np.ma.count_masked( temp_c) > 0  or np.ma.count_masked( ppfd) > 0\
    or np.ma.count_masked( co2) > 0:
        sys.exit("No masked values within arrays as input possible")

    elif np.ma.count( temp_c) == np.ma.count( ppfd) == np.ma.count( co2):
        pass

    # x1 == x2 != 1 and x3 == 1
    elif ( np.ma.count( temp_c) == np.ma.count( ppfd) != 1 and\
    np.ma.count( co2) == 1) or ( np.ma.count( temp_c) == np.ma.count( co2)\
    != 1 and np.ma.count( ppfd) == 1) or ( np.ma.count( co2)\
    == np.ma.count( ppfd) != 1 and np.ma.count( temp_c) == 1):
        pass
```

```
    # x1 == x2 == 1 and x3 != 1
    elif ( np.ma.count( temp_c) == np.ma.count( ppfd)== 1\
    and np.ma.count( co2) != 1) or ( np.ma.count( temp_c) ==\
    np.ma.count( co2) == 1 and np.ma.count( ppfd) != 1) or\
    ( np.ma.count( co2) == np.ma.count( ppfd) == 1 and\
    np.ma.count( temp_c) != 1):
        pass

    else:
        sys.exit("At␣least␣two␣input␣variables␣must␣have␣same\
␣␣␣␣␣␣␣␣length␣(mask␣==␣False).␣If␣there␣are␣two␣different\
␣␣␣␣␣␣␣␣shapes␣one␣has␣to␣be␣the␣length␣of␣1.")

    # GENERAL CONSTANTS
    TEMP_K_0  = 273.15      # [K] 0 degree Celsius in Kelvin
    TEMP_K_25 = TEMP_K_0 + 25.# [K] leaf temp at "normal" conditions
    TEMP_K_30 = TEMP_K_0 + 30.# [K] leaf temp at standard conditions
    PPFD_1000 = 1000        # PPFD standard conditions (umol m-2 s-1)
    PAR_ABS   = 0.860       # PAR absorbance factor Collatz, 1991
    R_GAS     = 8.314       # J K-1 mol-1
    O2I       = 200         # intracellular O2 conc ~ ambient O2 conc
    co2i      = co2 * 0.7   # intracellular CO2 conc (umol mol-1)

    CO2_std   = 400
    CO2I_std  = CO2_std * 0.7

    # SPECIES SPECIFIC PARAMETERS FOR PHOTOSYNTHESIS ACTIVITY FACTOR
    # FROM Grote et al. 2014 HERE USED AS CONSTANTS FOR ALL SPECIES
    C1          = 0.17650 # = 0.17650e-3 when constant relation to C2
    C2          = 0.00280 # = 0.00280e-3 here in nmol m-2 s-1 */
    GAMMA_MAX   = 34.0 # saturating amount of electrons (umol m-2 s-1)
    Q10KC       = 2.1   # Q10 factor for Rubisco carboxylation (/)
    Q10KO       = 1.2   # Q10 factor for Rubisco oxygenation (/)
    Q10VC       = 2.4   # Q10 factor for electron transport response (/)
    Q10R        = 2.0   # Q10 factor for photorespiration response (/)

    # SPECIES SPECIFIC PARAMETERS FOR ENZYMATIC ACTIVITY FACTOR
    # FROM Grote et al. 2014
    CT   = 32.86    # scaling constant (J mol-1 )
    DS   = 887.5    # entropy term of emission enzyme (J mol-1 K-1 )
    HA   = 83129    # activation energy of emission enzyme (J mol-1 )
    HD   = 284600   # deactivation energy of emission enzyme (J mol-1)

    # SPECIES SPECIFIC PARAMETERS FROM LandscapeDNDC LRESOURCES
    # FILE FROM 15 APRIL 2018
    if species == 'maize_2015':
        AEJM     = 77900
        KC25     = 650
        KO25     = 450
        QJVC     = 2.25
```

```
    THETA    = 0.97
    VCMAX25 = 130

elif species == 'rapeseed_2016':
    AEJM     = 37000
    KC25     = 260
    KO25     = 179
    QJVC     = 3.07
    THETA    = 0.9
    VCMAX25 = 61

elif species == 'ryegrass_2017':
    AEJM     = 46270
    KC25     = 260
    KO25     = 179
    QJVC     = 2.8
    THETA    = 0.9
    VCMAX25 = 60

elif species == 'grote_2014':
    AEJM     = 49884
    KC25     = 300
    KO25     = 300
    QJVC     = 2
    THETA    = 0.7
    VCMAX25 = 60
    HD       = 220000
    DS       = 703

else:
    sys.exit("The selected species is currently not supported.")

#print "Using species specific values for", species, ":"
#print "AEJM =", AEJM
#print "KC25 =", KC25
#print "KO25 =", KO25
#print "QJVC =", QJVC
#print "THETA =", THETA
#print "VCMAX25 =", VCMAX25

# CONVERSION
temp_k        = temp_c + TEMP_K_0 # temperature in kelvin
ppfd_absorbed = ppfd * PAR_ABS    # leaf absorbed radiation

# GET GAMMA EN RELATIVE TO STANDARDIZED ENVIRONMENTAL CONDITIONS
def get_gamma_en( tk):

    return np.exp( CT - HA / ( R_GAS * tk)) /\
        ( 1.0 + np.exp(( DS * tk - HD) / ( R_GAS * tk)))
    del tk
```

```
gamma_en      = get_gamma_en( temp_k)
gamma_en_norm = get_gamma_en( TEMP_K_30)

gamma_en_rel = gamma_en / gamma_en_norm
del gamma_en, gamma_en_norm


# GET GAMMA PH RELATIVE TO STANDARDIZED ENVIRONMENTAL CONDITIONS
# ALL PHOTOSYNTHESIS PARAMETERS TAKEN FROM Grote et al 2014
# FOLLOWING THE Farquhuar et al. 1980 APPROACH,
# REARANGED BY Collatz et al. 1991 and Oleson et al. 2010 IN CLM
def get_gamma_ph( tk, light_abs, ci):

    # KM: MICHAELIS-MENTEN COEFFICIENT FOR ELECTRON TRANSPORT
    kco2 = KC25 * np.power( Q10KC, ( tk - TEMP_K_25) / 10.)
    ko2  = KO25 * np.power( Q10KO, ( tk - TEMP_K_25) / 10.)
    km = kco2 * ( 1. + O2I / ko2)

    # J: ELECTRON PROVISION (umol m-2 s-1)
    ft = 1. / ( 1 + np.exp(( - HD + DS * tk) / ( R_GAS * tk)))
    j_max = QJVC * VCMAX25 * ft * np.exp( AEJM * ( tk -\
    TEMP_K_25) / ( R_GAS * TEMP_K_25 *  tk))

    j = ( light_abs + j_max - np.sqrt((  light_abs + j_max) *\
    ( light_abs + j_max) - 4.0 * THETA * light_abs * j_max )) /\
    ( 2.0 * THETA)

    del light_abs, j_max

    # JV: ELECTRON FLUX REQUIRED TO SUPPORT RUBISCO-LIMITED
    # CARBON ASSIMILATION (umol m-2 s-1)
    vcmax   = VCMAX25 * ft * np.power( Q10VC, ( tk - TEMP_K_25)\
    / 10. )
    co2comp = 0.5 * kco2 * O2I * 0.21 / ko2
    del kco2, ko2, ft

    jv = 4.0 * vcmax * ( ci + 2.0 * co2comp) / ( ci + km)
    del vcmax, km

    # GET LENGTH OF LONGEST VARIABLE FOR max AND min ARGUMENTS
    LENGTH_GAMMA_MAX = np.ma.count( j)
    if np.ma.count( jv) != np.ma.count( j):
        LENGTH_GAMMA_MAX = np.max( [np.ma.count( jv),\
        np.ma.count( j)])

    LENGTH_1 = np.ma.count( co2comp)
    if np.ma.count( co2comp) != np.ma.count( ci):
        LENGTH_1 = np.max( [np.ma.count( co2comp),\
        np.ma.count( ci)])
```

```
        return (C1 + C2 * np.max( np.array(( np.tile( -GAMMA_MAX,\
        LENGTH_GAMMA_MAX), j - jv)), axis = 0)) * j *\
            np.min( np.array(( np.tile( 1.0, LENGTH_1), ci /\
            co2comp)), axis = 0)

        del co2comp, j, jv, tk

    gamma_ph      = get_gamma_ph( temp_k, ppfd_absorbed, co2i)
    gamma_ph_norm = get_gamma_ph( TEMP_K_30, PPFD_1000 * PAR_ABS,\
                    CO2I_std)

    gamma_ph_rel = gamma_ph / gamma_ph_norm
    del gamma_ph, gamma_ph_norm

    return gamma_ph_rel * gamma_en_rel

    del gamma_ph_rel, gamma_en_rel


def guenther_seasonal_temperature_and_light_correction(\
    temp_c_light_umol, sef):

    temp_c, light_umol = temp_c_light_umol

    # CONSTANTS FROM GUENTHER ET AL., 1997
    ALPHA = 0.0027      # [-]
    C_L1  = 1.066       # [-]

    GAMMA_LIGHT = ( ALPHA * C_L1 * light_umol) /\
    np.sqrt( 1 + np.power( ALPHA, 2) * np.power( light_umol, 2))

    # CONSTANTS FROM GUENTHER ET AL., 1997
    TEMP_K_STANDARD = 303.15    # [K] leaf temp at standard conditions
    C_T1            = 95000     # [J mol-1]
    C_T2            = 230000    # [J mol-1]
    C_T3            = 0.961     # set GAMMA_TEMP=1 at standard cond.
    temp_k          = temp_c + 273.15   # [K] observed leaf temp
    R_GAS           = 8.314     # [J K-1 mol-1]
    T_M             = 314       # [K]

    GAMMA_TEMP = np.exp(( C_T1 * ( temp_k - TEMP_K_STANDARD)) /\
      ( R_GAS * temp_k * TEMP_K_STANDARD)) / ( C_T3 + np.exp(( C_T2 *\
      (temp_k - T_M)) / ( R_GAS * temp_k * TEMP_K_STANDARD)))

    return sef * GAMMA_TEMP * GAMMA_LIGHT
```

F.2. JJv implemented in LandscapeDNDC

```
/*!
 * @brief
 *
 *    This gas exchange module calculates only
 *    emission of biogenic volatile organic compounds.
 *    cf. Grote et al., 2014
 *
 *    implemented by: Felix Wi\ss (fw)
 *                    Ruediger Grote (rg) *
 * @date
 *    20.02.2015
 *
 * @author
 *    ruediger grote (rg)
 *    felix wiss (fw)
 */



#include  "physiology/vocjjv/vocjjv.h"
#include  "physiology/ld_vocemissionhelper.h"
#include  "physiology/ld_canopylayer.h"

#include  <cbm_rtcfg.h>

#include  <logging/cbm_logging.h>
#include  <constants/cbm_const.h>
#include  <math/cbm_math.h>


#define  get_config_item(__key__,__value__)
    this->io_kcomm->get_scratch()->get( __key__, __value__)


LMOD_MODULE_INFO(PhysiologyVOCJJV,TMODE_SUBDAILY,LMOD_FLAG_USER);

REGISTER_OPTION(PhysiologyVOCJJV, CalcSynthaseActivity,
    "Specifies␣whether␣voc␣synthase␣acitivity␣should␣be␣calculated
␣␣␣␣instead␣of␣using␣standard␣emission␣factors␣(EF_ISO,␣EF_MONO)
␣␣␣␣[bool]");

REGISTER_OPTION(PhysiologyVOCJJV, CalcParTempDependence,
    "PPFD␣and␣temperature␣dependence␣of␣last␣ten␣days␣will␣be
␣␣␣␣calculated␣[bool]␣(only␣if␣standard␣emission␣factors␣are␣used");

namespace ldndc {

PhysiologyVOCJJV::photosynth_t::photosynth_t()
    : par( 0.0), par24( 0.0), par240( 0.0), parabs( 0.0)
{
}
```

```
PhysiologyVOCJJV::foliage_t::foliage_t()
    : tempK( 0.0), tempK24( 0.0), tempK240( 0.0)
{
}
PhysiologyVOCJJV::temp_par_seasonality_t::temp_par_seasonality_t()
    : eopt_iso( 1.0), eopt_mono( 1.0), c_p( 1.0)
{
}

/* more detailed description in vocjjv.h */
double const  PhysiologyVOCJJV::BETA        = 0.09;
double const  PhysiologyVOCJJV::BETA_MONO_S = 0.1;
double const  PhysiologyVOCJJV::BETA_OVOC   = 0.09;
double const  PhysiologyVOCJJV::TREF        = 30.0 + cbm::D_IN_K;
double const  PhysiologyVOCJJV::PPFD0       = 1000.0;
double const  PhysiologyVOCJJV::TEMP0       = 25.0 + cbm::D_IN_K;
double const  PhysiologyVOCJJV::ABS0        = 0.860;
double const  PhysiologyVOCJJV::C1          = 0.17650;
double const  PhysiologyVOCJJV::C2          = 0.00280;
double const  PhysiologyVOCJJV::GAMMA_MAX   = 34.0;
double const  PhysiologyVOCJJV::CEO_ISO     = 2.0;
double const  PhysiologyVOCJJV::CEO_MONO    = 1.83;
double const  PhysiologyVOCJJV::PAR0_SUN    = 200;
double const  PhysiologyVOCJJV::PAR0_SHD    = 50;


PhysiologyVOCJJV::PhysiologyVOCJJV( MoBiLE_State *  _state,
        cbm::io_kcomm_t * _io,
        timemode_e  _timemode)
            : MBE_LegacyModel( _state, _timemode),

        ac( _state->get_substate_ref< substate_airchemistry_t >()),
        mc( _state->get_substate_ref< substate_microclimate_t >()),
        ph( _state->get_substate_ref< substate_physiology_t >()),

        m_setup( _io->get_input_class< input_class_setup_t >()),
        m_veg( &_state->vegetation)

{
}

PhysiologyVOCJJV::~PhysiologyVOCJJV()
{
}

lerr_t
PhysiologyVOCJJV::configure(
        ldndc::config_file_t const *)
{
    return  LDNDC_ERR_OK;
}
```

```
lerr_t
PhysiologyVOCJJV::initialize()
{
    CALC_SYNTHASE_ACTIVITY  =
        get_option< bool >( "CalcSynthaseActivity", false);
    CALCULATE_PAR_TEMP_TERM  =
        get_option< bool >( "CalcParTempDependence", false);
    return  LDNDC_ERR_OK;
}


lerr_t
PhysiologyVOCJJV::solve()
{
  this->step_init();

  leaf_emission_t  lemi;
  leaf_emission_t  leminorm;

  double const  tslength = cbm::SEC_IN_DAY *
    this->lclock()->day_fraction();
  double const  sim_day_fraction = LD_RtCfg.clk->day_fraction();

  for ( PlantIterator vt = this->m_veg->begin(); vt !=
    this->m_veg->end(); ++vt)
    {
      MoBiLE_Plant *  p = *vt;
      size_t const  fl_cnt = foliage_layer_count( p->height_max);
      for ( size_t  fl = 0;  fl < fl_cnt;  ++fl)
      {
      if (( p->mFol_fl[fl] > 0.0) && ( p->sla_fl[fl] > 0.0))
      {
          /* call function from vocemissionhelper */
          // emission factors can change only on daily basis
          if (( this->timemode() == TMODE_SUBDAILY) &&
              ( this->lclock()->is_position( TMODE_POST_DAILY)))
          {
              double const  nd_temp_fl = mc.nd_temp_fl[fl] +
                  mc.temp_fl[fl] * sim_day_fraction;
              double const  nd_rad_fl = mc.nd_rad_fl[fl] +
                  mc.rad_fl[fl] * sim_day_fraction;

              get_voc_emission_factors( *vt, fl,
                          CALC_SYNTHASE_ACTIVITY,
                          this->m_setup->latitude(),
                          this->lclock()->yearday(),
                          nd_temp_fl, nd_rad_fl);

          }
```

```
/* conversion of microclimate variables */
lemi.pho.par    = mc.rad_fl[fl] * cbm::FPAR *
  cbm::UMOL_IN_W;
lemi.pho.par24  = mc.rad24_fl[fl] * cbm::FPAR *
  cbm::UMOL_IN_W;
lemi.pho.par240 = mc.rad240_fl[fl] * cbm::FPAR *
  cbm::UMOL_IN_W;

lemi.fol.tempK  = mc.tFol_fl[fl] + cbm::D_IN_K;
lemi.fol.tempK24  = mc.tFol24_fl[fl] + cbm::D_IN_K;
lemi.fol.tempK240 = mc.tFol240_fl[fl] + cbm::D_IN_K;

/* normalized microclimate variables */
leminorm.pho.par      = PPFD0;
leminorm.pho.parabs   = PPFD0 * ABS0;
leminorm.fol.tempK    = TREF;

/* the foliage layer of the current loop */
lemi.foliage_layer      = fl;
leminorm.foliage_layer  = fl;

this->CalcLeafEmission( &lemi, &leminorm, *vt);

/* conversion from ug gDW-1 h-1 to umol m-2 per timestep */
double const  C  = (( p->mSap / fl_cnt + p->mCor / fl_cnt +
  p->mBud / fl_cnt + p->mFol_fl[fl]) * cbm::G_IN_KG) *
  ( tslength / cbm::SEC_IN_HR);

p->isoprene_emission_fl[fl]    = lemi.isoprene * C / 68.0;
p->ovoc_emission_fl[fl]        = lemi.ovoc * C / 44.0;
p->methanol_emission_fl[fl]    = lemi.methanol * C / 32.0;
p->acetaldehyde_emission_fl[fl]= lemi.acetaldehyde * C / 44.0;
p->ethanol_emission_fl[fl]     = lemi.ethanol * C / 46.0;
p->acetone_emission_fl[fl]     = lemi.acetone * C / 58.0;
p->acetic_acid_emission_fl[fl] = lemi.acetic_acid * C / 60.0;
p->mvk_macr_emission_fl[fl]    = lemi.mvk_macr * C / 71.0 ;
p->mek_emission_fl[fl]         = lemi.mek * C / 73.0;
p->benzene_emission_fl[fl]     = lemi.benzene * C /  79.0;
p->toluene_emission_fl[fl]     = lemi.toluene * C / 93.0;
p->hexenal_emission_fl[fl]     = lemi.hexenal * C / 98.0;
p->hexanal_emission_fl[fl]     = lemi.hexanal * C / 100.0;
p->xylenes_emission_fl[fl]     = lemi.xylenes * C / 106.0;
p->indole_emission_fl[fl]      = lemi.indole * C / 117.0;
p->monoterpenes_emission_fl[fl]= lemi.monoterpenes * C /
  136.0;
p->dmnt_emission_fl[fl]        = lemi.dmnt * C / 150.0;
p->camphor_emission_fl[fl]     = lemi.camphor * C / 152.0;
p->o_monoterpenes_emission_fl[fl]= lemi.o_monoterpenes * C /
  154.0;
p->sesquiterpenes_emission_fl[fl]= lemi.sesquiterpenes * C /
  204.0;
```

```
            }
            else
            {
              p->isoprene_emission_fl[fl]       = 0.0;
              p->ovoc_emission_fl[fl]           = 0.0;
              p->methanol_emission_fl[fl]      = 0.0;
              p->acetaldehyde_emission_fl[fl] = 0.0;
              p->ethanol_emission_fl[fl]       = 0.0;
              p->acetone_emission_fl[fl]       = 0.0;
              p->acetic_acid_emission_fl[fl]   = 0.0;
              p->mvk_macr_emission_fl[fl]      = 0.0;
              p->mek_emission_fl[fl]           = 0.0;
              p->benzene_emission_fl[fl]       = 0.0;
              p->toluene_emission_fl[fl]       = 0.0;
              p->hexenal_emission_fl[fl]       = 0.0;
              p->hexanal_emission_fl[fl]       = 0.0;
              p->xylenes_emission_fl[fl]       = 0.0;
              p->indole_emission_fl[fl]        = 0.0;
              p->monoterpenes_emission_fl[fl] = 0.0;
              p->dmnt_emission_fl[fl]          = 0.0;
              p->camphor_emission_fl[fl]       = 0.0;
              p->o_monoterpenes_emission_fl[fl] = 0.0;
              p->sesquiterpenes_emission_fl[fl] = 0.0;
          }
      }
  }
    return  LDNDC_ERR_OK;
}


void
PhysiologyVOCJJV::step_init()
{
    ph.ts_isoprene_emission = 0.0;
    ph.ts_monoterpene_emission = 0.0;
}


lerr_t
PhysiologyVOCJJV::CalcLeafEmission(
        leaf_emission_t *  _lemi,
        leaf_emission_t *  _leminorm,
        MoBiLE_Plant * _vt)
{
    size_t const  _fl = _lemi->foliage_layer;
    gamma_factor_t  gamma;
    _lemi->pho.parabs = _lemi->pho.par * ABSO;
    gamma.ph          = this->get_jjv_gamma_PH( _lemi, _vt);

    /* photosynthesis activity under standard conditions */
```

```
    gamma.phnorm      = this->get_jjv_gamma_PH_norm( _leminorm, _vt);

    /* relative bvoc activity factor for photosynthesis */
    gamma.phrel = 0.0;
    if ( gamma.phnorm > 0.0)
    {
        gamma.phrel = gamma.ph / gamma.phnorm;
    }

    /* enzymatic activity of isoprene and monoterpene synthase;*/
    this->get_jjv_gamma_EN( _lemi, _leminorm, _vt, &gamma);

    /* total scaling factor denovo synthesis */
    gamma.iso = 0.0;
    if ( gamma.ennorm_iso > 0.0)
    {
      gamma.iso = gamma.phrel * ( gamma.en_iso / gamma.ennorm_iso);
    }

    gamma.mono = 0.0;
    if ( gamma.ennorm_mono > 0.0)
    {
      gamma.mono = gamma.phrel * ( gamma.en_mono / gamma.ennorm_mono);
    }


    if ( CALCULATE_PAR_TEMP_TERM && !CALC_SYNTHASE_ACTIVITY)
    {
        KLOGINFO_ONCE("VOC␣standard␣emission␣factors␣are␣modified
␣␣␣␣␣␣␣␣␣␣according␣to␣past␣days␣temperature␣and␣radiation");
        this->get_temp_par_seasonality( _lemi);

    }
    else if ( CALCULATE_PAR_TEMP_TERM && CALC_SYNTHASE_ACTIVITY)
    {
        KLOGERROR("CalcSynthaseActivity:␣", CALC_SYNTHASE_ACTIVITY,
          "␣and␣CalcParTempDependence:␣", CALCULATE_PAR_TEMP_TERM,
          "␣at␣the␣same␣time␣is␣not␣meaningful␣:|");
        return LDNDC_ERR_FAIL;
    }

/* Multiply emission activity for LDF and LIF with emission factor*/
_lemi->methanol = _vt->parameters()->EF_METHANOL()  *
( _vt->parameters()->LDF_METHANOL() * gamma.mono + ( 1 -
_vt->parameters()->LDF_METHANOL()) * this->get_gamma_T(  _lemi,
_leminorm, _vt->parameters()->BETA_METHANOL()));

_lemi->acetaldehyde = _vt->parameters()->EF_ACETALDEHYDE()  *
( _vt->parameters()->LDF_ACETALDEHYDE() * gamma.mono + ( 1 -
_vt->parameters()->LDF_ACETALDEHYDE()) * this->get_gamma_T(  _lemi,
_leminorm, _vt->parameters()->BETA_ACETALDEHYDE()));
```

```
_lemi->ethanol = _vt->parameters()->EF_ETHANOL()  *
( _vt->parameters()->LDF_ETHANOL() * gamma.mono + ( 1 -
_vt->parameters()->LDF_ETHANOL()) * this->get_gamma_T(  _lemi,
_leminorm, _vt->parameters()->BETA_ETHANOL()));

_lemi->acetone = _vt->parameters()->EF_ACETONE()  *
( _vt->parameters()->LDF_ACETONE() * gamma.mono + ( 1 -
_vt->parameters()->LDF_ACETONE()) * this->get_gamma_T(  _lemi,
_leminorm, _vt->parameters()->BETA_ACETONE()));

_lemi->acetic_acid = _vt->parameters()->EF_ACETIC_ACID()  *
( _vt->parameters()->LDF_ACETIC_ACID() * gamma.mono + ( 1 -
_vt->parameters()->LDF_ACETIC_ACID()) * this->get_gamma_T(  _lemi,
_leminorm, _vt->parameters()->BETA_ACETIC_ACID()));

_lemi->mvk_macr = _vt->parameters()->EF_MVK_MACR()  *
( _vt->parameters()->LDF_MVK_MACR() * gamma.mono + ( 1 -
_vt->parameters()->LDF_MVK_MACR()) * this->get_gamma_T(  _lemi,
_leminorm, _vt->parameters()->BETA_MVK_MACR()));

_lemi->mek = _vt->parameters()->EF_MEK()  *
( _vt->parameters()->LDF_MEK() * gamma.mono + ( 1 -
_vt->parameters()->LDF_MEK()) * this->get_gamma_T(  _lemi,
_leminorm, _vt->parameters()->BETA_MEK()));

_lemi->benzene = _vt->parameters()->EF_BENZENE()  *
( _vt->parameters()->LDF_BENZENE() * gamma.mono + ( 1 -
_vt->parameters()->LDF_BENZENE()) * this->get_gamma_T(  _lemi,
_leminorm, _vt->parameters()->BETA_BENZENE()));

_lemi->toluene = _vt->parameters()->EF_TOLUENE()  *
( _vt->parameters()->LDF_TOLUENE() * gamma.mono + ( 1 -
_vt->parameters()->LDF_TOLUENE()) * this->get_gamma_T(  _lemi,
_leminorm, _vt->parameters()->BETA_TOLUENE()));

_lemi->hexenal = _vt->parameters()->EF_HEXENAL()  *
( _vt->parameters()->LDF_HEXENAL() * gamma.mono + ( 1 -
_vt->parameters()->LDF_HEXENAL()) * this->get_gamma_T(  _lemi,
_leminorm, _vt->parameters()->BETA_HEXENAL()));

_lemi->hexanal = _vt->parameters()->EF_HEXANAL()  *
( _vt->parameters()->LDF_HEXANAL() * gamma.mono + ( 1 -
_vt->parameters()->LDF_HEXANAL()) * this->get_gamma_T(  _lemi,
_leminorm, _vt->parameters()->BETA_HEXANAL()));

_lemi->xylenes = _vt->parameters()->EF_XYLENES()  *
( _vt->parameters()->LDF_XYLENES() * gamma.mono + ( 1 -
_vt->parameters()->LDF_XYLENES()) * this->get_gamma_T(  _lemi,
_leminorm, _vt->parameters()->BETA_XYLENES()));
```

```
_lemi->indole = _vt->parameters()->EF_INDOLE()  *
( _vt->parameters()->LDF_INDOLE() * gamma.mono + ( 1 -
_vt->parameters()->LDF_INDOLE()) * this->get_gamma_T(  _lemi,
_leminorm, _vt->parameters()->BETA_INDOLE()));

_lemi->monoterpenes = _vt->parameters()->EF_MONOTERPENES()  *
( _vt->parameters()->LDF_MONOTERPENES() * gamma.mono + ( 1 -
_vt->parameters()->LDF_MONOTERPENES()) * this->get_gamma_T(  _lemi,
_leminorm, _vt->parameters()->BETA_MONOTERPENES()));

_lemi->dmnt = _vt->parameters()->EF_DMNT()  *
( _vt->parameters()->LDF_DMNT() * gamma.mono + ( 1 -
_vt->parameters()->LDF_DMNT()) * this->get_gamma_T(  _lemi,
_leminorm, _vt->parameters()->BETA_DMNT()));

_lemi->camphor = _vt->parameters()->EF_CAMPHOR()  *
( _vt->parameters()->LDF_CAMPHOR() * gamma.mono + ( 1 -
_vt->parameters()->LDF_CAMPHOR()) * this->get_gamma_T(  _lemi,
_leminorm, _vt->parameters()->BETA_CAMPHOR()));

_lemi->o_monoterpenes = _vt->parameters()->EF_O_MONOTERPENES()  *
( _vt->parameters()->LDF_O_MONOTERPENES() * gamma.mono + ( 1 -
_vt->parameters()->LDF_O_MONOTERPENES()) * this->get_gamma_T(  _lemi,
_leminorm, _vt->parameters()->BETA_O_MONOTERPENES()));

_lemi->sesquiterpenes = _vt->parameters()->EF_SESQUITERPENES()  *
( _vt->parameters()->LDF_SESQUITERPENES() * gamma.mono + ( 1 -
_vt->parameters()->LDF_SESQUITERPENES()) * this->get_gamma_T(  _lemi,
_leminorm, _vt->parameters()->BETA_SESQUITERPENES()));

return  LDNDC_ERR_OK;
}

double
PhysiologyVOCJJV::get_gamma_T(
        leaf_emission_t *  _lemi,
        leaf_emission_t *  _leminorm,
        double _beta)
const
{
    /* light independent emission calculation */
    return  exp( _beta * ( _lemi->fol.tempK - _leminorm->fol.tempK));
}

double
PhysiologyVOCJJV::get_jjv_gamma_PH(
        leaf_emission_t *  _lemi,
        MoBiLE_Plant * _vt)
const
{
    size_t const  fl = _lemi->foliage_layer;
```

```
    /* electron usage for photosynthesis */
    /* km: michaelis-menten coefficient */
    double  km = 0.0;
    if ( _vt->ko2_fl[fl] > 0.0)
    {
        km = _vt->kco2_fl[fl] * ( 1.0 + _vt->o2i_fl[fl] /
        _vt->ko2_fl[fl]);
    }

    /* jj: electron provision (umol m-2 s-1) */
    double const  tmp_var = ( _lemi->pho.parabs + _vt->jMax_fl[fl]) *
    ( _lemi->pho.parabs + _vt->jMax_fl[fl]) - 4.0 * (*_vt)->THETA() *
    _lemi->pho.parabs * _vt->jMax_fl[fl];

    double  jj = 0.0;
    if ( tmp_var > 0.0)
    {
        jj = ( _lemi->pho.parabs + _vt->jMax_fl[fl] - sqrt( tmp_var))
         / ( 2.0 * (*_vt)->THETA());
    }

    /* jv: electron transport for C assimilation (umol m-2 s-1) */
    double  jv = 0.0;
    if (( _vt->co2i_fl[fl] + km) > 0.0)
    {
        /* co2comp25_fl: CO2 compensation point (umol mol-1) */
        jv = 4.0 * _vt->vcMax_fl[fl] * ( _vt->co2i_fl[fl] + 2.0 *
        _vt->co2comp25_fl[fl]) / ( _vt->co2i_fl[fl] + km);
    }

    /* excess energy after carbon assimilation) */
    if ( _vt->co2comp25_fl[fl] > 0.0)
    {
        return  (( C1 + C2 * std::max( -GAMMA_MAX, jj - jv)) * jj *
        std::min( 1.0, _vt->co2i_fl[fl] / _vt->co2comp25_fl[fl]));
    }
    else
    {
        return  0.0;
    }
}

double
PhysiologyVOCJJV::get_jjv_gamma_PH_norm(
        leaf_emission_t *  _lemi,
        MoBiLE_Plant * _vt)
const
{
    /* Calculation of gamma_PH under standard conditions */
    size_t const  fl = _lemi->foliage_layer;
```

```
    double  km = 0.0;
    if ( _vt->ko2_std_fl[fl] > 0.0)
    {
        km = _vt->kco2_std_fl[fl] * ( 1.0 + _vt->o2i_std_fl[fl] /
        _vt->ko2_std_fl[fl]);
    }

    double const  tmp_var = ( _lemi->pho.parabs +
      _vt->jMax_std_fl[fl]) * ( _lemi->pho.parabs +
      _vt->jMax_std_fl[fl]) - 4.0 * (*_vt)->THETA() *
      _lemi->pho.parabs * _vt->jMax_std_fl[fl];

    double  jj = 0.0;
    if ( tmp_var > 0.0)
    {
        jj = ( _lemi->pho.parabs + _vt->jMax_std_fl[fl] -
          sqrt( tmp_var)) / ( 2.0 * (*_vt)->THETA());
    }

    double  jv = 0.0;
    if (( _vt->co2i_std_fl[fl] + km) > 0.0)
    {
        jv = 4.0 * _vt->vcMax_std_fl[fl] * ( _vt->co2i_std_fl[fl] +
          2.0 * _vt->co2comp25_std_fl[fl]) / ( _vt->co2i_std_fl[fl] +
          km);
    }

    if ( _vt->co2comp25_std_fl[fl] > 0.0)
    {
        return  (( C1 + C2 * std::max( -GAMMA_MAX, jj - jv)) * jj *
          std::min( 1.0, _vt->co2i_std_fl[fl] /
          _vt->co2comp25_std_fl[fl]));
    }
    else
    {
        return  0.0;
    }
}


lerr_t
PhysiologyVOCJJV::get_jjv_gamma_EN(
        leaf_emission_t *  _lemi,
        leaf_emission_t *  _leminorm,
        MoBiLE_Plant *  vt,
        gamma_factor_t * _gamma)
const
{
    _gamma->en_iso       = exp( ( *vt)->CT_IS() - ( *vt)->HA_IS() /
      ( cbm::RGAS * _lemi->fol.tempK)) / ( 1.0 +
      exp(( ( *vt)->DS_IS() * _lemi->fol.tempK - ( *vt)->HD_IS()) /
```

```
      (cbm::RGAS * _lemi->fol.tempK)));

    _gamma->en_mono      = exp( ( *vt)->CT_MT() - ( *vt)->HA_MT() /
      ( cbm::RGAS * _lemi->fol.tempK)) / ( 1.0 +
      exp(( ( *vt)->DS_MT() * _lemi->fol.tempK - ( *vt)->HD_MT()) /
      (cbm::RGAS * _lemi->fol.tempK)));

    /* Calculate normalized emission from enzyme activity */
    _gamma->ennorm_iso   = exp( ( *vt)->CT_IS() - ( *vt)->HA_IS() /
      ( cbm::RGAS * _leminorm->fol.tempK)) / ( 1.0 +
      exp(( ( *vt)->DS_IS() * _leminorm->fol.tempK -
      ( *vt)->HD_IS()) / (cbm::RGAS * _leminorm->fol.tempK)));

    _gamma->ennorm_mono = exp( ( *vt)->CT_MT() - ( *vt)->HA_MT() /
    ( cbm::RGAS * _leminorm->fol.tempK)) / ( 1.0 +
    exp(( ( *vt)->DS_MT() * _leminorm->fol.tempK -
    ( *vt)->HD_MT()) / (cbm::RGAS * _leminorm->fol.tempK)));

    return  LDNDC_ERR_OK;

}


lerr_t
PhysiologyVOCJJV::get_temp_par_seasonality(
        leaf_emission_t *  _lemi)
const
{

    size_t const  _fl = _lemi->foliage_layer;

    /* fixed empirical coefficients from MEGAN2.1 */
    _lemi->tpar.eopt_iso  = 2.26;
    _lemi->tpar.eopt_mono = 2.26;
    _lemi->tpar.c_p       = 1.21;


    if ( _lemi->fol.tempK240 > 0.0)
    {
        /* temperature dependence of past days */
        _lemi->tpar.eopt_iso   = CEO_ISO  * exp( 0.05 *
        ( _lemi->fol.tempK24 - 297.15)) * exp( 0.05 *
        ( _lemi->fol.tempK240 - 297.15));

        _lemi->tpar.eopt_mono  = CEO_MONO * exp( 0.05 *
        ( _lemi->fol.tempK24 - 297.15)) * exp( 0.05 *
        ( _lemi->fol.tempK240 - 297.15));
    }

    if ( _lemi->pho.par240 > 0.0)
    {
```

```
        /* Factor for PPFD dependence of past days */
        double const  C_P_SUN = 0.0468 * exp( 0.0005 *
        ( mc.parsun24_fl[_fl] - PAR0_SUN)) *
          pow( mc.parsun240_fl[_fl], 0.6);

        double const  C_P_SHD = 0.0468 * exp( 0.0005 *
        ( mc.parshd24_fl[_fl] - PAR0_SHD)) *
          pow( mc.parshd240_fl[_fl], 0.6);

        _lemi->tpar.c_p = mc.sunlitfoliagefraction240_fl[_fl] *
          C_P_SUN + (( 1 - mc.sunlitfoliagefraction240_fl[_fl]) *
          C_P_SHD);

    }
    return  LDNDC_ERR_OK;
}
} /*namespace ldndc*/
```